USE OF EVAPORATIVE FRACTIONAL CRYSTALLIZATION IN THE PRETREATMENT PROCESS OF MULTI-SALT SINGLE SHELL TANK HANFORD NUCLEAR WASTES

A Thesis
Presented to
The Academic Faculty

by

Laurent Nassif

In Partial Fulfillment
of the Requirements for the Degree
Master of Science in the
School of Chemical and Biomolecular Engineering

Georgia Institute of Technology
May 2007

USE OF EVAPORATIVE FRACTIONAL CRYSTALLIZATION IN THE PRETREATMENT PROCESS OF MULTI-SALT SINGLE SHELL TANK HANFORD NUCLEAR WASTES

Approved by:

Dr. Ronald W. Rousseau, Chair and Advisor
School of Chemical and Biomolecular Engineering
Georgia Institute of Technology

Dr. Amyn S. Teja
School of Chemical and Biomolecular Engineering
Georgia Institute of Technology

Dr. Daniel Tedder
School of Chemical and Biomolecular Engineering
Georgia Institute of Technology

Date Approved: December 8th 2006

To Viola Karam Nassif

PREFACE

There currently are 53 million gallons of mixed and highly radioactive wastes awaiting treatment at the Hanford site in the State of Washington. These wastes are stored in 177 underground shielded tanks partitioned into 18 tank farms. Wastes have accumulated at the site since the Second World War and are a result of more than fifty years of nuclear materials production.

Waste is a term referring to liquids and solids that are radioactive and/or hazardous (DOE/EM-0319, 1997). The waste materials were previously disposed of by burial or by deep underground injection. Department of Energy wastes awaiting disposal are accumulated in containers, tanks, silos, buildings, and other structures along with the wastes that have been retrieved in site cleanups. All waste that falls under the responsibility of the US Department of Energy (DOE) is measured in terms of volume and radioactivity content (DOE/EM-0319, 1997). "Approximatively two-thirds of the legacy of waste managed by the Department of Energy was generated from nuclear weapons production. Some waste has been generated as a result of other DOE programs in basic research, nuclear power research, and other applied research and development activities. Additionally, some waste was generated as a result of producing nuclear fuel for the NNPP (Naval Nuclear Propulsion Program) and commercial nuclear power reactors" (DOE/EM-0319, 1997).

At the Hanford site, nuclear wastes have been generated by activities like those described above and include such as purification and chemical separation, mining, milling and refining, reactor operations, research, development and testing, fuel and target fabrication, enrichment and finally weapons components fabrication. Activities related to weapons production are responsible for 220 000 m^3 of the 239 000 m^3 of the total volume of high-level liquid wastes inventoried at the Hanford site. In terms of radioactivity, the nuclear weapons activities generated 320 million curies among the total 347 million curies disposed at Hanford (DOE/EM-0319, 1997).

Isotopes responsible for the radioactivity of the waste stored at Hanford are mainly uranium fission products that remain unspecified. Hence, a methodology was developed in order to select the most important radionuclides present in the Hanford waste along with their concentrations (Cowley et al., 1998). This methodology facilitated the identification of cesium (Lewis et al., 1965), technetium (Vance et al., 1998) and strontium (Fullam et al., 1976) as radioactive species present in Hanford waste. Among these radioactive isotopes, ^{137}Cs (cesium 137) has been identified as the major isotope remaining in the low and medium curie wastes that must be removed before immobilization.

However, radioactive isotopes represent only a small fraction of the waste. The bulk of the waste is composed of non-radioactive inorganic chemicals issued from the fuel reprocessing operations. More recently, the characterization of the solid phases in the waste have focused not only on quantifying amounts but also in speciation. Speciation studies showed the importance of the presence of several sodium double salts and of certain heavy elements. (Herting et al., 2003)

Since limited thermodynamic information was available for these sodium double salts at the conditions present in the Hanford tanks, there was a need for simulation tools in order to predict their thermodynamic behavior. The Environmental Simulation Program (developed by OLI system inc.) was chosen in order to simulate the salt cake dissolution, tank retrieval, and pipeline transfer operations. Experimental measurements of phase equilibrium was performed for 9 saltcakes in the high ionic strength inorganic system conditions of the Hanford waste tanks and compared to simulations. This allowed examining of the predictive aspect of the simulation program (Toghiani et al., 2002).

The treatment of both Low Level Liquid Waste (LLLW) and High Level Liquid Waste (HLLW) accumulated at Hanford site was initially intended to be performed by a single structure called the Waste Treatment Plant (WTP). It is intended to immobilize the liquid waste in borosilicate glass cast into stainless steel canisters. The filled canisters will be disposed of in a federal geologic repository.

The waste treatment plant facility was originally intended to integrate three main processes. A pretreatment unit would reduce the volume of High Level Waste to be treated. Then the liquid waste would be sent to the melter feed Vitrification system. Among the different technologies possible for the vitrification process we can mention the “in-can melter”, the “Pt Crucible” and the “Joule-heated” melter (Chapman et al., 1979). The vitrification plant at Hanford would use a continuous feed melter technology (Smith et al., 1990) where the feed is introduced continuously inside the melter box with a water-cooled nozzle. The refractory-lined melter box is equipped with a stainless steel cooling water jacket, heating electrodes, and off-gas vent. The off-gas system is

positioned from the exhaust opening in the melter cell to the exhaust duct of the plant's building. Its aim is to remove the particulates, the radionuclides, and reactive gases that have formed in the melter so that the exhaust gas meets regulations. The glass formed is then transferred to the canister by introducing vacuum inside the canister and using a canister-to-melter spout. The filled canister is then cooled on a stainless steel turntable and stored in the appropriate repository site. The melter cell is equipped with a closed circuit television in order to control the process.

The vitrification process is a common technique used for the HLLW treatment and has been used successfully in several other U.S. Department of Energy sites (Carreon et al., 2002), (Rabiger et al., 1995), (Colombo et al., 2003). This technology, which consists of the immobilization of the liquid waste into a borosilicate glass, has been investigated thoroughly during the years.

To demonstrate the feasibility of vitrification and the durability of the high-level waste glass, a high level waste sample from Hanford tank AZ-101 was processed to glass and analyzed with respect to chemical composition, radionuclide content, and waste loading capacity (Hrma et al., 2005,Part I). The vitrified borosilicate glass was then tested to demonstrate its compliance with regulatory requirements. Crystallinity testing was performed by quantitative X-Ray Diffraction (XRD) and image analysis was performed with scanning electron microscopy (SEM) micrographs. Glass leachability was measured with the product consistency test and the toxicity characteristic leaching procedure (Hrma et al., 2005, Part II). These results were compared with the non-radioactive simulant glass results and models were used in order to identify the

impact of spinels on glass composition and leachability (Wilson et al., 2002), (Mika et al., 2001).

In 2000, the U.S. Department of Energy awarded a 14 billion dollar contract for the construction of the Waste Treatment Plant and the cleaning of the Hanford site by the year 2030 (Smith et al., 1990). However, contractor and DOE Management issues have lead to higher costs, construction delays, and safety concerns. Since the WTP construction contract was awarded in 2000, the estimated building cost has increased more than 150 %, from 4.3 to 11 billion dollars. In addition, the completion date for the building of the WTP has been postponed by 6 years or more (Aloise et al., 2006). These issues were attributed to insufficient contractor performance in implementing the adequate nuclear safety requirements and in its project estimate, the DOE management issues, and technical challenges that arose.

Safety issues were also raised as an effect of extended storage time at Hanford site (DOEM/EM-0266, 1996), (DOEM/EM-0232 and DOEM/EM-0290, 1995-1996), (DOE, 1996). Many of Hanford's older single shell tanks have leaked and some one million gallons of waste are believed to have leaked from these tanks in the last fifty years (DOE/EM-0319, 1997). The double shell tanks, some of these having been built in the early 80's, were constructed to last for 50 years. However, the extension in the project completion time increased the risks of liquid waste or flammable gases leaking due to the aging of the waste (Bryan et al., 2003). Three additional main releases of radioactive materials have occurred since 1944. More than 200 million gallons of slightly radioactive water have been routinely discharged in Hanford soil leading to soil and groundwater contamination since 1951. Between 1944 and 1947 Iodine-131, a radioactive isotope with

a half life of eight days, was directly released in the atmosphere. Finally, between 1944 and 1971, radionuclides were directly released to the Columbia River through contaminated cooling water used for the fuel elements in the reactor core (DOE/EM-0319, 1997).

Based on this information related to cost, time and environmental issues, the U.S. Department of Energy has determined that the preferred alternative to remediate the Hanford tank waste would be to submit it to pretreatment. This process would separate the waste into Low Activity Waste (LAW) and High Level Waste (HLW), which would both be vitrified into borosilicate glasses (Carreon et al., 2002).

The LAW would be immobilized through bulk vitrification for on-site disposal, contrary to the HLW that would be immobilized as glass through the WTP for ultimate disposal in the national repository. The bulk vitrification process is well known at the Hanford site and experiments at the engineering scale have been performed with simulated waste solutions (Tyree), (Kaldor et al., 1985), (Huang et al., 1994). In these experiments, simulant was mixed with soil and small amounts of chemical additives before being melted at 1300 degrees Celcius. The melter used for the bulk vitrification process also acts as the final container for the immobilized waste and can be stored in situ. This vitrification method, by supplementing the WTP, would greatly decrease the final repository and overall project costs while accelerating the treatment of Hanford waste (Thompson et al., 2003).

Several methods have been proposed and studied for use in removing cesium from Hanford wastes. Such methods include ion exchange, solvent extraction, tetraphenylborate precipitation, nanofiltration-complexation and evaporative fractional

crystallization. Ideally, the selected technology will remove at least 99% of the cesium from the waste and add no additional waste streams to the process (Carreon et al., 2002).

The proposed ion exchange process uses a SuperLig® 644 resin material containing a poly (hydroxyarlyne) ligand, which is highly selective for the cesium cation. Research has proven that by operating two ion exchange columns in series, cesium removal yields can range from 99.4-99.98%. The reason for the range in cesium yields was found to be the potassium concentration in the feed stream; potassium competes with cesium for the ligand sites on the resin. This process is very attractive since the resin can be reused by eluting the column with nitric acid (removing the cesium) and regenerating the resin with sodium hydroxide. The downside to this technology is that it introduces an acid and base stream to the process, which could increase the total waste volume (Hassan et al., 2002).

A second possible method for removing cesium from Hanford wastes is an extraction process using magnetic microparticles. These particles are composed of magnetite (Fe_3O_4), crystalline silicotitanate (CST), and polyacrolein, and are known by the trade name MagAcryl^{TM}-CST. During the process cesium binds to the CST in the micropores and after an appropriate contact time a high gradient magnetic separator is used to separate the particles from the liquid stream. This method has proven to remove between 90-98% of the cesium in a single stage. The major drawback to this method is that magnetite is susceptible to dissolution under extreme conditions, and since the magnetic separation step relies on magnetite, dissolution would ruin this process (Kaminski et al., 2002).

Tetraphenylborate (TPB) precipitation is another alternative for cesium removal from Hanford wastes. To begin this process, aqueous NaTPB is mixed with the cesium containing waste. Ion exchange occurs between sodium and cesium and insoluble CsTPB is precipitated from the solution. This cesium precipitate is then separated, dissolved in a propylene carbonate stream, and sent to a three phase extraction. The extraction step involves an upper layer of tripropylamine, a middle layer of aqueous $NaNO_3$, and a lower layer of cesium-containing propylene carbonate. During the extraction process, ion exchange occurs again between cesium and sodium, with aqueous $CsNO_3$ being the final product of interest. TPB precipitation has proven to have a cesium removal yield of at least 99.8%, but there are several drawbacks to this method. These drawbacks include the additional process streams necessary for the separation process and the potential decomposition of TPB into benzene and other flammable organics (Ponder et al., 2001).

The fourth alternative method discussed here is nanofiltration-complexation. This process utilizes a cesium-selective ligand to form a cesium-ligand complex in the waste stream, which is then sent to a nanofiltration step. The ligand chosen for testing was tetrahydroxylated bis-crown-6 calix[4]arene. This process is attractive since it does not add additional wastes to the process, but studies have shown that a single stage of complexation-nanofiltration only removes 90% of the cesium in the feed stream (Chitry et al., 2001).

The pretreatment method selected and investigated in this thesis is fractional crystallization. This method "was already demonstrated in the laboratory for separating clean, virtually non-radioactive sodium nitrate from Hanford tank waste". Flowsheet modeling has shown that the process could reduce the volume of vitrified low

activity waste (LAW) by 80% to 90%, reducing disposal costs by an estimated $240 million, and would eliminate the need for building a $2.2 billion large scale vitrification plant (Herting et al., 1997).

The evaporative crystallization method uses experimental solubility data obtained for three main sodium salts present in the simulant solutions. The solubilities of sodium nitrate, sodium nitrate, and sodium aluminate were obtained as functions of the temperature and concentration of sodium hydroxide, nitrate, nitrate and aluminate. The effects of the other species present in simulated waste solutions were found to be negligible (Reynolds et al., 1985).

A general procedure for the evaporative fractional crystallization of simulated Hanford Waste Solutions was established. It concerns the crystal formation of burkeite and other sodium salts. This method would decrease the volume of radioactive waste, but also the sodium-to-sulfate molar ratio, which may limit the formation of stable glass matrices during vitrification (Geniesse, 2004). The application and improvement of this method, in the case of single shell tank wastes, is the aim of this thesis.

The crystal identification of the solid phases issued from research on Hanford simulated wastes are performed through Polarized Light Microscopy (PLM). For each of the different crystalline species commonly obtained from processes involving Hanford wastes (or simulated wastes), a listing of characteristics and full-color photographs were established. The crystalline characteristics described were the extinction position, the crystal morphology, the optic and elongation signs, the interference figure and birefringence (Herting et al., 1992). The precise inventory and

importance of the data collected on inorganic species likely to crystallize made of this technique the preferred method for crystal characterization.

The simulants were developed from available analysis data. Test on simulated waste are performed before the actual radioactive wastes. Laboratory testing with the radioactive wastes are to be handled under hot cell environment. The specific hot cell equipment to be used for the cesium removal pretreatment processes have been already developed (Hammit et al., 1979).

ACKNOWLEDGEMENTS

I would like to especially thank my parents, Atef and Christiane, and my brother Christian, without whose continuous support, love and faith in me I would not be here. I wish to express my deepest gratitude to my thesis advisor, Dr Ronald. W. Rousseau, for his knowledge, guidance and help and my main coworker and friend, George "Pj" Dumont, with whom I am sharing the work and results presented in this thesis. I wish to include to this research work the name of my two other coworkers, Cosmas Bayuadri and Hatem Alsyouri with whom we shared long hours to complete the experimental part of this project.

I wish to acknowledge the financial support for the research project provided by the U.S. Department of Energy's Office of Environmental Management (EM-21 – Office of Cleanup Technology) through CH2M HILL and COGEMA, Inc. The interaction with Eric Nelson has been beneficial in keeping the activities moving forward and focused on the project objectives. His style in reminding us of deadlines is commendable and effective.

Guidance from Dr. Daniel L. Herting of the CH2M HILL provided very helpful insights to many of the issues concerning fractional crystallization from the Hanford solutions. In addition, his knowledge and willingness to help our team learn to use polarized light microscopy in studying crystals produced in this work were invaluable.

Don Geniesse of COGEMA, Inc. provided knowledgeable and timely guidance with his simulations of fractional crystallization. He did not mind answering even the most mundane questions regarding the systems with which we worked, and he was especially helpful in responding to "what if" questions regarding process modifications.

The work benefited considerably from discussions with Tim Nordahl, President of Swenson Inc. He provided perspectives and suggestions regarding the most important data for taking the results of our work to a scaled-up process.

The experimental apparatus and procedures developed in this thesis benefited considerably from the input of John Smith and Dave Bechtold from CH2M HILL, whose practical point of view and experience in the field becomes a great asset for the project.

We express appreciation to Jeff Dillener of Galbraith laboratories and Victor De Jesus of GTRI at Georgia Tech for his diligence in working with us to provide analytical results that were as useful as possible. We also would like to thank Mike Buchanan at the IPST Center at Georgia Tech and Victor for his assistance with chemical analyses.

I would like to particularly thank past and present members of this research group for their valuable inputs, encouragement and friendship: Karsten Bartling, Stephanie Barthe, Krystle Chavez, Quinta Nwanosike, "Ov" Apichit Svang-Aryaskul, Ana Fernandez, Chee-wei Jenifer Luk, Jose Mendez del Rio and Young-soo Kim.

I give my sincere thanks to all my friends, professors, and staff I met at Georgia Tech and in Toulouse, France. I wish to especially thank Pr Patrick Garnier, Mr. Joel Bertrand, Pr. Xavier Joulia and Pr. Joel Albet from the INP Toulouse and LGC Toulouse.

Finally and most importantly, I dedicate this thesis to the loving memory of my grandmother, Viola Nassif, whose sincere love and faith inspired me to be the person I am and the one I aim to become.

TABLE OF CONTENTS

LIST OF TABLES

LIST OF FIGURES

LIST OF ABBREVIATIONS

Abbreviations and Acronyms

ACS	American Chemical Society
ASTM	American Society of Testing Materials
CD	Compact Disk
CSD	Crystal Size Distribution
CST	Crystalline Silicotitanate
DAQ	Data Acquisition
DF	Decontamination Factor
DOE	Department Of Energy
ECN	Engineering Change Notice
ESP	Environmental Simulation Program
GTRI	Georgia Tech Research Institute
HLLW	High Level Liquid Waste
HLW	High Level Waste
LAW	Low Activity Waste
LLLW	Low Level Liquid Waste
MSE	Mixed Solvent Electrolyte
MW	Molecular Weight
NNPP	Naval Nuclear Propulsion Program
OD	Outside Diameter
PLM	Polarized Light Microscopy
PTFE	Poly Tetrafluoroethylene
QA	Quality Assurance
SOW	Statement Of Work
SST	Single-Shell Tank
TPB	Tetraphenylborate
WTP	Waste Treatment and Immobilization Plant
XRD	X Ray Diffraction

Units

ft	foot
g	gram
°C	degrees centrigrade
wt%	weight percent
mol	mole
M	molar
L	Liter
mL	milliliter
ppm	parts per million
Ci	curies
mm	millimeter
mA	milliampere
Ω	ohms
pH	potential of Hydrogen – measure of acidity or alkalinity
in	inch
µm	micrometer
h	hour
min	minute

SUMMARY

The purpose of the work described in this thesis was to explore the use of fractional crystallization as a technology that can be used to separate medium-curie waste from the Hanford Site tank farms into a high-curie waste stream, which can be sent to a Waste Treatment and Immobilization Plant (WTP), and a low-curie waste stream, which can be sent to Bulk Vitrification.

The successful semi-batch crystallization of sodium salts from two single shell tank simulant solutions (SST Early Feed, SST Late Feed) demonstrated that the recovered crystalline product met the purity requirement for exclusion of cesium, sodium recovery in the crystalline product and the requirement on the sulfate-to-sodium molar ratio in the stream to be diverted to the WTP.

In this thesis, experimental apparatus, procedures and results are given on scaled-down experiments of SST Early Feed for hot-cell adaptation along with operating parameters and crystallization mechanism studies on early feed multi-solute crystallization. Moreover, guidance is given regarding future steps towards adapting the technology to multi-salt crystallization kinetic parameter estimates and modeling.

KEY WORDS

Crystallization, Evaporative Fractional Crystallization, Nuclear Waste Pretreatment, Cesium Removal, Hanford, SST Early and Late feed, Multi-solute, Multi-salts, Simulant Testing.

CHAPTER 1: INTRODUCTION

1.1 OBJECTIVES

The following study assesses the objectives fixed by the Pretreatment Testing and Demonstration Program. The overall objective of the Program is to demonstrate that fractional crystallization is an effective way to condition feed streams for the CH2M HILL Low Activity Waste (LAW) supplemental treatment system. The program is divided into two phases, Phase I and Phase II, which essentially differ only in the nature of the feed material. Phase I uses a non-radioactive simulant for the solutions being treated, while Phase II includes the use of mainly actual tank waste samples for testing in a radioactive hot cell.

Minimum separation goals were provided (in order of priority) in the Statement of Work for ^{137}Cs activity (<0.05 Ci/L or 2.89E-03 g/L in a 5 molar (M) sodium solution, based on 20% ^{137}Cs to total cesium) in the recovered stream going to the pretreatment facility, sodium removal (50%), and sulfate-to-sodium M ratio (<0.01) in the stream going to the Waste Treatment and Immobilization Plant. The preliminary thermodynamic models applied by COGEMA, Inc. for each of the simulant feeds indicated that these goals can theoretically be met by fractional crystallization. The models further indicated that it was possible to approach the desired removal levels (<0.0012 Ci/L or 6.93E-05 g/L, 90%, and ≤ 0.0022, respectively). These are to be achieved by crystallization of sodium salts, especially those containing nitrate, carbonate and sulfate ions, while leaving the highly soluble cesium in solution.

1.2 FRACTIONAL CRYSTALLIZATION

When a solution has a single species that can be crystallized by cooling, evaporation, addition of a non-solvent or some other means of concentrating the solution, such an operation may be thought of as simple crystallization. However, when a solution contains multiple solutes, solutes may be expected to come out of solution (crystallize) when each has reached its solubility limit. For example, suppose a solution contains three solutes (A, B, and C) that all saturate the solution as solvent is evaporated from a solution, and the solution also contains additional solutes whose concentrations increase as evaporation occurs, but do not reach saturation. Figure 1 illustrates the hypothetical distribution of products if the solution is progressively saturated with A, then B, and finally C in the course of evaporating solvent from the solution. The unique behavior of each solute is readily apparent: similar to the behavior of burkeite, the stoichiometry of A limits its production after one of its constituents is depleted. The mass of crystalline B accumulates rapidly immediately after it saturates the solution, but its production decreases slowly thereafter. The mass of crystalline C builds slowly after saturation and then rapidly as the end of the operation is approached. Clearly, the point at which the slurry is sent to a solid-liquid separator will influence the composition of the final product and, concomitantly, the characteristics of the separation.

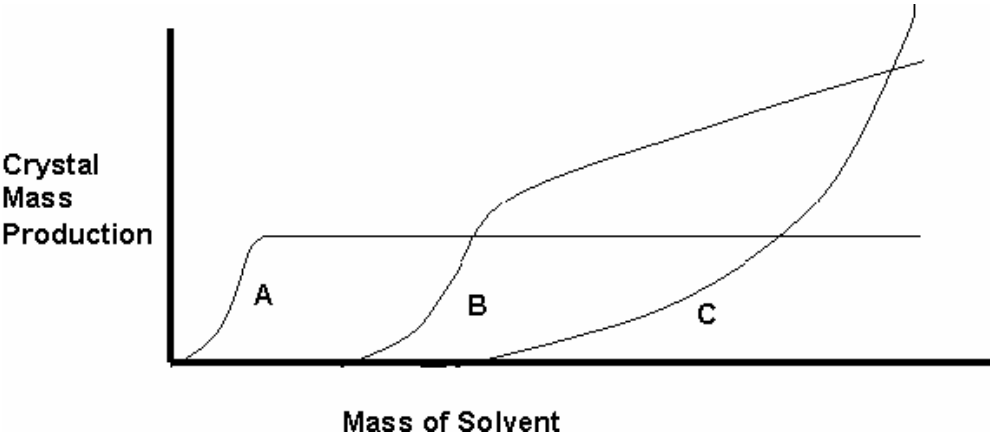

Figure 1. Hypothetical Product distribution from Fractional Crystallization: Solution Becomes Saturated with Solutes at Different Times in the Evaporation.

Now consider a different situation, one in which the solutes achieve saturation at roughly the same time in process. Assuming that all nucleate and grow as such conditions are achieved, the product generation is expected to look more like that in Figure 2. In this situation, separation of species from one another by simple fractional crystallization is not possible; instead, this instance of fractional crystallization only facilitates separation of a physical mixture of the crystalline solutes from the residual mother liquor.

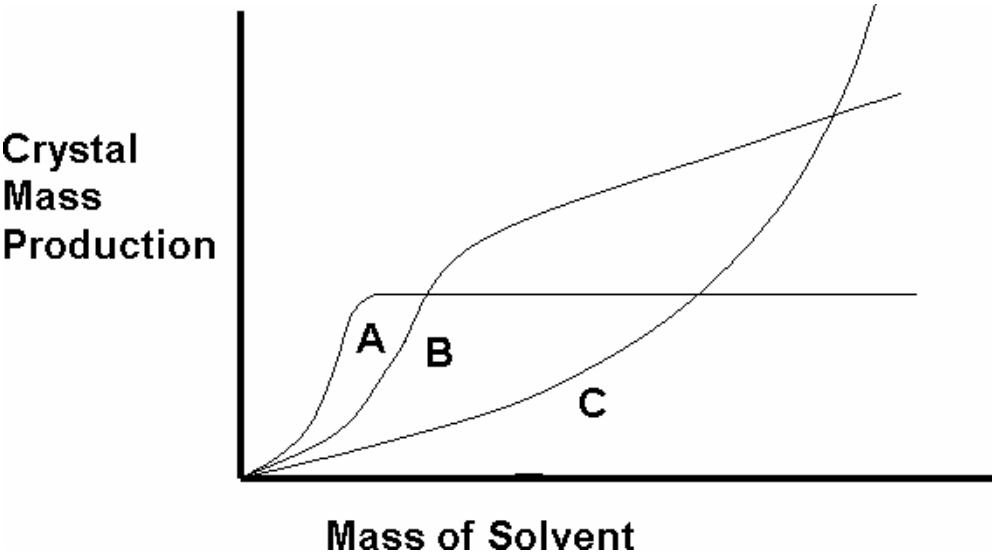

Figure 2. Hypothetical Product Distribution from Fractional Crystallization: Solution Becomes Saturated with Solutes at Roughly the Same Times in the Evaporation.

In the simulation files provided by CH2M HILL, the feed contained sodium carbonate, sodium sulfate, sodium nitrate, sodium hydroxide and aluminum hydroxide in proportions similar to Single-Shell Tank (SST) Early Feed Solution. The total solute concentration was adjusted so that the solution would reach saturation at 60°C after 200 grams (g) of water had been evaporated. Note that in Figure 3, burkeite saturates the solution after approximately 200 g of water have been evaporated. At that point in the process, the only solid that forms is burkeite and the mass of crystals of this species continues to grow, without other crystalline material being formed, until approximately 380 g of water have been evaporated. At that point, sodium nitrate begins to come out of solution and the mass of these crystals increases rapidly. At about the same time, sodium carbonate monohydrate saturates the solution and crystals of this species begin to form.

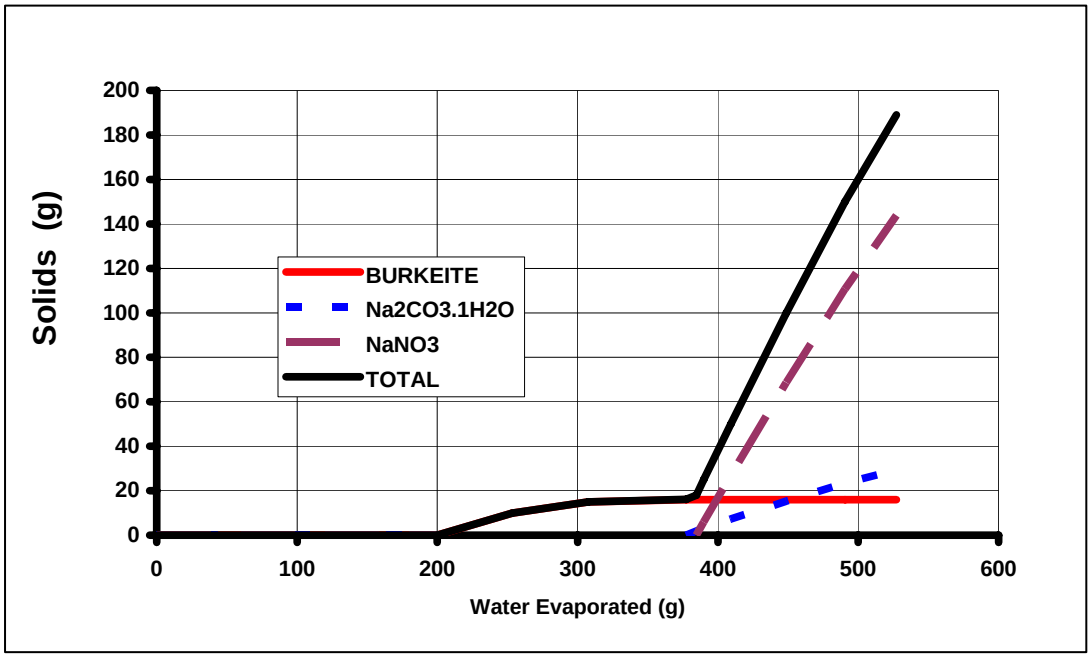

Figure 3. Mass of Crystals Produced in Simulated Evaporation of Solutions Containing Sodium Carbonate, Sodium Sulfate, and Sodium Nitrate at 60°C (LAB3.XLS).

The behavior described is expected to be characteristic of all three simulant solutions: SST Early Feed Solution FY05, SST Late Feed Solution, and SST Early Feed Solution FY06. Since the objective of the operation is to remove a significant fraction (more than 50%) of the sodium salts from the feed solution, irrespective of the counter ion, this behavior presents no apparent problem.

1.3 SEPARATION OF CRYSTALS FROM MOTHER LIQUOR

As described in the preceding section, the formation of crystals removes sodium salts and other species from solution. For this to be an effective separation process, the crystals must then be separated from the residual mother liquor by solid-liquid segregation. It is possible to do this by filtration, centrifugation, or other commonly used techniques. However, the nature of the crystals, in particular their morphology and size distribution, determine how easily they can be segregated from the mother liquor. In general, a narrow crystal size distribution leads to easier separation than one that is broad; bulky crystals as opposed to flakes or needles also mean an easier separation.

For single-solute simple crystallization, the size distribution is determined by the nucleation and growth kinetics of the crystalline species. In fractional crystallization of the type characterized by the behavior in Figure 3, the nucleation and growth kinetics of each species leads to a determination of the final crystal size distribution.

As will be described in later sections of this thesis, considerable effort went into developing a means to segregate the complex crystalline solids from the mother liquor on a laboratory scale. Similar effort led to the development of a means to wash the mother liquor from the interstices of filter cakes produced in the experimental program. A secondary part of this

work led to development of washing procedures that allowed sieve analyses to determine product crystal size distributions without significant distortion by crystal agglomeration.

1.4 CERTIFICATION RUNS AND CHEMICAL ANALYSIS

The culmination of studies leading to process protocols for each of the feed solutions (SST Early Feed and SST Late Feed) was performance of runs that were designed to test those protocols against the process specifications cited earlier. The masses of each stream have been determined carefully, and appropriate samples were sent to Galbraith Laboratories (Galbraith) or Georgia Tech Research Institute (GTRI) for analysis. These results, which were obtained using Quality Assurance (QA) certified techniques, form the basis of demonstrating the applicability of the fractional crystallization pretreatment technology.

1.5 COMPARING ANALYTICAL RESULTS TO PROCESS OBJECTIVES

As stated above, the objectives of the technology described in the present report involve the cesium content of the recovered crystals, the recovery of sodium in the solid product, and the separation of sulfate ions from the liquid destined for feed to the Waste Treatment and Immobilization Plant. Minimum and desired targets for these criteria are as follows:

- Obtain a crystalline product that upon dissolution in water to a 5 M sodium concentration has a Cs content low enough to produce a specific activity of less than 0.05 Ci/L, and preferably less than 0.0012 Ci/L.
- Recover at least 50% of the sodium from the feed solutions as crystalline product, and preferably at least 90%.
- Produce a filtrate that has a molar ratio of sulfate to sodium less than 0.01, and preferably less than 0.0022.

The analytical results obtained from Galbraith and GTRI provide compositions of samples in wt % for major components and parts per million (ppm), which is mass of a species per million mass units of the sample. There are at least two ways to use such information to compare the outcome of a fractional crystallization run with Objective 1.

One method uses the compositions of the streams and estimates of the fraction of the total cesium in the streams of interest that is present as ^{137}Cs. To illustrate the methodology, assume that a sample of the final product crystals has been analyzed and found to contain 25 wt% sodium (Na) and 0.2 ppm cesium (Cs). The basis of calculation for determining if the product meets Objective 1 is to estimate the activity of a solution of this material containing 5 mole Na/L. As specified in the SOW, it may be assumed that there is 1 g ^{137}Cs/5 g Cs in typical streams at Hanford. It may also be assumed that the activity of ^{137}Cs is 86.58 Ci per g of ^{137}Cs. This means, then, that the specific activity associated with the product is

$$5\frac{\text{mol Na}}{\text{L}}\times\frac{23\text{ g Na}}{\text{mol Na}}\times\frac{100\text{ g}}{25\text{ g Na}}\times\frac{0.2\text{ g Cs}}{1{,}000{,}000\text{ g}}\times\frac{86.58\text{ Ci}}{\text{g }^{137}\text{Cs}}\times\frac{1\text{ g }^{137}\text{Cs}}{5\text{ g Cs}}=0.0016\frac{\text{Ci}}{\text{L}} \quad \text{(E-1)}$$

This value can be compared to the criterion in Objective 1.

A second method for estimating the approach to Objective 1 is in terms of a decontamination factor (DF), defined as the activity of ^{137}Cs in real waste or the total cesium concentration in a simulant feed at 5 M sodium concentration divided by the corresponding activity or concentration in the salt recovered from the fractional crystallization process, also at a 5 M sodium concentration. The decontamination factors corresponding to Objective 1 are as given in Table 1.

Table 1. Required Decontamination Factors to Meet Objective on ^{137}Cs Activity.

Feed Solution to Fractional Crystallization	^{137}Cs activity (Ci/L)		Decontamination Factor (*DF*)	
	Minimum	Desired	Minimum	Desired
SST Early Feed	0.05	0.0012	1.15	48
SST Late Feed	0.05	0.0012	—[1]	14

The decontamination factors can be estimated from the following relationship:

$$DF = \frac{\left[\text{activity of } ^{137}\text{Cs (at 5 M Na)}\right]_{\text{feed}}}{\left[\text{activity of } ^{137}\text{Cs (at 5 M Na)}\right]_{\text{waste}}} = \frac{\left[\dfrac{\text{ppm Cs}}{\text{wt \% Na}}\right]_{\text{feed}}}{\left[\dfrac{\text{ppm Cs}}{\text{wt \% Na}}\right]_{\text{waste}}} \tag{E-2}$$

where the compositions in the term on the farthest right are given by the analyses of crystals produced in the operation. For example, suppose the feed to a process contains 10 wt% sodium and 0.20 ppm Cs, and crystals produced contain 28 wt% sodium and 0.04 ppm Cs. Such results correspond to a DF of 14, which has been calculated as follows:

$$DF = \frac{\left[\dfrac{0.20 \text{ ppm Cs}}{10 \text{ wt\% Na}}\right]_{\text{feed}}}{\left[\dfrac{0.04 \text{ ppm Cs}}{28 \text{ wt\% Na}}\right]_{\text{waste}}} = 14 \tag{E-3}$$

The objectives of the work presented in this thesis are hence to:

- prove the feasibility of using crystallization for the pretreatment of SST Early and Late Feed solutions. This would be assessed by performing two certification runs and attest that results meets the three requirements described in Section 1. This objective is associated with the establishment of procedures and apparatus to be used and potentially reproduced at Hanford site.

[1] Activity of feed is below minimum required; therefore minimum DF does not apply.

- improve the developed procedures and apparatus for the SST Early Feed simulated waste and prove their possible adaptation to hot-cell environment. This goal would be achieved by performing a certification run on a modified simulated waste composition noted FY06. Improvements are displayed in terms of improving experimental results and meeting required values by assessing procedures and equipment modifications.
- identify the solid phases present as the results of SST Early and Late Feed simulated wastes and the potential growth mechanism associated with their formations. This would be attested by PLM analysis of the solids and slurry streams produced by the preliminary and certification runs on SST solutions. This study would be accompanied by a first estimate of growth rate for the main crystalline species crystallized (i.e sodium nitrate, sodium carbonate monohydrate and burkeite).
- identify the effect of operating parameters variation on crystallization. This will be displayed by studying the effect of operating temperature, condensate-to-feed ratio value, evaporation profile and evaporation rate on SST Feed solutions.
- prepare future research and experiments on crystallization modeling. This is achieved by the last two objectives.

CHAPTER 2: APPARATUS AND PROCEDURES

The experimental apparatus and procedures used in performing the certification runs (the essential runs described in the Statement of Work) evolved as experience was gained in working with the different solutions comprising SST Early Feed and SST Late Feed. The evolution resulted from knowledge learned about feed-specific characteristics and interrelationships between solute crystallization and crystallizer configuration. The original system configuration is shown schematically in Figure 4. Although the same basic configuration was used in all runs, several modifications were made to address problems associated with accumulation of crystal encrustations on the walls and baffles of the crystallizer. The key modification was to add the capability of periodic addition of feed solution so that the active volume in the crystallizer was constant. Figure 5 is a photograph of the modified apparatus with a feed vessel positioned above the crystallizer. Note also that the reflux condenser has been removed from the system as it was considered unnecessary when the system was operated in the constant-volume mode.

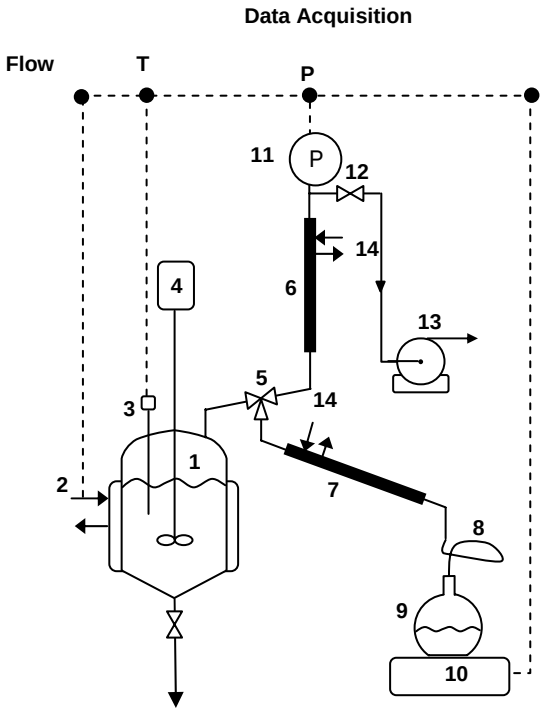

Figure 4. Schematic Flowsheet of System Used in All Crystallization Runs.

(1) Crystallizer, (2) Heating Fluid, (3) Thermocouple, (4) Motor to Drive Stirrer, (5) 3-Way Valve, , (6) Reflux condenser, (7) Product Condenser, (8) Flexible Tube Adapter, (9) Condensate Collection Flask, (10) Digital Balance, (11) Pressure Sensor, (12) On-Off Valve Plus Metering Valve, (13) Vacuum Pump, (14) Cooling Water.

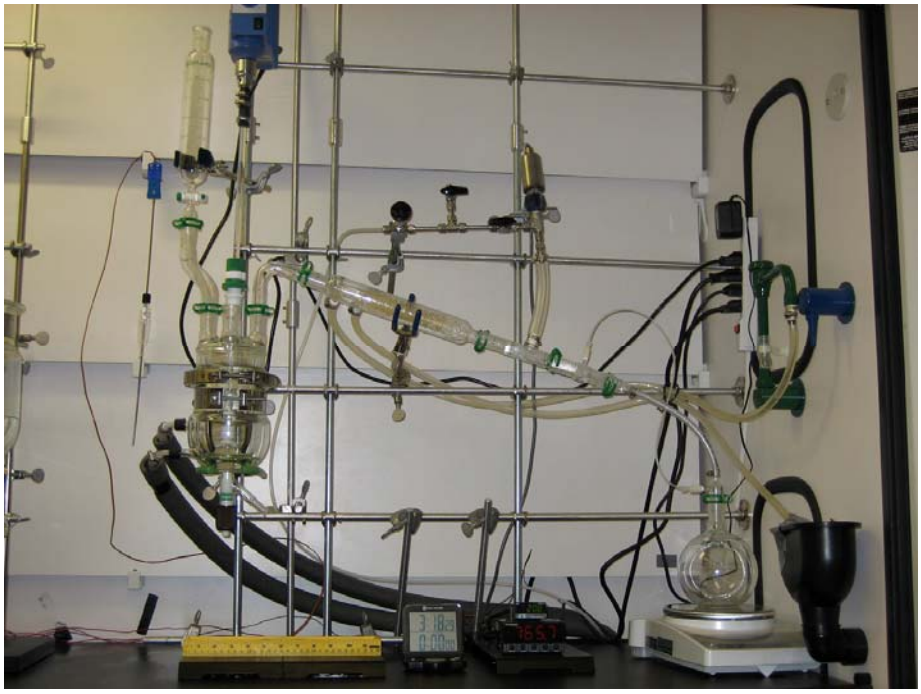

Figure 5. Evaporative Crystallization System with 300-mL Crystallizer Installed.

2.1 EQUIPMENT

The following items of equipment are described: crystallizers, filtration and crystal-washing apparatus, data-logging software and hardware, and analytical equipment (sieves and ro-tap, polarized light microscope, balances).

2.1.1 CRYSTALLIZERS

The vessels used as crystallizers were of 1-L, 600-mL, 300-mL and 100-mL nominal sizes, and the 1-L vessel is shown in Figure 6. The reason different sizes were used was to facilitate multiple-stage batch and semi-batch operations in which the volume of feed available for successive stages was reduced because of the vapor generated in preceding stages. For example, this would mean that if the batch feed was 1 L and 400 mL of condensate were generated in the first stage of operation, the available feed for the second stage would be approximately 600 mL, and so forth for subsequent stages.

The internals of the crystallizers included four equally spaced baffles that were contoured so that they rested on the curved portion of the vessel. The baffle cages for the three crystallizers are shown in Figure 7. They were manufactured in-house and designed so that they did not interfere with the impeller and accommodated other crystallizer internals. The four metal baffles fit snugly against the crystallizer wall.

Figure 6. 1-L Vessel Used as a Crystallizer

Figure 7. Baffles Used in the Three Crystallizers.

From Left to Right in Each Photograph: 1-L, 600-mL, and 300-mL Baffle Cages.

The heads for the crystallizers had four openings: one was used for the agitator, one for vapor withdrawal, one for insertion of a thermocouple, and one for addition of feed or seed crystals. The feed vessel shown sitting atop the crystallizer in Figure 5 was used to add feed solution during the course of a run. The vessel has a valve that allows regulation of the flow of

feed solution into a short length of glass tubing leaving the vessel. A length of tygon tubing is connected to the glass tubing, and the end of the tygon tubing is adjusted so that the feed falls onto the active surface near the agitator in the crystallizer; in other words, the apparatus is designed so that the feed can be rapidly and thoroughly distributed upon entering the crystallizer.

The temperature of the crystallizer contents was measured by the thermocouple and readings were recorded on a computer. Heat was added to the system by a heating fluid that was pumped through the jacket of the crystallizer. The rate of evaporation was manipulated by adjusting the temperature of the heating fluid.

As vapor was generated in the crystallizer, it passed into a heat exchanger where it was condensed. The heat exchanger had cooling water flowing through a jacket. The condensate flowed from the heat exchanger through a flexible tube to a collection vessel resting on a balance. The condensate collection receiver was equipped with a pressure equalization Teflon tube to prevent accumulation of the condensate on top of the receiver. Readings from the balance were transmitted to and stored on a computer. A vacuum pump reduced the pressure in the system to the desired value.

The agitators used in the crystallizers varied according to the size of the vessel. For the 1-L and 600-mL vessels, two impellers were used. They are shown in Figure 8. A third smaller impeller of the same type as that shown on the left of Figure 8 was used in the 300-mL and 100-mL vessel when crystallizations from SST solutions were performed. The mixing intensity was controlled by an adjustable speed motor connected by a rubber tube to the glass shaft turning the impellers. It was important to have good mixing to keep the crystals, especially the larger ones, from settling to the bottom of the vessel; on the other hand, excessive intensity splashed liquid

on the upper walls of the crystallizer, which contributed to scaling problems and subjected crystals in the system to possible attrition (breakage).

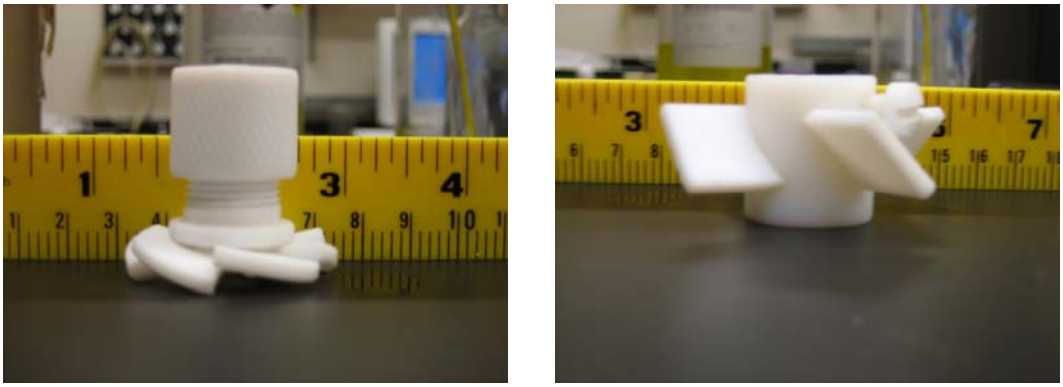

Figure 8. Impellers Used in the Stirred-Tank Crystallizers.

Both impellers were used in the 1-L and 600-mL crystallizers, with the one on the right positioned approximately a few mm from the surface of the slurry, while the one on the left was close to the bottom of the vessel. The impeller on the left was used alone in the 300-mL and 100-mL crystallizers.

2.1.2 FILTRATION AND CRYSTAL WASHING

Two types of devices were used to perform filtration and washing on the crystals recovered from the SST solutions crystallizations. The first apparatus used to filter crystals from the slurry and to wash mother liquor from the filter cake is shown in Figure 9. It was designed by the research team at Georgia Tech; the design criteria included (1) a slurry volume of 800 mL, (2) the dimensions of the crystallizer and medium-frit filter previously purchased, and (3) the manufacturing limitations of the provider (Chemglass). The final drawings of the apparatus were sent to Chemglass for a quote and design confirmation, and the details of the apparatus manufactured by Chemglass are provided in Appendix A.

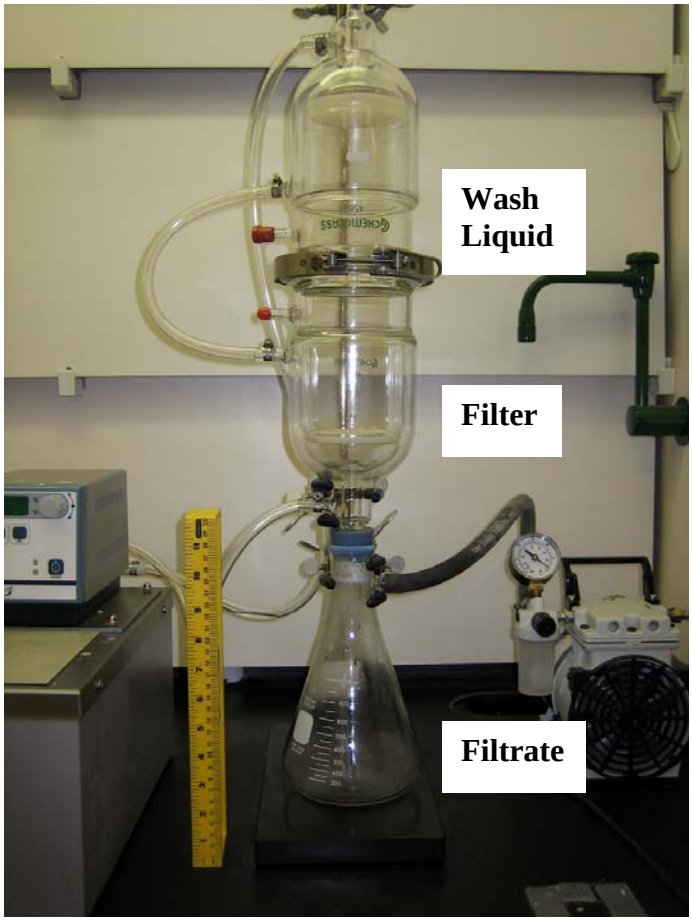

Figure 9. Apparatus Used for Filtration and Washing.

The filter has a glass frit onto which the process slurry was poured. It also could be possible to transfer the slurry directly from the crystallization vessel to the filter by drawing it through flexible tubing and into an opening just below the clamping ring. A vacuum was drawn on the filtrate receptacle, and the frit captured the crystals and separated them from the filtrate, which flowed through the frit and into the receptacle. At the conclusion of the filtration step, wash liquid (usually an aqueous solution saturated with the major solutes) was added to the upper vessel and then was drawn from the feed vessel through a perforated plate that dispersed

the liquid over the filter cake. The filter and wash-liquid receptacles were jacketed and a fluid at a temperature corresponding to that of the crystallizer flowed through the jacket. The objective was to maintain the temperature of the process slurry at a near-constant value. The vacuum pump in the picture pulled a vacuum in the filtrate receptacle.

This apparatus allowed filtration and washing to be performed under isothermal conditions since both top and bottom parts possessed a double jacket. It also provided good distribution of the washing liquid by forcing it to flow through a plate perforated with holes having a diameter of 1 mm. The distribution of the wash liquid provided superior washing efficiency. The system can be operated at atmospheric conditions or under vacuum.

The second apparatus used to perform the filtration and washing of the slurry corresponded to a regular double jacket medium frit filter, purchased from Chemglass. This device was used on the final experiments (from Run 38b to Run 51) due to its ease of implementation and operation under hot cell conditions. This very simple device had the advantages to allow performing filtration and washing under isothermal conditions and allow mixing of the filter cake during the two operations. The crystal washing was performed by pouring the wash solution onto the filter cake, mixing and pulling the vacuum through the medium frit filter. This method will be referred to the slurrying method in the following sections.

2.1.3 DATA LOGGING SOFTWARE AND HARDWARE

The data-acquisition system monitored temperature and pressure inside the crystallizer, along with the mass of condensate collected on the balance. Temperature was measured with a hastalloy thermocouple (T-type C-276 purchased from Chemglass) while pressure was monitored with an Omega transducer. These sensing devices were connected to meters for direct display of readings; analog temperature controller/display (CNi3253, Omega) and process meter

controller (DP25B-E, Omega) for pressure reading. These meters were connected to a data acquisition (DAQ) board (PMD-1208FS, Measurement Computing) for continuous recording of data. This board accepted voltage signals for data storage and connected to the computer through a USB port. The pressure transducer and temperature meter gave current outputs (4-20 mA), so 250 Ω resistors (249XBK-ND, Digi-Key) were used to convert the current signals to voltage signals compatible with the DAQ board. The digital balance used to measure the condensate mass (PB1502-S Mettler Toledo obtained from VWR) was connected to the computer through a RS-232 port. Due to the fact that multiple RS-232 ports were needed, a computer board was installed that provided four RS-232 connections (PCI-COM232/4-9, Measurement Computing). Readings from the DAQ board and the RS-232 ports were collected in a LabView program and the voltage signals from the DAQ board were calibrated to the corresponding temperature and pressure values. A simplified layout of the DAQ connections is shown in Figure 10.

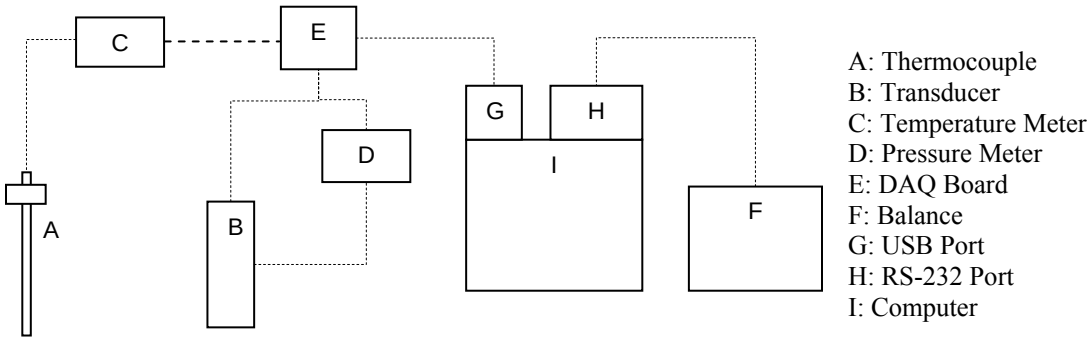

Figure 10. Data Acquisition System Setup.

2.1.4 ANALYTICAL EQUIPMENT

2.1.4.1 SIEVES AND ROTAP

Crystal size distribution (CSD) analysis was conducted by sieving on a Ro-Tap test sieve shaker (RX-29, serial 24210, Tyler) utilizing US standard sieve nests obtained from Dual

Manufacturing Co. The sieving apparatus is shown in Figure 11. The shaker features a combination circular motion along with a vertical vibration induced by an upper hammer tapping that allows good size segregation of crystals as they attempt to pass through the sieving apertures. The shaker can accommodate test sieves of 3-in., 6-in., or 8-in. diameter and can be adjusted to fit various numbers of sieves depending on their depth. In the present work, 3-in. diameter x 1-in. depth test sieves were used and the shaker was adjusted to accommodate a stack of 11 sieves, including the pan. Shaking time can be adjusted by turning a thumb screw until the desired value appears in a digital window. The shaker is placed on a stand inside a Ro-Tap sound enclosure cabinet to reduce the noise level.

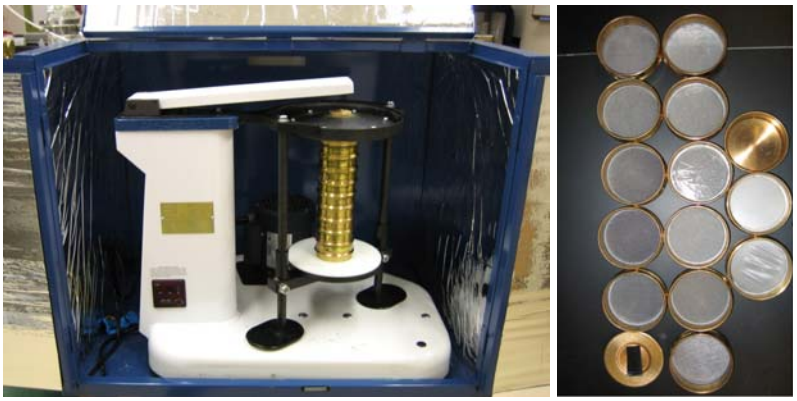

Figure 11. Ro-Tap Test Sieve Shaker Placed Inside a Sound Enclosure Cabinet (Left) and Test Sieving Nests Top View (Right).

The test sieves are US standard sieves with brass frames and stainless-steel mesh. Table 2 shows the sieves available for the current analyses; they ranged in nominal aperture from 10 to 1180 μm. They were selected so that the ratio of aperture sizes on consecutive sieves is almost $\sqrt{2}$. Sieve tests were typically performed using the 38 to 850 μm nests, unless the operation involved particularly large or small crystals. In these cases the 10-, 20-, or 1180-μm sieves were used to provide a more accurate distribution. The sieves can hold about 27 g of sample mass, but only 15 to 20 g were used.

Table 2. Sieves Used for CSD Analysis.

No.	ASTM Sieve No.	Nominal Sieve Opening (μm)
1	16	1180
2	20	850
3	30	600
4	40	425
5	50	300
6	70	212
7	100	150
8	140	106
9	200	75
10	270	53
11	400	38
12	635	20
13	850	10

All Sieves From Dual Manufacturing Co.

2.1.4.2 POLARIZED LIGHT MICROSCOPE (PLM)

PLM images were obtained on a Meiji Techno trinocular polarizing microscope (Model ML9300), which is illustrated in Figure 12. Images are either observed in the eyepiece and/or acquired on a computer. The source of light in the microscope is provided by a Koehler-type illuminator with intensity controlled by a knob (6). The substage polarizer (5) is fully rotatable, sending polarized light within angles between 0–360 degrees up to the specimen. When the polarizer is swung-out, the light is un-polarized. The analyzer (16) is a slide-in plate mounted in an in-tube slider positioned after the specimen which moves the analyzer in and out of the optical path. When the analyzer is "in" and the polarizer (5) is swung in and set at 0 degrees, the elements are crossed and the field of view is said to be extinguished. In this condition the field of view is dark, except for an optically active specimen in the field path, which rotates the polarization angle and becomes visible against the dark background.

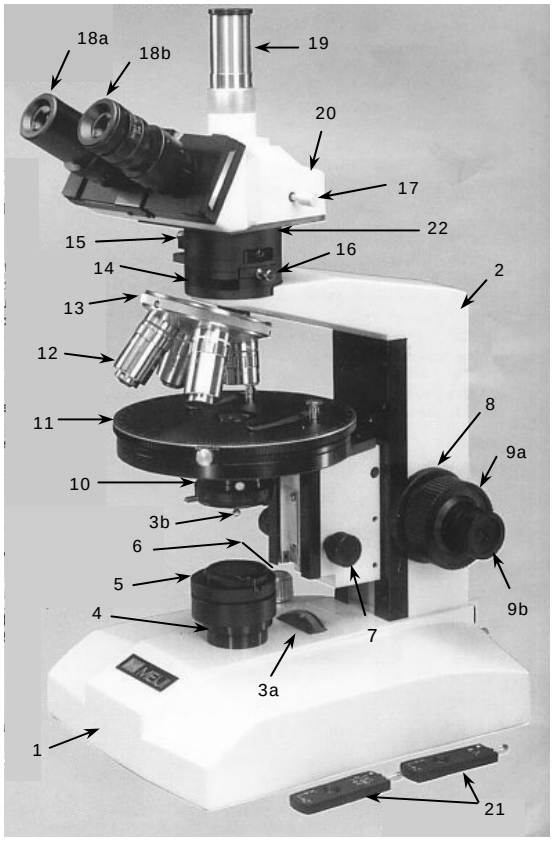

1 Microscope base
2 Microscope limb
3 Iris control (a) field (b) aperture
4 Koehler type illuminator
5 Polarizer, rotatable swing-out
6 Light intensity control knob
7 Substage focus control
8 Tension control knob
9 Focus (a) coarse (b) fine
10 Substage condenser (N.A. 1.25)
11 Rotating stage
12 Objective lenses (4, 10, 40, 60X)
13 Objective revolving nosepiece
14 Compensator slot
15 Bertrand lens aperture
16 Analyzer slider
17 Beam splitter lever
18 10X eyepiece (a) wide field (b) focusing cross-line
19 Photo tube
20 Rotatable 360°/60° inclination
21 Compensator plates (red and ¼ wave-length)
22 Switch-over beam splitter

Parts not shown in Figure
Camera attached to photo tube
Computer for image processing
Wrenches for objective centering

Figure 12. Polarized Light Microscope Used in this Project.

Other elements of the microscope serve to improve the image quality. The iris diaphragm (3) and the condenser (10), a lens between the illuminator and specimen, are used to control the angle of the illumination cone that passes through optical train and improve the contrast. The circular stage (11) rotates through a full 360 degrees, with angular measurement ability, to facilitate orientation studies in polarized light. The objectives (12) are mounted in a rotatable ball bearing nosepiece (13) allowing easy swing of the required objective in the optical path. Objectives with 4X, 10X, 40X and 60X magnifying powers were utilized in this study. A 100X

objective is also available but was not used. If the 100X objective is to be used, immersion oil must be applied to the specimen slide so when the objective is swung in, as the slide and the 100X objective are in good and bubble-free contact. The beam splitter (22) is used to switch the image between the binocular eyepiece (18) and the digital camera photo tube (19).

The focusing knob (9) allows course and fine adjustment of the distance between the specimen and objective for sharper images. The compensator (or retardation) plate (21) is a crystal that is selectively placed between the sample and analyzer to introduce a known optical path length difference to the re-combined light ray components and shift the colors of the generated images. The plates are sliding in a slot (14) cut in the tube just above the objective nosepiece (13). The microscope visual images can be observed through the eyepieces (18) or more conveniently snapped on a computer using a camera attached to the phototube (19). A photo camera (Sony DKC-5000, serial 10322) was used to generate digital images on a computer employing Image-Pro Plus (version 4.5.1.22, serial 41N40000-13717, Media Cybernetics Inc.) for image processing and manipulation.

A preparatory step to PLM operation is the preparation of good specimen slides with uncrowded fields (few crystals with empty spaces). Crystals are best viewed mounted in their mother liquor or in some solvent which will not dissolve the crystals, e.g., paraffin oil. Mounting them in air causes a large change in refractive index at the air-crystal interface and reduces the image resolution. Samples from crystallization experiments are normally taken from the slurry (or flash) solution at the end of the run using a plastic pipette. A small drop of the slurry is placed at the center of a 3”×1” plain slide (Part 2947, Corning) and preheated to the slurry temperature (40-60ºC). Then the drop is covered with a 22 mm circular glass cover (Part 12-546-1, Fisher Scientific) to spread the sample drop over the cover area. To test dry crystals, a

small drop of paraffin oil (HR3-411, Hampton Research) is placed on the slide and a small number of the dry crystals are spread over the oil before they are covered with the circular glass. The circular cover should rest evenly on the slide without any air spaces or crystal stacking. Such flaws can be fixed by gentle tapping on the cover with a spatula or by mild movement of the glasses.

The microscope may require some initial adjustments before its use; the major ones are illumination setup and objective centering. They would lead to good focusing, overlapping, and centering of the specimen image in the field of view, either in the eyepiece or computer preview screen. Illumination setup normally should be performed on each objective upon the use of microscope. A detailed procedure for optical setup and illumination adjustment is provided in Appendix B. Objective centering is required less frequently if the microscope is properly treated. However, it should be tested from time to time to ensure good centering of the image. Centering can be simply tested by observing a crystal sample in the eyepiece with cross-line (18b). If the focused image of the crystal strays from the center of the cross-line upon stage (11) rotation, then the objective is slightly off the optical axis. The objective (12) can be centered using two hexagon keys supplied with the microscope accessories according to the procedure summarized in Appendix B. The centering test must be performed for all the objectives attached to the nosepiece (13).

It should be noted that initial adjustments of the microscope while observing the crystal specimen through the binocular eyepiece (18) will also adjust the image in the computer display if the digital camera is well aligned with the optical path. The computer display is more convenient although the field of view is somewhat more limited than the binocular eyepiece especially at high magnifications. Size scales can be added to the recorded images for crystal size

analysis. However, this requires a size calibration for each magnification objective using a 2.5 mm stage micrometer slide graduated with precise grids of 25, 100, 500, and 1000 μm. This can be done by snapping an image of the scaled grids of the micrometer slide with each objective and use a grid of known length in the image to calibrate the length estimated by the Image-Pro Plus software. Details of the calibration procedure are provided in Appendix B.

For PLM characterization of the crystallization runs, a sample is taken from the slurry solution and mounted on a preheated slide as described before. The slide is preheated to the temperature of slurry to minimize formation of additional crystals on the slide by cooling; therefore, the slides should be tested immediately after preparation.

To characterize:

- Turn on the illuminator and pass some light by switching the intensity control knob (6);
- Turn on the digital camera button and start the Image-Plus Pro imaging software menu on the computer desktop;
- From the main menu select the Video/Digital icon on the tool bar or from *Acquire* → *Video/Digital* commands to activate the Preview Page for video capturing and image setup.;
- Start the live preview by pressing "Start Preview." The preview will look white if the analyzer (16) is out. Make sure the substage polarizer (5) is swung in and set at 0 degrees then slide the analyzer plate (16) in. The live preview gets black because the polarizer and analyzer are crossed which prevents any light from passing through;

- Place the crystal slide on the rotatable stage (11) with the sample centered in the field of light and rotate the smallest objective, 4X, into position for focus. Crystal bodies should appear on the live preview;
- Modify the light intensity using the control knob (6) then focus down on the crystal slides with coarse and fine focus (9) until details can be seen. Most of the crystals in this study had a grey color with poor contrast so the red compensator (21) was used most of the time. The compensator turns the background into pink and improves the crystal coloring;
- Scan the whole crystal slide and study various crystals available in the sample. Crystal types can be identified from the shape and color of the crystals. Also rotate the stage about the axis of crystals and observe the change in colors and the extinction positions. These observations can be used to distinguish crystals which have similar shapes, e.g., sodium nitrate vs. sodium nitrite, sodium oxalate vs. sodium phosphate, etc.;
- Switch to higher power objectives by revolving the nosepiece (11) to enlarge crystal view and get more details. Switching between objectives requires re-adjustment of the lighting intensity and focusing;
- Desired PLM images can be recorded by pressing "Snap" from the Preview Page window. The recorded image will appear separately behind the live preview screen; and,
- Add a scale to the recorded image by pressing the Spatial Calibration icon (the vernier icon on the top right) on the tool bar or by selecting *Measure* → *Calibration* → *Spatial* sequence from the command Menu. A new small

calibration window will open. From that window select the objective power from the drop menu list (4X, 10X, 40X, or 60X) then press "Mark" to write the desired scale, e.g. 100μ for the 10X images. The scale bar will appear on the image. Move it to the desired location on the image then right click to fix it there. The image is finally renamed and saved in the desired location. These steps are repeated for every recorded image from the slide.

Crystal identification is carried out by comparing the crystal images obtained from our crystallization runs with typical PLM image of crystals found in Hanford waste tanks. The typical images were provided on a CD (Herting et al., 2002).

2.1.4.3 BALANCES

Three different digital balances were used. Condensate mass was determined on a Mettler Toledo digital balance (PB1502-S, obtained from VWR) attached through DAQ board to a computer for continuous recording of the mass. Another Mettler Toledo digital balance (PG2002-S) was utilized for assorted measurements of beakers, chemicals, sieves, and experimental accessories. When extremely small masses were involved, a sensitive balance (Ohaus Analytical Plus, AP2500, serial M99315) was used; e.g., this balance was used for weighing small quantities of cesium nitrate in the preparation of simulant solutions.

2.1.5 CHEMICALS

Chemicals used in this project were sodium hydroxide pellets (NaOH, ACS grade), potassium nitrate (KNO_3, ACS grade), sodium nitrate ground ($NaNO_3$, ACS grade), sodium sulfate anhydrous (Na_2SO_4, ACS grade), sodium chloride (NaCl, ACS grade), sodium carbonate anhydrous (Na_2CO_3, ACS grade), sodium oxalate ($Na_2C_2O_4$, ACS grade), and sodium

dichromate dihydrate ($Na_2Cr_2O_7 \cdot 2H_2O$, ACS grade) all from EMD Chemicals Inc., and sodium aluminate anhydrous ($NaAlO_2$, technical grade), sodium nitrite ($NaNO_2$, 97 + % ACS reagent), sodium phosphate dodecahydrate ($Na_3PO_4 \cdot 12H_2O$, 98 + % ACS reagent), sodium fluoride (NaF, 99 + % ACS reagent), sodium acetate trihydrate ($NaC_2H_3O_2 \cdot 3H_2O$, ACS reagent) and cesium nitrate ($CsNO_3$, 99.99%) from Sigma-Aldrich. A polydimethylsiloxane heating fluid for the heater/circulator (Dow Corning 200, 5) was purchased from Ashland, Georgia.

2.2 CRYSTALLIZATION EXPERIMENTAL PROCEDURES

2.2.1 GENERAL OPERATIONS

There were two types of crystallization runs performed in the study: batch and semi-batch. Most of the early runs in Phase I were batch and, thus, involved adding a feed charge to the crystallizer prior to the start of the run and removal of product slurry after the requisite amount of vapor had been generated. Variables in such runs include the rate at which vapor is generated, operating temperature (pressure), and whether or not seed crystals are added.

Prior to the start of either a batch or a semi-batch run, water was boiled in the crystallizer to saturate dead spaces in the system with water. A known mass of deionized water was charged to the crystallizer and boiled for at least 20 minutes. This procedure saturated dead spaces in the glassware with around 15 g of water (determined from a mass balance around the system). A batch or semi-batch crystallization could then be done with the apparatus, and closure of mass balances around the system was enhanced.

Several difficulties were encountered with batch operation that led to use of the alternative semi-batch procedure for the certification runs. The primary and overriding difficulty was the quantity of vapor that must be produced to obtain the desired yield of solute. This led to production of a slurry of much reduced volume in a crystallizer of fixed dimensions. For

example, the agitator in the largest crystallizer was designed to provide good mixing when the active volume was around 1000 mL; after nearly 60% of the charge had been vaporized, the remaining fraction may very well fall at or below the impeller used to mix the slurry. In either case, the contents of the crystallizer were poorly mixed. Furthermore, as the level in the crystallizer fell, the exposed, wet walls of the crystallizer had a tendency for scale to form on them. This resulted in what was called accumulation in the system. An additional problem with using pure batch operation was that the amount of material recovered from the first stage of a two-stage process was too small to provide good operation in the second stage.

In the semi-batch procedure, an initial charge of the feed material was added to the crystallizer, and the conditions throughout the system were brought to their desired state: the pressure in the system was set, flow of cooling water through the jacket of the condenser started, mixing in the crystallizer begun, and all monitoring instrumentation started. At this point the flow of the heating fluid was started, and the temperature of the material in the crystallizer began to rise to a value that corresponded to the system pressure. When vapor began to form and produce condensate that entered the receptacle on the balance, the temperature of the heating fluid was adjusted to set the rate at which vapor was generated.

As vapor was generated, the feed solution was added manually from the vessel atop the crystallizer so as to maintain the level in crystallizer. This was done carefully so that the vacuum in the system was not broken. Vapor generation continued until crystals were observed in the crystallizer. At this point the evaporation was stopped and additional feed, which was unsaturated, was added to dissolve all of the crystals in the system. From this point on, the rate of evaporation was much slower than had been the case in the earlier phases of the run. Figure 15 shows data from an early run in which this procedure was developed.

The approach was chosen so as to minimize run time by rapidly evaporating water while the solution was undersaturated, but then to eliminate all crystals that had been formed under such conditions; this was followed by slowly evaporating solvent to minimize nucleation in relationship to crystal growth.

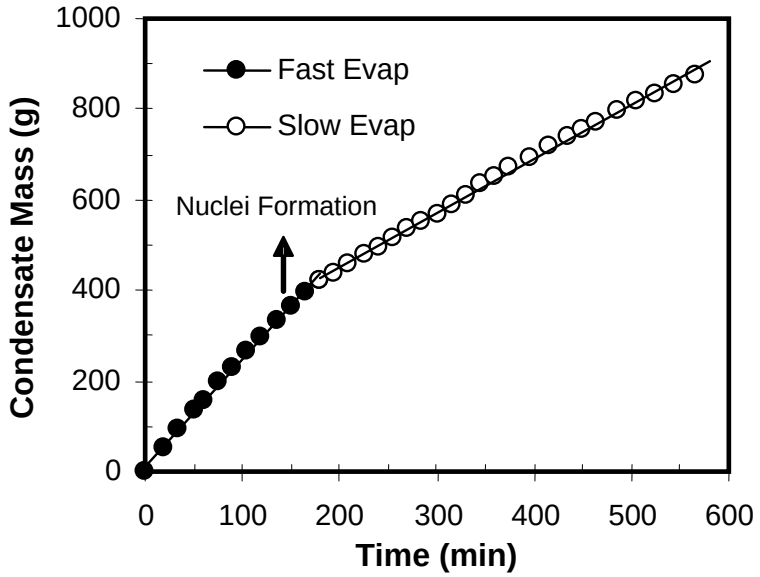

Figure 13. Plot of Mass of Condensate Generated from an Early Semi-Batch Run in Which Rapid Evaporation to Saturation Was Followed by Dissolution of Crystals and Subsequent Slow Evolution of Vapor.

The vacuum in the system had to be adjusted during a run to control the temperature of slurry in the crystallizer. This was necessary because there was an increase in the concentrations of non-crystallizing species as solvent was evaporated. The concomitant decrease in vapor pressure required an increase in temperature or decrease in pressure to continue evaporation. The regulating valve on the vacuum pump was closed slightly to increase the vacuum drawn in the equipment. Unfortunately, this tended to increase violent boiling of the solution in the vessel,

which often led to splashing of the slurry on the upper walls of the crystallizer. Gradual closing of the valve somewhat mitigated this problem.

When the desired amount of condensate had been collected (as determined by a condensate-to-feed ratio set by a corresponding simulation), the monitoring Labview software was stopped and the final slurry was collected for subsequent treatment and characterization.

2.2.2 WASHING AND FILTRATION

The slurry was drained from the bottom opening of the crystallizer into a beaker, which had been heated to the temperature of the slurry, and transferred to the jacketed filter. In order to maintain a constant temperature, heating fluid at the crystallization temperature was pumped through the jacketed portion of the apparatus. As the slurry was transferred to the filter, a vacuum pump pulled a vacuum in the filtration flask in which the filtrate was collected. During filtration, the top half of the apparatus was disconnected from the filter, leaving the funnel open to the air.

The rate of slurry addition to the filter depended on the difficulty of filtration; this is generally a function of the size of the crystals, as fine crystals, especially when part of a broad distribution, have a tendency to plug the filter and slow the rate of filtration. When extreme problems of this kind were encountered the difficulty was mitigated by using three jacketed filters mounted in parallel so as to process the slurry as rapidly as possible. It was important to keep access to the slurry during the filtration step in order to mix it with a Teflon spatula. Such mixing sped filtration by alleviating filter plugging.

After the filtration step, the filtration flask was changed, the mass of unwashed solids determined, and the wet crystals returned to the filter. The top half of the apparatus was placed in

position and sealed. At this time the upper valve was put in the closed position and the washing solution loaded into the funnel. The vacuum pump was turned on to decrease the pressure inside the vessel and then the upper valve was opened to distribute the solution through the perforated plate.

2.2.3 ACCUMULATION REMOVAL

Accumulation of crystalline material on the walls of the crystallizer above the baffle cage was considered another major product from a run. Although attempts were made to minimize the amount of this material, it was almost always found after a run had been completed. Of course, it had to be collected at the end of a run and its mass determined for closure of mass balances.

In order to collect the accumulation, the condenser and agitator (with its motor) were removed from the apparatus and the vessel lid was removed. The solids that remained on the walls and baffles were collected carefully using a spatula; they were then weighed and stored in a sealed bottle for further analysis. Solids that could not be recovered contributed to non-closure of mass balances.

2.2.4 PREPARATION OF WASH SOLUTIONS

All stages of the certification runs included a washing step that used an aqueous solution of sodium nitrate and sodium carbonate. Sodium hydroxide was also included in the wash solution so that alkaline conditions were maintained. In all cases, the wash solution was prepared in a beaker of known mass and the salts were added in measured quantities. Water was added slowly to the salt mixture and the beaker was placed on a hot plate stirrer, which turned a magnetic stir bar that had been placed in the beaker, and the solution was brought to the desired

temperature. Once the solution reached the appropriate temperature, additional water was added until all crystals had dissolved. Before using the wash solution, the full beaker was weighed to determine the amount of water added to the solution.

2.2.5 STAGE TWO PREPARATION

In a two-stage crystallization run, the filtrate from the first stage was the feed to Stage 2. A known amount of water was added to the filtrate to dissolve any crystals that had formed as the filtrate cooled. This also was necessary to preserve the integrity of samples of the filtrate; i.e., without dilution, the filtrate quickly became a two-phase mixture that would have been difficult to analyze. In any case, the diluted filtrate was used as feed for the second stage, and the ratio of pure filtrate to dilution water was used in mass balance calculations. All other procedures for operating the second stage were identical to those followed for the first stage.

2.2.6 MASS BALANCE AND LOSS ESTIMATE

Continual improvement in procedures led to mass balance closures to within 3% for each stage of the certification runs. The tare weights of all beakers and flasks were determined before use and after they were filled with the designated process stream (slurry, accumulation, etc.). The beakers were also weighed after they have been emptied to determine the amount of residual mass remaining in the beaker. Other possible losses of mass came from (1) the crystallization vessel, (2) the filtration apparatus, and (3) the washing apparatus. In order to account for accumulations in each apparatus, they were each washed with a known amount of water, and the collected water was weighed to determine the amount that remained in the apparatus. In order to account for wash water that remained on the inner wall of the vessel or filters, a dry laboratory

paper of measured mass was used to collect this water. To close the mass balance further, all the accessories (Teflon and metal spatulas) used during the experiments were washed with a known amount of water. The addition of a trap before the vacuum pump reduced water loss through the pump during a run and collected water could be included in the overall mass balance.

The overall mass balance data are presented in tables similar to that shown in Table 3. These tables give the mass and species composition of each element and provide data in three columns: (1) *Input*, corresponding to the feed and wash solution, (2) *Output*, including the condensate water ("cond"), the washed solids (final crystals obtained after the washing step), the filtrate (liquid obtained at the end of the filtration step), the spent wash (liquid obtained at the end of the washing step) and the accumulation (solids remaining on the wall of the crystallizer at the end of the evaporation), and (3) *Loss,* which corresponds to the difference between the total input mass and the total output mass. Percentage loss is given as two values in the bottom two rows. The first corresponds to the overall closure percentage when no observable mass losses are accounted for. The second is the closure value deduced after all known losses are accounted for (following the procedures explained above). The mass balance data are also represented by a flow diagram summarizing the mass and flow patterns of all streams in addition to various processes and stages used in the experiment. Figure 16 gives an example of such a flow diagram.

Table 3. Example of a Mass Balance Table (SST Early Feed Run Prior to Certification Run).

	Input (g)		Output (g)					Loss (g)
Species	**Feed**	**Wash**	**Cond**	**Washed Solids**	**Filtrate**	**Spent Wash**	**Accum. Solids**	
	6479.97							
H_2O		330.58	4482.99					
Na_2CO_3		56.36						
$NaNO_3$		233.2						
Solution				469.25	1205.2	639.91	4.16	
Total	6479.97	620.14	4482.99	469.25	1205.2	639.91	4.16	298.6
Combined	7100.11		6801.51					298.6
						Loss (%)		4.21%
						Corrected loss (%)		3.5 %

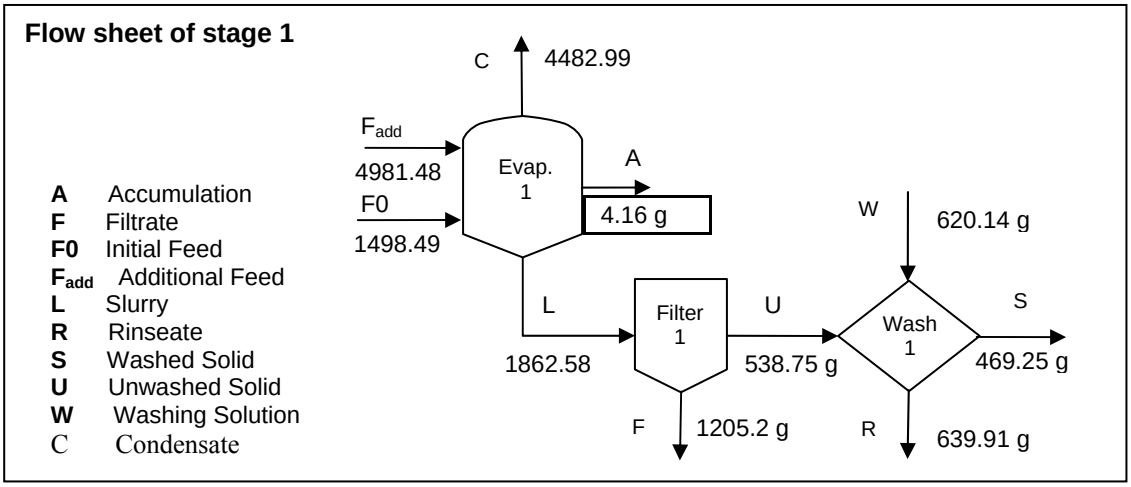

Amounts shown in grams.

Figure 14. Example of Flow Diagram.

2.2.7 CHEMICAL ANALYSIS

Chemical analysis was required in order to perform species mass balances and determine whether or not specifications given in the SOW had been met. For each stage in the certification runs the following samples were taken: feed solution, filtrate, spent wash, unwashed crystals, accumulation, and final crystals. These samples can be seen graphically in a two-stage schematic shown below in Figure 15. In order to ensure homogeneity in the samples and eliminate sampling uncertainties with two-phase mixtures, dilution water was added to the spent wash, filtrate, unwashed crystals, and accumulation. The amount of water added to each pure sample was recorded so mass balance calculations could be performed accurately. The only samples sent for analysis in solid form were the final crystals obtained from the Runs 26 and 27.

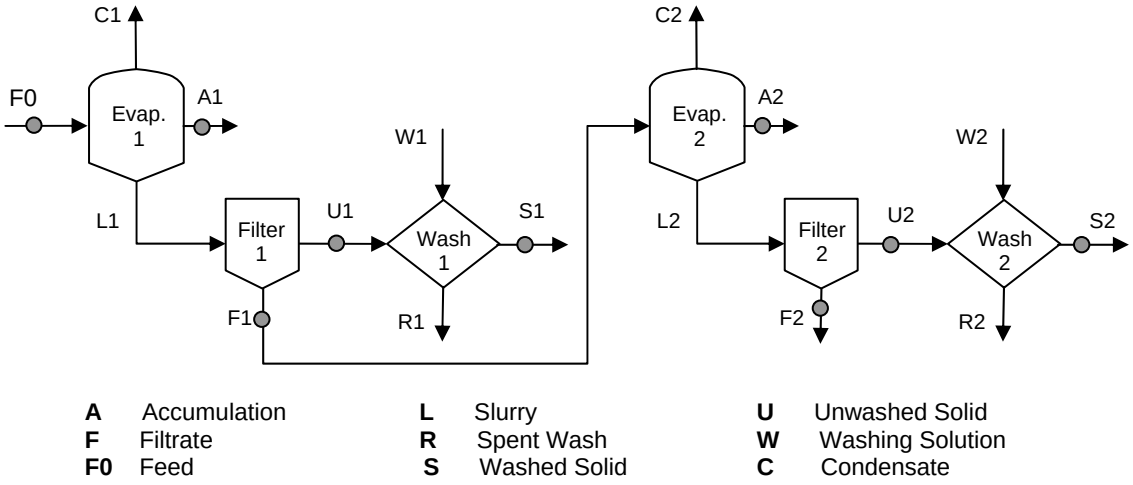

(Sample points marked with gray circles. The DST run also includes carbonation steps which are not shown here.)

Figure 15. Schematic of the Two-Stage Certification Runs.

2.2.8 SIEVING PROCEDURE

Crystal agglomeration was the major problem affecting CSD analyses throughout the test runs. Microscopic observation of samples taken directly from the crystallizer proved that agglomeration plaguing CSD analysis was not a result of events within the crystallizer, but rather an artifact associated with filtration and drying of product crystals. It was caused by residual traces of mother liquor on crystal surfaces after filtration and/or washing that led to crystallization of solute from the mother liquor as the solvent was evaporated; as this material crystallized it bound adjacent crystals into agglomerates. To reduce this phenomenon, two extra steps were introduced to the procedures followed prior to sieving. First, the final washed crystals were flushed with a hydrophilic solvent (acetone) to wash any residual mother liquor from the crystals and reduce the extent of agglomeration. Then after drying, the crystals were subjected to a manual, gentle separation process to disrupt any remaining agglomerates. The overall sieving procedure summarized below was applied to all certification runs.

All of the product crystals that had been washed with saturated solution were placed in the washing/filtration apparatus and washed with an approximately equivalent mass of acetone. The acetone was introduced from the top part of the washing apparatus and was evenly distributed over the crystal sample upon being drawn into the filtering flask. The crystals were then collected, spread wide on a pan and left overnight to allow evaporation of residual solvent.

Washing with acetone did not totally eliminate agglomeration, but significantly reduced it; some crystal agglomerates still appeared in the dried crystals. These agglomerates would contribute significantly to the sieve fraction larger than 500 μm and negligibly to the fraction less than 200 μm. It was found that these agglomerates could be disrupted with gentle manipulation using a spatula. Microscopic observation confirmed that such manipulation did not break the

constituent crystals, but it did improve the true representation of single crystals that is required for representative CSD data.

The selection of sieve sizes to use in an analysis depended on the size of crystals generated in a run. Guidance was obtained from the simulation files (e.g., sodium nitrate is often over 100 μm while burkeite is about 20 μm) and from visual observations of crystals grown during the experiment. All sieve analyses were performed with the 38 to 850 μm test sieves. If fine crystals (< 38 μm) were significant in the crystal sample (by having large mass collected in the bottom pan), they were further separated by using 10- and 20-μm sieves in place of the two largest aperture sieves.

Each sieve analysis was performed with 10 sieves in a nest, in addition to the bottom pan and the cover. The sieves were rinsed with hot water and dried in an oven prior to use. The empty weight of individual sieves was recorded and they were stacked in a nest, from top to bottom in order of decreasing openings. A 15 to 20 g sample of the crystals to be analyzed was then added to the top-most sieve and covered. The sieve stack was assembled and loaded in the Ro-Tap. The timer was adjusted to 30 min and the machine was started.

When the operation was completed, the stack was removed and each sieve was weighed; the tare weights of the sieves were subtracted from the final weights to determine the mass of crystals recovered on each sieve. By definition, the crystals collected in each nest ranged in size from the aperture of the sieve opening to that of the sieve above the one being analyzed; for example, crystals collected in the 38-μm sieve were between 38 and 53 μm (the upper nest according to Table 2) in size. These data were then used to evaluate the crystal size distribution, which could be expressed as histograms, density functions, or cumulative distributions. Samples were collected from several of the sieves and held in vials for further analysis by polarized light

microscopy. Such analyses facilitated determination of the crystal composition in each size range and detection of crystal breakage or agglomeration. A simplified sieve test procedure is present in appendix C.

2.2.9 KINETIC PARAMETER ESTIMATE PROCEDURE

In order to estimate crystallization parameters such as growth rates, the largest crystal sizes were identified for each of the main crystalline species (sodium nitrate, sodium carbonate monohydrate, sodium oxalate and burkeite). Nine samples were taken from each of the largest sieve sizes and analyzed through PLM imaging. When several morphologies were observed for a single crystalline species, as for sodium nitrate, the longest side was selected as the reference for the growth rate calculations. A SST Early Feed crystallization experiment was realized under identical conditions to the certification run 38b. To the basic apparatus, the sampling capability was added in order to determine the nucleation time of the main crystalline species. These values were compared to the simulation predictions and used in growth rate calculations.

Estimations of the growth rates were performed based on (1) the observed maximum crystal dimension, (2) the observed nucleation time, and (3) the simulation file prediction. The relation used to perform the calculations was as follow:

$$G = \frac{(L_{MAX})}{(t_{end} - t_{nucleation})} \qquad \text{(E-4)}$$

Where G was the crystal growth rate and had the unit of micrometers per minute, L_{MAX} was the maximum length of the crystalline species and had the units of micrometers, t_{end} and $t_{nucleation}$ were the experimental ending time and nucleation time respectively. Both times were expressed in minutes.

2.2.10 PRELIMINARY RUNS

To become familiar with the experimental apparatus and prepare for certification runs, numerous runs were performed on simple salt solutions. A total of 55 runs (including the Certification Runs) were done in the laboratory. The simple salt solutions began with sodium nitrate and evolved to a more complicated mixture of sodium nitrate, sodium carbonate, and sodium sulfate and also included attempts at seeding (see Appendix F). Initial runs were purely batch crystallizations where the heating bath was maintained at a constant temperature and pure water was used for crystal washing. During these runs experience was gained with the crystallization equipment, which led to the final apparatus design and crystallization procedure. The procedure involved running semi-batch crystallizations at constant volume, varying the heating rate to promote crystal growth, and washing with a saturated solution to maximize the mass of final crystals. A listing of all crystallization runs is given in Appendix G.

2.3 MODIFICATIONS FOR HOT-CELL IMPLEMENTATION

2.3.1 CRYSTALLIZATION APPARATUS

The constancy and control of the operating temperature is a key issue for the scale down crystallization to be performed in the hot cell environment. The experimental apparatus was modified to achieve a higher vacuum (lower pressure) so that the system temperature could be maintained as the dissolved solids content increased. A vacuum pump with an ultimate pressure of $1.5^{x}10^{-2}$ torr (compared to 9 torr that could be achieved by the previous pump used for Phase I experiments) was installed in the system.

With the help of a tesla coil, it was determined that there were a few small leaks around the necks of both Stage 1 and Stage 2 crystallizers. The leaks were sealed by a glass shop as

described below in more detail. In addition, the vacuum was also increased by reducing the resistance to gas flow between the crystallizer and the pump. This was done by replacing the ¼ in. OD- (0.035–in. wall) stainless steel tubing with 3/8–in. tygon vacuum tubing and by eliminating two unnecessary control valves. With these changes, shown in Figures 1B and 1C, the system achieved a pressure of 7 torr.

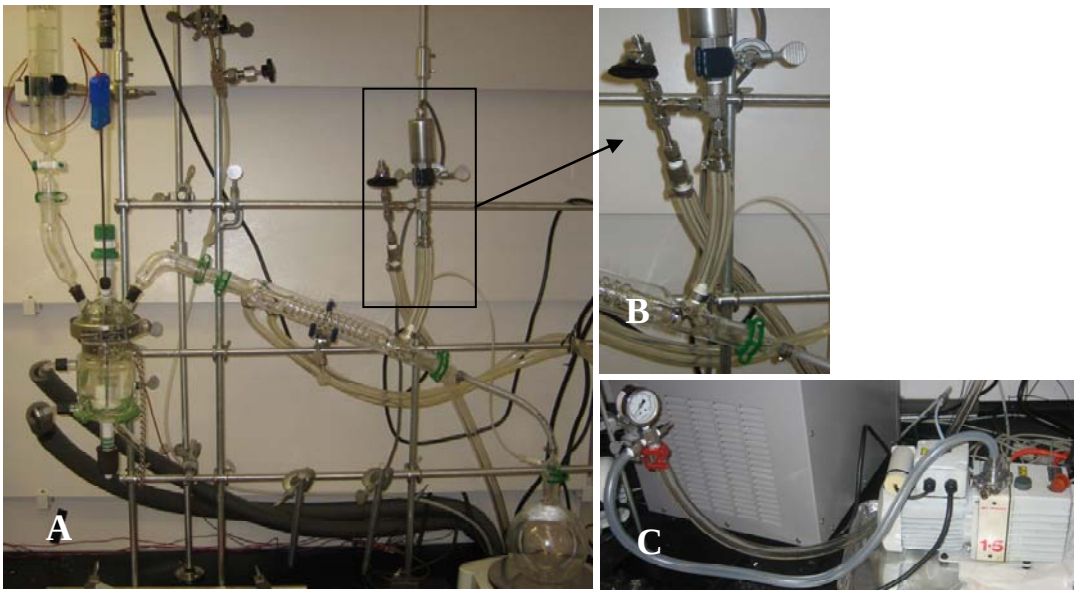

Figure 16: New equipment setup, a) main view, b) zoom on pressure sensor, c) new vacuum system.

The glass connections of the 300-mL vessel lid were treated with ground glass and sealed with wax as presented in Figure 17. The wax (Apiezon® W) is resistant to a temperature of 150 ˚C and is not likely to add any impurities to the slurry during the runs. The tesla coil was used to demonstrate that the treatment of the vessel lid eliminated the leaks described above. In addition, having one continuous piece of glass makes assembly of the apparatus much easier. This should be especially helpful for the case of hot cell experiments.

Figure 17: 300-mL vessel lid

Similar modifications were performed on the 100-mL vessel lid, as shown in Figure 18. In addition to sealing the connections, the enlarging adapter was eliminated to simplify the equipment and reduce its length.

Figure 18: 100-mL vessel lid

Another modification was the improvement of the condenser, which was flattened on downstream side to avoid collection of water in a dead space. In addition, the condenser length was considerably reduced by adding the vacuum outlet and the pressure equalization opening to the condenser. This eliminates the connecting adapters that were previously used for these purposes. The new condenser, shown in Figure 19, will improve water collection, reduce the size of the apparatus, and simplify assembly.

Figure 19: New Condenser

2.3.2 CRYSTALLIZATION PROCEDURE

2.3.2.1 HEATING MEDIUM

Due to restrictions at the Hanford laboratories, silicone oil could not be used as a heating medium. For this reason, water was used to replace silicone oil. The use of water induced the formation of gas bubbles in the double jacket that revealed to be only temporary and disappeared after the first experiment. These bubbles would not directly affect the crystallization run, but would be likely to reduce the heat transfer efficiency. The use of water also induced a limitation on the evaporation rate since the evaporation is controlled by the temperature difference between the heating medium and the slurry temperature. To perform crystallization under very high evaporation rate, the temperature of the heating fluid might be increased to a temperature close to

the water boiling point making necessary the regular control of the water level inside the heating bath.

2.3.2.2 ACCUMULATION HANDLING

A simpler way to handle the accumulation generated during the process was developed. After draining the slurry, the accumulated crystals were redissolved by adding a known amount of water to the crystallizer. This allowed estimation of the mass of accumulation, and it also eliminated the need to disassemble the apparatus for cleaning. This simple method should be particularly useful for hot-cell experiments.

2.3.2.3 CONTROL SYSTEMS

In order to help automate the crystallization process for future hot cell experiments, two control systems were proposed.

The first controlled the heating bath temperature using the scheme in Figure 20. The heating bath would be controlled through LabView by specifying a temperature difference between the slurry and the heating fluid. For example, during the initial phase of each stage, this difference could be set to 15 ^{o}C for rapid evaporation, and then lowered to 5 ^{o}C for the portion of the run during which there is slow evaporation. In Figure 20, the temperature difference is set to 5 ^{o}C, and if the temperature difference drops below that value the program will increase the heating bath temperature. This program has been added to the laboratory control scheme and was used in the majority of the SST solutions experiments.

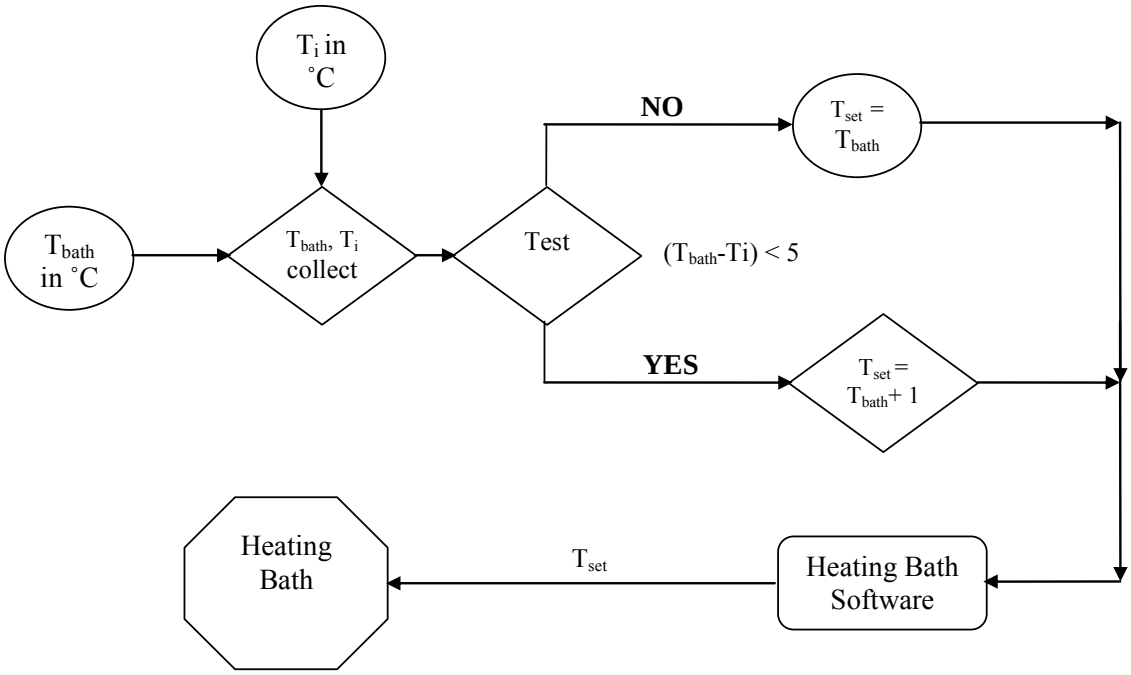

Figure 20. Heating bath control diagram.

The second process improvement involves control of the system pressure. Reducing the pressure too rapidly causes intense boiling and subsequent accumulation of crystal mass on the walls of the crystallizer. Digital regulators, such as the one manufactured by J-KEM Scientific, Inc, can be automatically controlled through LabView software, and are advertised to regulate the pressure within +/- 0.1 torr. This device would increase the sensitivity of the manually operated valve used to reduce the pressure inside the crystallizer. The proposed control system is outlined in Figure 21.

In this control system the pressure will be varied based on the slurry temperature. If the temperature of the slurry begins to rise above the target value (40 ^{o}C in the above example), a new pressure set point will be created and the regulating valve will close slightly to reduce the

pressure and, thereby, maintain a constant temperature. Maintaining the pressure in this manner should reduce the amount of accumulation that forms on the walls of the vessel.

Implementing the control schemes described above should eliminate most of the manual tweaking of controls during the crystallization process. This may facilitate operations in controlled hot-cell environments.

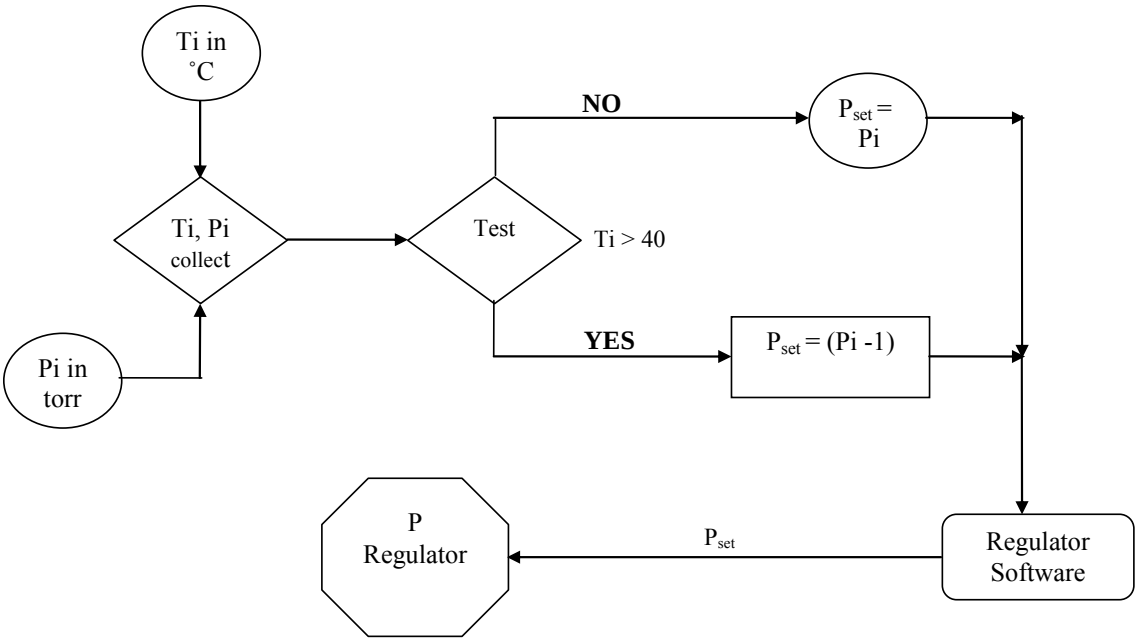

Figure 21. Pressure control diagram.

CHAPTER 3: CERTIFICATION RUNS

3.1 EARLY FEED SOLUTION CERTIFICATION RUN

The Certification Run was performed using a feed solution that had been prepared according to procedures provided by CH2M HILL (Herting and Nelson, 2004). The procedures led to formulation of a feed solution having the composition given in Table 4.

Table 4. Composition of SST Early Feed Solution FY05.

Chemical	MW	Intended Molarity
$NaAlO_2 \cdot 2H_2O$	118.0	0.48
NaOH	40.0	1.65
Na_2CO_3	106.0	0.58
$Na_2C_2O_4$	134.0	0.01
KNO_3	101.1	0.03
$NaNO_3$	85.0	3.87
$NaNO_2$	69.0	0.82
Na_2SO_4	142.0	0.14
$Na_3PO_4 \cdot 12H_2O \cdot 0.25NaOH$	390.1	0.04
NaCl	58.4	0.08
NaF	42.0	0.015
$Na_2Cr_2O_7 \cdot 2H_2O$	298.0	0.04
$CsNO_3$	194.9	0.0035 g/L

3.1.1 OPERATING CONDITIONS

The two-stage crystallization was conducted using the 1-L crystallizer for Stage 1 and the 300-mL crystallizer for Stage 2. The procedures used in performing the crystallizations followed

the semi-batch approach outlined in Section 2.0. Each stage was operated under a variable evaporation-rate profile, as shown in Figure 22, to reduce formation of fines.

The evaporation rate was controlled by varying the temperature difference between the heating medium and the slurry. This was done by adjusting the temperature of the heating fluid and the operating pressure of the crystallizer. In the more rapid evaporation step of Stage 1, vapor was generated at a rate of 143 g/h by adjusting the temperature of the heating fluid to 65 °C and the pressure in the crystallizer to 95 mm Hg, at which the slurry temperature stabilized at 37 °C.

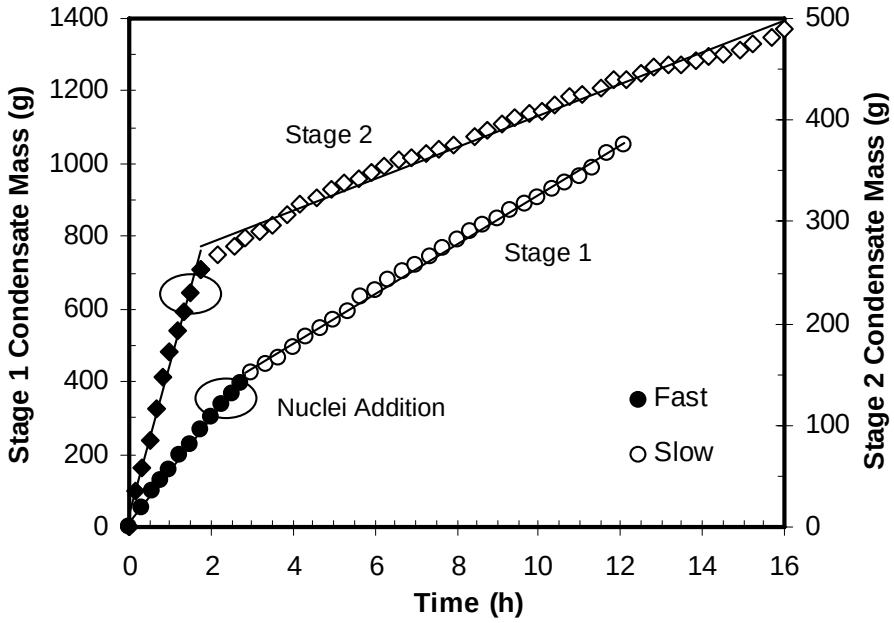

Figure 22. Mass of Condensate Generated as a Function of Run Time for Stage 1 and Stage 2 of Run 26 (SST Early Feed Solution).

Evaporation continued for 2.8 h, which is when crystals began appearing in the system. At that point, the addition of simulant feed to return the level in the crystallizer to its initial position re-dissolved all crystals that had been formed. After this point, the evaporation rate was reduced to 68 g/h by reducing the temperature of the heating fluid to 50 °C; the temperature of the solution in the crystallizer stabilized at 40 °C. Evaporation proceeded at these conditions for over 10 h, at which time the target condensate-to-feed mass ratio was achieved (see Appendix D). The ending condensate-to-feed ratio for the first stage was 0.33, while the target ratio given by the batch simulation from COGEMA, Inc. (SST1SIM.BIN/SST1SIM.xls) was 0.329.

An important issue in this run was the formation of froth during the first stage. This behavior was characterized by intense bubbling, which entrained some of the simulant solution upward and onto the upper walls of the crystallizer. The crystallization of solute on the walls increased accumulation of solids during the run. The total amount of accumulation was 56 g, which can be attributed primarily to the entrainment. It should be noted, however, that this accumulation represents a very small fraction of the feed mass of over 3200 g. The filtrate from the first stage was diluted with water and used as feed for the second stage. The 300-mL crystallizer was used for Stage 2 because the volume of filtrate from the first stage was substantially less than that available for operation of Stage 1. The target condensate-to-feed ratio obtained from the above-cited simulation was adjusted to 0.44 in order to account for the dilution water added. Because the volume of the second-stage crystallizer was 300 mL, only a fraction of the diluted filtrate (70%) was required for its operation. The evaporation rate for Stage 2 followed the same pattern as was used for Stage 1, as shown in Figure 22. Evaporation rates were 148 g/h and 16 g/h in the fast and slow regimes, respectively. The slurry temperature at the end of the run was 52 ºC and the actual condensate-to-feed ratio achieved was 0.45.Although the

goal was to operate this stage at 40°C, the temperature increased to 52°C during the operation. This increase was due to changes in the slurry density and solution concentration, which caused the boiling point of the slurry to increase. The limitations of the vacuum pump were reached during this stage, making an increase in slurry temperature inevitable.

3.1.2 BALANCES ON TOTAL MASS

The means used to satisfy mass balances were described in Section 2.0. The objectives of this process are (1) to determine the fate of species entering the process, and (2) to use mass balances to identify potential problems with the operating procedures.

The schematic diagram in Figure 23 illustrates an overall mass balance around Stage 1 of Run 26. Included in the figure are definitions of quantities used in closing mass balances around each of the units in the stage. As shown in Table 5, the difference between input and output for each of these units was as follows: evaporation, 0.45%; filtration, 0.33%; washing, 0.73%.

Stage 1. Evaporative crystallization in Stage 1 is represented schematically in Figure 23. The figure shows the masses of vapor generated and either recovered in the condensate receiver or the cold trap protecting the vacuum pump, crystals that accumulated on the walls of the vessel, material that adhered to the vessel and was lost in the transfer process, and the recovered slurry. Unfortunately, a spill occurred during the transfer of the slurry from the crystallizer to the filtration apparatus. The run was continued because the loss could be quantified in terms of total mass at 200 g. A description of how the spill was quantified is provided in Appendix E.

The slurry recovered from the evaporative crystallization was filtered as shown schematically in Figure 23. The unwashed crystals leaving the filter correspond to the mass of solids recovered at the end of the filtration. The filtrate was collected inside the vacuum flask,

and the funnel loss corresponds to the loss recovered after filtration by washing the filtration funnel with a known amount of water and using a dry paper of known mass to collect the water accumulated on the wall of the apparatus.

The unwashed crystals were washed as shown schematically in Figure 23. The mass of unwashed crystals entering the washing step correspond to the mass coming from the filtration step, after subtracting the amount lost in the intermediary beaker and the amount removed as a sample. The beaker loss was small because the solids recovered are relatively dry and do not stick to the glass wall of the beaker. The crystals leaving the washing step are the product from Stage 1, while the spent wash and funnel loss are defined as shown in Figure 23.

Stage 2. Figure 24 is a schematic diagram for Stage 2 of Run 26. Each process unit functioned as described in the discussion of Stage 1, and the methods of closing total mass balances also were the same. The results of these analyses are shown in Table 5.

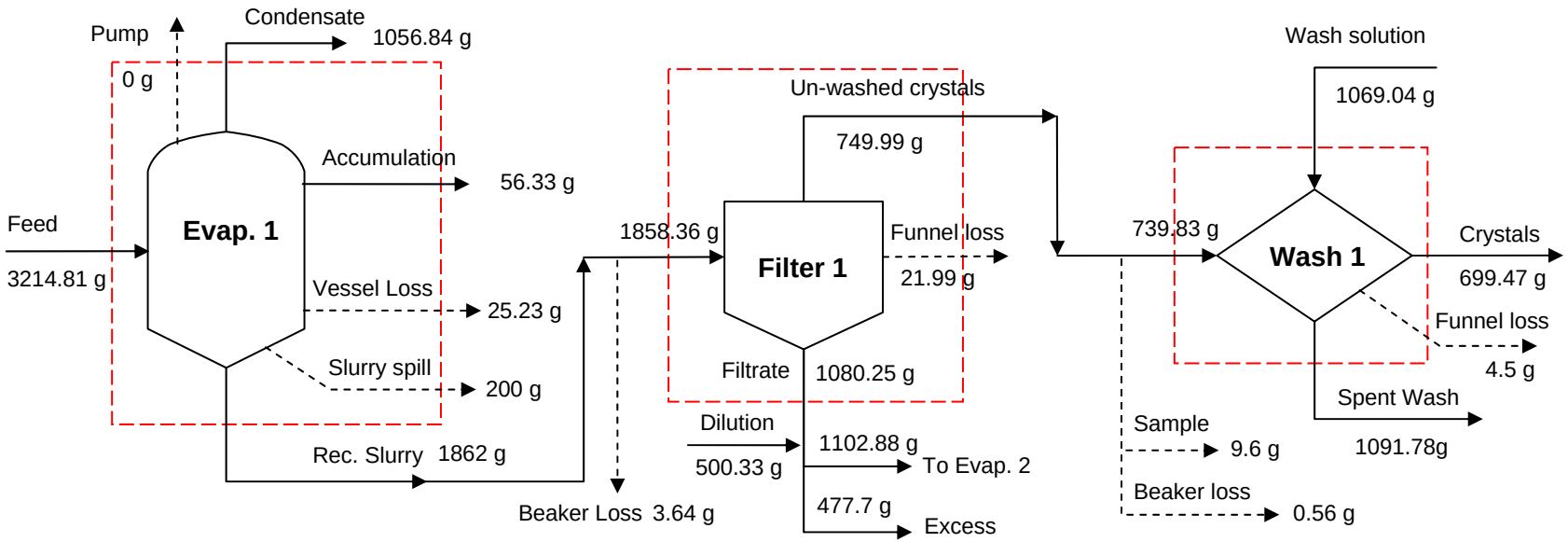

Pump	Mass of the condensate collected in the cold trap protecting the vacuum pump.
Slurry Spill	A spill that took place during transfer of the slurry between units. This was estimated at 200 g.
Rec. Slurry	Mass of slurry recovered from the crystallizer. Due to the slurry spill that occurred during Stage 1, this is an estimated value.
Vessel Loss	Mass recovered by washing the vessel with a known amount of water.
Dilution	Water added to the filtrate to dissolve any precipitated crystals.
Funnel Loss	Mass recovered by washing the funnel with a known amount of water and then drying with paper of a known weight. Performed after the filtration and washing operations.
Beaker Loss	Mass of slurry lost in the several beakers necessary for the transfer from the vessel to the filter.
Sample	Mass collected from the un-washed crystals for chemical analysis.

Solid arrows are the process streams and the dotted arrows represent quantified losses. Closure on a total mass balance was performed for each dashed box around a process unit.

Figure 23. Overall Mass Balance in Stage 1 of SST Early Feed Solution Run 26.

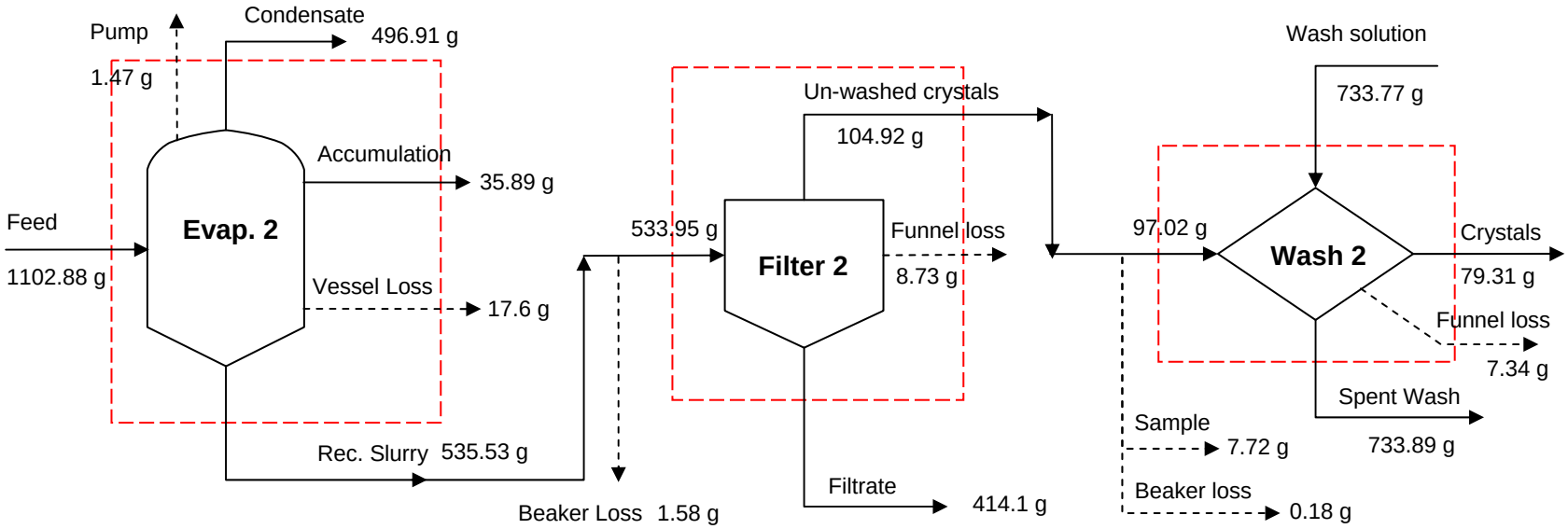

Pump	Mass of the condensate collected in the cold trap protecting the vacuum pump.
Rec. Slurry	Mass of slurry recovered from the crystallizer.
Vessel Loss	Mass recovered by washing the vessel with a known amount of water.
Funnel Loss	Mass recovered by washing the funnel with a known amount of water and then drying with paper of a known weight. Performed after the filtration and washing operations.
Beaker Loss	Mass of slurry lost in the several beakers necessary for the transfer from the vessel to the filter.
Sample	Mass collected from the un-washed crystals for chemical analysis.

Solid arrows are the process streams and the dotted arrows represent the losses. Closure on a total mass balance was performed for each dashed box around a process unit.

Figure 24. Overall Mass Balance in Stage 2 of SST Early Feed Solution Run 26.

Table 5. Mass Balances Around Process Units of Run 26 (SST Early Feed Solution).

Unit	Input (g)	Output (g)	Difference (g)	% Closure of Mass Balance
Evaporator 1	3214.81	3200.40	14.41	0.45
Filtration 1	1858.36	1852.23	6.13	0.33
Washing 1	1808.87	1795.75	13.12	0.73
Evaporator 2	1102.88	1087.40	15.48	1.40
Filtration 2	533.95	527.75	6.20	1.16
Washing 2	830.79	820.54	10.25	1.23

3.1.3 CHARACTERIZATION OF CRYSTAL PRODUCT

Polarized Light Microscopy. Samples of crystals removed from the slurry produced in each stage were examined by polarized light microscopy (PLM). Images obtained from the examinations are shown in Figure 25. The samples were obtained from the slurry product immediately at the end of operation of each crystallization stage. The major crystals expected from the first stage were sodium nitrate and sodium carbonate monohydrate, whereas sodium oxalate and burkeite crystals were expected in lesser amounts. Sodium nitrate (Figure 25A), sodium carbonate monohydrate (rainbow pattern in Figure 25A), and sodium oxalate (needle shapes in Figures 25A and 25B) were observed as expected. However, no burkeite crystals were found in the images, which could be due to three possibilities: (1) the quantity of burkeite crystals was too low to be detected, and/or (2) the samples were not representative of the overall slurry composition, and/or (3) no burkeite was produced. Sodium nitrate, sodium carbonate monohydrate, and burkeite were also expected from the second stage of this run. PLM images display the presence of sodium nitrate in large quantities (Figures 25C and 25D) along with sodium carbonate (Figure 25D). Again, no burkeite crystals were detected, which is consistent with the fact that the simulation (SST1SIM.BIN/SST1SIM.xls) predicted that only 0.1 g of this

species would be produced. Sodium nitrite crystals were not explicitly observed in these images from the slurry; however, such crystals were identified in the images of crystals after sieving. Another interesting crystal type in the PLM images is that of the yellow-blue crystals displayed in Figures 25B through 25D; these are thought to be sodium sulfate.

Sieve Analyses. A fraction of the crystals obtained at the end of each stage of Run 26 was washed with acetone as described in Section 2.0 and allowed to air dry overnight. Applying the sieving procedure outlined in Section 2.0 to a 15- to 20-g sample from each fraction gave the results in Figure 26.

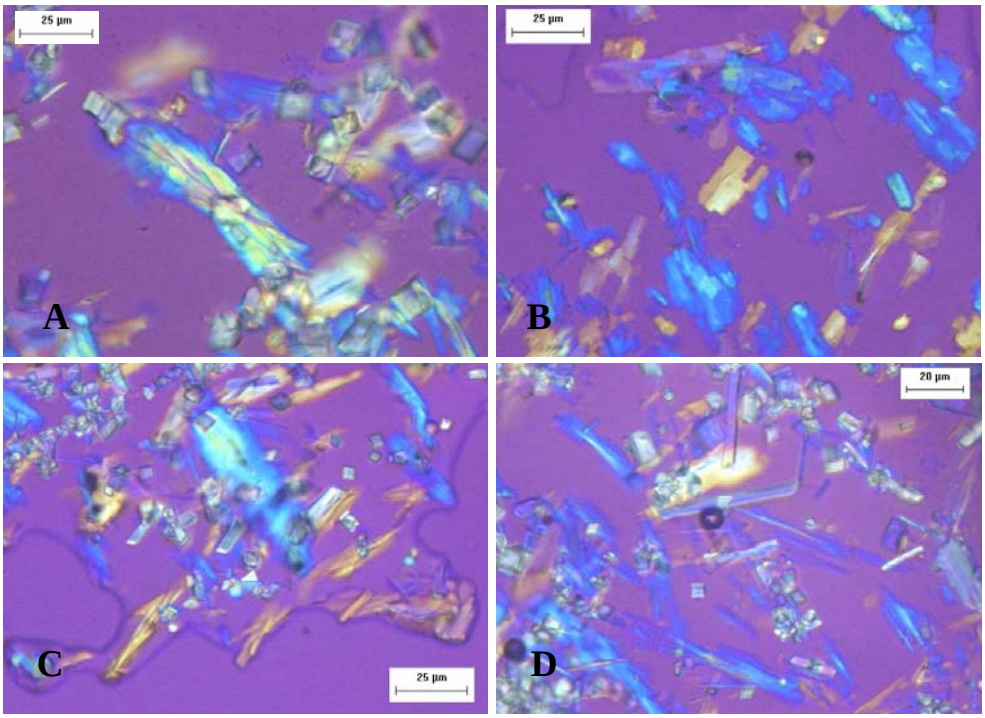

Images A and B were obtained from Stage 1 and Images C and D were obtained from Stage 2.

Figure 25. PLM Images of the Crystals Obtained from the Certification Run (Run 26) on SST Early Feed Solution.

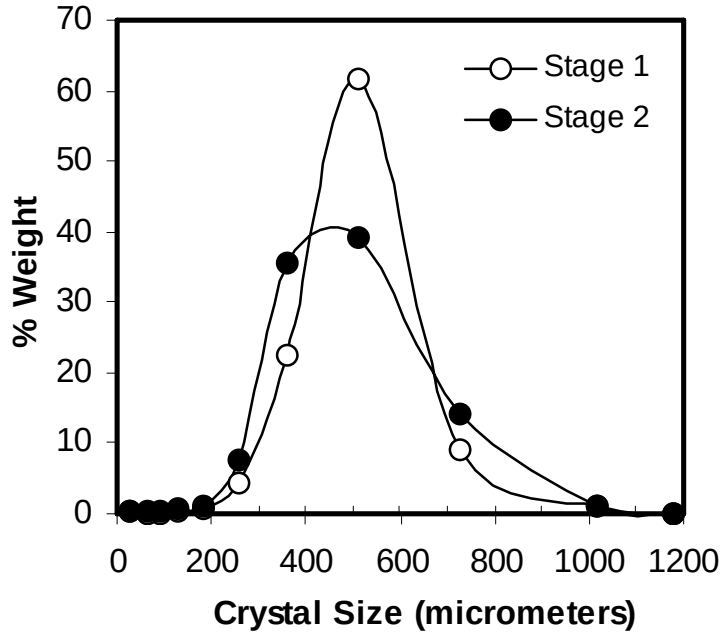

Figure 26. Crystal Size Distribution of the Products From SST Early Feed Solution.

Crystals from Stage 1 exhibit a sharp and uniform size distribution with a mode near 500 μm. Crystals from Stage 2 have a broader distribution with a mode at approximately 450 μm. In each case, the mode is expected to be dominated by sodium nitrate crystals. The simulation cited earlier predicted the formation of large quantities (> 75 wt%) of sodium nitrate in each stage.

A small amount of crystals below 100 μm were also observed, especially in stage two. These are thought to be dominated by sodium carbonate monohydrate, burkeite, and sodium oxalate. According to the simulation, these fine species should represent about 20 wt% of the total product mass, with the majority being sodium carbonate monohydrate. Less than 2% of these crystals were observed in the size range below 100 μm and the remaining are expected to be agglomerated together or part of the large species of sodium nitrate.

Species Distribution. The sieved crystalline products were used to analyze the distribution of chemical species within different size ranges. Figures 27 and 28 display PLM images of crystals from Stages 1 and 2 of Run 26, respectively.

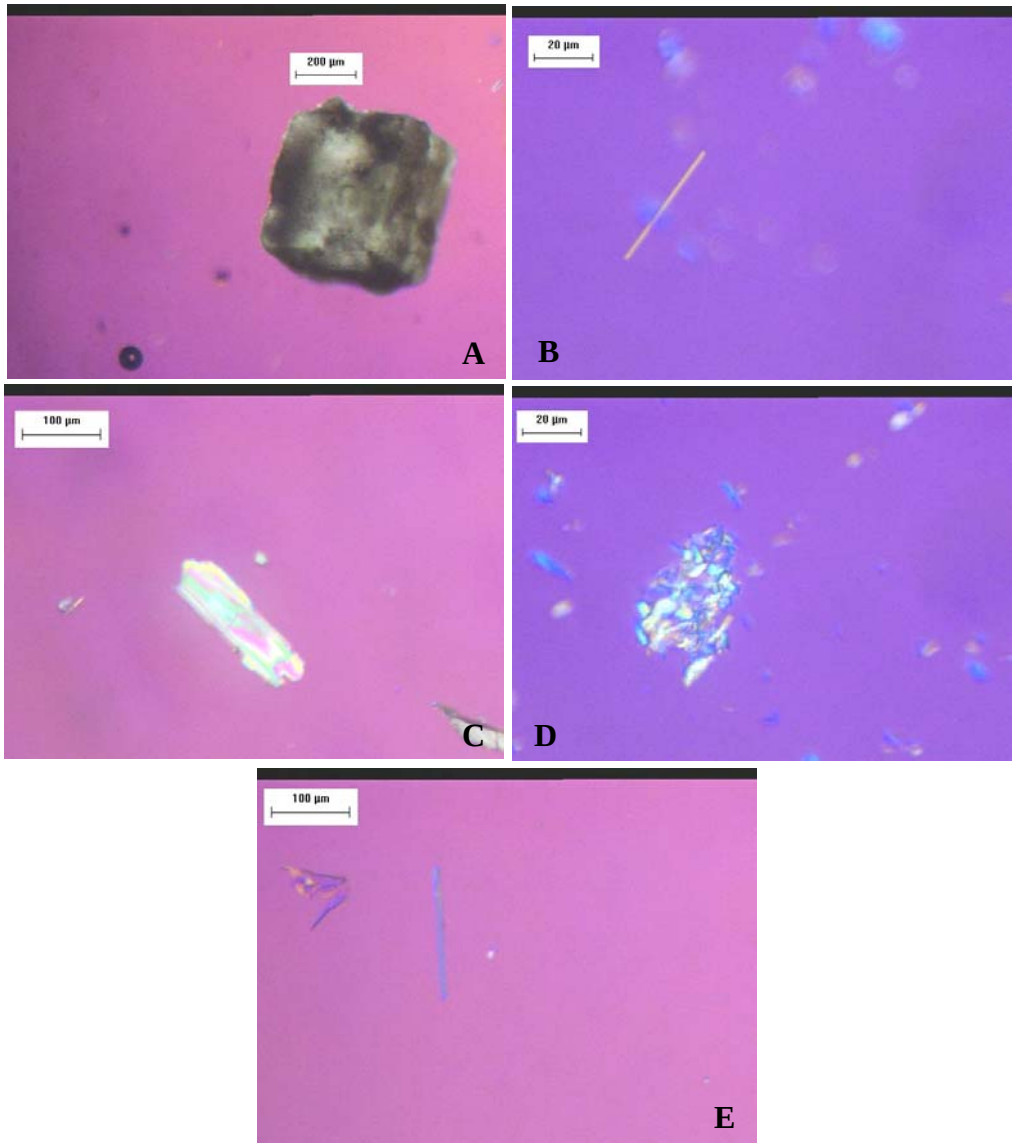

Figure 27. PLM Images of the Sieved Crystals from Stage 1.

As seen in Figure 26, the mode for Stage 1 crystals was near 500 µm. PLM images verified that this size range corresponded to sodium nitrate crystals (see Figure 27A). No

agglomerates were observed at this size range. Crystals observed in the 53 to 75 μm size range included mainly sodium carbonate monohydrate and sodium oxalate (Figure 27B), and sodium nitrate. Sodium carbonate monohydrate and sodium oxalate were also observed in sieves up to 200 μm (Figure 27C and 27E). The simulation also predicted formation of a reasonable amount of burkeite (7 wt% of the total product) in Stage 1. Although none of these crystals were identified in PLM imaging of slurry samples (presented in the previous section) Figure 27D shows what is thought to be a burkeite crystal.

Figure 28 shows PLM images of crystals from Stage 2. The sodium nitrate image in Figure 28A is of crystals taken from near the mode of 450 μm. Only a few agglomerates are found at that size range, but an apparent example is shown in Figure 28B. Since the individual crystals composing this agglomerate have sizes around 350 μm, the size of the agglomerate exceeds 700 μm. This leads to the conclusion that these agglomerates were formed after the sieving process, since the mode size is bounded by sieves of 425 μm and 600 μm. Analysis of the 50 μm size sieve displayed a mix of sodium nitrate (Figure 28E) sodium carbonate (Figure 28F) and sodium oxalate (Figure 28C). What is believed to be a burkeite crystal has also been observed (Figure 28D).

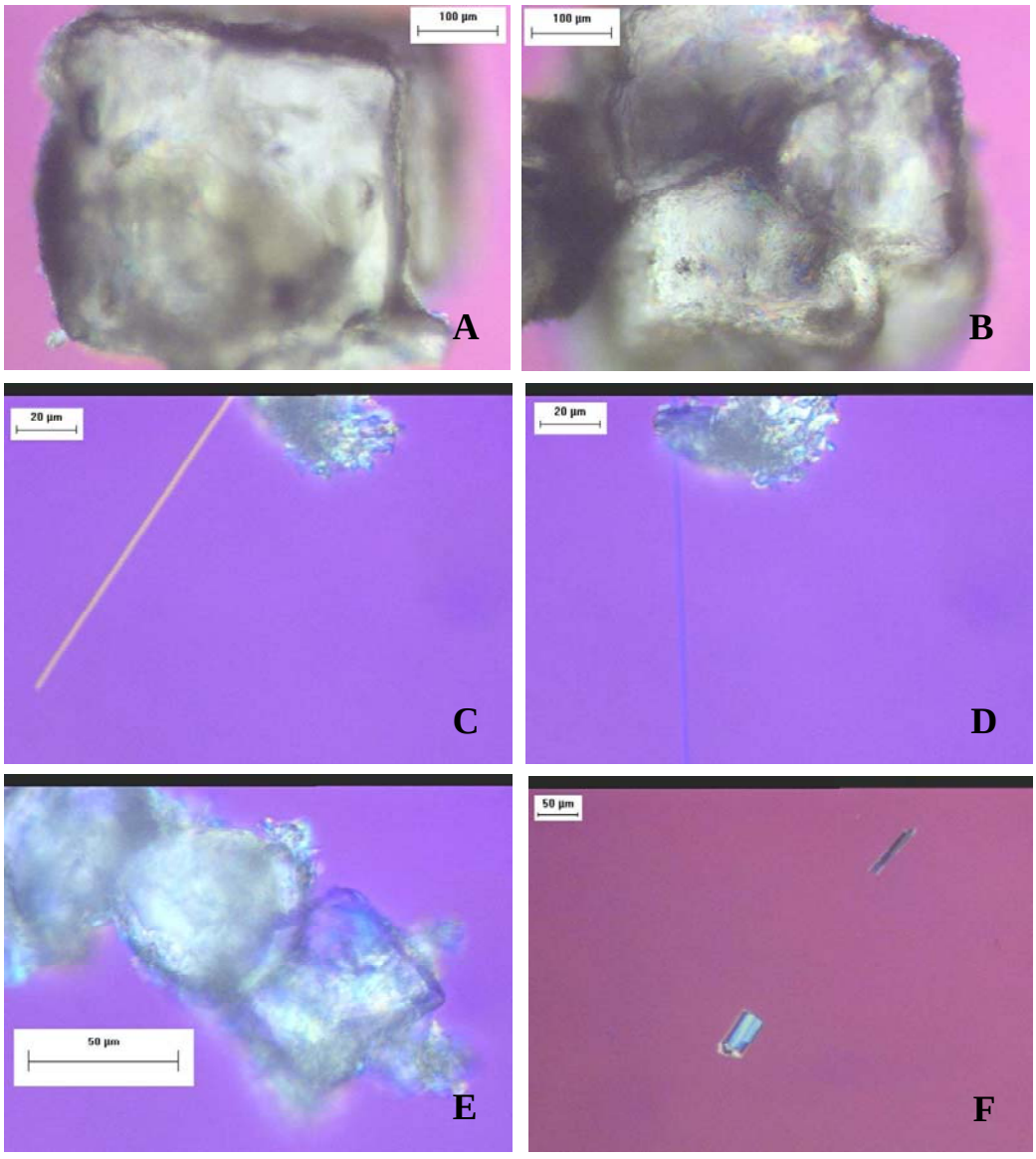

Figure 28. Images of Sieved Crystals from Stage 2.

3.1.4 SPECIES ANALYSIS AND MASS BALANCES

Figures 23 and 24 illustrate the accounting associated with the total mass entering and leaving Stage 1 and Stage 2. These have been used as the basis for balances on total mass that are illustrated in Figure 29 for Run 26, which is the Certification Run for SST Early Feed Solution. Table 6 shows the stream values, and it also gives the amounts of sodium nitrate and sodium carbonate that entered the system with the wash solution. (Recall that this solution was saturated with respect to these two solutes so as to reduce the dissolution of crystals in the filter cake. This was justified by recognizing that it more closely represented a continuous operation.)

The results of the balances on total mass show that 299.1 g were lost in Stage 1, but that 265.5 g could be accounted for using the methods described in Section 2.0 and with the estimation of 200 g for the slurry spill. This meant that the unaccounted for loss was estimated to be 33.6 g; another way of saying this is that the balance on total mass was closed to within 0.8%. Addressing Stage 2, there was a loss of 76.6 g, of which 44.6 g were unaccounted for; in other words the total mass balance closed to within 1.7%.

Samples of each stream were obtained and sent to Galbraith Laboratories for chemical analyses (Appendix H). The samples were of the feed solution, filtrate, spent wash, unwashed crystals, washed crystals, and accumulation. All samples except for the final crystals were sent for analysis in liquid form in order to give a homogeneous sample. Results obtained from Galbraith were tabulated in a spreadsheet and the mass of each ionic species was calculated at each sample point in the process.

Table 7 gives inputs, outputs, and closures of mass balances around the entire process for each species. Details of the stage-wise species mass balances are given in Tables 8 and 9. For

species analysis it was assumed that the total amount of filtrate from Stage 1 was used as feed for Stage 2. In reality, only a portion of the filtrate from Stage 1 was used as the feed for Stage 2, so the output streams from Stage 2 were scaled accordingly. It was also assumed that the relative amounts of each output stream in Stage 2 would remain constant when using the total filtrate from Stage 1.

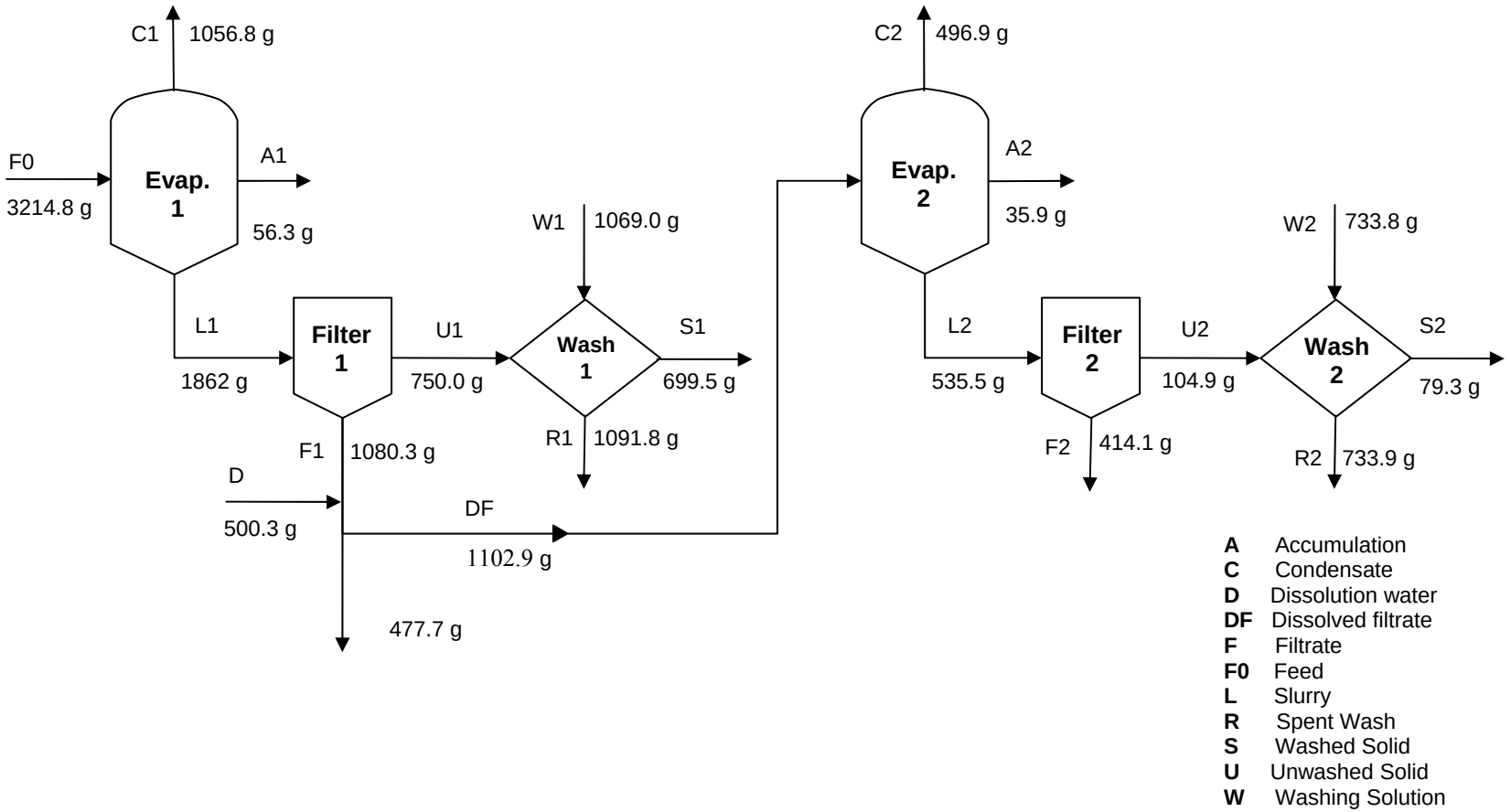

Figure 29. Balances on Total Mass for Each Process Unit in Run 26.

Table 6. Balances on Total Mass Around Each Unit in Run 26 (SST Early Feed Solution).

Stage 1	**Input (g)**		**Output (g)**					**Loss (g)**
Species	**Feed**	**Wash**	**Cond**	**Washed Solids**	**Filtrate**	**Spent Wash**	**Accum**	
Early feed	3214.8							
H_2O		634.1	1056.8					
Na_2CO_3		98.9						
$NaNO_3$		336.0						
Solution				699.5	1080.3	1091.8	56.3	
Total	3214.8	1069.0	1056.8	699.5	1080.3	1091.8	56.3	299.1
Combined	4283.8		3984.7					299.1
						% Loss		7.0%
						Accounted loss (g)		265.5
						% Corrected Loss		0.8%

Stage 2	**Input (g)**		**Output (g)**					**Loss (g)**
Species	**Feed**	**Wash**	**Cond**	**Washed Solids**	**Filtrate**	**Spent Wash**	**Accum**	
Stage 1 Filtrate	753.8							
H_2O	349.1	413.2	496.9					
Na_2CO_3		75.8						
$NaNO_3$		244.8						
Solution				79.3	414.1	733.9	35.9	
Total	1102.9	733.8	496.9	79.3	414.1	733.9	35.9	76.6
Combined	1836.7		1760.1					76.6
						% Loss		4.2%
						Accounted loss (g)		44.6
						% Corrected Loss		1.7%

Table 7. Species Mass Balances for SST Early Feed solution Run 26.

Species	Input (g)	Output (g)	Closure (%)
Cs^{+}	6.45E-03	4.70E-03	27.1
Na^{+}	764.03	696.76	8.8
Al^{3+}	35.85	33.88	5.5
CrO_4^{2-}	22.06	18.37	16.7
F^{-}	0.662	0.124	81.2
NO_2^{-}	89.55	79.59	11.1
NO_3^{-}	1076.03	1035.26	3.8
PO_4^{3-}	9.03	4.01	55.6
SO_4^{2-}	31.89	27.04	15.2
$C_2O_4^{2-}$	2.07	1.21	41.8
CO_3^{2-}	199.81	205.10	-2.6
H_2O	3693.04	3239.71	12.3
OH^{-}	165.40	85.81	48.1

Two other issues had to be considered when performing calculations on the data from Run 26. The first issue only became clear in analyzing the data on the feed composition that were provided by Galbraith Laboratories. The analytical results corresponded to the composition of SST Late Feed Solution, which could only have been the case if there was a labeling error in the Georgia Tech laboratory or a mistake in handling by Galbraith Laboratories. If necessary, another feed sample could be taken for analysis. However, the feed solution was prepared as described earlier in this section and the composition resulting from that preparation is expected to correspond to that in Table 4. Stated simply, the feed composition was taken to correspond to that expected from following the previously referenced simulant preparation instructions from

CH2M HILL. This feed composition also was used in the simulation file SST1SIM.xls. The slurry spill that occurred during Stage 1 of this run was not accounted for in Tables 7, 8, and 9.

Table 8. Species Mass Balances for SST Early Feed Solution Run 26 Stage 1.

Stage 1	Input (g)		Output (g)					Closure
Species	**Feed**	**Wash**	**Condensate**	**Filtrate**	**Spent Wash**	**Crystals**	**Accumulation**	**%**
Cs^{+}	6.45E-03	0	0	4.81E-03	2.09E-04	4.50E-04	6.88E-05	14.1
Na^{+}	488.18	133.82	0	217.44	146.21	199.71	13.69	7.2
Al^{3+}	35.85	0	0	31.37	1.40	3.25	0.48	-1.8
CrO_4^{2-}	22.06	0	0	17.10	0.71	1.77	0.26	10.1
F^{-}	0.662	0	0	0.007	0.005	0.064	0.001	88.3
NO_2^{-}	89.55	0	0	76.72	3.46	7.65	1.21	0.6
NO_3^{-}	574.95	245.13	0	181.54	252.67	351.90	22.64	1.4
PO_4^{3-}	9.03	0	0	2.78	0.34	0.43	0.08	59.9
SO_4^{2-}	31.89	0	0	2.42	3.18	20.38	1.24	14.6
$C_2O_4^{2-}$	2.07	0	0	0.18	0.11	0.67	0.04	51.5
CO_3^{2-}	82.32	56.01	0	8.02	57.60	76.30	3.15	-4.9
H_2O	1712.83	634.08	1056.84	465.15	621.99	37.27	12.50	6.5
OH^{-}	165.40	0	0	77.53	4.11	0.07	1.05	50.0

Table 9. Species Mass Balances for SST Early Feed Solution Stage 2.

Stage 2	Input (g)			Output (g)					Closure
Species	**Filtrate 1**	**Dilution**	**Wash**	**Condensate**	**Filtrate**	**Spent Wash**	**Crystals**	**Accumulation**	**%**
Cs^{+}	4.81E-03	0	0	0	3.70E-03	1.09E-04	6.22E-05	1.04E-04	17.4
Na^{+}	217.44	0	142.03	0	143.87	149.21	31.34	12.74	6.2
Al^{3+}	31.37	0	0	0	26.31	0.81	0.88	0.77	8.3
CrO_4^{2-}	17.10	0	0	0	14.27	0.41	0.52	0.43	8.6
F^{-}	0.007	0	0	0	0.036	0.010	0.007	0.001	-652.3
NO_2^{-}	76.72	0	0	0	59.43	3.41	2.38	2.06	12.3
NO_3^{-}	181.54	0	255.95	0	53.82	262.67	67.86	23.69	6.7
PO_4^{3-}	2.78	0	0	0	2.37	0.63	0.07	0.10	-14.2
SO_4^{2-}	2.42	0	0	0	1.02	0.62	0.46	0.14	7.7
$C_2O_4^{2-}$	0.18	0	0	0	0.14	0.21	0.01	0.02	-113.1
CO_3^{2-}	8.02	0	61.49	0	1.37	60.75	5.20	0.73	2.1
H_2O	465.15	753.80	592.33	712.14	227.66	558.06	4.23	9.02	16.6
OH^{-}	77.53	0	0	0	63.16	14.96	0.72	1.74	-3.9

3.1.5 COMPARISON TO MINIMUM AND DESIRED TARGETS

As described in Section 2.0, Stage 2 was operated using only a fraction of the total filtrate produced in Stage 1. In the calculations to evaluate the approach to the process criteria, the mass balances shown in Tables 7, 8, and 9 were scaled as if all of the filtrate had been used in the process. This is a standard approach for scaling up or scaling down process flowsheets (Felder and Rousseau). Specifically, the sodium balance for Stage 2 sodium was scaled according to the amount of filtrate from Stage 1 that was used to feed Stage 2. It was also assumed that the sodium collected in the accumulation from each stage would be found as crystal mass in an ideal process. Another assumption used in the sodium calculations was that the 200 g of estimated slurry spill had the same composition as the recovered slurry. Using this assumption, the 200 g was split up into filtrate mass, crystal mass, and mass taken away with the spent wash. Results of these calculations are given in Table 10 and show that the sodium recovery was 58.1%, which exceeds the minimum target.

Table 10. Sodium Balance and Recovery for SST Early Feed Solution Run 26.

Stream	Unit Value (g)	Totals (g)
Input		488.18
Crystals/Stage 1	221.16	
Accum/Stage 1	13.69	
Crystals/Stage 2	34.7	
Accum/Stage 2	14.1	
Output		283.66
Recovery		58.1%

Cesium activity was calculated directly from the chemical analyses performed by Galbraith Laboratories on the washed crystals obtained from Stages 1 and 2. Table 11 shows the analytical results for sodium and cesium and the calculated activities expected for dissolution of

each of the filter cakes and for the combined filter cakes. It is assumed that 20% of the cesium in Hanford waste is in the form of ^{137}Cs, and that the activity of ^{137}Cs is 86.58 Ci/g. As shown, the value for the combined solids is significantly better than the minimum requirement of 0.05 Ci/L. The estimated decontamination factor associated with blending the two products of washed crystals from Stages 1 and 2 is 7.98. This value is well above the minimum (1.15) given in Section 1.6, but significantly below that desired (48).

Table 11. Compositions of Filter Cakes from SST Early Feed Solution Run 26 with Estimated Activities and Decontamination Factors.

	mass (g)	wt % Na	Ppm Cs	Ci/L	DF
Stage 1	699.47	28.4	0.64	0.0112	5.4
Stage 2	113.66	27.2	0.54	0.0099	6.9
Combined	813.13	28.2	0.626	0.0110	5.5

The sulfate-to-sodium molar ratio in the filtrate streams from Stages 1 and 2 were calculated using the relative amounts of the two ions in the filtrate streams as determined by Galbraith Laboratories. The results given in Table 9 show that the combined filtrates from Run 26 exceed the minimum requirement of 0.01 and nearly meet the desired target of 0.0022 moles of sulfate ion per mole sodium ion.

Table 12. Compositions of Filtrate Streams from SST Early Feed Solution Run 26 and Associated Sulfate-to-Sodium Molar Ratio.

	Wt % Na	wt% SO_4	Molar Ratio Sulfate:Sodium
Stage 1	20.13	0.22	0.0027
Stage 2	24.24	0.17	0.0017
Combined	21.59	0.21	0.0023

3.2 LATE FEED SOLUTION CERTIFICATION RUN

The Certification Run was performed using a feed solution that had been prepared according to procedures provided by CH2M HILL (Herting and Nelson, 2004). The procedures led to formulation of a feed solution having the composition given in Table 13.

Table 13. Composition of Phase I SST Late Feed Solution.

Chemical	MW	Intended Molarity
$NaAlO_2 \cdot 2H_2O$	118.0	0.04
NaOH	40.0	0.01
Na_2CO_3	106.0	0.24
$Na_2C_2O_4$	134.0	0.01
KNO_3	101.1	0.01
$NaNO_3$	85.0	1.59
$NaNO_2$	69.0	0.07
Na_2SO_4	142.0	0.17
$Na_3PO_4 \cdot 12H_2O \cdot 0.25NaOH$	390.1	0.05
NaCl	58.4	0.01
NaF	42.0	0.10
$Na_2Cr_2O_7 \cdot 2H_2O$	298.0	0.009
$CsNO_3$	194.9	0.00035 g/L

3.2.1 OPERATING CONDITIONS

The two-stage crystallization was conducted using the 1-L crystallizer for Stage 1 and the 300-mL crystallizer for Stage 2. The procedures followed in performing the crystallizations were outlined in Section 2.0. Each stage was operated under a variable evaporation-rate profile to reduce formation of fines, as shown in Figure 30.

The evaporation rate was controlled by varying the temperature difference between the heating medium and the slurry. This was done by adjusting the temperature of the heating fluid and the pressure of the vessel. In the more rapid evaporation step of Stage 1, vapor was generated at a rate of 330 g/h by adjusting the temperature of the heating fluid to 100 °C and the pressure in the crystallizer to 127 mm Hg, at which the slurry temperature stabilized at 54 °C. Evaporation continued for 3.7 h, which is when crystals began appearing in the system. After observation of the crystals, additional simulant feed was added to return the level in the

crystallizer to its initial position and concomitantly re-dissolve all crystals that had been formed. Furthermore, the evaporation rate was reduced to 74 g/h by reducing the temperature of the heating fluid to between 65 and 70°C; the temperature of the solution in the crystallizer stabilized at 60°C. Evaporation proceeded at these conditions for over 35 h, at which time the target condensate-to-feed mass ratio was achieved (see Appendix D). The ending condensate ratio for the first stage was 0.68, the same as the target ratio given by the batch simulation from COGEMA, Inc. (SST2.BIN/SST2SIM1.xls).

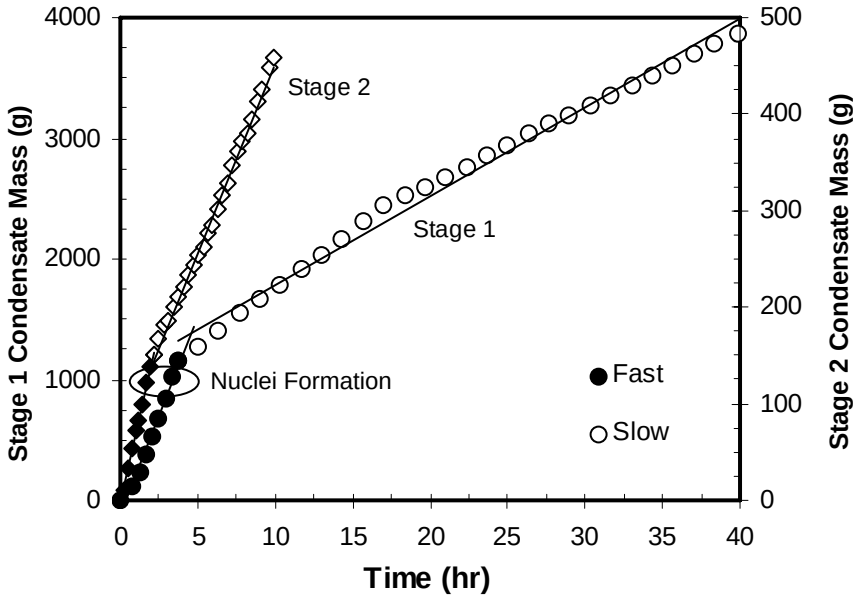

Figure 30. Mass of Condensate Generated as a Function of Run Time for Stage 1 and Stage 2 of Run 27 (SST Late Feed).

The filtrate from the first stage was diluted with water and used as feed for the second stage. The target condensate-to-feed ratio from the above-cited simulation was adjusted to 0.537 in order to account for the dilution water added. Because the volume of the second-stage crystallizer was 300 mL, only a fraction of the diluted filtrate was required for its operation. The evaporation rate for Stage 2 followed the same pattern as was used for Stage 1; evaporation rates

were 128 g/h and 60 g/h in the fast and slow regimes, respectively. The slurry temperature at the end of the run was 40ºC and the actual condensation ratio achieved was 0.535. The major issue encountered during operation of this stage was the generation of a relatively large amount (126 g) of accumulation on the walls of the crystallizer, which is thought to have been caused by intense boiling near the end of the run. This level of accumulation has only been observed in the 300-mL crystallizer, and it seems to be due to the shape and small size of the vessel, although there is insufficient evidence to be certain.

Because of the large amount of accumulation in the original operation of Stage 2, this portion of the run was repeated using the remaining diluted filtrate from Stage 1. A lower heating rate was used near the conclusion of the run to try to reduce the amount of accumulation. With the reduced evaporation rate (40 g/h compared to 60 g/h in the original trial), splashing was reduced but was not completely eliminated. In fact, there was more accumulation (158 g) in this trial. The problem with this trial was that there remained insufficient filtrate from Stage 1 to operate the crystallizer at a fixed level above the baffle cage. The target condensate-to-feed ratio of 0.537 could only be reached by allowing the level in the crystallizer to fall, and even so the condensate-to-feed ratio achieved was only 0.49. Even so, the mass balance and species analysis results of the second stage belong to the repeated run.

3.2.2 BALANCE ON TOTAL MASS

The means used to satisfy mass balances were described in Section 2.0. The objectives of this process are (1) to determine the fate of species entering the process, and (2) to use mass balances to identify potential problems with the operating procedures.

Figure 31 is a schematic diagram illustrating the results of the overall mass balance around Stage 1 of Run 27. Included in the figure are definitions of quantities used in closing

mass balances around each of the units. As shown in Table 14, the difference between input and output for each of these units was as follows: evaporation, 0.08%; filtration, 1.78%; washing, 2.32%.

Stage 1. Evaporative crystallization in Stage 1 is represented schematically in Figure 31. The figure shows the masses of vapor generated and either recovered in the condensate receiver or the cold trap protecting the vacuum pump, crystals that accumulated on the walls of the vessel, material that adhered to the vessel and was lost in the transfer process, and the recovered slurry.

The slurry recovered from the evaporative crystallization was filtered as shown schematically in Figure 31. The unwashed crystals correspond to the mass of solids recovered at the end of the filtration. The filtrate is the mass of filtrate collected inside the vacuum flask, and the funnel loss corresponds to the loss recovered after filtration by washing the filtration funnel with a known amount of water and using a dry paper of known mass to collect the water accumulated on the wall of the apparatus.

The unwashed crystals were washed as shown schematically in Figure 31. The unwashed crystals correspond to mass coming from the filtration step after subtracting the amount lost in the intermediary beaker and the amount removed as a sample. The beaker loss was small because the solids recovered are relatively dry and do not stick to the glass wall of the beaker. The final crystals, spent wash, and funnel loss are as defined.

Stage 2. Figures 32 and 33 are schematic diagrams of two trials for Stage 2 of Run 27. As explained earlier, the reason for performing two trials was the large mass of accumulated crystals found in the crystallizer at the end of the first trial. Each process unit functioned as described in the discussion of Stage 1, and the methods of closing total mass balances also were the same. The results of these analyses are shown in Table 14.

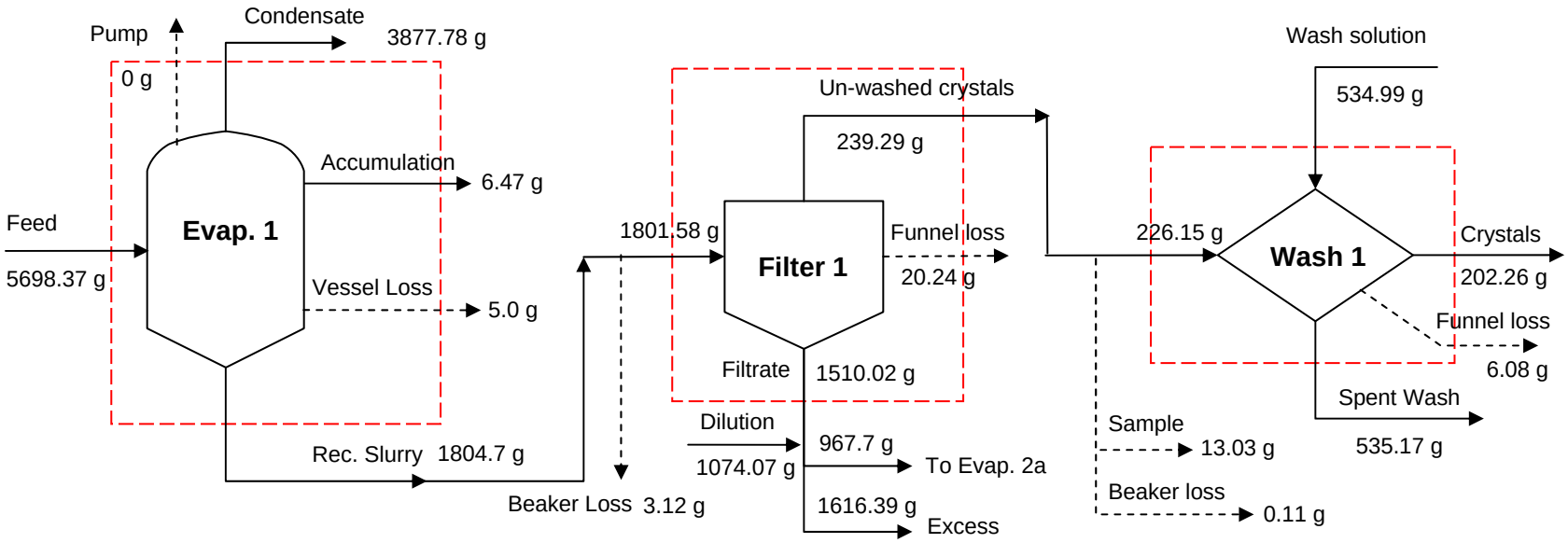

Pump	Mass of the condensate collected in the cold trap protecting the vacuum pump.
Rec. Slurry	Mass of slurry recovered from the crystallizer.
Vessel Loss	Mass recovered by washing the vessel with a known amount of water.
Dilution	Water added to the filtrate to dissolve any precipitated crystals.
Funnel Loss	Mass recovered by washing the funnel with a known amount of water and then drying with paper of a known weight. Performed after the filtration and washing operations.
Beaker Loss	Mass of slurry lost in the several beakers necessary for the transfer from the vessel to the filter.
Sample	Mass collected from the un-washed crystals for chemical analysis.

Solid arrows are process streams and dotted arrows represent quantified losses. Closure on a total mass balance was performed for each dashed box around a process unit.

Figure 31. Overall Mass Balance on Stage 1 of Run 27 (SST Late Feed Solution).

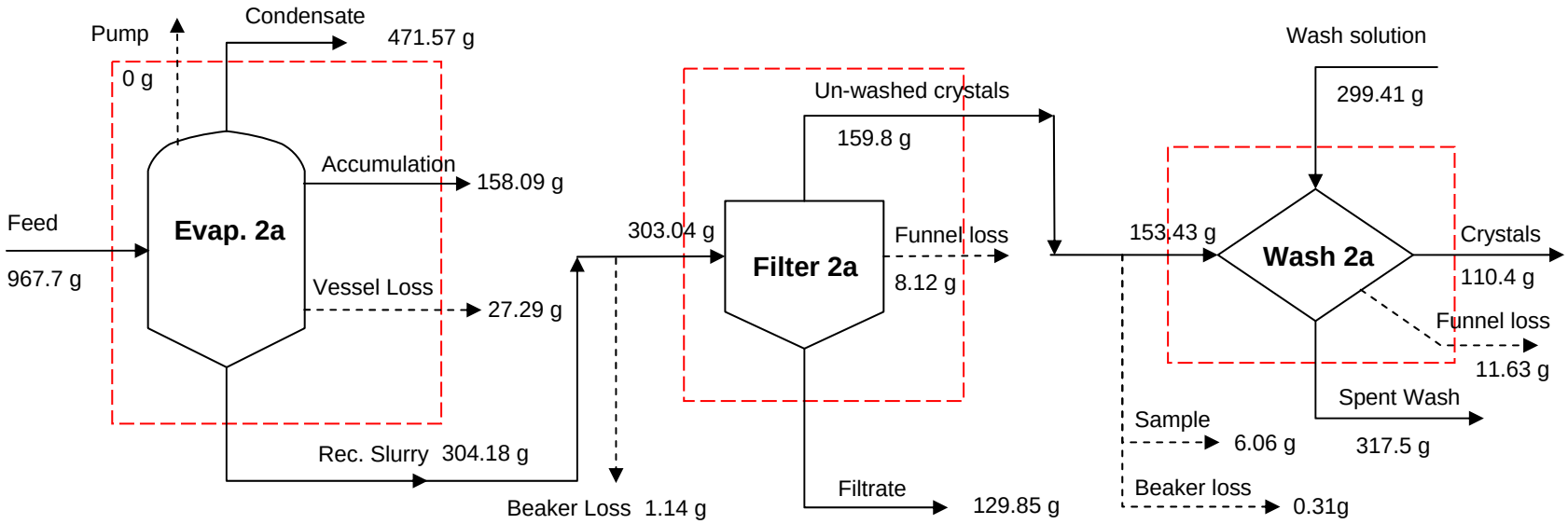

Pump	Mass of the condensate collected in the cold trap protecting the vacuum pump.
Rec. Slurry	Mass of slurry recovered from the crystallizer.
Vessel Loss	Mass recovered by washing the vessel with a known amount of water.
Funnel Loss	Mass recovered by washing the funnel with a known amount of water and then drying with paper of a known weight. Performed after the filtration and washing operations.
Beaker Loss	Mass of slurry lost in the several beakers necessary for the transfer from the vessel to the filter.
Sample	Mass collected from the un-washed crystals for chemical analysis.

Solid arrows are process streams and dotted arrows represent losses. Closure on a total mass balance was performed for each dashed box around a process unit.

Figure 32. Overall Mass Balance on Stage 2 of Run 27 (SST Late Feed Solution).

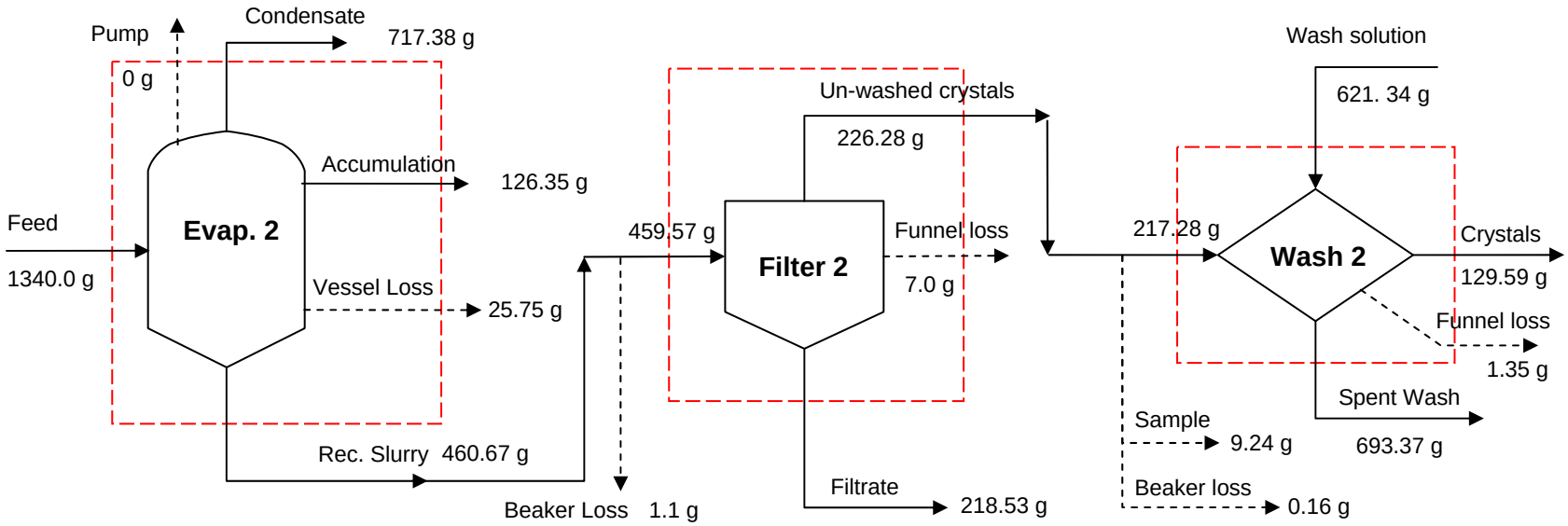

Pump	Mass of the condensate collected in the cold trap protecting the vacuum pump.
Rec. Slurry	Mass of slurry recovered from the crystallizer.
Vessel Loss	Mass recovered by washing the vessel with a known amount of water.
Funnel Loss	Mass recovered by washing the funnel with a known amount of water and then drying with paper of a known weight. Performed after the filtration and washing operations.
Beaker Loss	Mass of slurry lost in the several beakers necessary for the transfer from the vessel to the filter.
Sample	Mass collected from the un-washed crystals for chemical analysis.

Solid arrows are process streams and dotted arrows represent losses. Closure on a total mass balance was performed for each dotted box around a process unit.

Figure 33. Overall Mass Balance on Stage 2, Trial 2 of Run 27 (SST Late Feed Solution).

Table 14. Mass Balances Around Process Units of Run 27 (SST Late Feed Solution).

Unit	Input (g)	Output (g)	Difference (g)	% Closure of Mass Balance
Evaporator 1	5698.37	5693.95	4.42	0.08
Filtration 1	1801.58	1769.55	32.03	1.78
Washing 1	761.14	743.51	17.63	2.32
Evaporator 2a	967.70	961.13	6.57	0.68
Filtration 2a	303.04	297.77	5.27	1.74
Washing 2a	452.84	439.53	13.31	2.94
Evaporator 2	1340.00	1330.15	9.85	0.74
Filtration 2	459.57	451.81	7.76	1.69
Washing 2	838.62	824.31	14.31	1.71

Streams from SST Late Feed Solution Stage 2a were used in chemical analyses.

3.2.3 CHARACTERIZATION OF CRYSTAL PRODUCT

Polarized Light Microscopy. Samples of crystals removed from the slurry produced in each stage were examined using polarized light microscopy (PLM). Images obtained from the examinations are given in Figure 34. From these, six different crystalline species can be identified: burkeite (Figure 34A), trisodium fluoride sulfate (the six-sided purple crystals with pyramid-like shapes in Figure 34B), sodium oxalate (the needle shapes in Figure 34C), sodium carbonate monohydrate (Figure 34C), sodium phosphate (long yellow-blue needles in Figures 34D and 34E), and sodium nitrate (Figures 34A through 34F). The simulation (SST2.BIN/SST2SIM1.xls) predicted formation of all of these crystals at the conditions of the run, except for sodium phosphate.

Sieve Analyses. A fraction of the crystals obtained at the end of Stage 1 of Run 27 was washed with acetone as described in the previous Section and allowed to air dry. The crystals were then divided into three samples of between 15 to 20 g each, and subjected to the sieving procedure described in Section 2.0. Results are shown in the histogram of Figure 35 for two of the samples.

The CSD is bimodal, with the first mode appearing at about 15 μm and the second at about 212 μm. Both modes are relatively sharp, which indicates a fairly narrow distribution around each.

The mass of crystals above 300 μm represents 12 % of the total sieved mass (obtained from a cumulative distribution). On the other hand the amount of crystals collected in the pan represents only 0.15% of the mass and is negligible.

Sieve results obtained on crystals obtained from Stage 2 of Run 27 are shown in Figure 36. The mass distribution has a single mode at about 360 μm. This size is between the 300- and 425-μm sieves, and the mass of crystals recovered in this size range represented 36% of the crystal mass.

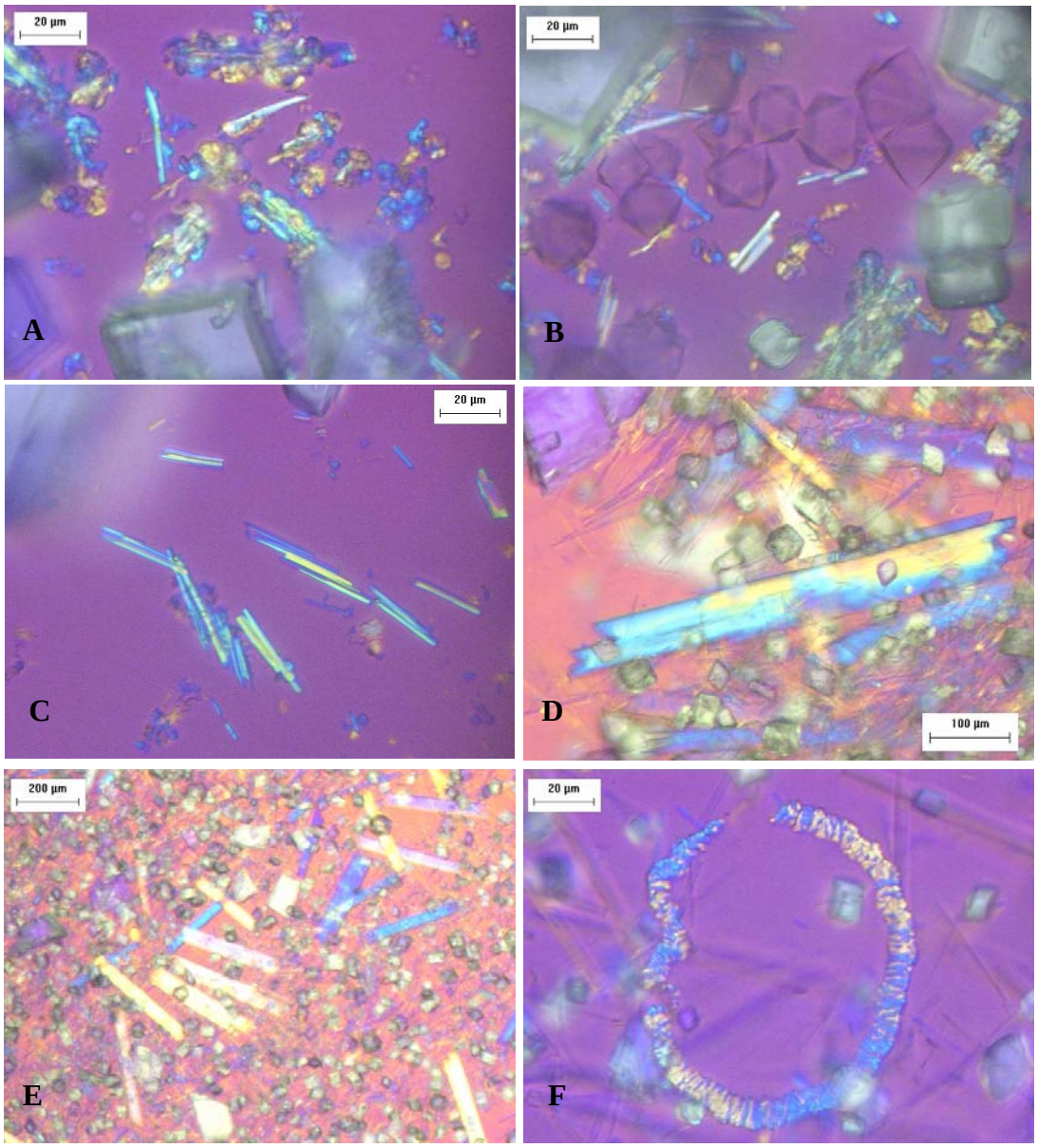

Images A through C were obtained from samples taken from the Stage 1 slurry while Images D through F were obtained from Stage 2 slurry.

Figure 34. PLM Images of the Crystals Obtained from the Certification Run (Run 27) on SST Late Feed Solution.

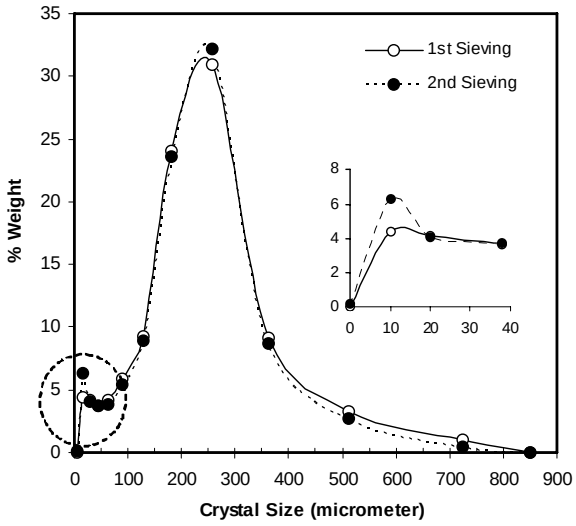

Inset is a magnification of the 0-40 μm range.

Figure 35. Sieve Analysis of Crystals from Stage 1 of Run 27.

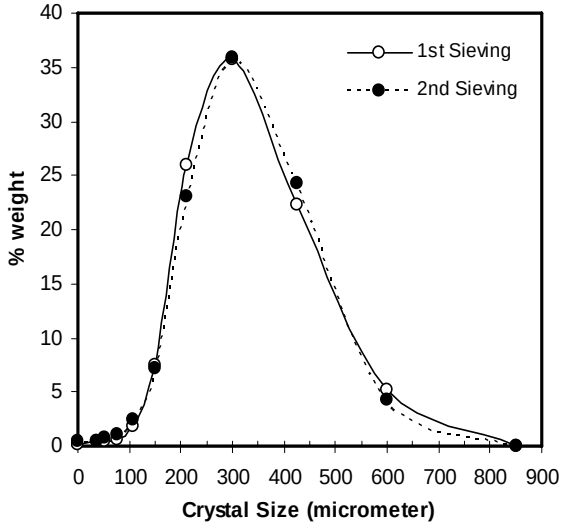

Figure 36. CSD Late Feed Second Stage.

On the one hand, the mass of crystals obtained above the size of 600 μm represents 4 % of the total sieved mass. The amount of large aggregates has then been reduced. On the other hand the amount of crystals collected in the sieves with a mesh opening lower than 100 μm represents only 10 % of the total mass. No fines have been obtained for this second stage. Hence the crystal size is definitely in the higher range size comparing to the previous run which is in agreement with an expected majority of sodium nitrate crystals and an extended growing time during the run. No fines were obtained and the amount of likely aggregates was reduced.

The mode size is expected to correspond to sodium nitrate crystals. The other crystals expected are sodium carbonate and in very low amount sodium oxalate and burkeite. However taking into account that no burkeite was observed during the stage one, and that the sodium carbonate (that were not expected for stage one) were observed, the PLM images are expected to present mainly sodium nitrate crystals.

Species Distribution. As described in Section 1.0, fractional crystallization generates a product that contains several chemical species. The distribution among various size fractions of the product depends upon the interplay between the solid-liquid equilibrium and nucleation and growth kinetics of each species.

Samples from several sieves were analyzed to determine how the species formed were distributed according to size. Figure 37 shows PLM images of crystals from Stages 1 and 2 of Run 27.

Several species were identified in the product from Stage 1. PLM images were generated on three samples taken from each sieve. Those found on the sieve with the smallest opening are characteristic of the oblong shape of sodium carbonate (Figure 37A) and small rod (or prismatic) shape of sodium oxalate (Figure 37B). Note that the crystals are not broken or aggregated.

Neither sodium carbonate nor sodium oxalate crystals were observed in samples from the 106-μm sieve, although crystals of trisodium fluoride sulfate were found along with a small amount of sodium nitrate. Crystals in the vicinity of the second mode (212 μm) appear to be only sodium nitrate. Again they do not involve aggregates or broken crystals. The sodium nitrate crystals are all independent (no aggregates) which allows us to validate the sieving procedure and the CSD (See Figure 37D). The largest sieve mainly had particles that were agglomerates. Burkeite was not found in samples from any of the sieves.

Crystals in the vicinity of the mode from the second stage (350 μm) show nicely formed sodium nitrate crystals (See Figure 37E and 37F.). There were no agglomerates or broken crystals in the observations.

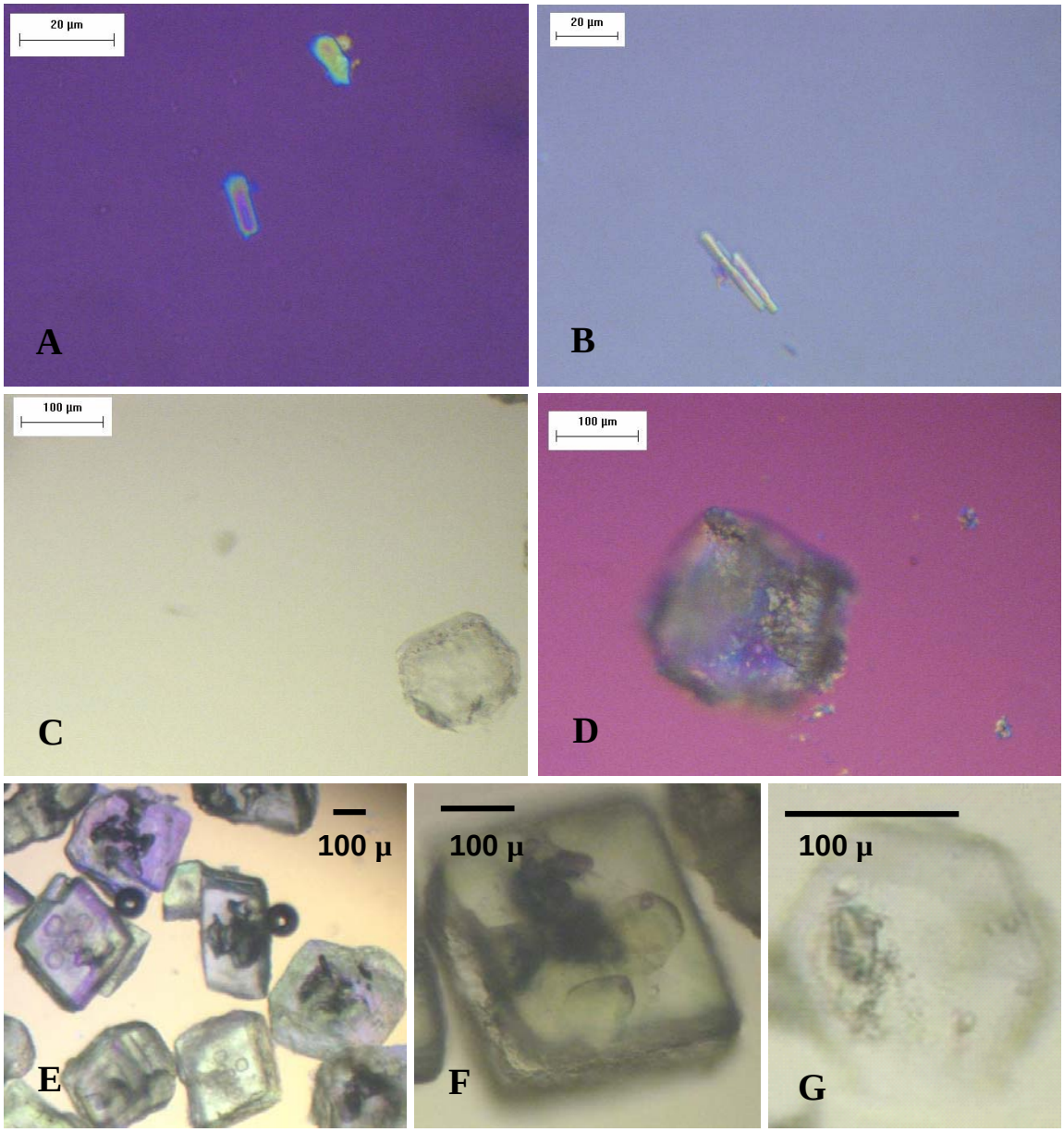

Crystals in Panel A and B were removed from the 106-µm sieve used in the sieve analysis from Stage 1 and appear to be sodium carbonate and sodium oxalate, respectively. Crystals in Panels C and G are trisodium fluoride sulfate, while those in D, E, and F are sodium nitrate.

Figure 37. PLM Images of Crystals from Stages 1 and 2 of Run 27.

3.2.4 SPECIES ANALYSES AND BALANCES

Figures 31, 32, and 33 illustrate the accounting associated with the total mass entering and leaving Stage 1 and both trials of Stage 2. These have been used as the basis for the balances on total mass that are illustrated in Figure 38 for Run 27, which is the Certification Run for SST Late Feed Solution. It should be noted that the second trial of Stage 2 provided the data included in Figure 38. Table 15 shows the stream values, but it also identifies the amount of sodium nitrate and sodium carbonate that entered the system with the wash solution. (Recall that this solution was near saturation with respect to these two solutes so as to reduce the dissolution of crystals in the filter cake. This was justified by recognizing that it more closely represented a continuous operation.)

The results of the balances on total mass show that 101.6 g were lost in Stage 1, but that 47.6 g could be accounted for using the methods described in Section 2.0. This meant that the unaccounted for loss was 54.0 g; another way of saying this is that the balance on total mass was closed to within 0.9%. Addressing Stage 2 (trial 2): there was a loss of 80.0 g, of which 25.4 were unaccounted for; in other words the total mass balance closed to within 2.0%. Similar results were obtained and are shown for the initial Stage 2 trial.

Samples of each stream were obtained and sent to Galbraith Laboratories for chemical analyses (Appendix H). The samples were of the feed solution, filtrate, spent wash, unwashed crystals, washed crystals, and accumulation. All samples except for the final crystals were sent for analysis in liquid form in order to give a homogeneous sample. Results obtained from Galbraith were tabulated in a spreadsheet and the mass of each ionic species was calculated at each sample point in the process.

Table 16 gives inputs, outputs, and closures of mass balances around the entire process for each species. Details of the stage-wise species mass balances are given in Tables 17 and 18. For species analysis it was assumed that the total amount of filtrate from Stage 1 was used as feed for Stage 2. In reality, only a portion of the filtrate from Stage 1 was used as the feed for Stage 2. It was also assumed that the relative amounts of each output stream in Stage 2 would remain constant when using the total filtrate from Stage 1.

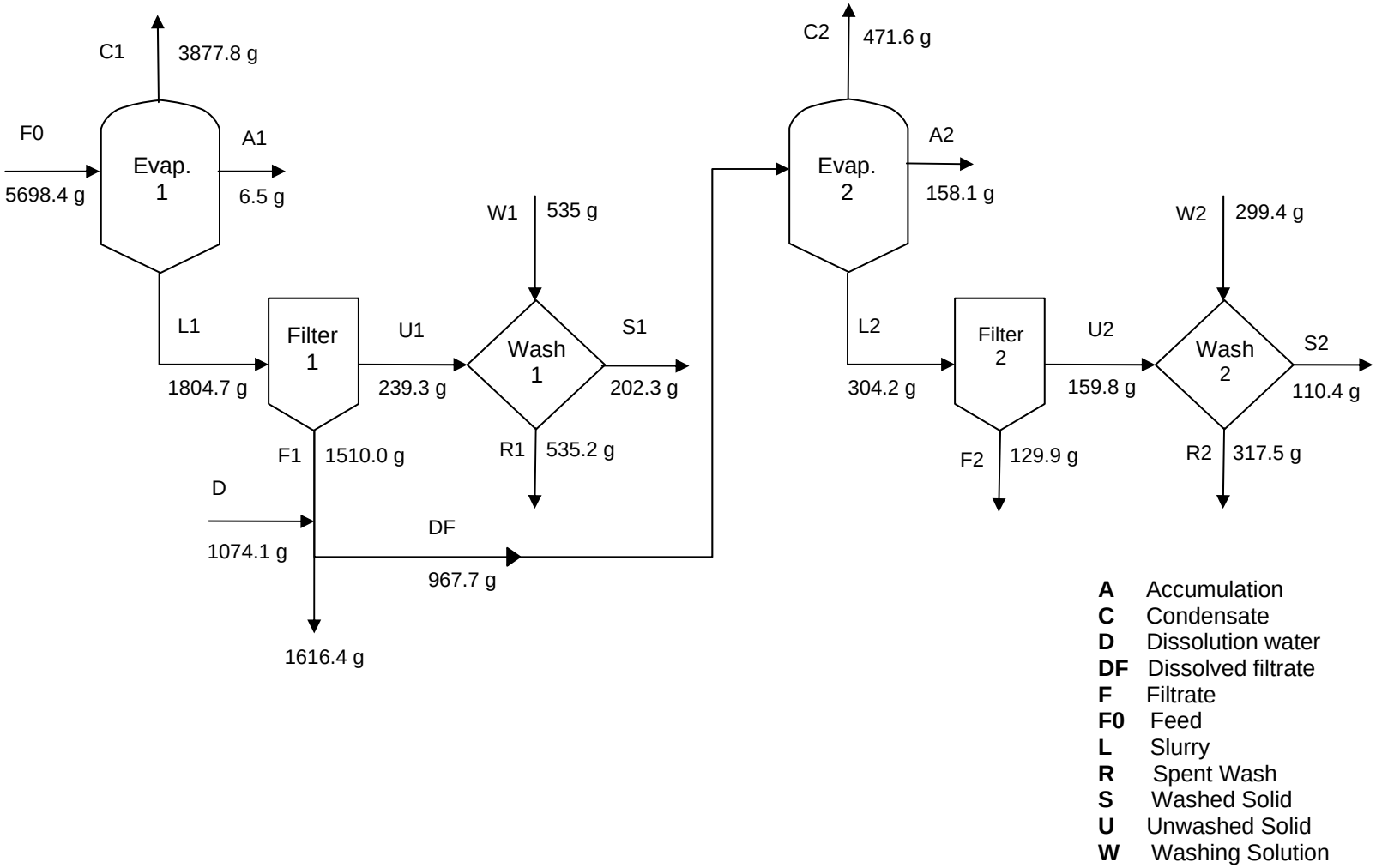

Figure 38. Balances on total Mass for Each Process Unit in Run 27.

Values for Stage 2 come from Trial 2.

Table 15. Balances on Total Mass for Each Unit in Run 27 (SST Late Feed Solution).

Stage 1	**Input (g)**		**Output (g)**					**Loss (g)**
Species	**Feed**	**Wash**	**Cond**	**Washed Solids**	**Filtrate**	**Spent Wash**	**Accum.**	
Late Feed	5698.4							
H_2O		283.1	3877.8					
Na_2CO_3		49.1						
$NaNO_3$		202.8						
Solution				202.3	1510.0	535.2	6.5	
Total	5698.4	535.0	3877.8	202.3	1510.0	535.2	6.5	101.6
Combined	6233.4		6131.8					101.6
						% Loss		1.6%
						Accounted loss (g)		47.6
						% Corrected Loss		0.9%

Stage 2a (trial 2)	**Input (g)**		**Output (g)**					**Loss (g)**
Species	**Feed**	**Wash**	**Cond**	**Washed Solids**	**Filtrate**	**Spent Wash**	**Accum.**	
Filtrate stage 1	565.5							
H_2O	402.2	162.6	471.6					
Na_2CO_3		36.7						
$NaNO_3$		100.1						
Solution				110.4	129.9	317.5	157.8	
Total	967.7	299.4	471.6	110.4	129.9	317.5	157.8	80.0
Combined	1267.1		1187.1					80.0
						% Loss		6.3%
						Accounted loss (g)		54.6
						%Corrected Loss		2.0%

Stage 2(trial 1)	**Input (g)**		**Output (g)**					**Loss (g)**
Species	**Feed**	**Wash**	**Cond**	**Washed Solids**	**Filtrate**	**Spent Wash**	**Accum**	
Filtrate stage 1	783.0							
H_2O	557.0	347.6	717.4					
Na_2CO_3		73.3						
$NaNO_3$		200.4						
Solution				129.6	218.5	693.4	126.4	
Total	1340.0	621.3	717.4	129.6	218.5	693.4	126.4	76.0
Combined	1961.3		1885.3					76.0
						% Loss		3.9%
						Accounted loss (g)		44.6
						%Corrected Loss		1.6%

Table 16. Species Mass Balances for SST Late Feed Solution Run 27.

Species	Input (g)	Output (g)	Closure (%)
Cs^{+}	1.01E-03	9.62E-04	4.4
Na^{+}	498.61	476.84	4.4
Al^{3+}	6.60	6.23	5.6
CrO_4^{2-}	10.12	9.56	5.5
F^{-}	10.60	11.06	– 4.4
NO_2^{-}	16.53	15.17	8.2
NO_3^{-}	828.48	825.96	0.3
PO_4^{3-}	23.78	21.16	11.0
SO_4^{2-}	79.96	73.43	8.2
$C_2O_4^{2-}$	4.32	4.11	4.9
CO_3^{2-}	152.17	148.18	2.6
H_2O	6463.81	6191.97	4.2
OH^{-}	11.94	8.05	32.6

Table 17 Species Mass Balances for SST Late Feed Solution Run 27 Stage 1.

Stage 1	Input (g)		Output (g)					Closure
Species	**Feed**	**Wash**	**Condensate**	**Filtrate**	**Spent Wash**	**Crystals**	**Accumulation**	**%**
Cs^{+}	1.01E-03	0	0	1.14E-03	2.84E-05	7.92E-06	3.43E-06	-16.9
Na^{+}	307.66	76.16	0	231.27	75.99	58.30	2.10	4.2
Al^{3+}	6.60	0	0	6.12	0.16	0.13	0.01	2.7
CrO_4^{2-}	10.12	0	0	9.80	0.24	0.09	0.02	-0.3
F^{-}	10.60	0	0	0.04	0.17	10.00	0.59	-1.8
NO_2^{-}	16.53	0	0	15.20	0.36	0.11	0.05	5.0
NO_3^{-}	485.45	147.97	0	455.45	151.97	27.82	0.33	-0.3
PO_4^{3-}	23.78	0	0	21.87	0.89	1.50	0.04	-2.2
SO_4^{2-}	79.96	0	0	7.73	2.58	60.56	2.62	8.1
$C_2O_4^{2-}$	4.32	0	0	0.63	0.13	2.74	0.06	17.8
CO_3^{2-}	68.97	27.78	0	48.32	26.78	20.19	0.11	1.4
H_2O	4672.43	283.08	3877.78	703.67	275.58	20.62	0.53	1.6
OH^{-}	11.94	0	0	9.92	0.31	0.20	0.01	12.5

Table 18. Species Mass Balances for SST Late Feed Solution Run 27 Stage 2.

Stage 2	Input (g)			Output (g)					Closure
Species	**Filtrate 1**	**Dilution**	**Wash**	**Cond**	**Filtrate**	**Spent Wash**	**Crystals**	**Accumulation**	**%**
Cs^{+}	1.14E-03	0	0	0	4.80E-04	1.53E-04	2.35E-05	2.67E-04	18.8
Na^{+}	231.27	0	114.80	0	51.49	119.49	78.62	90.84	1.6
Al^{3+}	6.12	0	0	0	3.17	0.85	0.27	1.65	3.2
CrO_4^{2-}	9.80	0	0	0	5.06	1.41	0.21	2.54	5.9
F^{-}	0.039	0	0	0	0.020	0.061	0.072	0.159	-706.6
NO_2^{-}	15.20	0	0	0	8.06	2.27	0.10	4.23	3.5
NO_3^{-}	455.45	0	195.06	0	69.31	211.67	167.34	197.50	0.7
PO_4^{3-}	21.87	0	0	0	5.71	4.24	2.06	6.72	14.4
SO_4^{2-}	7.73	0	0	0	4.10	1.15	0.19	2.22	0.9
$C_2O_4^{2-}$	0.63	0	0	0	0.50	0.14	0.03	0.51	-88.2
CO_3^{2-}	48.32	0	55.42	0	14.14	55.44	17.67	13.86	2.5
H_2O	703.67	1074.10	434.20	1259.27	181.71	450.94	27.24	98.30	8.8
OH^{-}	9.92	0	0	0	3.58	0.14	0.98	2.82	24.1

3.2.5 COMPARISON TO MINIMUM AND DESIRED TARGETS

As described in Section 2.0, Stage 2 was operated using only a fraction of the total filtrate produced in Stage 1. In the calculations to evaluate the approach to the process criteria, the mass balances shown in Tables 16, 17, and 18 were scaled as if all of the filtrate had been used in the process. This is a standard approach for scaling up or scaling down process flowsheets (Felder and Rousseau). Specifically, the sodium balance for Stage 2 sodium was scaled according to the amount of filtrate from Stage 1 that was used to feed Stage 2. It was also assumed that the sodium collected in the accumulation from each stage would be found as crystal mass in an ideal process. Results of these calculations are given in Table 19 and show that the sodium recovery was 74.7%, which significantly exceeds the minimum target.

Table 19. Sodium Balance and Recovery for SST Late Feed Solution Run 27.

Stream	Unit Value (g)	Totals (g)
Input		307.66
Crystals/Stage 1	58.30	
Accum/Stage 1	2.10	
Crystals/Stage 2	78.62	
Accum/Stage 2	90.84	
Output		229.86
Recovery		74.7%

Cesium activity was calculated directly from the chemical analyses performed by Galbraith Laboratories on the washed crystals obtained from Stages 1 and 2. Table 20 shows the analytical results for sodium and cesium and the calculated activities expected for dissolution of each of the filter cakes and for the combined filter cakes. It is assumed that 20% of the cesium in Hanford waste is in the form of ^{137}Cs, and that the activity of ^{137}Cs is 86.58 Ci/g. As shown, the values for the combined solids is significantly better than the minimum value of 0.05 Ci/L and

even exceeds the desired target of 0.0012 Ci/L. The estimated decontamination factor associated with blending the two products of washed crystals from Stages 1 and 2 is 14.8. This value is above both the minimum and desired value of 14 given in Section 1.6

Table 20. Compositions of Washed Crystals from SST Late Feed Solution Run 27 with Estimated Activities and Decontamination Factors.

	mass (g)	wt % Na	Ppm Cs	Ci/L	DF
Stage 1	202.26	30.9	0.042	0.0007	24.5
Stage 2	294.79	25.8	0.077	0.0015	11.2
Combined	497.05	27.88	0.063	0.0011	14.8

The sulfate-to-sodium molar ratio in the filtrate streams from Stages 1 and 2 were calculated using the relative amounts of the two ions in the filtrate streams as determined by Galbraith Laboratories. The results given in Table 21 show the minimum requirement of 0.01 mole sulfate ion per mole sodium ion as matched in this run.

Table 21. Compositions of Filtrate Streams from SST Late Feed Solution Run 27 and Associated Sulfate-to-Sodium Molar Ratio.

	wt % Na	wt% SO4	molar ratio sulfate:sodium
Stage 1	15.32	0.51	0.0080
Stage 2	14.85	1.18	0.0191
Combined	15.22	0.64	0.0100

3.3 SCALE DOWN EARLY FEED CERTIFICATION RUN

The Certification Run was performed using a feed solution that had been prepared according to procedures provided by CH2M HILL (Geniesse, Herting and Nelson, 2006). The procedures led to formulation of a feed solution having the composition given in Table 22.

Table 22. New composition of SST Early Feed Solution.

Chemical	MW	Intended Molarity
$NaAlO_2 \cdot 2H_2O$	118.0	0.26
NaOH	40.0	0.62
Na_2CO_3	106.0	0.61
$Na_2C_2O_4$	134.0	0.01
KNO_3	101.1	0.02
$NaNO_3$	85.0	3.26
$NaNO_2$	69.0	0.51
Na_2SO_4	142.0	0.13
$Na_3PO_4 \cdot 12H_2O \cdot 0.25NaOH$	390.1	0.05
NaCl	58.4	0.07
NaF	42.0	0.01
$Na_2Cr_2O_7 \cdot 2H_2O$	298.0	0.02
$CsNO_3$	194.9	0.005 g/L

3.3.1 OPERATING CONDITIONS

The two-stage crystallization was conducted using the 300-mL crystallizer for Stage 1 and the 100-mL crystallizer for Stage 2. The procedures followed in performing the crystallizations were outlined in Section 2.0. Each stage was operated under a constant evaporation-rate profile, as shown in Figure 39.

The evaporation rate was controlled by varying the temperature difference between the heating medium and the slurry. This was done by adjusting the temperature of the heating fluid

and the pressure of the vessel. In the Stage 1 of the certification run, vapor was generated at a rate of 26 g/h by setting the temperature of the heating fluid to 77 °C and adjusting the pressure in the crystallizer during the run, so that the slurry temperature stabilized at 66 °C. Evaporation proceeded at these conditions for over 30.5 h, at which time the target condensate-to-feed mass ratio was achieved (see Appendix D). The ending condensate ratio for the first stage was 0.481, close to the target ratio of 0.474 given by the batch simulation from COGEMA, Inc. (EARLY_FEED_FINAL_LABORATORY_FLOWSHEET.xls).

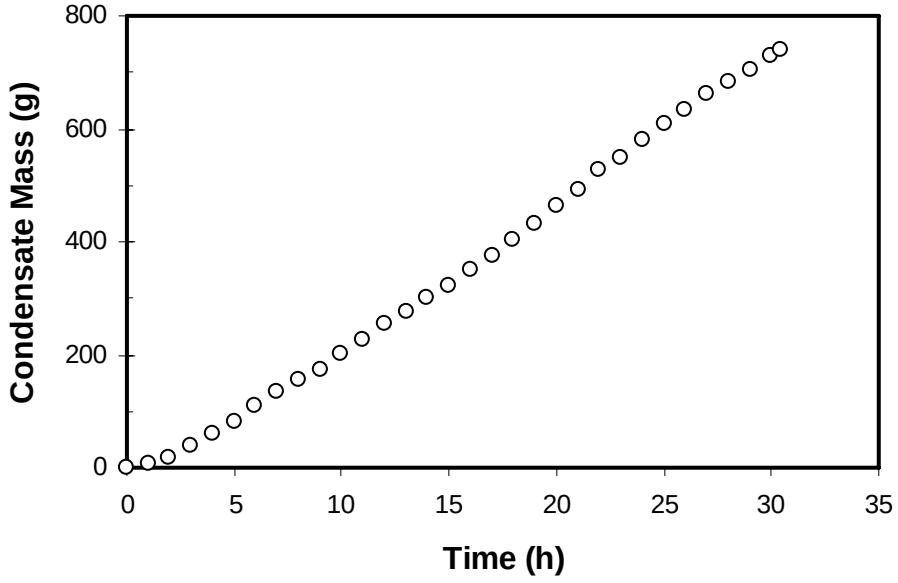

Figure 39. Mass of Condensate Generated as a Function of Run Time for Stage 1 of Run 38b (SST Early Feed).

Temperature and pressure profiles for Stage 1 of Run 38b are presented in Figure 40. Throughout the run the temperature was controlled to within +/- 1 ^{o}C of the target value of 66 ^{o}C. The pressure profile displays the step-wise changes in vacuum level, which corresponds to adjustments in the regulating valve.

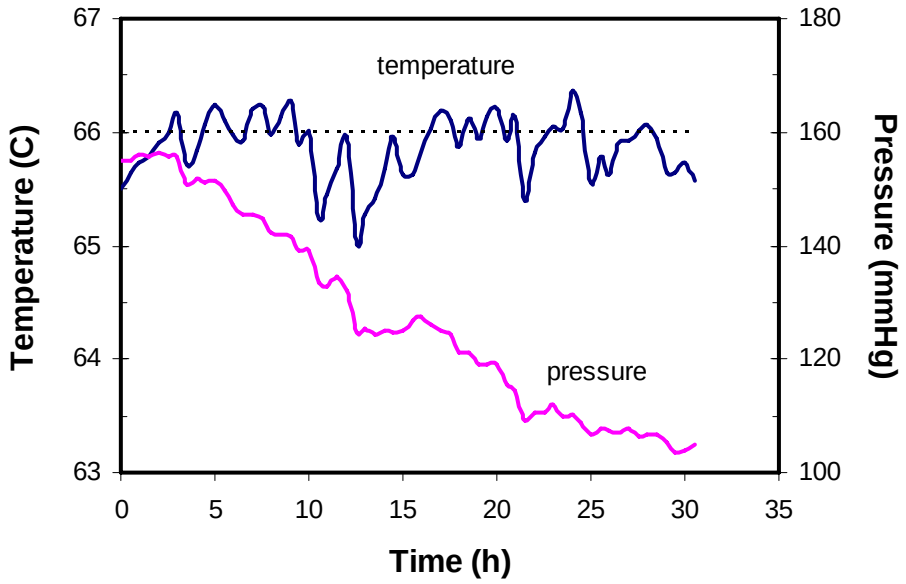

Figure 40. Temperature and pressure profiles for Stage 1 of Run 38b. The dotted line represents the target operating temperature of 66 ^{o}C.

The filtrate from the first stage was diluted with water and used as feed for the second stage. The target condensate-to-feed ratio from the above-cited simulation was adjusted to 0.627 in order to account for the dilution water added. Because the volume of the second-stage crystallizer was 100 mL and the run was performed under constant feed addition, all the diluted filtrate was required for its operation. The evaporation rate for Stage 2 followed the same pattern as was used for Stage 1; but with a constant evaporation rate of 39 g/h, as shown in Figure 41. Evaporation proceeded at these conditions for over 12.9 h, at which time the target condensate-to-feed mass ratio was achieved. The slurry temperature during the run was 66ºC and the actual condensation ratio achieved was 0.626.

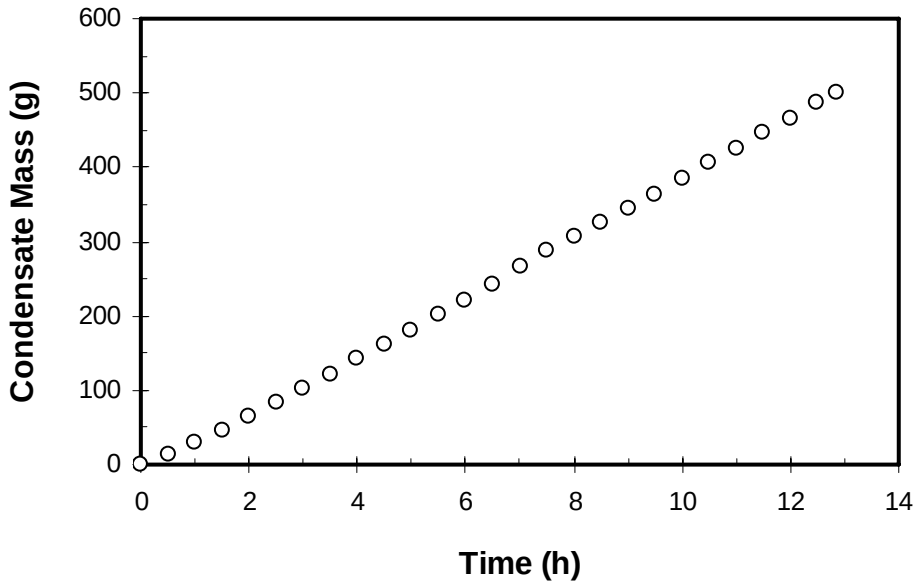

Figure 41. Mass of Condensate Generated as a Function of Run Time for Stage 2 of Run 38b (SST Early Feed).

Temperature and pressure profiles from Stage 2 of Certification Run 38b are presented in Figure 42. Except for an unexplained excursion at around 7 h, the temperature was controlled to within ± 1 ^{o}C of the target value of 40 ^{o}C. The pressure profile reflects the step-wise changes in vacuum associated with manual adjustments of the regulating valve.

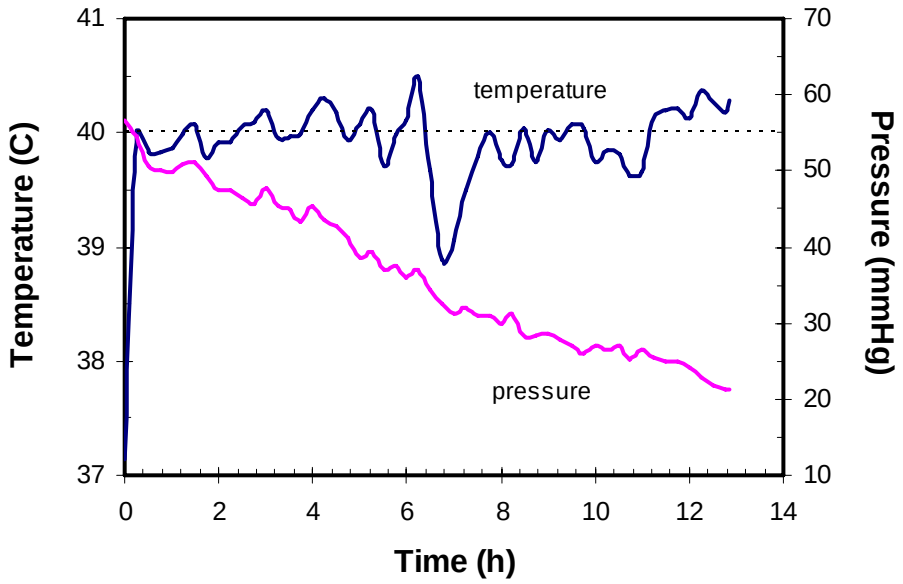

Figure 42. Temperature and pressure profiles for Stage 2 of Run 38b. The dotted line represents the target operating temperature of 40 ^{o}C.

3.3.2 BALANCES ON TOTAL MASS

The means used to satisfy mass balances were described in Section 2.0. The objectives of this process are (1) to determine the fate of species entering the process, and (2) to use mass balances to identify potential problems with the operating procedures. The mass balance procedure was modified for the runs following the Early Feed Run 34, as the unwashed solids were not removed from the process previous to washing and their mass was not measured.

Figure 43 is a schematic diagram illustrating the results of the overall mass balance around Stage 1 of Run 38b. Included in the figure are definitions of quantities used in closing mass balances around each of the units. As shown in Table 23, the difference between input and output for each of these units was as follows: evaporation, 0.13%; filtration and washing, 0.47%. Since the unwashed solids mass was not measured, a mass balance around the combined

filtration-washing step was performed along with a mass balance closure around the evaporation unit.

Stage 1. Evaporative crystallization in Stage 1 is represented schematically in Figure 43. The figure shows the masses of vapor generated and either recovered in the condensate receiver or the cold trap protecting the vacuum pump, crystals that accumulated on the walls of the vessel, material that adhered to the vessel and was lost in the transfer process, and the recovered slurry.

The slurry recovered from the evaporative crystallization was filtered as shown schematically in Figure 43. The unwashed crystals correspond to the mass of solids recovered at the end of the filtration and estimated by performing a mass balance closure around the filtration unit. The filtrate is the mass of filtrate collected inside the vacuum flask, and the funnel loss corresponds to the loss recovered after filtration and crystal washing by washing the filtration funnel with a known amount of water and using a dry paper of known mass to collect the water accumulated on the wall of the apparatus.

The unwashed crystals were washed as shown schematically in Figure 43. The unwashed crystals mass was not determined since the unwashed crystals were not removed from the process, but an estimate of this mass was determined by the means of mass balance closure around the filtration unit. The final crystals, spent wash, and funnel loss are as defined.

Stage 2. Figure 44 is a schematic diagram of Stage 2 of Run 38b. The process unit functioned as described in the discussion of Stage 1, and the methods of closing total mass balances also were the same. The results of these analyses are shown in Table 23.

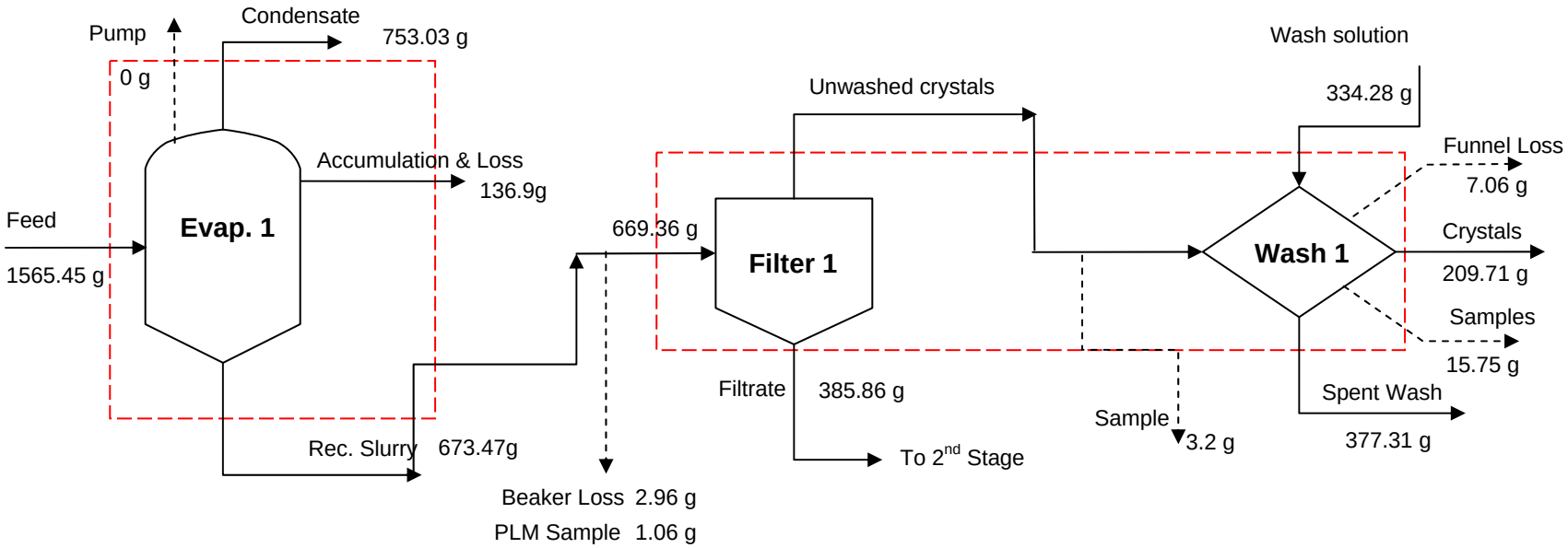

Pump	Mass of the condensate collected in the cold trap protecting the vacuum pump.
Rec. Slurry	Mass of slurry recovered from the crystallizer.
Accumulation & Loss	Mass recovered by washing the vessel with a known amount of water.
Funnel Loss	Mass recovered by washing the funnel with a known amount of water and then drying with paper of a known weight. Performed after the filtration and washing operations.
Beaker Loss	Mass of slurry lost in the beaker necessary for the transfer from the vessel to the filter.
Sample	Mass collected from the unwashed crystals or washed crystals.
PLM Sample	Mass taken from the slurry for PLM imaging.

Figure 43. Overall Mass Balance on Stage 1 of Run 38b (SST Late Feed Solution).

Solid arrows are process streams and dotted arrows represent quantified losses. Closure on a total mass balance was performed for each dashed box around a process unit.

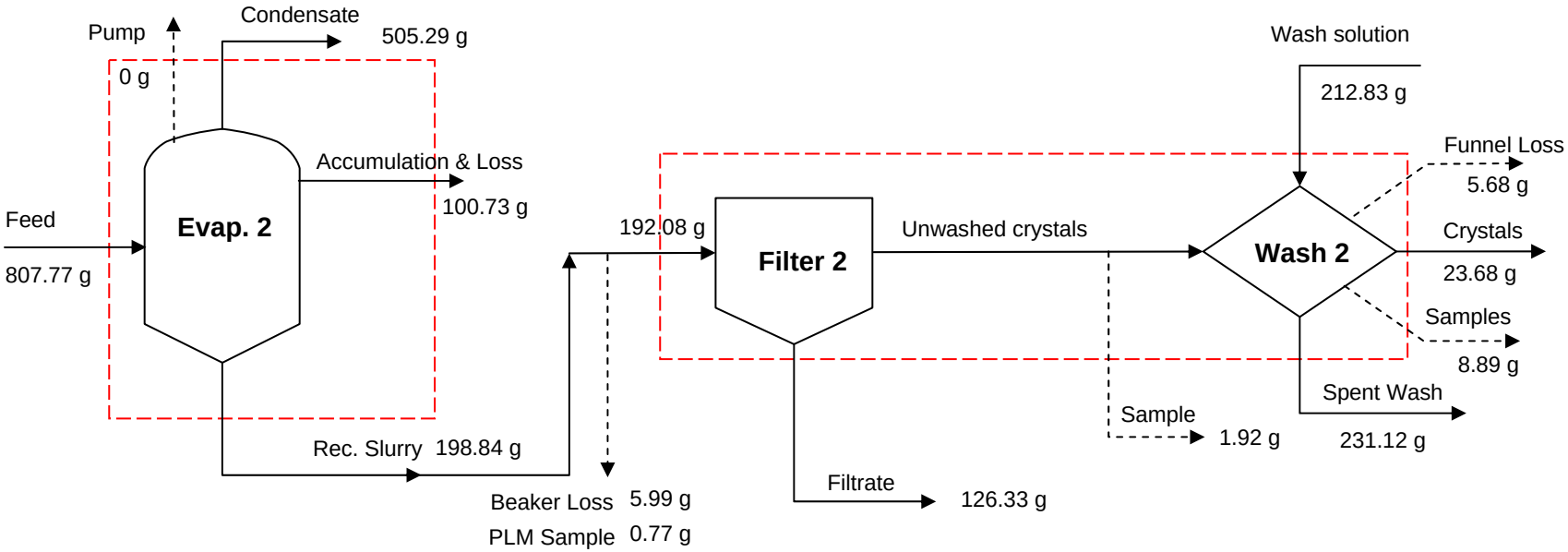

Pump	Mass of the condensate collected in the cold trap protecting the vacuum pump.
Rec. Slurry	Mass of slurry recovered from the crystallizer.
Accumulation & Loss	Mass recovered by washing the vessel with a known amount of water.
Funnel Loss	Mass recovered by washing the funnel with a known amount of water and then drying with paper of a known weight. Performed after the filtration and washing operations.
Beaker Loss	Mass of slurry lost in the beaker necessary for the transfer from the vessel to the filter.
Sample	Mass collected from the unwashed crystals or washed crystals.
PLM Sample	Mass taken from the slurry for PLM imaging.

Solid arrows are the process streams and the dotted arrows represent the quantified losses. Closure on a total mass balance was performed for each dashed box around a process unit.

Figure 44. Overall Mass Balance on Stage 2 of Run 38b (SST Early Feed Solution).

Table 23. Mass Balances Around Process Units of Run 38b (SST Early Feed Solution FY06).

Unit	Input (g)	Output (g)	Difference (g)	% Closure of Mass Balance
Evaporator 1	1565.45	1563.4	2.05	0.13
Filtration & Washing 1	1003.64	998.89	4.75	0.47
Evaporator 2	807.77	804.86	2.91	0.36
Filtration & Washing 2	404.91	397.62	7.29	1.80

3.3.3 CHARACTERIZATION OF CRYSTAL PRODUCT

Polarized Light Microscopy. Samples of crystals removed from the slurry produced in each stage were examined using polarized light microscopy (PLM). Images obtained from the examinations are given in Figures 45 and 46, for the first and second stage respectively. From Figure 45, four different crystalline species can be identified: burkeite (Figure 45B, 45C and 45F), sodium oxalate, sodium carbonate monohydrate (Figure 45C and 45E), and sodium nitrate (Figures 45A through 45H). In addition to burkeite crystals, sodium carbonate and sodium nitrate were found in large amounts, along with trace amounts of sodium sulfate and sodium oxalate crystals. Figure 45 displays also PLM images of samples taken from the unwashed crystals produced in the run. These display sodium nitrate crystals over a size range from 100 to 500 μm, while sodium carbonate monohydrate crystals had a maximum size of around 200 μm. The single burkeite crystals had a size of about 20 μm and a size range between 30 to 50 μm when presenting different sections. A trace amount of sodium sulfate was also identified. Figure 46 displays PLM images taken from the slurry of the second stage of Certification Run 38b. They show the exclusive presence of sodium nitrate in the slurry of Stage 2. The sodium nitrate crystals have different geometries and a large spread in their size range (from 10 μm to several hundreds of micrometers).

The simulation (EARLY_FEED_FINAL_LABORATORY_FLOWSHEET.xls) predicted formation of all of these crystals at the conditions of the run.

Sieve Analyses. A fraction of the crystals obtained at the end of Stage 1 of Run 38b was washed with acetone as described in the previous Section and allowed to air dry. The crystals were then divided into three samples of 15 g each and subjected to the sieving procedure described in Section 2.0. Results are shown in the histogram of Figures 47 and 48.

These samples gave nearly identical results, and they display a mode size around 350 μm. In addition, the curves show that only 5% of the crystal mass is below 75 μm. This mass is expected to correspond mostly to burkeite, since these crystals were observed in PLM images and are typically grown to small sizes. The distribution is relatively narrow and gives a coefficient of variation of 34.7%, where

$$CV = \frac{100(d_{84\%} - d_{16\%})}{2d_{50\%}} \qquad \text{(E-5)}$$

Appendix I gives details on the coefficient of variation calculation for the first stage of Run 38b.

Figures 47 and 48 present a comparison of the CSDs obtained from the first stages of Run 38b and practice Run 37, an Early Feed run realized under very similar conditions. Figure 47 shows the reproducibility of the CSD results; both curves have the same mode size and nearly the same spread. Figure 48 shows the cumulative mass distributions, which highlight the fact that Run 37 produced slightly larger crystals.

Sieve results obtained on crystals obtained from Stage 2 of Run 38b are shown in Figures 49 and 50. The CSD displays a mode size around 500 μm. In addition, the curve shows that less than 5% of the crystal mass is below 100 μm. Consistent with the PLM images in Figure 46, the

curve is expected to be comprised of only sodium nitrate crystals. The distribution is relatively narrow and gives a coefficient of variation of 36.6 %, where

$$CV = \frac{100(d_{84\%} - d_{16\%})}{2d_{50\%}}$$

Figure 50 shows the cumulative mass distribution from Stage 2 of Run 38b. It highlights the fact that a relatively small mass of fines and relatively large crystals were produced.

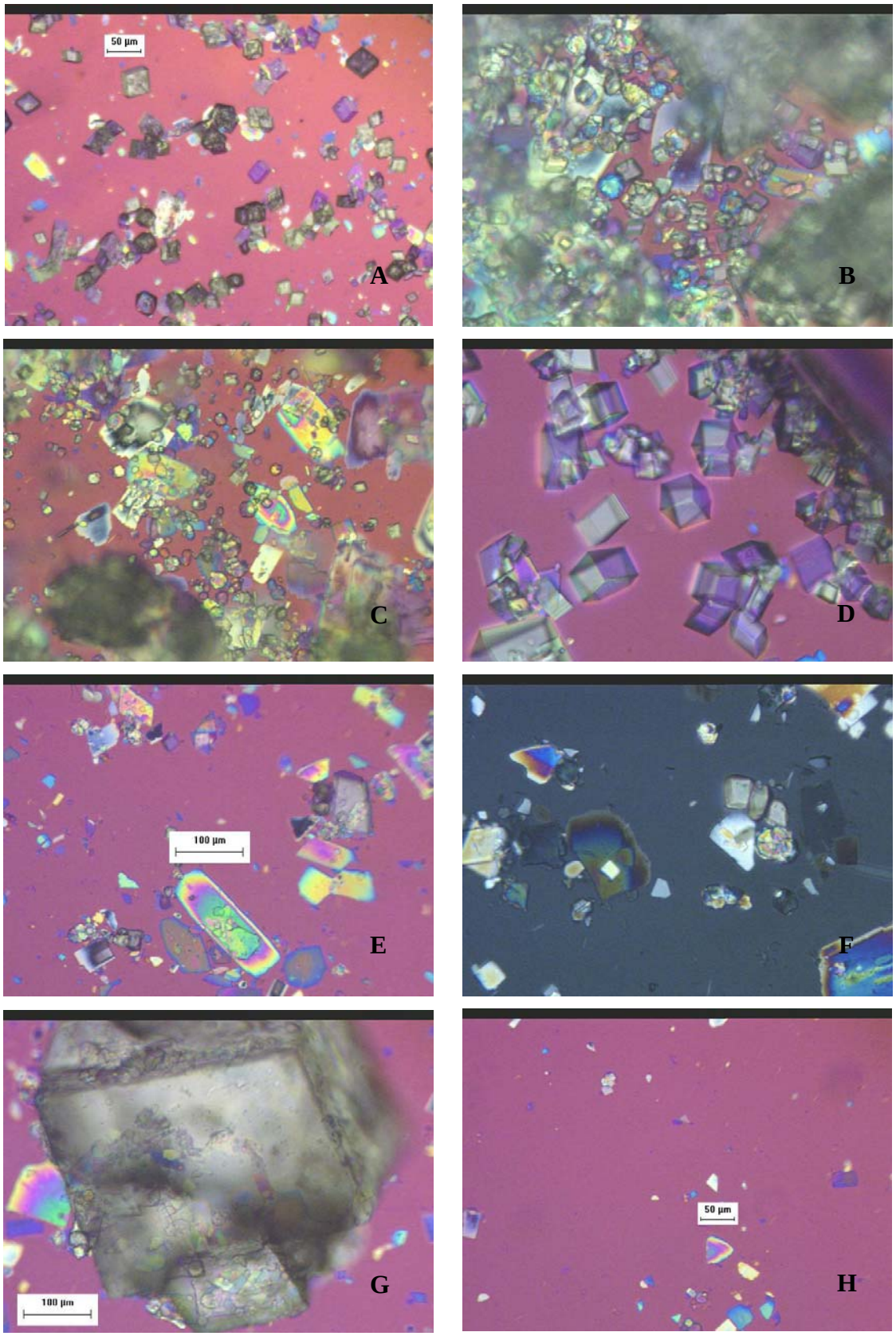

Figure 44. PLM Images of the Crystals Obtained from the First Stage Slurry and unwashed crystals of Certification Run 38b on SST Early Feed Solution.

Images A through D were obtained from samples taken from the Stage 1 slurry while Images E through H were obtained from Stage 1 unwashed crystal sample.

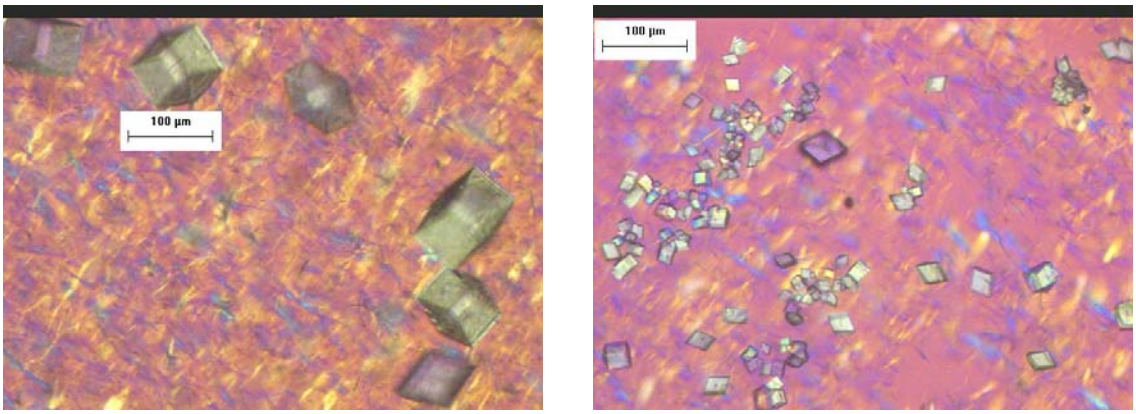

Figure 46. PLM Images of the Crystals Obtained from the Second Stage Slurry of Certification Run 38b on SST Early Feed.

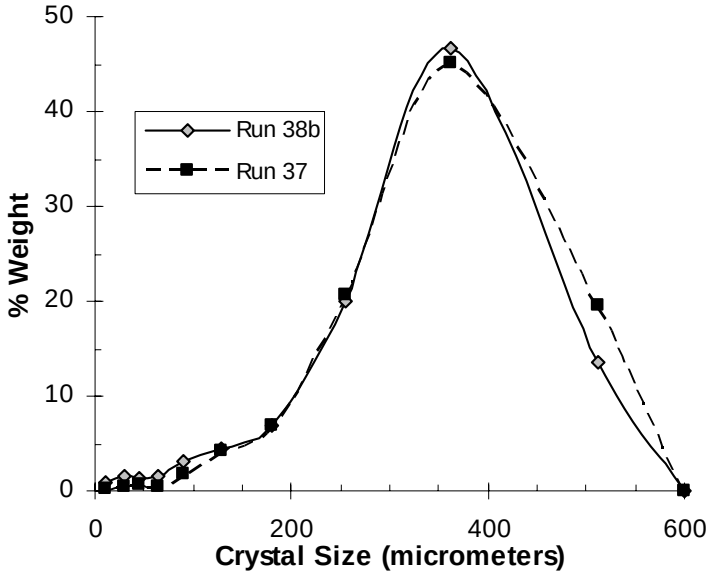

Figure 47. Sieve Analysis of Crystals from Stage 1 of Run 38b.

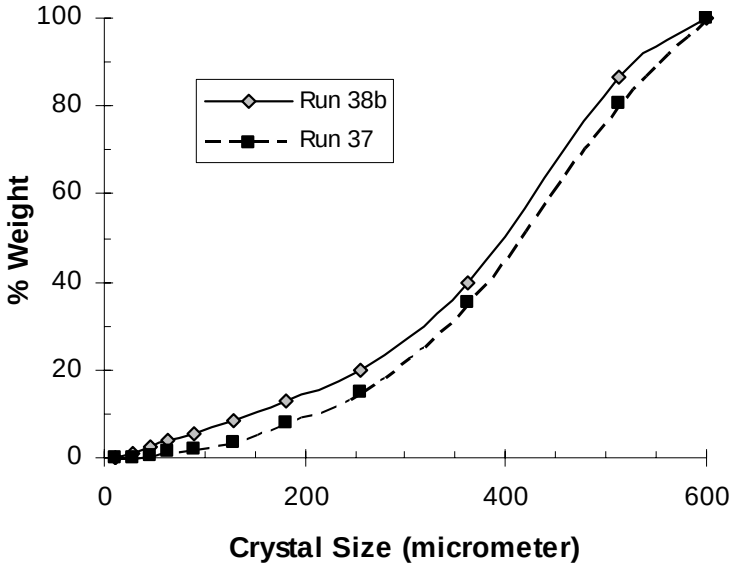

Figure 48. Cumulative Distribution of Crystals from Stage 1 of Run 38b.

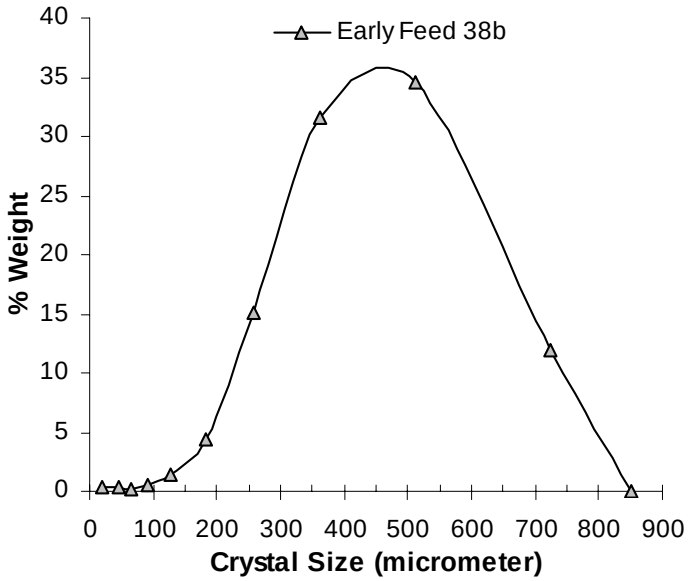

Figure 49. Sieve Analysis of Crystals from Stage 2 of Run 38b.

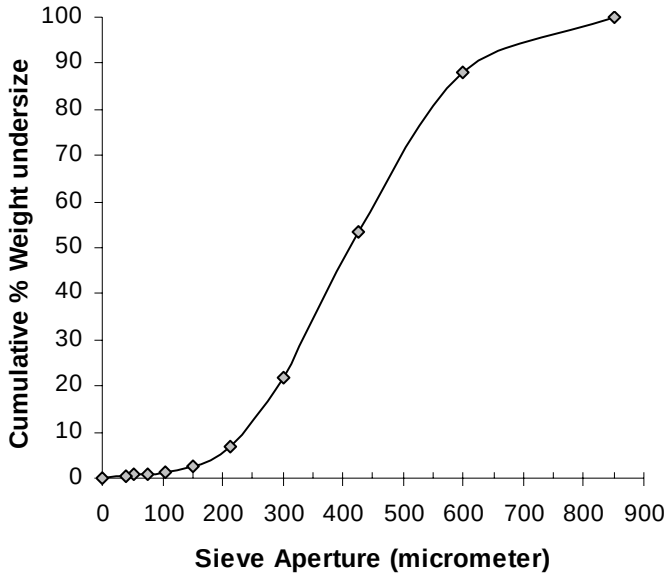

Figure 50. Cumulative Distribution of Crystals from Stage 2 of Run 38b.

Species Distribution. As described in Section 1.0, fractional crystallization generates a product that contains several chemical species. The distribution among various size fractions of the product depends upon the interplay between the solid-liquid equilibrium and nucleation and growth kinetics of each species.

Samples from several sieves were analyzed to determine how the species formed were distributed according to size. Figures 51 and 52 shows selected PLM images of crystals from Stage 1 of Run 38b.

Several species were identified in the product from Stage 1. PLM images were generated on three samples taken from each sieve. Those found on the sieve with the smallest opening are characteristic of the oblong shape of sodium carbonate (Figure 51A and 51B), the round shape of burkeite crystals (Figure 51A) and small rod (or prismatic) shape of sodium oxalate. Note that the crystals are not broken or aggregated. Sodium carbonate monohydrate (Figure 51C and 51D) and burkeite crystals (Figure 51C) are the only crystals observed in the vicinity of the first mode (30 μm). The irregularity, potentially considered as a second mode, observed in the 50-150 μm

size range appeared to be mainly composed of sodium carbonate crystals associated to burkeite agglomerates around the 50 μm bound (Figure 51E), and sodium nitrate crystals around the 150 μm bound (Figure 51F). Only trace amount of sodium carbonate were observed in samples from the 150-212μm sieve, and no sodium oxalate crystals were observed from the 20-38 μm sieve. Crystals in the vicinity of the second mode (350 μm) appear to be only sodium nitrate. Again they do not involve aggregates or broken crystals. The sodium nitrate crystals are all independent (no aggregates) which allows us to validate the sieving procedure and the CSD (Figure 51G). The largest sieve mainly had particles that were agglomerates. Figure 52 confirmed the presence of three different shapes or forms of burkeite crystals, which may result from three different growth mechanisms: (1) single round crystals of 20 μm, (2) heterogeneous crystals resulting from the growth of burkeite around one or more sodium nitrate or sodium carbonate crystals, and (3) subdivided burkeite crystals resulting from single crystal growth, agglomeration, and association. Another important remark is the high proportion of heterogeneous burkeite crystals in the crystalline population.

Crystals in the vicinity of the mode from the second stage (500 μm) show nicely formed sodium nitrate crystals. There were no agglomerates or broken crystals in the observations.

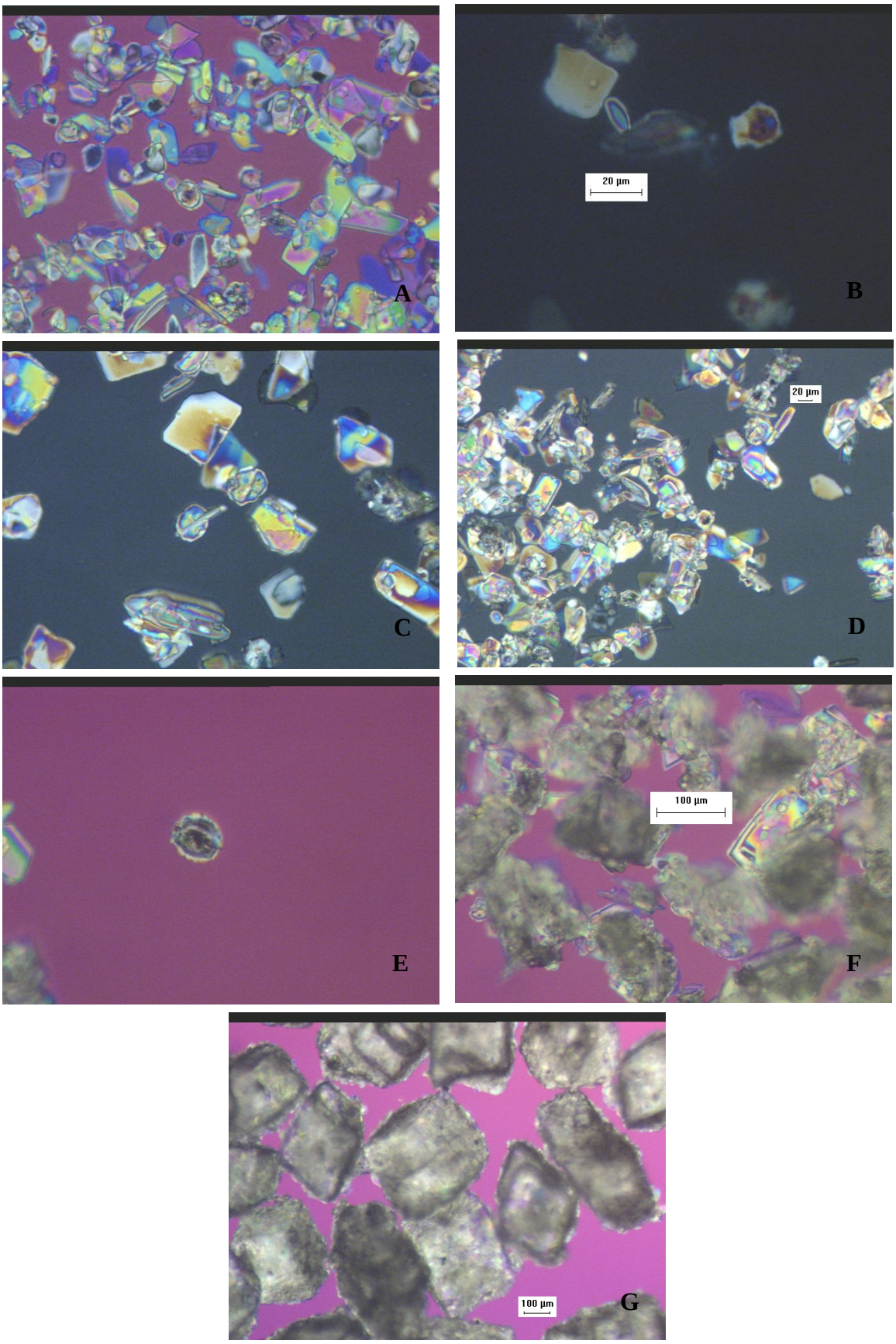

Figure 51. PLM Images of Sieved Crystals from Stage 1 of Run 38b.

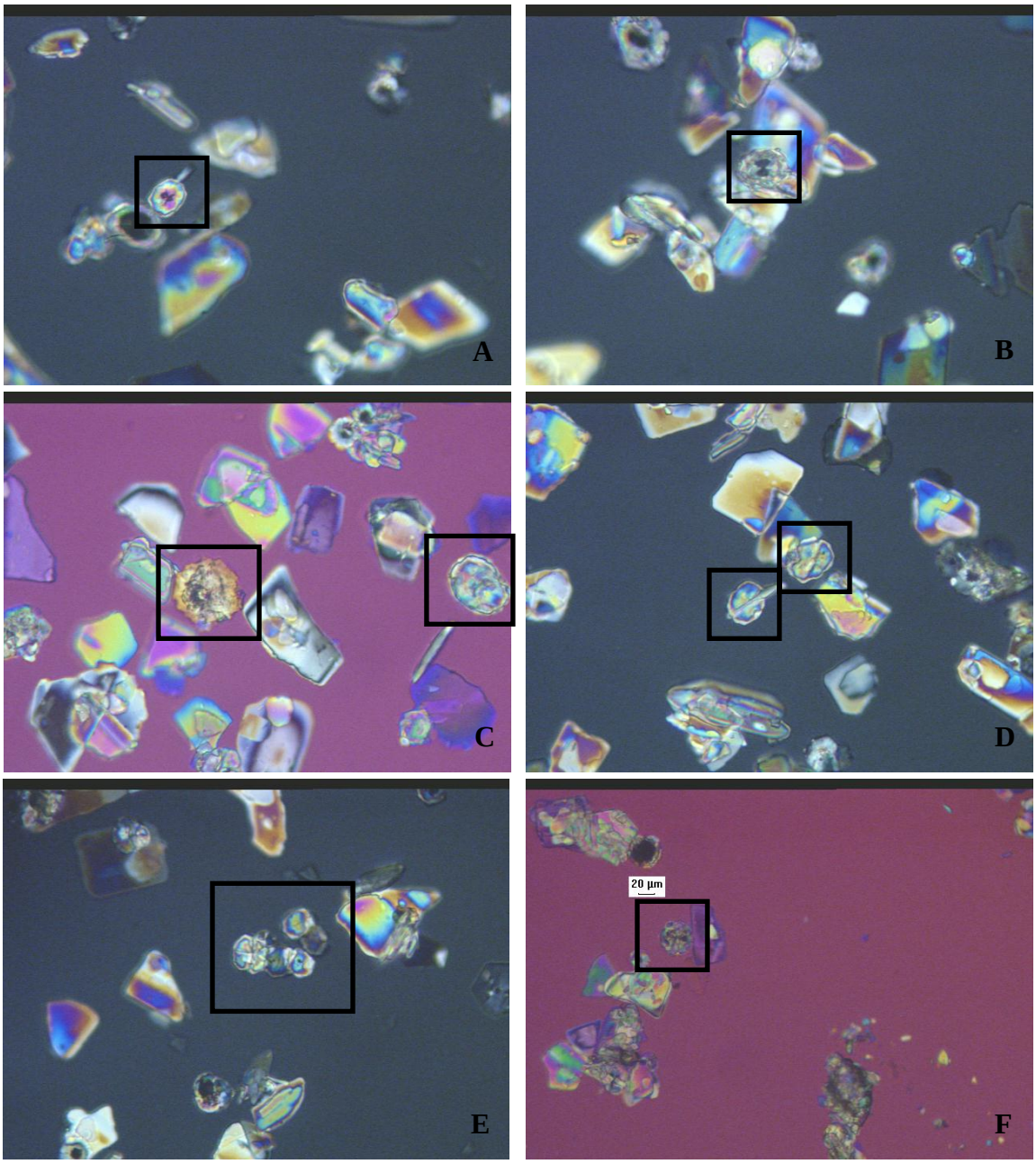

Figure 52. PLM Images of Sieved Burkeite Crystals from Stage 1 of Run 38b.

Crystals in panel A and B are heterogeneous burkeite crystals, presenting more likely nuclei of sodium nitrate and carbonate monohydrate as inclusion. Crystals in panel C are two different morphologies of burkeite crystals. Crystals in panels D and E are single homogenous burkeite crystals and "flower like" habit of burkeite agglomerate, while panel F displays a random shape agglomerate of burkeite crystals.

3.3.4 SPECIES ANALYSIS AND MASS BALANCES

Figures 43 and 44 illustrate the accounting associated with the total mass entering and leaving Stage 1 and Stage 2. These have been used as the basis for the balances on total mass that are illustrated in Figure 53 for Run 38b, which is the Certification Run for the SST Early Feed Solution FY06. Table 24 shows the stream values.

The results of the balances on total mass show that 36.92 g were lost in Stage 1, but that 28.47 g could be accounted for using the methods described in Section 2.0. This meant that the unaccounted for loss was 8.45 g; another way of saying this is that the balance on total mass was closed to within 0.4%. Addressing Stage 2: there was a loss of 33.45 g, of which 10.9 were unaccounted for; in other words the total mass balance closed to within 1.0%.

Samples of each stream were obtained and sent to GTRI Laboratories for chemical analyses (Appendix J). The samples were of the feed solution, filtrate, spent wash, wash solution, unwashed crystals, washed crystals after each wash, and accumulation. All samples were sent for analysis in liquid form in order to give a homogeneous sample. Results obtained from GTRI were tabulated in a spreadsheet and the mass of each ionic species was calculated at each sample point in the process.

Table 25 gives inputs, outputs, and closures of mass balances around the entire process for each species. Details of the stage-wise species mass balances are given in Tables 26 and 27. Note that the final and sample crystals are combined under the appellation “crystals” in Tables 26 and 27. The cesium value displayed in this column was hence not the one used for the calculation of the decontamination factor.

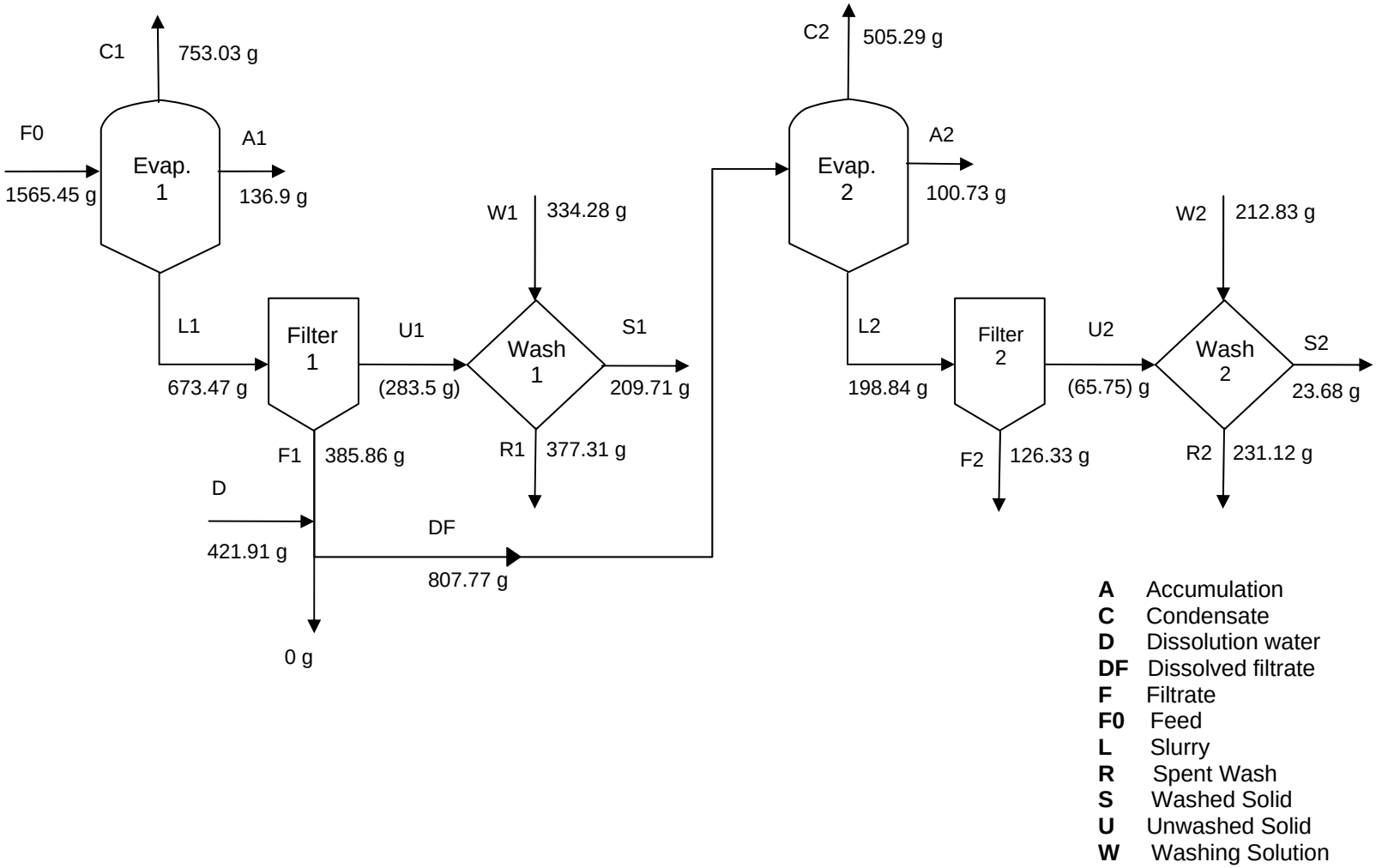

Figure 53. Balances on total Mass for Each Process Unit in Run 38b.

Table 24. Balances on Total Mass for Each Unit in Run 38b (SST Early Feed Solution).

Stage 1	**Input (g)**		**Output (g)**					**Loss (g)**
Species	**Feed**	**Wash**	**Cond**	**Washed Solids**	**Filtrate**	**Spent Wash**	**Accum.**	
Early Feed	1565.45							
H_2O			753.03					
Na_2CO_3								
$NaNO_3$								
Solution		334.28		209.71	385.86	377.31	136.9	
Total	1565.45	334.28	753.03	209.71	385.86	377.31	136.9	36.92
Combined	1899.73		1862.81					36.92
						% Loss		1.9%
						Accounted loss (g)		28.47
						% Corrected Loss		0.4%

Stage 2	**Input (g)**		**Output (g)**					**Loss (g)**
Species	**Feed**	**Wash**	**Cond**	**Washed Solids**	**Filtrate**	**Spent Wash**	**Accum**	
Filtrate stage 1	352.62							
H_2O	455.15		505.29					
Na_2CO_3								
$NaNO_3$								
Solution		212.83		23.68	126.33	231.12	100.73	
Total	807.77	212.83	505.29	23.68	126.33	231.12	100.73	33.45
Combined	1020.6		987.15					33.45
						% Loss		3.2%
						Accounted loss (g)		23.25
						%Corrected Loss		1.0%

Table 25. Species Mass Balances for SST Early Feed Solution Run 38b.

Species	Input (g)	Output (g)	Closure (%)
Al	11.9	10.8	9.4
Cr	2.35	2.28	3.0
Cs	4.93E-03	3.49E-03	29.3
SO_4	18.6	13.1	29.9
P	2.50	1.85	26.0
Na	343.7	308.3	10.3

Table 26. Species Mass Balances for SST Early Feed Solution Run 38b Stage 1.

Stage 1	Input (g)		Output (g)					Closure
Species	**Feed**	**Wash**	**Condensate**	**Filtrate**	**Spent Wash**	**Crystals**	**Accumulation**	**%**
Al	11.9	0	0	9.72	1.86	4.82E-02	1.12	-7.2
Cr	2.35	0	0	1.94	0.39	1.52E-02	0.26	-11.4
Cs	4.93E-03	0	0	2.95E-03	1.40	1.76E-05	3.98E-04	21.5
SO_4^{2-}	18.6	0	0	1.10	0.71	6.44	4.51	29.6
P^-	2.50	0	0	1.59	0.38	1.42E-02	0.23	11.3
Na	234.8	65.6	0	84.0	78.1	76.9	41.7	6.6

Table 27. Species Mass Balances for SST Early Feed Solution Run 38b Stage 2.

Stage 2	Input (g)			Output (g)					Closure
Species	**Filtrate 1**	**Dilution**	**Wash**	**Condensate**	**Filtrate**	**Spent Wash**	**Crystals**	**Accumulation**	**%**
Al	8.89	0	0	0	4.66	1.22	4.69E-02	1.15	20.3
Cr	1.78	0	0	0	0.95	0.26	9.55E-03	0.25	17.3
Cs	2.70E-03	0	0	0	1.51E-03	4.52E-04	1.55E-05	3.68E-04	13.0
SO_4^{2-}	1.01	0	0	0	0.60	0.19	2.00E-02	0.14	5.8
P^-	1.45	0	0	0	0.55	0.21	1.54E-02	0.35	23.1
Na	76.7	0	39.5	0	27.5	46.7	9.76	18.0	12.2

3.3.5 COMPARISON TO MINIMUM AND DESIRED TARGET

Table 28 displays the results on the three requirements for Certification Run 38b. The values displayed are based on the chemical analysis performed by GTRI.

Table 28. Comparison of Required and Desired Outcomes to Experimental Results.

SST Early Feed	Stage	Required	Actual	Desired
Cs Decont. Factor	1	1.15	210	48
	2	1.15	66	48
	Total	1.15	162	48
Sodium Recovery	Total	50%	63.4%	90%
Sulfate-to-Sodium	1	0.01	0.0032	0.0022
	2	0.01	0.0052	0.0022
	Total	0.01	0.0037	0.0022

Table 28 shows that the sodium recovery was 63.4%, which exceeds the minimum target of 50% as given in section 1.6.

The cesium activity was calculated directly from the chemical analyses performed by GTRI on the washed crystals obtained from Stages 1 and 2. The estimated decontamination factor associated with blending the two products of washed crystals from Stages 1 and 2 is 162. This value is above both the minimum and desired value of 48 given in Section 1.6

The sulfate-to-sodium molar ratio in the filtrate streams from Stages 1 and 2 were calculated using the relative amounts of the two ions in the filtrate streams as determined by GTRI. The results given in Table 28 show a sulfate to sodium ratio of 0.0037, which exceeds the minimum requirement of 0.01 mole sulfate ion per mole sodium ion.

CHAPTER 4: SOLID PHASES IDENTIFICATION AND KINETICS

The solid phases obtained from the crystallization of the different SST solutions are composed of a great variety of crystals, mainly sodium salts. The diversity of the crystallization conditions may lead to different crystal morphologies, growth mechanisms, habits or even to new occurrences of well-known crystalline species. The following section aims to provide an overview of the crystalline species observed and identified in the solid phases of the Early and Late Feed. Crystal identification was based on two techniques: (1) polarized light microscopy applied to solid samples and (2) X-Ray Diffraction applied to sieved crystals samples. The following sections show the interaction between the different species, represented by mixed or heterogeneous crystals.

The second part of this study investigates the growth of the crystalline species by following two different approaches: (1) a descriptive approach based on microscopic observations that display the mechanisms of crystal growth, and (2) a quantitative approach that consists of a first estimate of the growth kinetics of the main species obtained from certification runs.

4.1 CRYSTALLINE SPECIES INVENTORY

4.1.1 SODIUM NITRATE

The sodium nitrate crystals were observed with six major morphologies that will be, for reason of simplicity, denoted as (1) cubic, (2) tetragonal, (3) orthorhombic, (4) triclinic, (5) trigonal and (6) monoclinic.

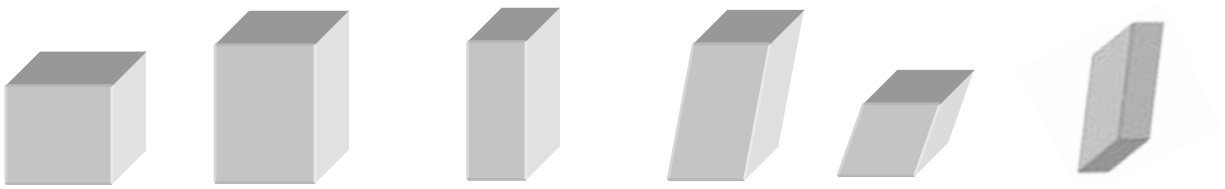

(1) Cubic (2) Tetragonal (3) Orthorhombic (4) Triclinic (5) Trigonal (6) Monoclinic

When all angles are 90 degrees and two or three of the edges have identical sizes the crystals are referred as tetragonal and cubic respectively. These two crystal shapes are presented in Figure 54.

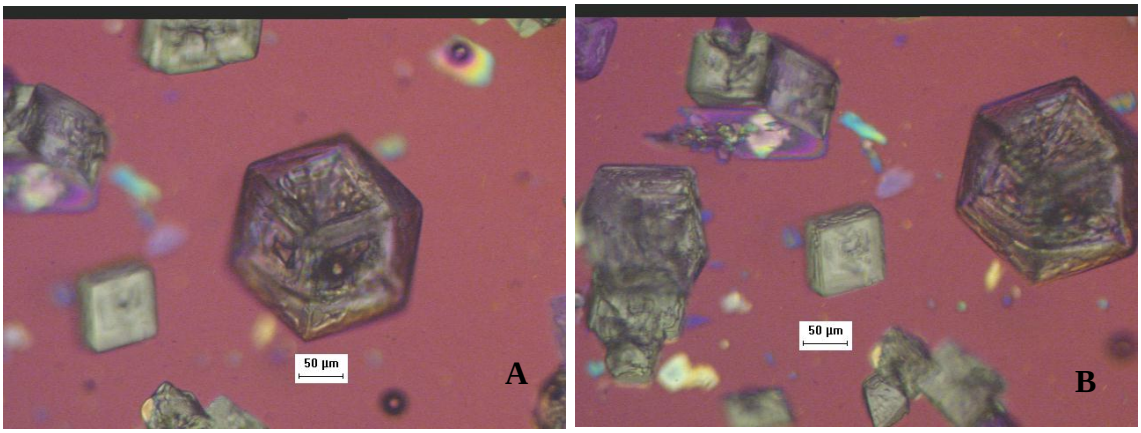

In Figure 54, panel A corresponds to cubic shape and panel B to tetragonal shape.

Figure 54. Cubic and tetragonal morphologies of sodium nitrate

The crystals presenting three different edge lengths are either orthorhombic (with all angles at 90°), triclinic (with all angles different from 90°) or monoclinic (two angles equal to

90°). The trigonal shape possesses three equal edges associated with three equal angles different from 90°. This crystalline habit is the most common representation of sodium nitrate crystals in early and late feed experiments. Figure 55 displays orthorhombic (Figure 55 A), triclinic (Figure 55B), monoclinic (Figure 55C) and trigonal (Figure 55D) sodium nitrate.

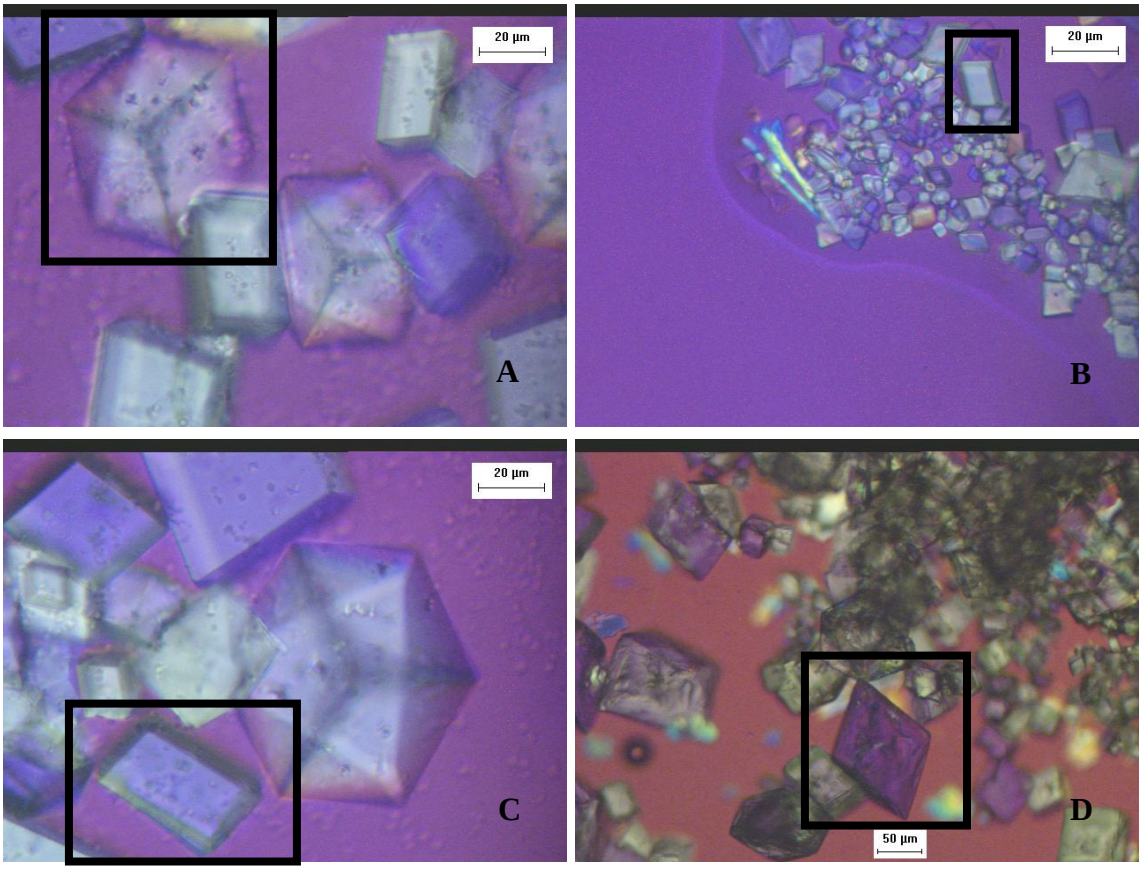

Figure 55. Orthorhombic, triclinic, monoclinic and trigonal morphologies of sodium nitrate

Two additional morphologies of the sodium nitrate crystals were observed: (1) octahedron and (2) cubo-octahedron crystals. These were obtained more rarely during Early Feed runs than the preceding shapes. Figure 56 presents selected examples of these sodium nitrate occurrences.

(7) Octahedron (8) cubo-octahedron

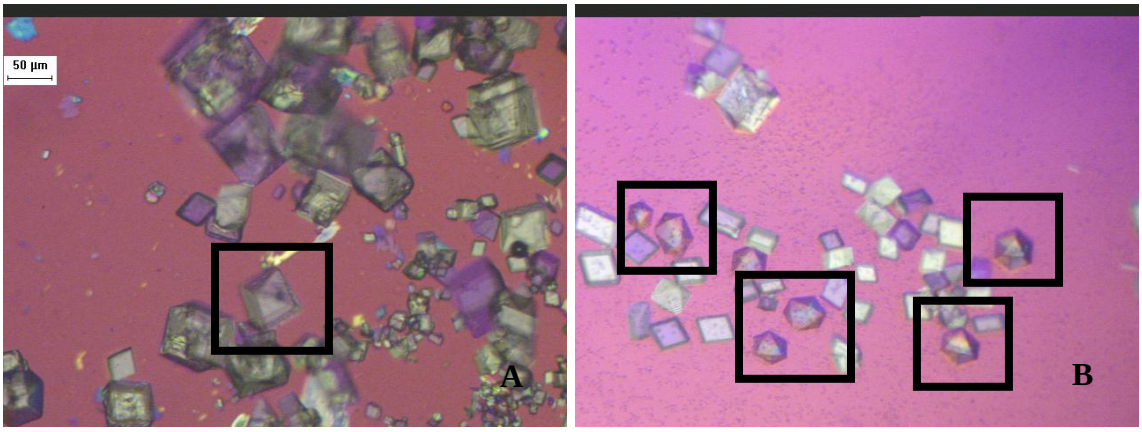

Figure 56. Orthorhombic, triclinic, monoclinic and trigonal morphologies of sodium nitrate

Two different techniques were used to characterize the solid phase in Early and Late Feed experiments as (1) PLM imaging and (2) X-Ray Diffraction. Through PLM microscopy, two main elements allowed identification of sodium nitrate crystals, as (1) the crystal extinction position and (2) the crystal size. The extinction position is defined as the relative position between the crystal and the microscope polarizer at which the crystal displays a color identical to the background. The sodium nitrate crystals are at their extinction position when placed in opposition to the polarizer. Figure 57 displays the extinction position of the sodium nitrate crystal.

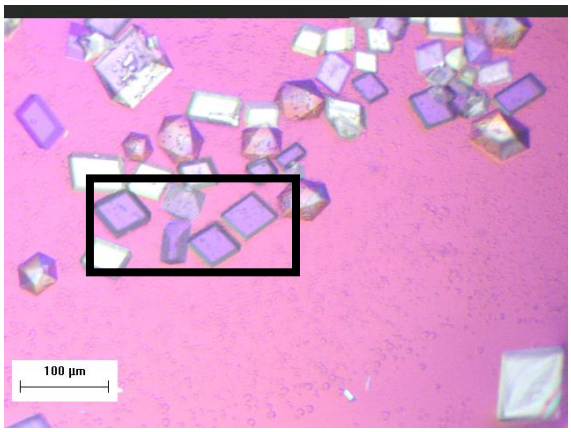

Figure 57. Orthorhombic, triclinic, monoclinic and trigonal morphologies of sodium nitrate

For this particular study (Early and Late Feed crystallization under operating conditions described in Section 3), crystal size is also an element that was used for solid phase identification. Only sodium nitrate crystals grew to sizes above 250 µm, an assertion that was validated by XRD analysis of crystals from the larger sieve sizes.

The notations used in this section correspond to observed shapes or habits and do not refer to the actual crystalline system followed by the sodium nitrate crystal. However, analyses and observations performed on the sieved crystals led to the hypothesis that sodium nitrate formed in possesses two main crystal systems under these multi-solute crystallization conditions: trigonal and cubic. All the sodium nitrate morphologies described in this section were proved to be formed by the growth along one or several edges of single trigonal or cubic nitrate.

4.1.2 SODIUM CARBONATE

Four crystalline shapes have been identified for homogenous sodium carbonate crystals as (1) prismatic “fat canoe” shape, (2) prismatic “rounded fat canoe” shape, (3) “knife” or triangular shape and (4) random rainbow colored shapes.

(1) Fat canoe (2) Rounded Fat canoe (3) Knife or Triangular

Prismatic shapes were observed with either a “fat canoe” habit or a “completely prismatic” habit. The “fat canoe” habit corresponds to a rectangular shape with rounded edges whereas the completely prismatic shape has perfectly straight edges. The edges present different lines of colors and rainbow colors go from the periphery to the center of the crystal.

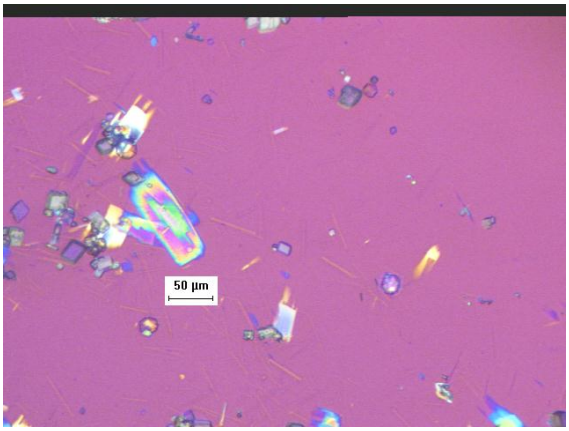

Figure 58. Prismatic shape of sodium carbonate

Four different occurrences of prismatic “fat canoe” habit were observed in the SST Early and Late Feed samples. The distinction was made based on shape and color considerations. Based on the shape, when the prismatic crystal has grown on its width it is referred to the rounded fat canoe shape (Figure 59A), whereas when it has grown on its length it is referred to the elongated fat canoe shape (Figure 59B).

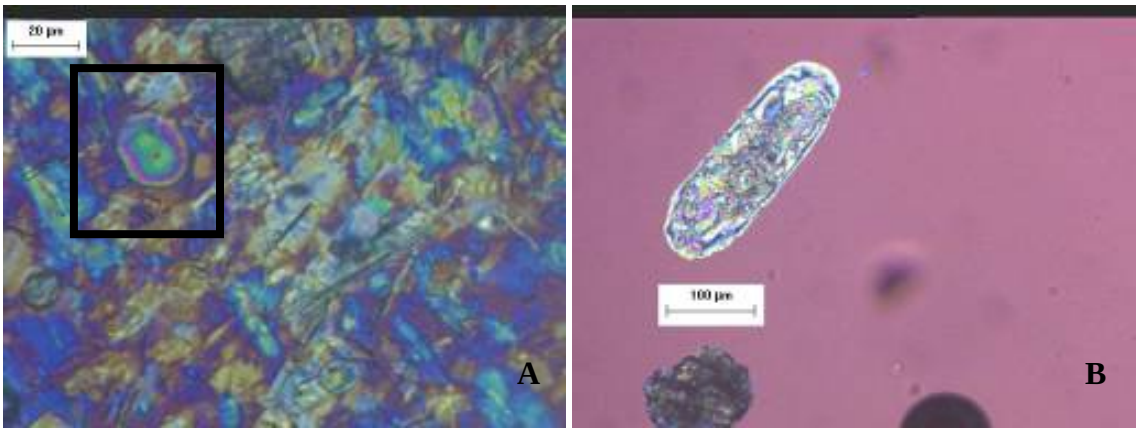

Figure 59. Prismatic shape of sodium carbonate

Based on the color, the sodium carbonate crystal might possess either one simple rainbow (Figure 60A) or two different rainbows (Figure 60B). The latest occurrence of sodium carbonate monohydrate crystals is referred as "masquerade mask" habit, and was rarely observed among the Early and Late Feed solid samples.

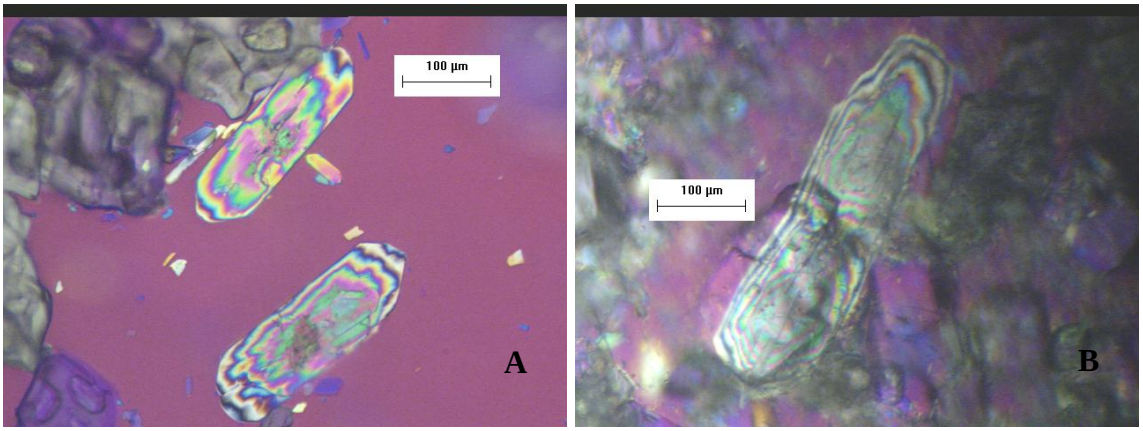

Figure 60. Prismatic shape of sodium carbonate

The last two occurrences of sodium carbonate crystals are the triangular shape and the "elongated triangular shape". The triangular shape presents rainbow colors (becoming white, grey and black when inversing the polarizer) and perfectly defined lines of colors on the edges, which exclude the possibility that this shape corresponds to the remnants of crystal breakage.

The other variation of the triangular shape sodium carbonate crystals is the elongated triangular shape. This occurrence has two straight edges and a curved one giving it the shape of a knife. From now on it will be referred as “knife habit” of sodium carbonate monohydrate crystals.

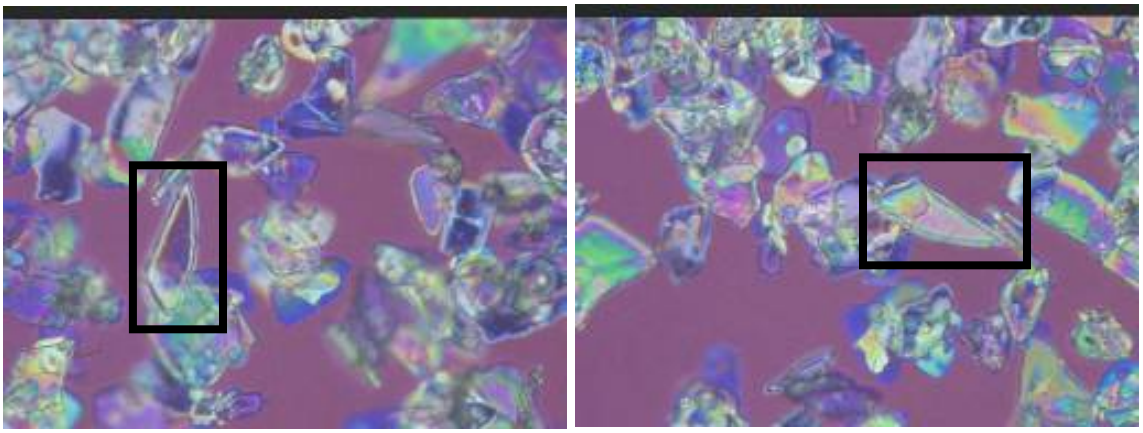

Figure 61. “Knife habit” surrounded by random shapes of sodium carbonate

The observations of the color and color changes, along with the XRD analysis confirmed the nature of these crystals as sodium carbonate monohydrate crystals. The perfectly defined edges, with different rainbow lines on each of the three sides, eliminates the possibility of crystal breakage. Sieving experiments have shown that the “knife habit” is recovered in the small size pan, on contrary to the prismatic shape that was observed with a maximum size of 250 μm. The collection of the knife habit among the random shaped carbonate, and the similarities between the “knife” and “fat canoe” morphologies suggests that the knife habit is an intermediary morphology between the random and the prismatic shape carbonate. If sieving experiments and PLM images suggest that the knife shape is likely to grow into prismatic fat canoe, the constant observation of this morphology in SST Early Feed samples and the precision of its shape suggest that it is more than a random growth of carbonate crystal.

4.1.3 BURKEITE CRYSTAL

Four main different habits of the burkeite crystals were observed as (1) a round shape single crystal (Figure 62A), (2) a round blue or yellow shape divided in several sections (Figure 62B), (3) a larger yellow and blue globular habit of burkeite (Figure 62C) and (4) the flower like habit of burkeite crystals (Figure 62D).

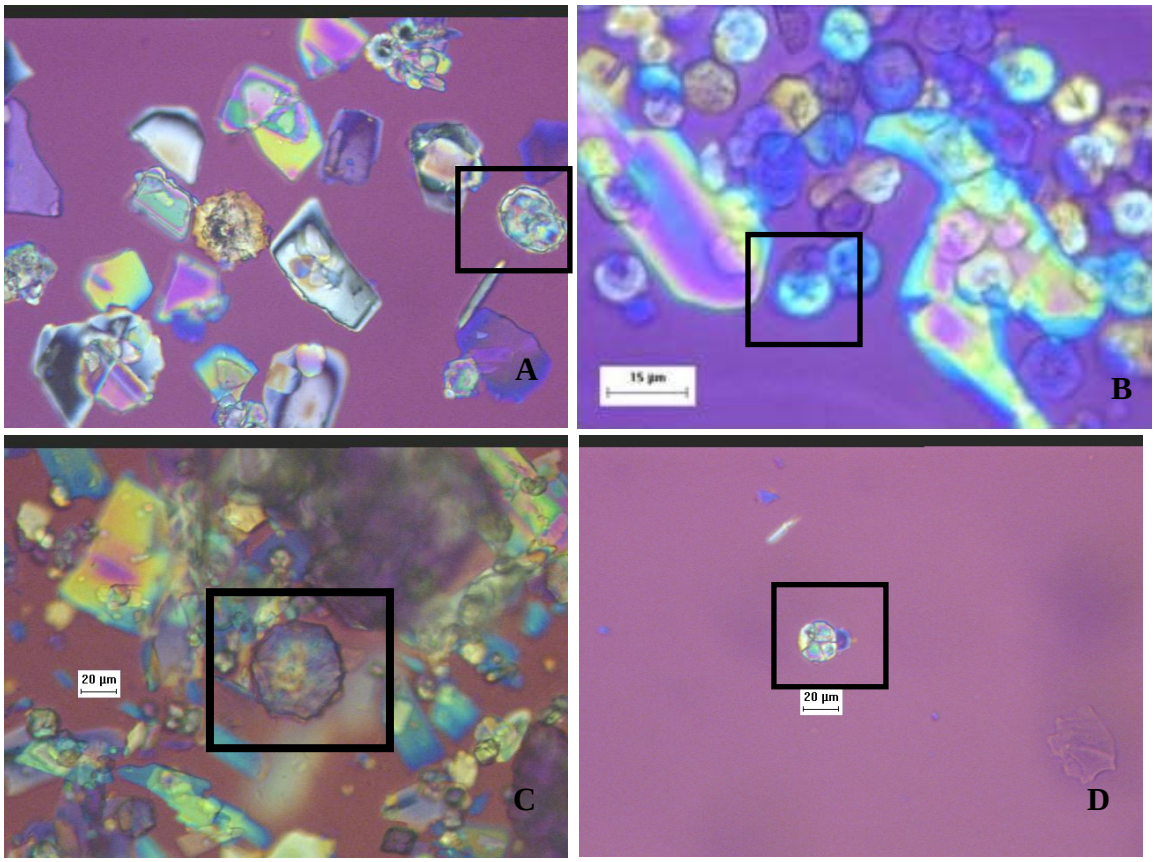

Figure 62. The Four Main Occurrences of Burkeite Crystals

The first most common representation of burkeite crystals is the single, globally round shape crystals (Figure 63A and 63B). These crystals were observed at a size ranging from 15 to 30 µm with an average crystal size of 20 µm in the majority of the Early Feed runs. The line of colors, at the edges of the crystal, is characteristic of this occurrence of burkeite and attests to a circular growth pattern.

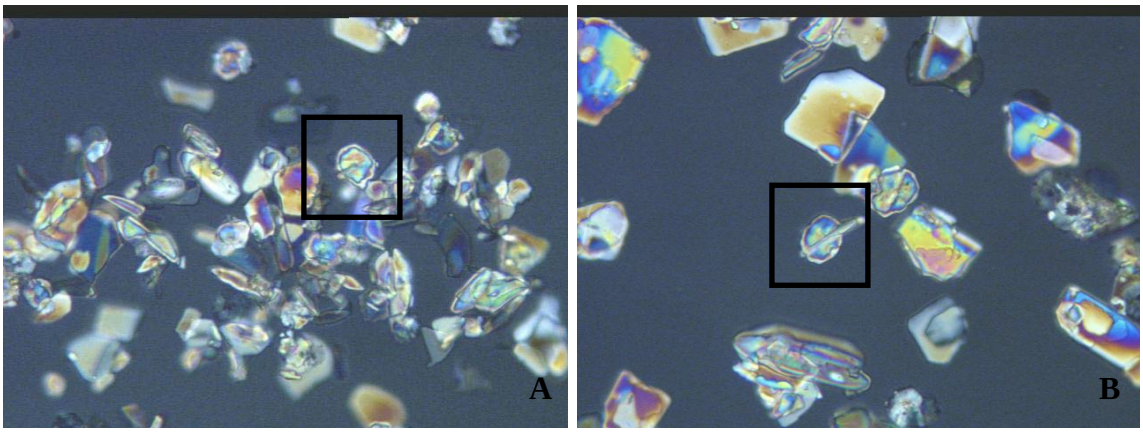

Figure 63. Single Round Habit of Burkeite Crystals

It is interesting to notice that this habit of burkeite is also the one most affected by heterogeneous growth conditions. Figure 64 displays some of this heterogeneous crystals involving single round shape burkeite and sodium nitrate inclusions.

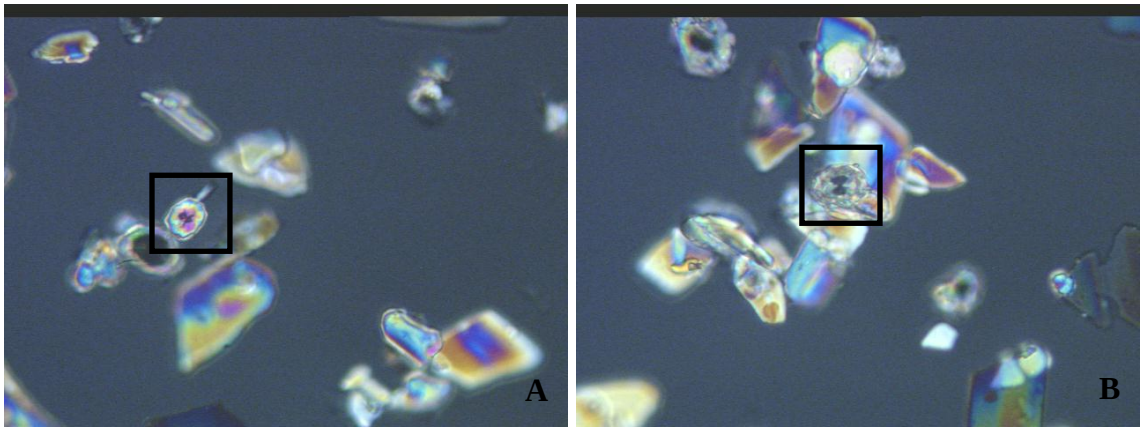

Figure 64. Heterogeneous Form of Single Round Habit of Burkeite Crystals

The second main occurrence of burkeite crystals were the round shape crystals divided into several sections (2 to 4 sections). Their color was blue or yellow or blue and yellow depending on their position with respect to the microscope polarizer (Figure 65A and 65B). The size of the crystals varied from 5 µm to 35 µm. The slightly higher size range and the irregular number of internal division suggest a possible formation of this habit through agglomeration.

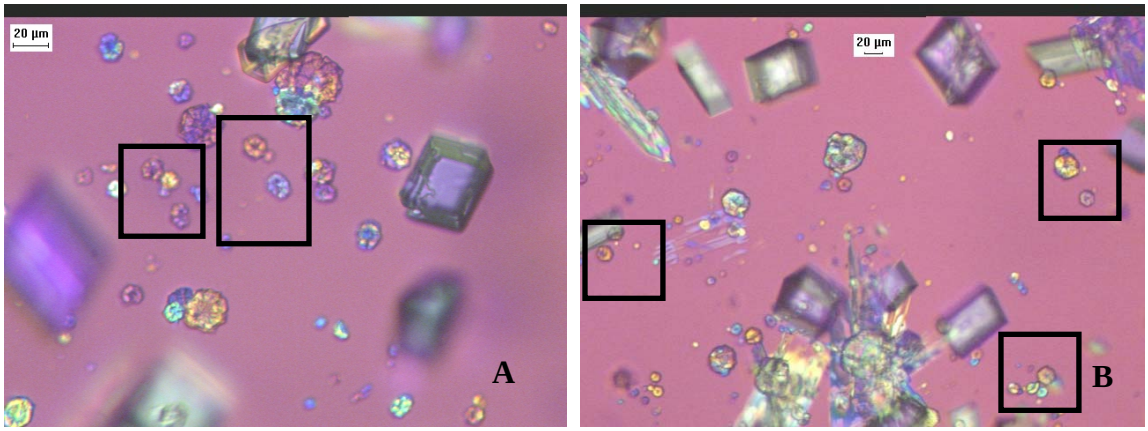

Figure 65. Subdivided Round shape Habit of Burkeite Crystals

Burkeite crystals might be encountered as "globular" habit. Similar to the burkeite displayed in Figure 65, their color was blue or yellow or blue and yellow depending on their position with respect to the microscope polarizer (Figure 66A and 66B). The size of the crystals varied from 20 µm to 55 µm. The similarities with the preceding burkeite habit and the high crystal size suggest that the "globular" habit is an agglomerate of divided habit structure and single round burkeite.

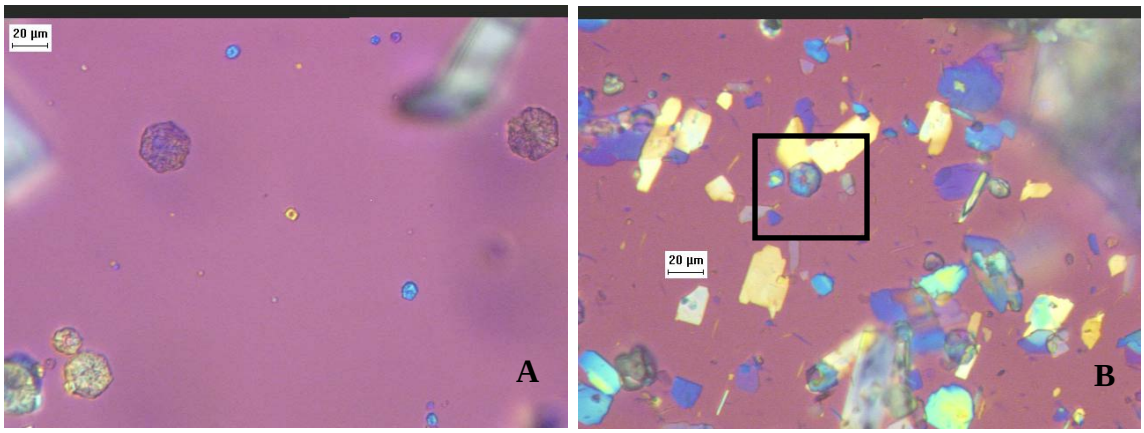

Figure 66. "Globular" Habit of Burkeite Crystals

Burkeite crystals may be encountered as "flower like" habit as presented in Figure 67 below. This habit of burkeite corresponds to a crystal composed of several division issued from the round single crystal shapes described in Figures 63 and 64. The "flower like" habit is hence a

very specific agglomerate of burkeite and might be considered homogenous (Figure 67A) or heterogeneous (Figure 67B) depending on the nature of the single crystals that composed it.

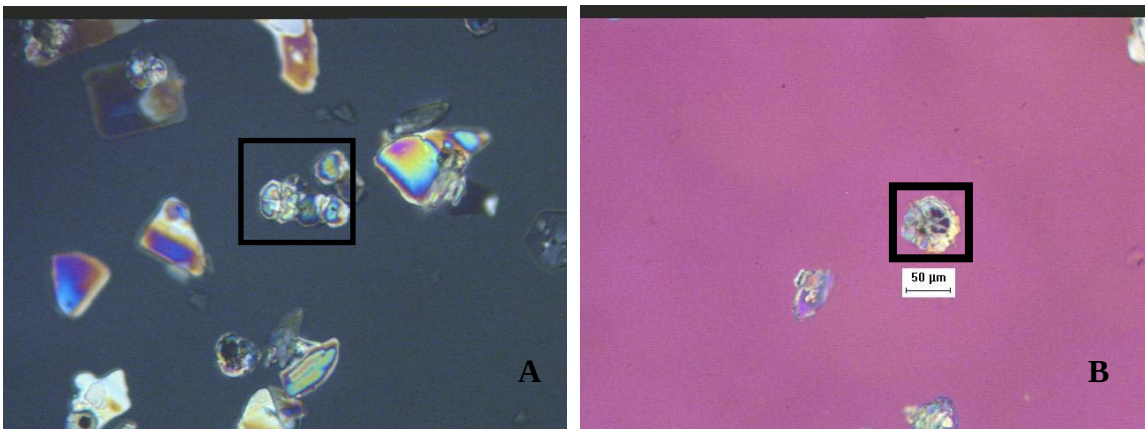

Figure 67. "Flower Like" Habit of Burkeite Crystals

One of the other occurrences of burkeite crystals in the solid phases of Early and Late Feed is as large agglomerate. It appears that burkeite has the tendency to form agglomerates as displayed in Figure 68, that were observed with a crystal size up to 60-65 µm. These agglomerates were however found in small proportion in the final crystals recovered from the crystallization runs.

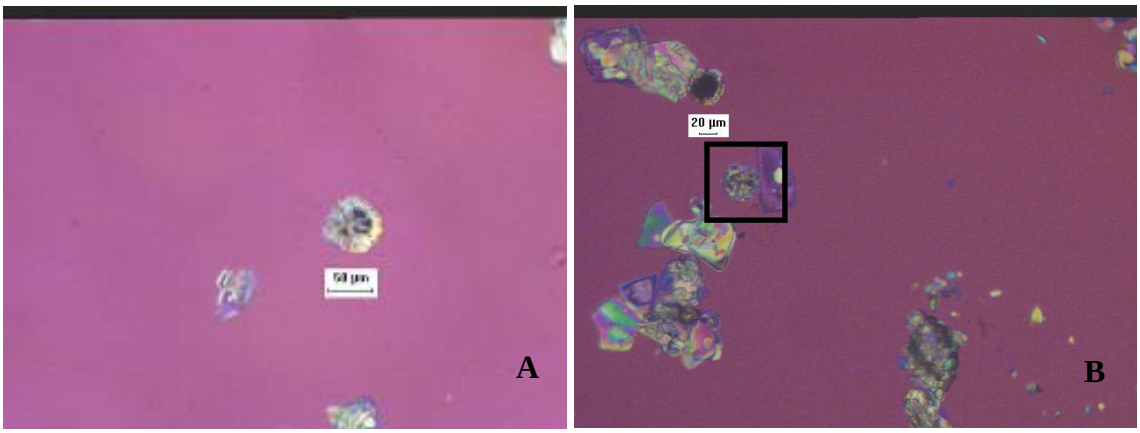

Figure 68. Agglomerates and Clusters of Burkeite Crystals

A blue or yellow hexagonal crystalline species was observed in the range of the burkeite crystals and is potentially one of its habits (Figure 69A and 69B). Characterization of crystalline species might be achieved when the concentration of the species in the solid sample is sufficient to be detected by X-Ray diffraction. For this particular crystal, no proof of its burkeite nature was found due to low concentration of this crystal in the sieving pan.

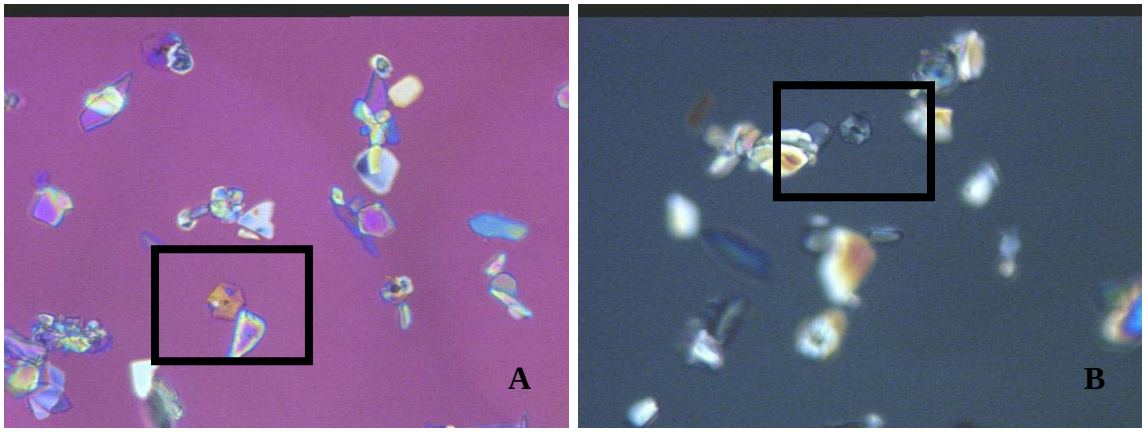

Figure 69. Blue-Yellow Hexagonal Crystal

4.1.4 SODIUM OXALATE

The sodium oxalate crystals were observed with one unique needle or rod like shape.

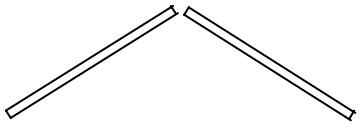

Long blue or yellow needle

They were identified as sodium oxalate based on their color (blue or yellow depending on the crystal position with respect to the polarizer) and their size ranging from 10 to 100 μm. The

high pH of the SST Feed solutions (close to 15) explained the very low thickness of the oxalate crystals (only one or two micrometers). Figure 70 presents the two orientations of sodium oxalate crystals.

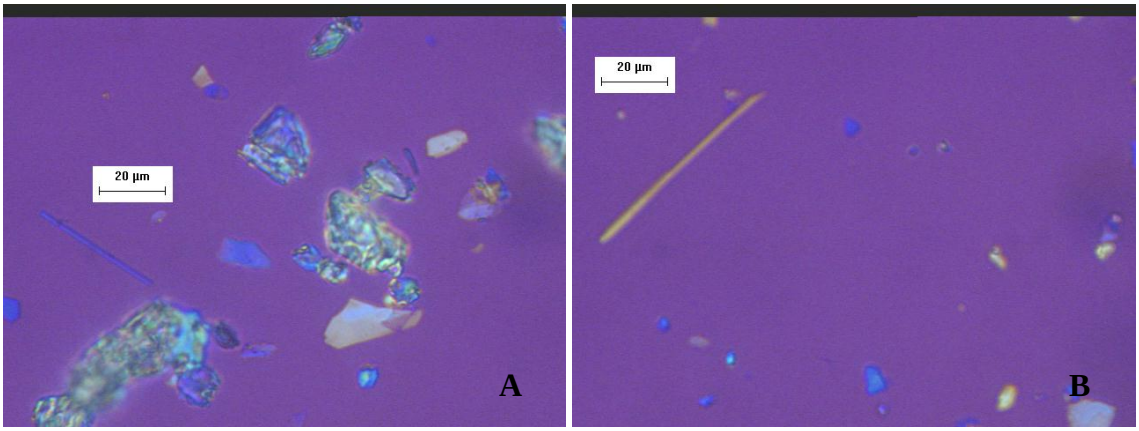

Figure 70. Blue and Yellow Orientations of Sodium Oxalate Crystals

4.1.5 TRISODIUM FLUORIDE SULFATE

The simple six-sided crystals, observed in the solid samples of SST Feed crystallization, were identified as trisodium fluoride sulfate crystals. Their color is similar to the background regardless of their position of the polarizer. There size ranged between 80 and 120 µm as displayed in Figure 71.

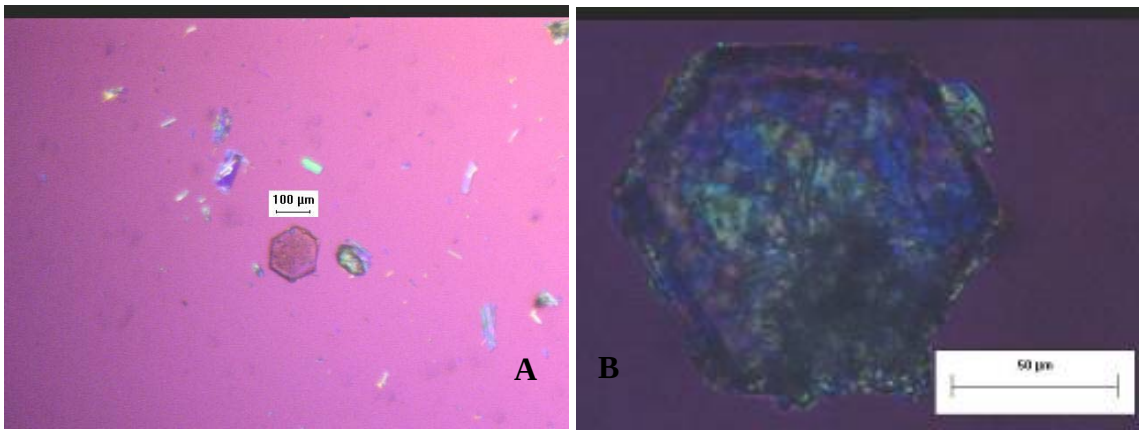

Figure 71. Hexagonal Shape of Trisodium Fluoride Sulfate Crystals

4.1.6 SODIUM NITRITE

Two different occurrences of sodium nitrite crystals were observed in the early and late feed crystallization performed as (1) trigonal and tetragonal and (2) prismatic flake with straight colored edges. These two different occurrences of sodium nitrite crystals are displayed in Figures 72A and 72B. The latest morphology was observed very rarely and in trace amounts.

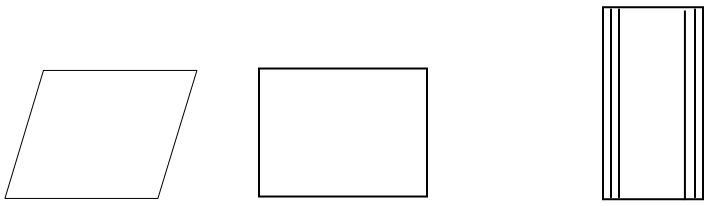

(1) Trigonal and tetragonal (2) Prismatic flake

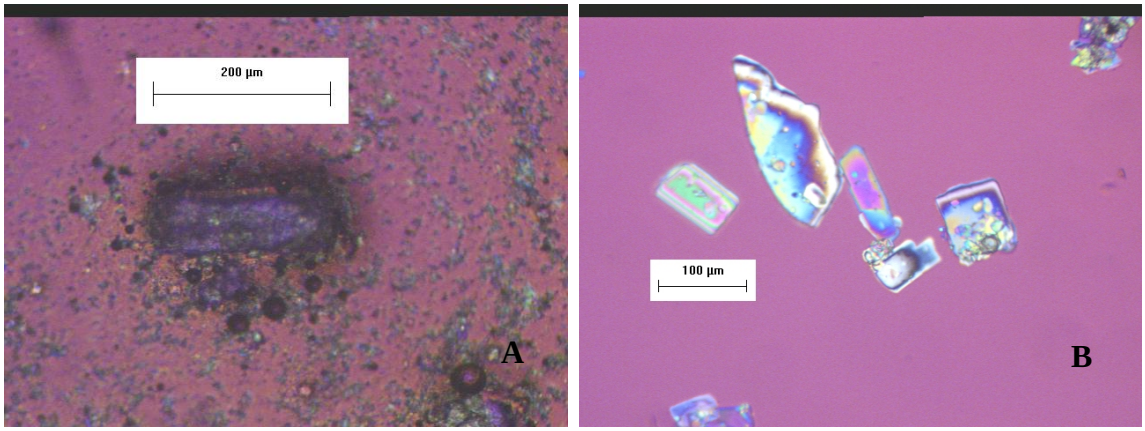

Figure 72. Hexagonal Shape of Trisodium Fluoride Sulfate Crystals

Trigonal and tetragonal shapes are differentiated from sodium nitrate crystals by their extinction position (Figure 72A). As seen in section 4.1.1, sodium nitrate crystals have a white color when placed parallel to the polarizer and a purple color (same color as the background also called extinction position) when placed in opposition to the polarizer. Sodium nitrite crystals (Figure 72A) possess a parallel extinction position.

Another occurrence of sodium nitrite was detected as a prismatic flake with straight colored edges. These crystals were however observed in trace amounts in Early Feed experiments and at a size range around 100 µm (Figure 72B). The edges present different lines of color and the center is generally turquoise surrounded by purple. Due to low concentration of this species, identification as sodium nitrite could not be confirmed by X-Ray Diffraction.

4.1.7 SODIUM SULFATE

(1) Yellow random shape (2) Blue random shape

The sodium sulfate crystals were observed as flake crystals, with generally a triangular shape that has the color blue or yellow depending on the orientation of the polarizer (Figure 73A and 73B). They were observed in the Early and Late Feed experiments in the 10 to 50 µm size range. Their amount varied in the last Early Feed runs depending on the formation of burkeite crystals. When burkeite crystals were produced the sodium sulfate were found in trace or small amounts whereas when no burkeite crystals were produced they were observed in important amounts associated with increased proportions of sodium carbonate crystals.

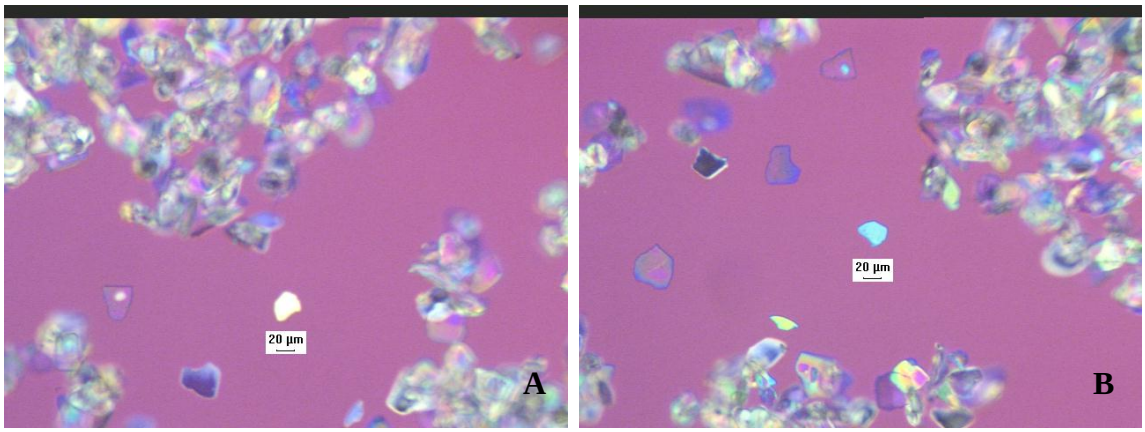

Figure 73. Blue and Yellow Orientation of odium Sulfate

4.1.8 SODIUM PHOSPHATE

The sodium phosphate crystals were observed with one unique needle or rod like shape but with four different habits as (1) single elongated needles, (2) star like habit of small needles, (3) prismatic small needle shape and (4) long and large needles.

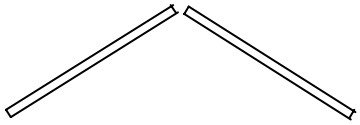

(1) Long blue or yellow needle

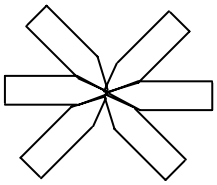

(2) Stars like habit

A new habit of small (10 µm size) rod shaped crystals have been observed as they tend to agglomerate as "stars" (Figure 74). These rods have been identified as sodium phosphate crystals based on (1) their extinction position (blue or yellow when placed in opposition), (2) their size of 10 µm and (3) based on the expectations of Late Feed run.

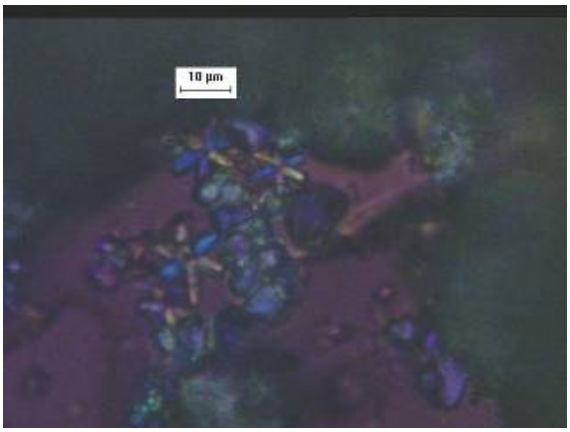

Figure 74. Stars Like Habit of Sodium Phosphate

The rod shape habits (elongated and large) are the only habits that were observed as part of the SST Feed solid phases. The two other occurrences, small needles and star like habit, are expected to only form from cooling crystallization.

4.1.9 MIXED CRYSTALS

The term "mixed species" is employed in this paragraph to describe the crystals that present mixed crystalline matrices. This includes, for instance, crystals resulting from a change in the conditions of crystallization that induce a change in crystal shape (same species but with two different matrices) or crystallization of a secondary species around the basic shape of a main species (referred to as heterogeneous crystallization).

Three mixed shapes or species were observed in the Early and Late Feed runs as (1) a round shape surrounding a square shape, (2) a six sided shape surrounding a round shape and (3) a round shape surrounding a fat canoe prismatic shape.

These crystals were identified as the product of heterogeneous crystallization of (1) burkeite around a sodium nitrate crystal, (2) trisodium fluoride sulfate around a burkeite crystal and (3) burkeite crystal around a sodium carbonate monohydrate crystal.

4.1.9.1 BURKEITE WITH SODIUM NITRATE CORE

Figure 75 displays a mixed burkeite and sodium nitrate crystal. The overall shape and the color of the outside layer are very similar to the main occurrence of burkeite crystals as described in Section 4.1.3. In the center of the crystal appears a cubic shape which is believed to be to a sodium nitrate crystal. The hypothesis of sodium nitrate crystals seems the most probable due to (1) the fact that sodium nitrate is the only species that was observed with a cubic morphology in the SST Feed samples, (2) the other mixed species observed possess center shapes that are either cubic, prismatic or rectangular and (3) sodium nitrate is the only species with sodium carbonate that was likely to be nucleated early enough during the run to have a 20 µm layer of burkeite growing around.

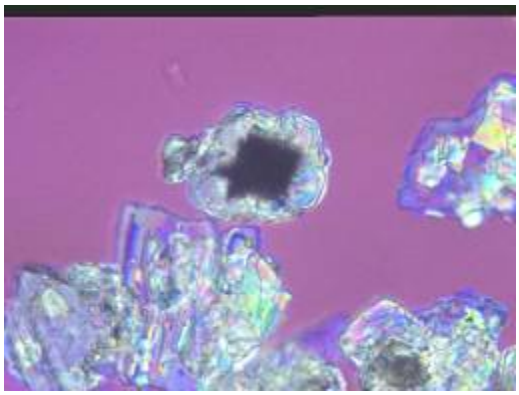

Figure 75. Mixed Burkeite and Sodium Nitrate Crystal

Please note that the XRD patterns identified sodium nitrate crystals among the solid samples collected from the lower sieve size where mixed species where observed in important proportions. The possibility of having two crystals superposed was investigated by moving the crystalline form in suspension in the silicone oil used for the PLM imaging. The experiment proved that Figure 75 corresponds to a unique crystal and not two superimposed crystals.

4.1.9.2 TRISODIUM FLUORIDE SULFATE INCLUDING BURKEITE CRYSTAL

The other form of mixed crystals observed was the hexagonal matrix that was grown around a round or oval crystal (Figure 76). The mixed hexagonal shape has been observed in the final product in association with simple six-sided crystals, identified as trisodium fluoride sulfate crystals in Section 4.1.5. The size of 100 µm and the hexagonal shape allows the identification of the exterior matrix as trisodium fluoride sulfate. The inside matrix might either be (1) a burkeite crystal, (2) another crystalline species or (3) another occurrence of trisodium fluoride sulfate. However the apparent inner structure is identical to the round shape single burkeite crystals described in Section 4.1.3. In addition, burkeite is the only species that nucleates soon enough during the run (burkeite being one of the first species to nucleate) to reach this overall crystal size and be included into a six sided shape.

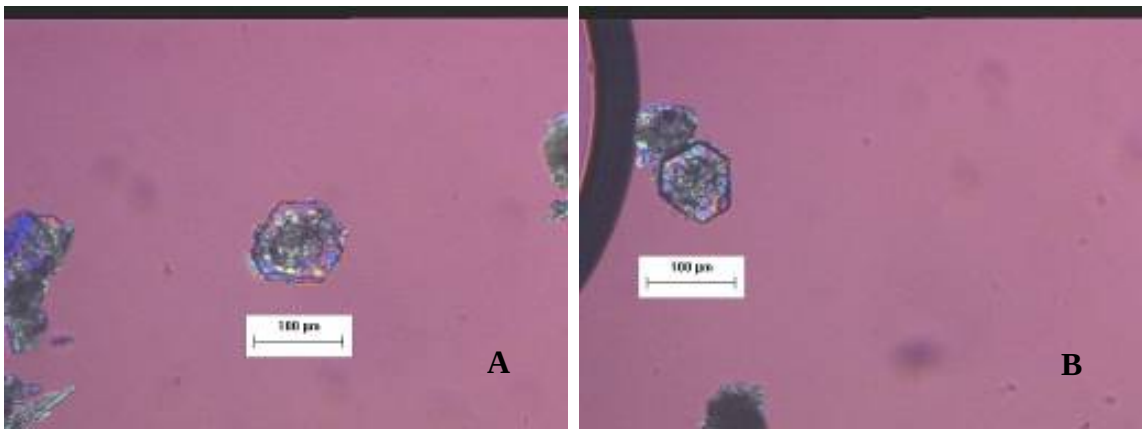

Figure 76. Mixed Trisodium Fluoride Sulfate and Burkeite Crystal

4.1.9.3BURKEITE INCLUDING SODIUM CARBONATE CRYSTAL

Figure 77 displays a mixed burkeite and sodium nitrate crystal. The overall shape and the color of the outside layer are very similar to the main occurrence of burkeite crystals as described in Section 4.1.3. In the center of the crystal appears two prismatic shaped crystals which are

believed to be two sodium carbonate monohydrate crystals. The mechanisms of heterogeneous growth and argument for the identification of the core as sodium carbonate are similar to those described in Section 4.1.9.1.

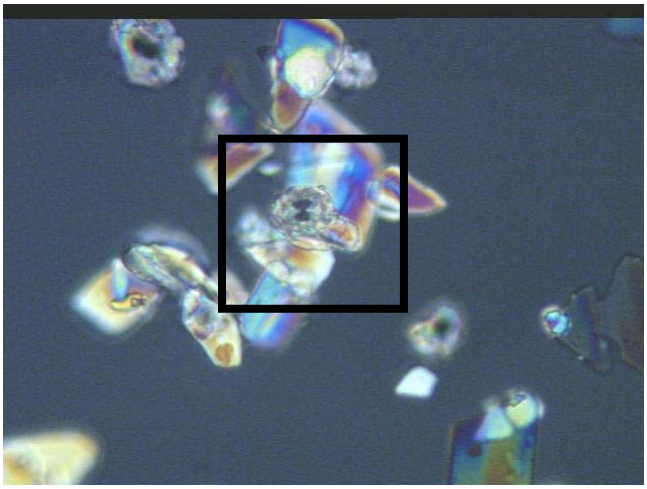

Figure 77. Mixed Burkeite and Sodium Carbonate Crystal

4.1.10 UNIDENTIFIED SOLID PHASES

Figure 78 displays several round shaped crystalline species that were observed in the slurry sample recovered from the preliminary Early Feed runs and have not been identified. Several elements are characteristics from the burkeite crystals as (1) the round shape of the crystals and (2) the division of the crystals in 2 or 3 sections. The size of 50 µm has however never been observed for single homogenous burkeite crystal. On the other hand, several elements are characteristics of the rounded fat canoe habit of sodium carbonate crystals such as (1) the rainbow colors and successive lines on the edges and (2) the size ranging between 50 to 60 µm.

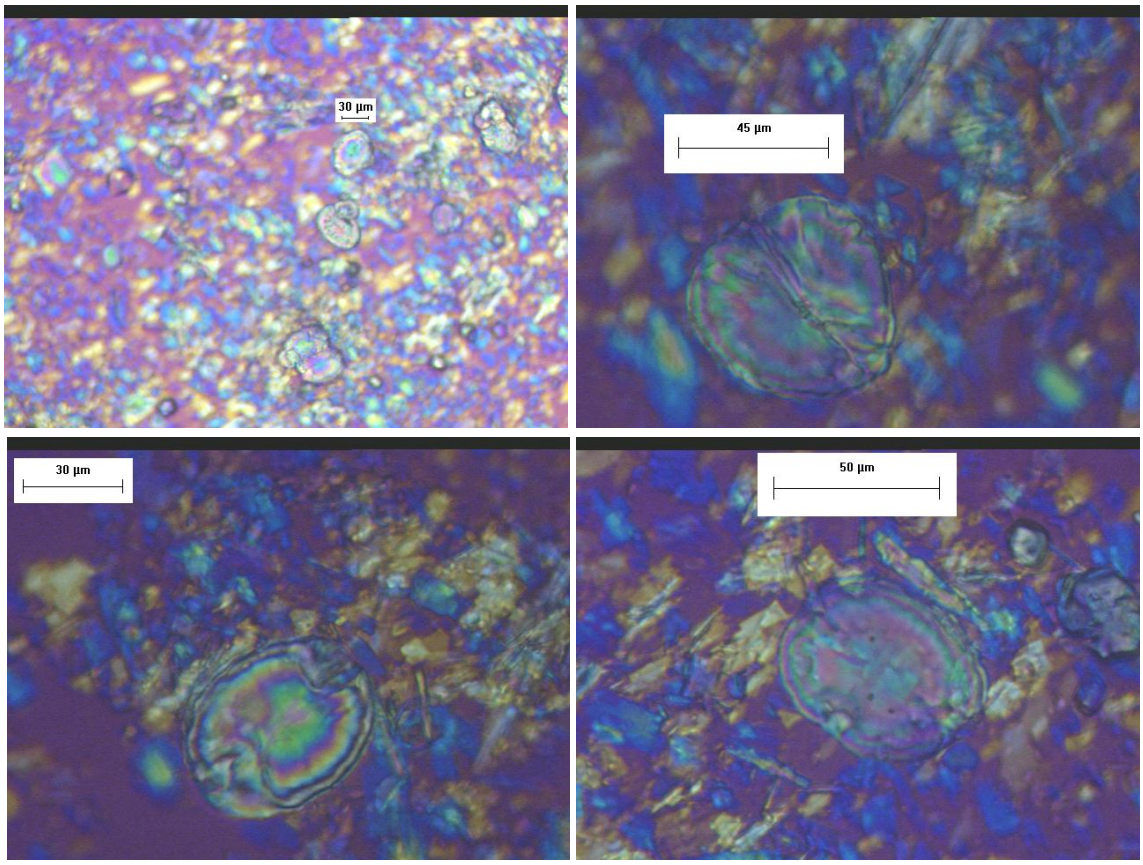

Figure 78. Mixed Burkeite and Sodium Carbonate Crystal

The XRD identification was not performed on this sample and no identification can be concluded for this new crystalline species. These crystals were observed with the rounded fat canoe habit of the sodium carbonate crystals. It is hence believed that these crystals are (1) either a new habit of sodium carbonate, (2) a new habit of the largest single burkeite crystals observed so far or (3) a mixed crystalline species of carbonate and sulfate.

4.2 CRYSTAL GROWTH MECHANISMS

The observation through PLM imaging of the different product recovered from the Early and Late Feed runs allows not only the identification of crystalline species but provides also

elements on the crystal growth. The PLM images obtained from the crystals and crystalline structure were studied in order to identify the growth mechanisms for the main species.

Three methods may be used to determine the growth mechanism of a crystal. The first possibility is to grow the crystal in a cell that has a camera that allows the recording of the growth with respect to time. This technique is hard to establish under the specific conditions of the SST Feed crystallization and is expensive. The second method is to take regular samples from the slurry during crystallization and analyze the variation with respect to time between two successive samples. The last method used is to sieve the crystals recovered from the crystallization, recuperate the crystals collected in each sieve and analyze them through PLM imaging. For regular shape species the sieve sizes are related to time and crystal growth as the more we go on the larger sieve, the more crystals had time to grow. By taking PLM images from the successive sieve size a sequence of growth may be determined.

Both of the last two experiments were performed and the results from the last will be displayed in this section.

4.2.1 TRISODIUM FLUORIDE SULFATE

Two different crystal growth mechanisms were observed for the trisodium fluoride sulfate species denominated as homogenous, when the core of the crystal is trisodium fluoride sulfate, and heterogeneous, when the core is a different crystalline species.

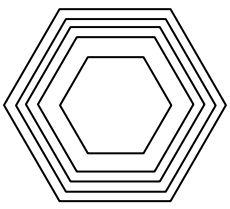

(1) Homogenous crystal growth

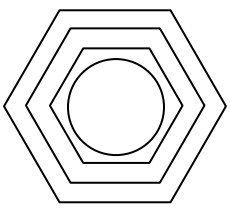

(2) Heterogeneous crystal growth

The mixed hexagonal shape has been observed in the final product in association with simple six sided crystals, identified as trisodium fluoride sulfate crystals in section 4.1.5.

By changing the parameters of the microscope, the crystal structure of the trisodium fluoride sulfate crystals have been revealed (Figure 79). The crystal is composed of regular layers of hexagonal shape. The crystal observed below displayed 4 hexagonal layers and a hexagonal core. The trisodium fluoride sulfate crystals are hence forming a core of a certain radius and grow by creating regular hexagonal layer around this core. The measurements of the core radius and of the different layers provide valuable information on the kinetics parameters related to the trisodium fluoride sulfate in a multi-salt solution.

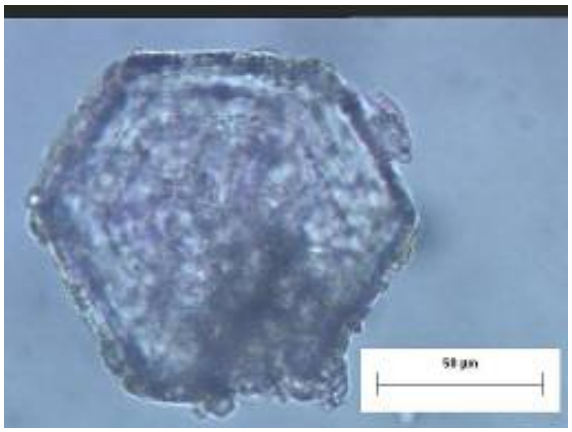

Figure 79. Structure of the Trisodium Fluoride Sulfate Crystal

The different layers indicate both the growth rate and the evolution of the growth rate with time.

The observations of the heterogeneous crystals displays that the creation of the hexagonal layer, and hence the crystal growth, is dependant on the shape of the crystal core. For instance in Figure 76B the hexagonal layer is of constant thickness but of irregular shape. This is due to the

fact that the core crystal displays a slightly oval shape. On contrary, in Figure.76A the inner crystal is a perfect round burkeite crystal, and the outside layer is hence a perfectly regular hexagon.

Since only one hexagonal layer was formed and the core crystal has a size of 25 to 30µm, the heterogeneous growth of this crystal had happened relatively late during the run. In conclusion the PLM images displayed in Figure 76A and 76B lead to the following growth mechanism: (1) burkeite is nucleated early in the run;(2) the burkeite grows for extended period of time; (3) when nucleation of trisodium fluoride sulfate is reached, trisodium fluoride sulfate begins to grow on the burkeite crystal;(4) the trisodium fluoride sulfate grows on the burkeite core by successive hexagonal layer of constant thickness.

4.2.2 BURKEITE CRYSTALS

Two crystal growth mechanisms were observed for the burkeite crystals.

The first one is the heterogeneous crystallization. This happens when a burkeite crystal grows around a sodium nitrate or sodium carbonate crystals as described in section 4.1.9.1 and 4.1.9.3. Figure 80A and 80B present two examples of single heterogeneous burkeite crystal. A colored circle close to the edge of the crystal and the regular round shape of the burkeite crystal shows that the single burkeite crystals grows in circle from the center of the crystal to the periphery.

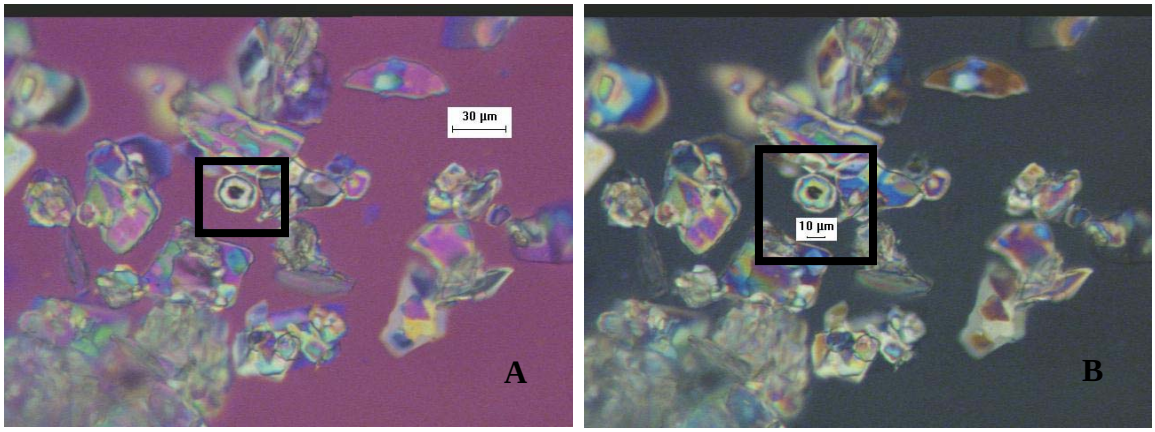

Figure 80. Growth of the Single Heterogeneous Burkeite Crystal

The second growth mechanism is growth by agglomeration. This phenomenon was determined thanks to (1) the crystals included in the core of the burkeite crystals that was used as a tracer and (2) the correlation between sieving and PLM imaging techniques.

It was observed that the burkeite crystals grow until an average size of 20 to 30µm. Then they gathered and began forming groups of three or four crystals. They got closer and closer, clustered and their core crystal moved to the extremity of the burkeite crystal as they are pressed on against the other. When the three or four burkeite were agglomerated their cores were regrouped and the resulting crystal appeared as a globally round shape with one central core and three or for sections inside. This growth by agglomeration is the mechanism responsible for the occurrence of burkeite as round shape with several sections. Figure 81A and 81B displayed examples of heterogeneous burkeite crystals that agglomerate.

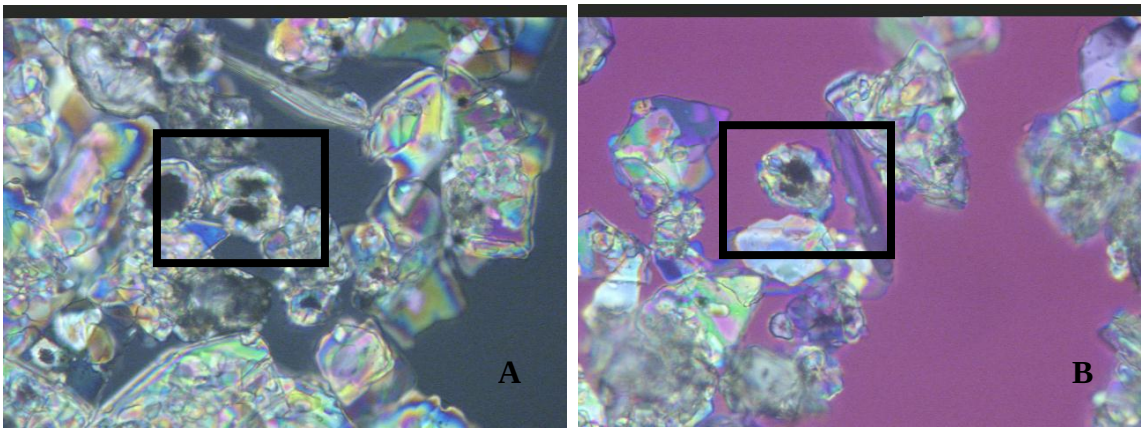

Figure 81. Agglomeration of Single Heterogeneous Burkeite Crystal

A SST Early Feed run (run 52) was performed with regular sampling of the slurry solution to validate with a secondary method the observations and conclusions made from the sieved crystals.

Based on the PLM images of crystals from successive pan sizes, it has been envisioned that the flower like habit of burkeite crystals was formed by agglomeration of smaller single entities of burkeite crystals. Figure 82 displayed an example of flower like habit of burkeite crystal where the 4 entities issued from single crystal are apparent.

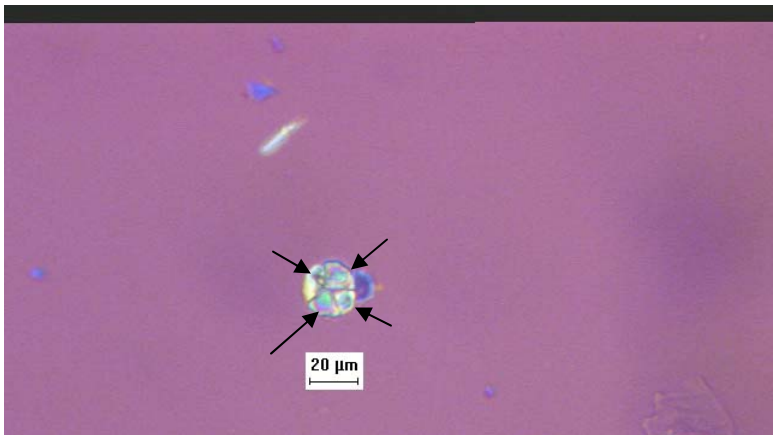

Figure 82. Structure of the Flower Like Habit of Burkeite Crystal

The PLM images taken at different operating times from the different samples also display this aggregation. Figure 83 below is an illustration of this phenomenon. Three single crystals of 5 µm (Figure 83A) appear to cluster near each other and gather into a 15-µm agglomerate (Figure 83B). These small agglomerates may then aggregate with several other single crystals and form a higher aggregate entity of burkeite with sizes ranging from 20 to 25 µm (Figure 83C). These aggregates evolve then as "flower like" habit of burkeite crystals (Figure 83D).

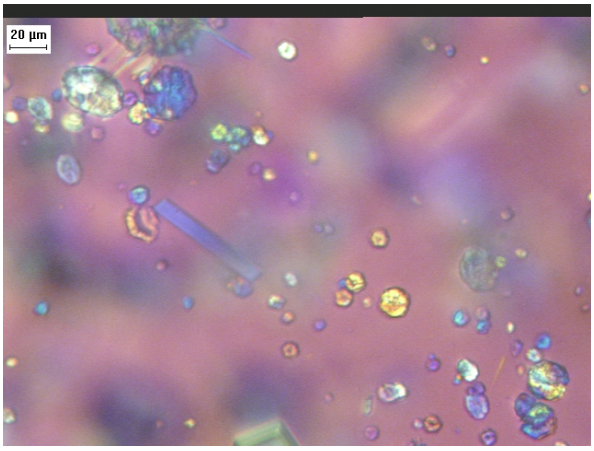

Figure 83A: Single burkeite crystals (average size of 8 µm)

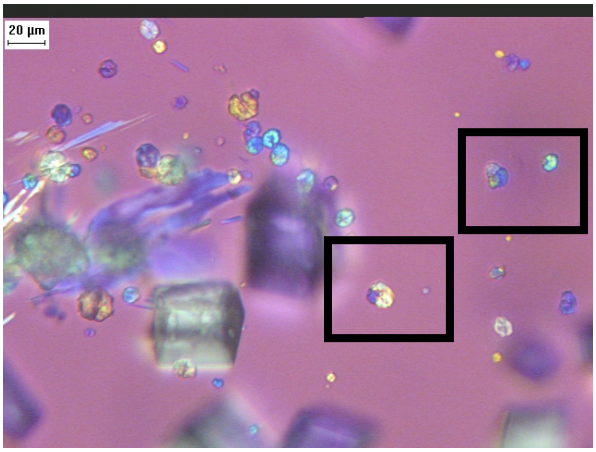

Figure 83B: Agglomeration of three burkeite crystals (structure of 15 µm)

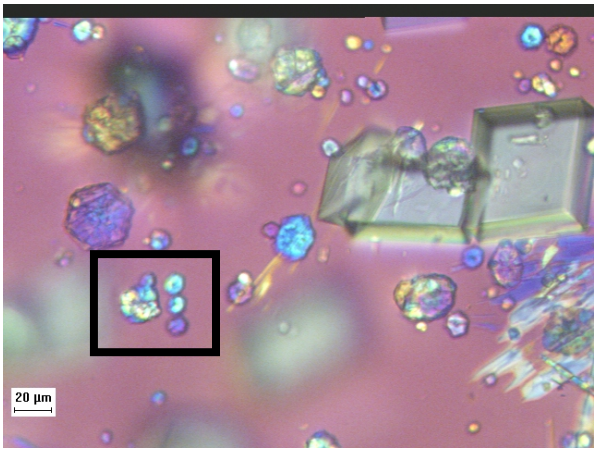

Figure 83C: Agglomeration of six burkeite crystals (structure of 22 µm)

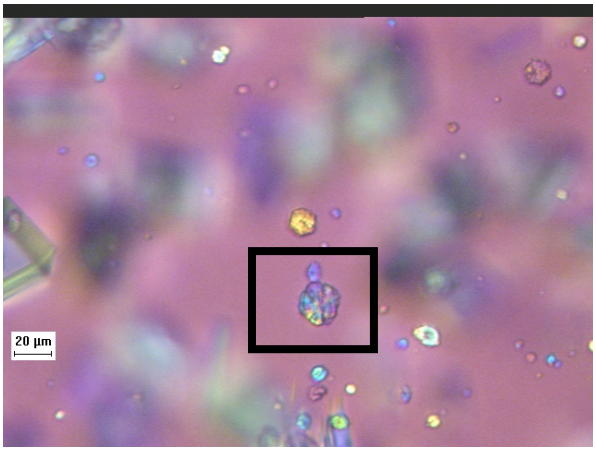

Figure 83D: Resulting "flower like" habit of burkeite crystals

Figure 83. Formation of Flower Like Habit of Burkeite Crystal By Agglomeration

4.3 CRYSTAL AVERAGE GROWTH RATE ESTIMATE

An estimate of the growth rate of the three main species (sodium nitrate, sodium carbonate monohydrate and burkeite crystals) was determined. Calculations were performed based on the simulation values (nucleation points) and experimental values from Run 52 applied to the observations of Run 38b. The main results are summarized in Table 29.

Table 29. Average Growth Rate Estimate for the Three Main Species during Certification Run 38b.

Parameters	Sodium nitrate	Sodium carbonate	Burkeite
Condensate to feed ratio at nucleation (simulation)	0.38	0.33	0.09
Condensate to feed ratio at nucleation (experimental)	0.24	0.28	0.09
Time at nucleation (simulation) (in min)	720	1067	232.6
Time at nucleation (experimental) (in min)	669.6	841	232.6
Time at end of crystallization (in min)	1830	1830	1830
Maximum crystal size (in µm)	550	250	45
Average Growth rate (simulation) in $\mu m.min^{-1}$	0.495	0.327	0.028
Average growth rate (experimental) in $\mu m.min^{-1}$	0.474	0.253	0.028

Note that these values correspond to an estimate of an average growth rate calculated based on equation E-4 and that appendix K displays sample calculations associated with growth rate estimate.

Note also that observations of run 52 proved that an average growth rate is probably representative of sodium nitrate and sodium carbonate crystals growth but does not represent very well the growth of burkeite. In other words, it has been proven that burkeite crystals do not have a constant growth rate throughout the entire crystallization run.

CHAPTER 5: INFLUENCE OF CRYSTALLIZATION VARIABLES

5.1 INFLUENCE OF EVAPORATION PROFILE

5.1.1 Concave evaporation profile

5.1.1.1 Objectives

A crystallization run (run 51) was performed on the FY06 simulated Early Feed solution. Run 51 was performed to examine the effect of a variable evaporation rate on crystal size distribution (particularly burkeite size) and solid-liquid separation. The run was performed in a single stage and the condensate-to-feed ratio was comparable to that from Certification Run 38b described in section 3.3. The evaporation rate was increased slowly throughout the run. Specifically, the evaporation profile consisted of (1) a slow evaporation rate during the period of burkeite nucleation and growth, (2) the typical evaporation rate[2] at the point of sodium carbonate and nitrate nucleation and initial growth, and (3) an increased evaporation rate towards the end of the run. This profile allowed further study of burkeite growth and determined the maximum burkeite crystal size obtained under slow evaporation.

The simulation graph for a typical Early Feed run is shown in Figure 84. This graph was used as a reference to determine the evaporation profile used in Run 51.

[2] This was a rate of ~25 g/h, identical to that used in Certification Run 38b.

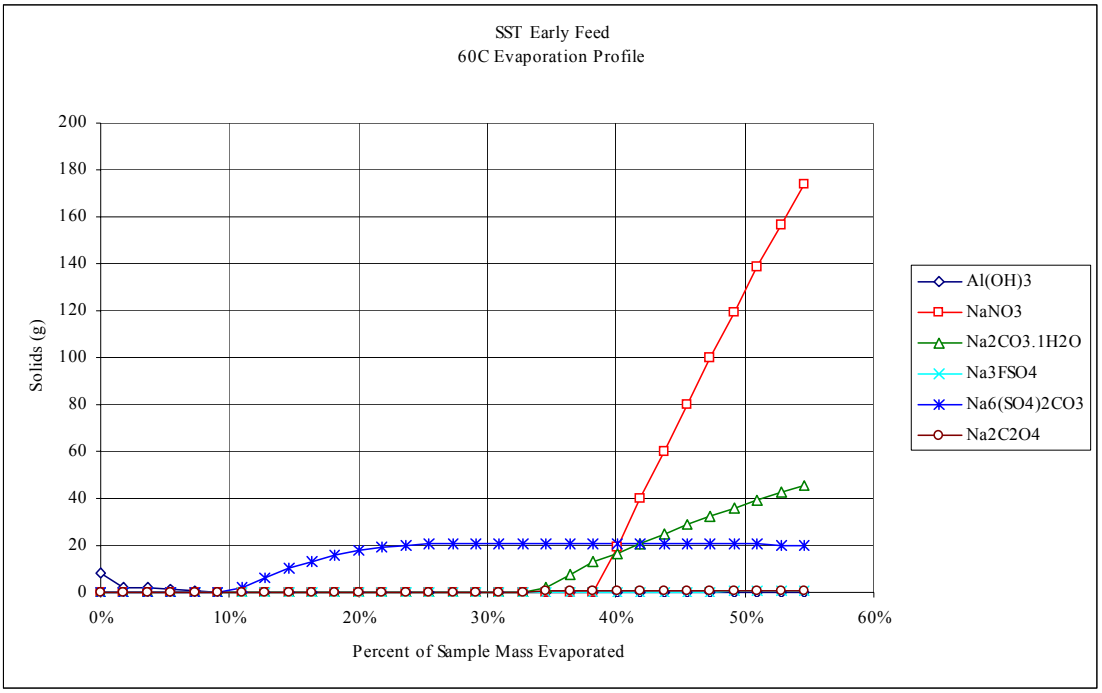

Figure 84. Simulation of Early Feed Crystallization.

Figure 84 shows the mass of the three primary species (burkeite, sodium carbonate, and sodium nitrate) that is crystallized as a function of the percentage of the sample evaporated. The figure assumes that the system is equilibrated at 60 °C; i.e., it is assumed that the solution is at saturation throughout the evaporative process. That being the case, Figure 84 can be used to define four different operating regimes: (1) burkeite is nucleated and most of the crystal mass of burkeite is generated in the region between 8 and 20% evaporation; (2) between 20 and 28% evaporation, there is little additional crystal mass formed in the system; (3) between 28 and 35% evaporation, sodium carbonate and sodium nitrate nucleate and begin to grow, but there is little if any additional crystallization of burkeite; (4) between 35% evaporation and the end of a run, sodium carbonate and sodium nitrate crystals continue to grow, but there is no additional burkeite crystallization.

The goal of Run 51 was to produce a smaller number of burkeite crystals, but to increase their size. Accordingly, a very slow evaporation rate was used during Regime 1. The rate was increased somewhat during Regimes 2 and 3, and it was increased further during Regime 4 to reduce the total operating time of the run. Two additional effects are expected as (1) heterogeneous burkeite crystals might be produced during Regime 3 and (2) increasing the evaporation rate in Regimes 3 and 4 might influence the spread of sodium nitrate and sodium carbonate crystals, thereby affecting the solid-liquid separation .

5.1.1.2 Operating conditions

The regimes described above were used to generate the evaporation profile for Run 51. Specifically, the run was started (Regime 1) with an evaporation rate of about 10 g/h and it was slowly increased to favor burkeite growth throughout Regime 2. At the end of Regime 2, the evaporation rate reached 25 g/h, which is equal to the value used in Run 38b). This evaporation rate was maintained throughout Regime 3, and it was then increased in Regime 4 (i.e., after the nucleation of sodium carbonate and sodium nitrate).

The temperature and pressure histories from Run 51 are shown in Figure 85. The run temperature was controlled to within +/- 1 ^{o}C of the target value of 66 ^{o}C. The pressure profile reflects the step-wise changes in vacuum that are associated with manual adjustments of the regulating valve.

The mass of vapor generated as a function of time is shown in Figure 86. The target and actual condensate-to-feed ratios for this run were 0.474 and 0.483, respectively. The operating time for the run was 33 hours. Overall and detailed mass balances are provided in the Appendix L.

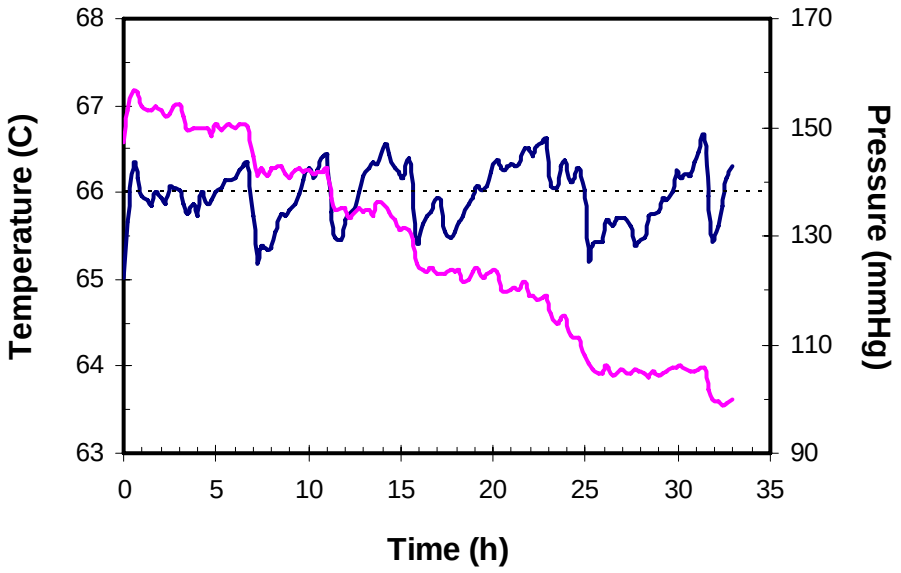

Figure 85. Temperature and Pressure Profiles for Run 51. The dotted line represents the target operating temperature of 66 ^{o}C.

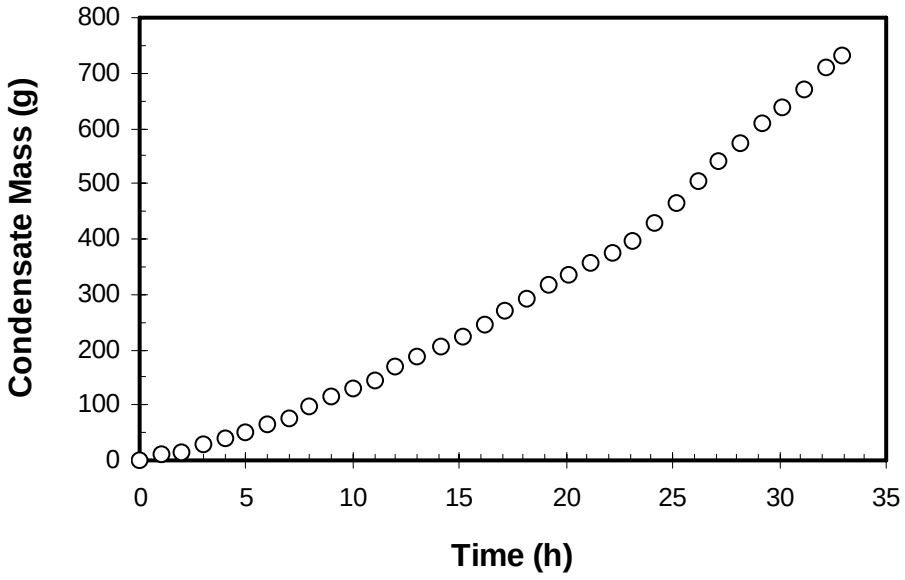

Figure 86. Evaporation Profile for Run 51.

5.1.1.3 Slurry composition and crystal size distribution

Samples were taken from the slurry of Run 51 for PLM analysis. Images from this analysis displayed the presence of sodium nitrate, sodium carbonate monohydrate, burkeite, sodium sulfate, and sodium oxalate. Selected images are shown in Figure 87.

Very large quantities of sodium nitrate crystals were observed in the samples. These crystals ranged in size from several microns up to 300 to 400 μm. The average size was similar to that found in Run 38b, but their spread about the mean was greater. Based on microscopic observations of the slurry and sieved crystals, it would seem that a significant fraction of the small sodium nitrate crystals (below a few μm) were either redissolved during the washing steps or passed through the medium-frit filter.

Sodium carbonate monohydrate crystals were present in important amounts with an average size around 100–150 μm. Sodium oxalate crystals were observed in trace amounts, which is similar to amounts produced in Run 38b. Burkeite crystals were observed in smaller amounts but as larger crystals (single crystals with an average size from 40 to 50 μm). The burkeite crystals observed in the slurry were less numerous, had a smaller spread, and were larger than those seen in Run 38b. These observations are in agreement with the predicted effects of the evaporation profile applied to Run 51.

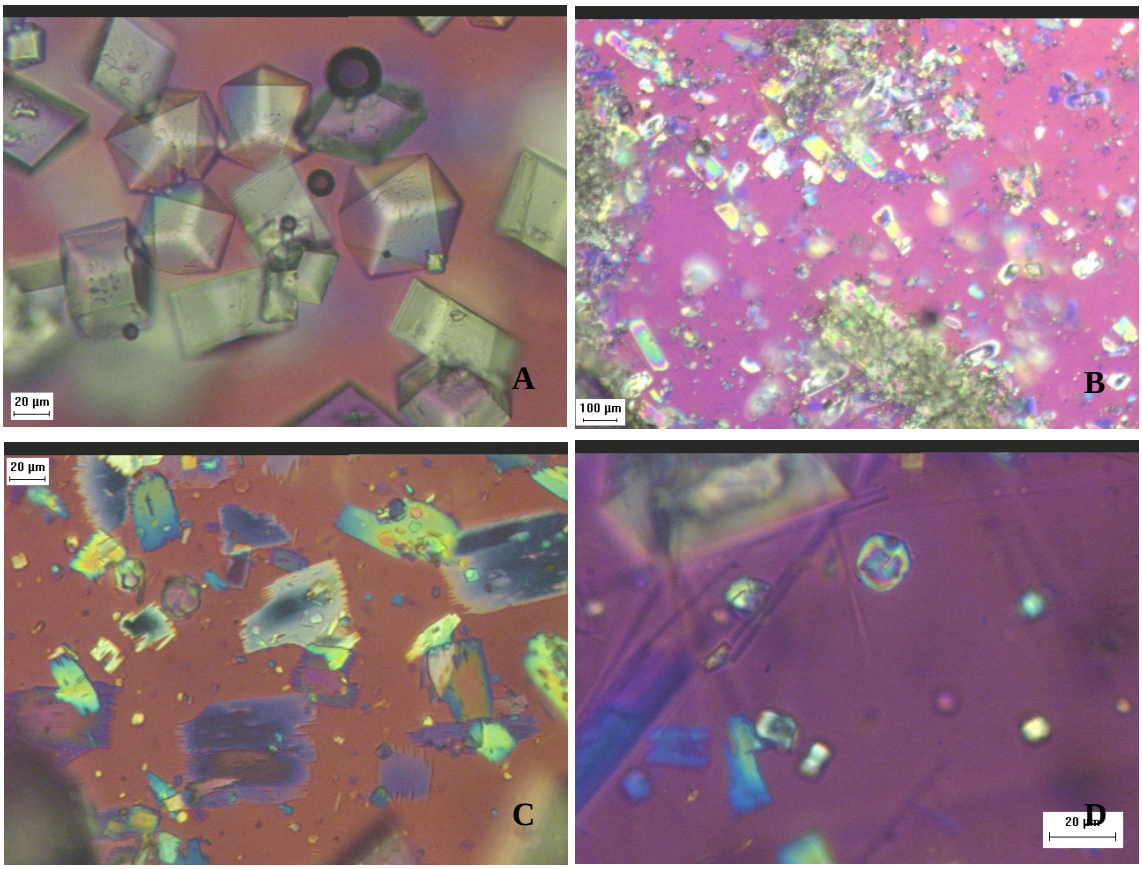

In panel A sodium nitrate crystals, in panel B sodium carbonate (sizes ranging from 100 to 150µm), in panel C burkeite crystals and sodium oxalate in background and in panel D. homogenous burkeite crystals

Figure 87. PLM Images of Run 51 Slurry

The slower evaporation rate in Run 51 apparently increased burkeite growth, leading to a higher average size and smaller number of crystals. On the other hand, the varying evaporation rate in the region of sodium carbonate monohydrate and sodium nitrate crystal nucleation led to slightly larger sizes and may have changed the spread of the size distribution of these crystals.

The CSD produced in Run 51 is shown in Figure 88. It shows (1) the same mode size that was produced in Run 38b, but with a smaller percentage of crystals at this size, (2) a slightly smaller general spread and (3) a slightly greater spread for sodium nitrate crystals.

The first section of the CSD from Run 51 is very close to that from Certification Run 38b, but the crystals obtained are slightly smaller than in Run 38b (a slightly smaller amount between 0 and 50 μm and a smaller amount between 50 and 200 μm). The crystals corresponding to this size range (0–50 μm) are mainly burkeite and sodium carbonate. Hence, the burkeite crystals have an average size larger than those from Run 38b and the sodium carbonate crystals have a larger spread and a slightly higher average size.

In the second section of the curve, between 200 and 600 μm, the crystals obtained (mainly sodium nitrate crystals) from Run 51 have a similar size to those from Run 38b, but a larger spread. These observations are further illustrated in Figure 89 and Table 30.

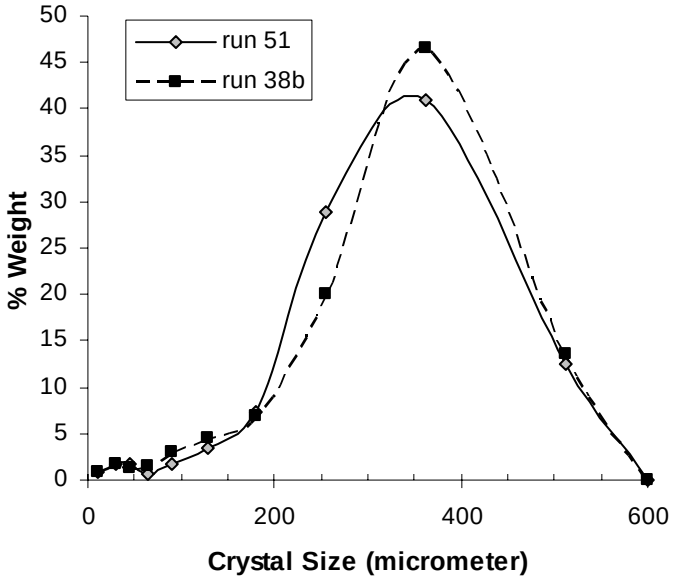

Figure 88. CSDs for Runs 38b and 51.

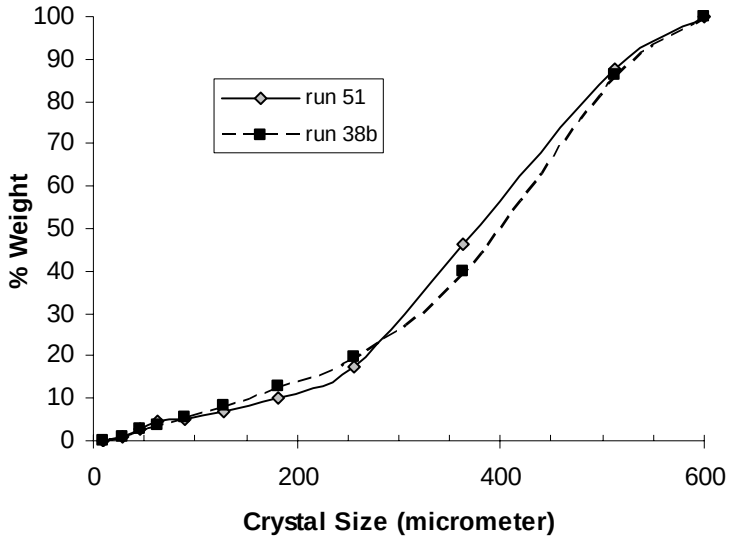

Figure 89. Cumulative mass distributions for Runs 38b and 51.

Table 30. CSD comparison for Runs 38b and 51.

Criteria	Early Feed 38b	Early Feed 51
Coefficient of variation	34.7	33.1
Percent crystal mass at mode size	46.62	40.97
Percent crystal mass below 50µm	3.82	3.63

5.1.1.4 Solid-liquid separation

The criteria used to evaluate the effect of evaporation rate on the solid-liquid separation steps in Runs 38b and 51 are shown in Table 31.

A key point illustrated in Table 31 is the difference between the mass of final crystals from the two runs; a far greater amount was produced in Run 51. The main explanation for this is

that accumulation in Run 51 was 60 g less than that in Run 38b. Also there was a slightly increased condensate-to-feed ratio in Run 51.

Table 31. Comparisons between Runs 38b and 51.

Criteria	Early Feed 38b	Early Feed 51
Evaporation rate (g/hr)	~ 25	Variable, increased from ~10 g/h to ~40 g/h during the run
Condensate-to-Feed Ratio	0.481	0.483
Washes necessary for major mother liquor removal	3	3
Filtration & Washing Time	Typical	Decreased
Slurry cake composition	Powder-like with large-medium crystals	Powder-like with larger crystals
Mass of final crystals	Typical (210 g)[3]	Increased (275 g)
Color of final crystals	White with slight yellow color	White color
Ease of operation	No filter plugging, easy to stir	No filter plugging, easy to stir

5.1.1.5 Crystal identification

Samples were taken from the sieved crystals of Run 51 for PLM analysis. Images from this analysis displayed the presence of sodium nitrate, sodium carbonate monohydrate, burkeite, sodium sulfate, and sodium oxalate. Selected images are shown in Figure 90.

[3] The value of 210 g in Run 38b corresponds to the final mass of crystals collected after the washing steps. This does not account for the samples collected from the unwashed crystals or those collected after each wash step, which totaled 19 g.

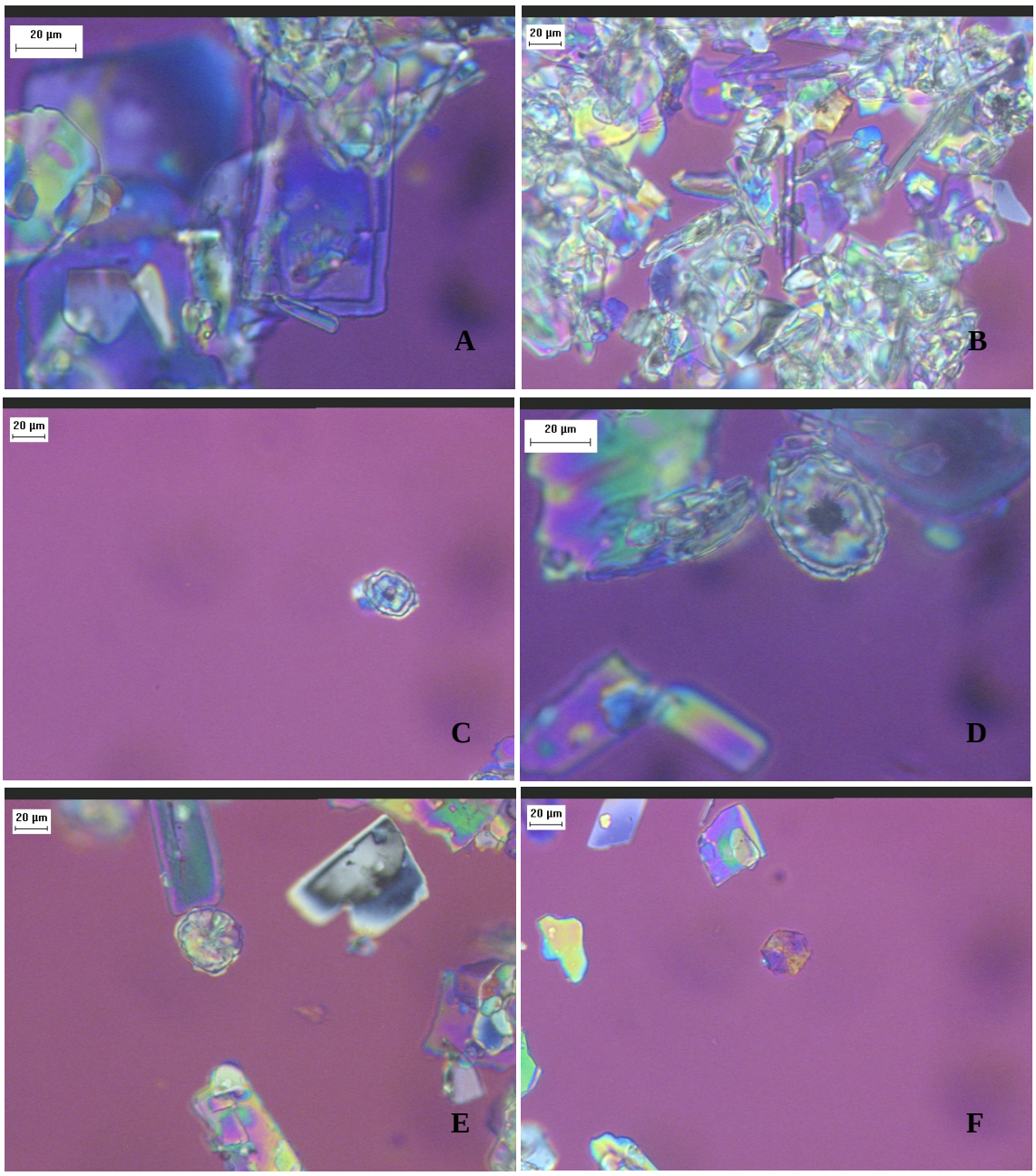

In panel A and B, sodium nitrate at lower size and as needle, in panel C and D, homogenous and heterogeneous burkeite crystal, in panel E and F, zoom on flower like habit and other occurrence of burkeite.

Figure 90. PLM Images on Sieved Crystals from Run 51

Images of sieved crystals show that the burkeite crystal spread was reduced compared to that from Run 38b. For a similar crystal mass, the burkeite was produced as a smaller number of larger crystals. The mode size for the burkeite crystals is 40-50 μm. The amount of heterogeneous crystals was reduced compared to other Early Feed runs, however their proportion is still important. The slower evaporation rate at the start of the run reduced the nucleation rate of burkeite and favored burkeite growth. This led to fewer, but larger burkeite crystals. However, the increased evaporation rate at latter stages of the run created the heterogeneous burkeite crystals observed in PLM images.

PLM images also displayed the presence of sodium nitrate crystals on the lower sieves. This was not the case in Run 38b and is a sign that the spread of the sodium nitrate crystals was increased. The sodium nitrate crystals presented a similar mode size to Run 38b and included large crystals. Once again, the small sodium nitrate crystals and the increased spread are likely due to the increased evaporation rate towards the end of the run.

These assessments explain the process ease that was observed during filtration and washing. The reduced number of small burkeite crystals avoided the potential filter plugging. Also, the slightly larger average size of the carbonate and nitrate crystals simplified the filtration and washing steps, compensating for the increased crystal mass.

5.1.1.6 Conclusions

Run 51 achieved its objectives. By applying a concave evaporation profile, burkeite crystals were produced at lower number but increased size. The size range of burkeite crystals displayed in run 51 represents the highest obtained by crystallization with Early Feed. On the other expectation that the evaporation profile would modify the solid liquid separation revealed

to be true. By increasing the size of the burkeite crystals and the spread of the sodium nitrate crystals a more homogenous crystal population was obtained which facilitated the filtration.

5.1.2 Convex evaporation profile

5.1.2.1 Objectives

A crystallization run (run 50a) was performed on the FY06 simulated Early Feed solution. The purpose of Run 50a was to study the effect of the evaporation rate profile on product crystal size distribution, burkeite crystal inclusions (Figure 91A and 91B), and solid-liquid separation. The run was performed in a single stage and the condensate-to-feed ratio was equal to that used in Certification Run 38b.

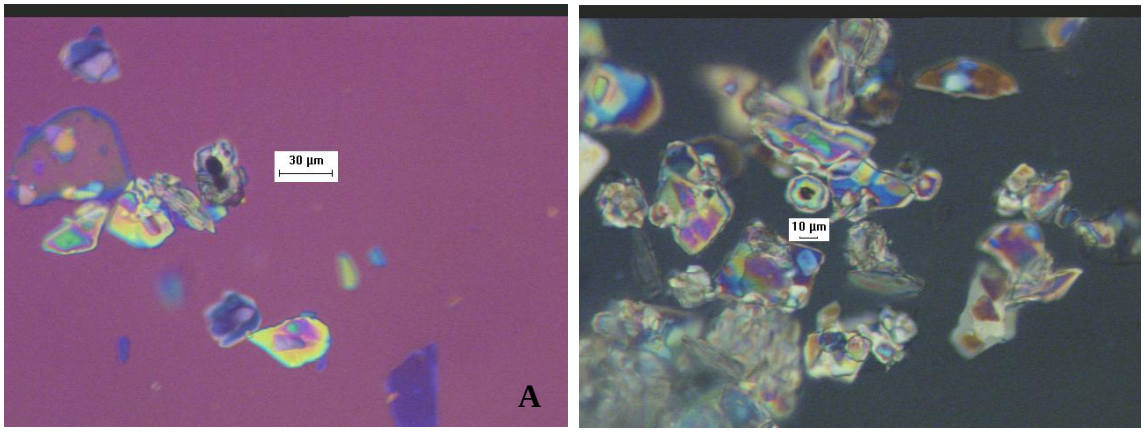

Figure 91. Heterogeneous Burkeite Crystals Obtained in Prior Early Feed Runs.

It was observed in previous Early Feed runs that a portion of the burkeite crystals recovered at the end of crystallization were heterogeneous. As seen in Figure 91, the core of these crystals were composed of small crystals, mainly sodium nitrate, around which burkeite had grown. It is believed that by reducing the proportion of heterogeneous burkeite crystals, the crystal purity can be enhanced (heterogeneous crystals are more likely to capture mother liquor than homogenous crystals).

It was hypothesized that the formation of heterogeneous burkeite crystals could be minimized by increasing burkeite nucleation and reducing the nucleation of non-burkeite species. Run 50a attempted to do this through variation of the evaporation rate during the run.

5.1.2.2 Operating conditions

The variation of evaporation rate with run time was based on the simulation shown in Figure 84 and the previous Early Feed experiments. Specifically, the variation in evaporation rate consisted of (1) a very high evaporation rate prior to saturation of the solution, (2) a high evaporation rate during the run segment in which burkeite nucleation was expected (and before sodium nitrate or carbonate nucleation), and (3) a slow evaporation rate during the segment in which nucleation and growth of sodium nitrate and sodium carbonate monohydrate were expected.

Temperature and pressure profiles from Run 50a are shown in Figure 92. The run temperature was controlled to within +/- 1 ^{o}C of the target value of 66 ^{o}C. The pressure profile reflects the step-wise changes in vacuum that are associated with manual adjustments of the regulating valve.

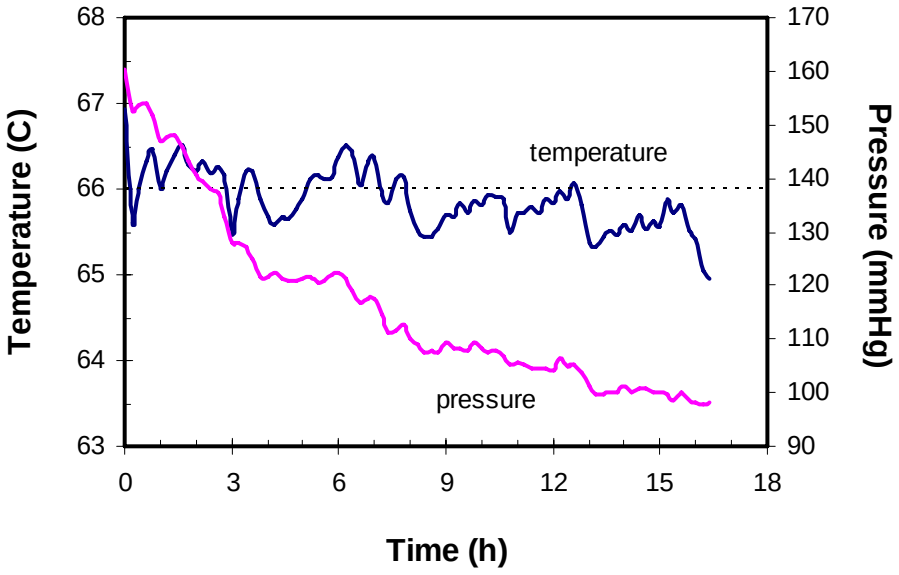

Figure 92. Temperature and Pressure Profiles for Run 50a. The dotted line represents the target operating temperature of 66 oC.

The mass of vapor generated as a function of time is shown in Figure 93. The target and actual condensate-to-feed ratios for this run were 0.474 and 0.475, respectively. The operating time for the run was 16.5 hours. Overall and detailed mass balances are provided in Appendix L.

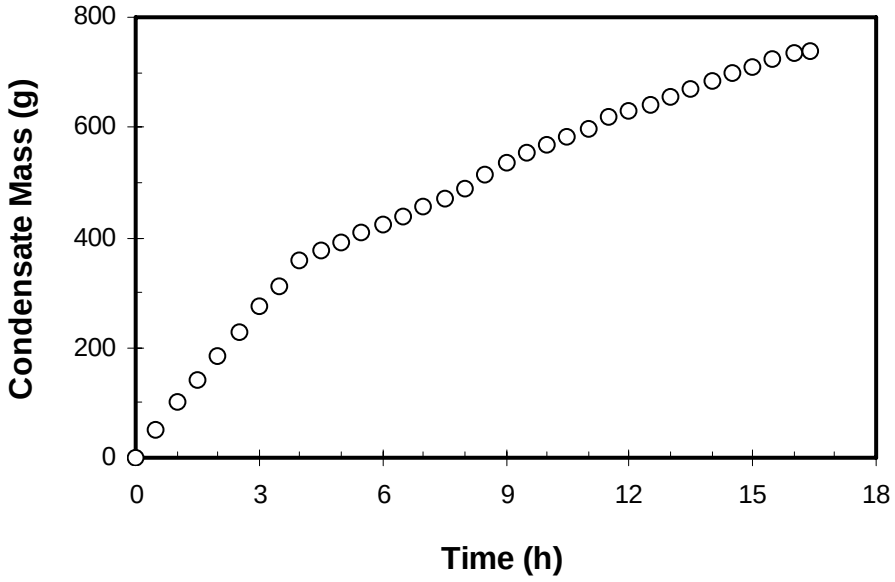

Figure 93. Evaporation Profile for Run 50a.

5.1.2.3 Slurry composition and Crystal size distribution

Samples were taken from the slurry of Run 50a for PLM analysis. Images from this analysis displayed the presence of sodium nitrate, sodium carbonate monohydrate, burkeite, sodium sulfate, and sodium oxalate. Selected images are shown in Figure 94. Large amounts of sodium nitrate crystals were observed. Their size ranged from several microns up to sizes of 300-400 μm. There were few large (>500 μm) single sodium nitrate crystals observed. Despite a similar average size, the amount of small sodium nitrate crystals appears to be lesser than in Run 38b. The small sodium nitrate crystals, with a size of only a few microns, are expected to go through the medium-frit filter and be collected in the filtrate.

Sodium carbonate monohydrate crystals were present in important amounts. Their average size was around 50-100 μm. Sodium oxalate crystals were observed in trace amounts, similar to Run 38b. The burkeite crystals were observed in reasonable amounts, and their average

size was smaller than in Run 38b. Burkeite crystals were present at a lower size range (20 µm or less) than in Run 38b (30-50 µm) and generally appeared as single crystals. The burkeite crystals observed in the slurry displayed a greater proportion of homogenous crystals than those seen in Run 38b. Both observations are in agreement with the expected effects of the evaporation profile applied to Run 50a.

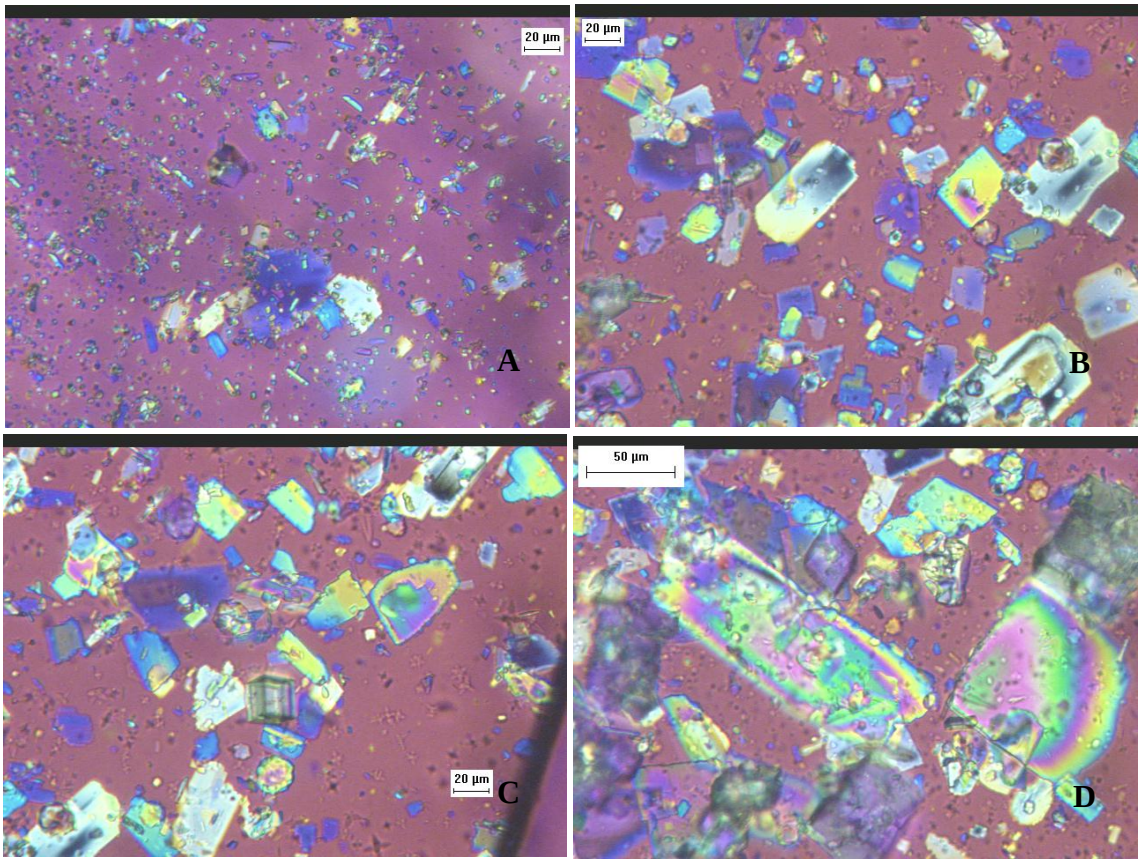

Panel A, sodium nitrate nuclei, panel B and D, sodium carbonate monohydrate 50 to 100µm and sizes slightly higher than 100µm, panel C, burkeite crystals with sizes less or equal to 20µm.

Figure 94. PLM Images from the Slurry of Run 50a

The increased evaporation rate in Run 50a apparently increased burkeite nucleation, leading to a smaller average size. On the other hand, the similar (slightly lower) evaporation rate in the region of sodium carbonate monohydrate and sodium nitrate crystal nucleation led to

similar size ranges of these crystals. These effects combined to increase the proportion of burkeite nuclei with respect to nitrate nuclei during the period of burkeite growth and hence reduced the proportion of heterogeneous burkeite at the end of the run.

The CSD of Run 50a is shown in Figure 95. The figure displays (1) the same mode size as Run 38b, but with a smaller percentage of crystals at this size, (2) a slightly larger general spread, (3) a slightly different first mode and (4) a slightly greater amount of large crystals (crystals over 500 μm).

The first section of the CSD, Run 50a is very close to that of Certification Run 38b. However, the crystals obtained are slightly smaller than in Run 38b (a slightly higher amount between 0 and 50 μm and a slightly smaller amount between 50 and 200 μm). The crystals corresponding to this size range (0-50 μm) are mainly burkeite and sodium carbonate. Hence, the burkeite crystals have an average size smaller than those from Run 38b.

In the second section of the curve, between 200 and 600 μm, the crystals obtained (mainly sodium nitrate crystals) are larger for Run 50a than for Run 38b. This discrepancy may be reduced if the agglomeration analysis proves a higher percent of agglomerates in the higher sieve size for Run 50a.These observations are further illustrated in Figure 96 and Table 32.

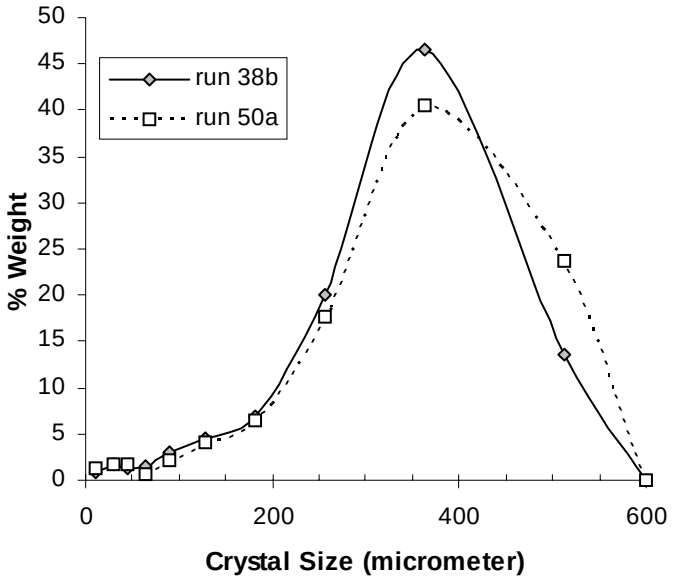

Figure 95. CSDs for Runs 38b and 50a.

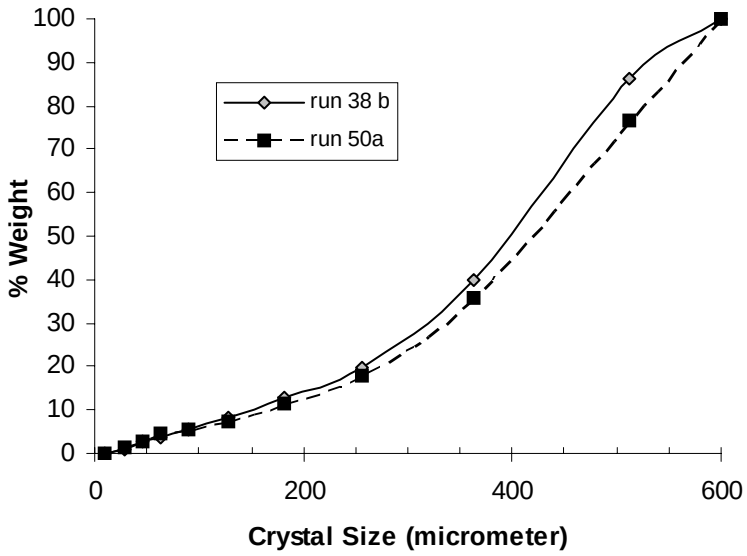

Figure 96. Cumulative Mass Distributions for Runs 38b and 50a.

Table 32. CSD Comparison for Runs 38b and 50a.

Criteria	Early Feed 38b	Early Feed 50a
Coefficient of variation	34.7	39.4
Percent crystal mass at mode size	46.62	39.7
Percent crystal mass below 50μm	3.82	5.2

5.1.2.4 Solid-liquid separation

Several criteria were used to evaluate the effect of evaporation rate on the solid-liquid separation steps in Runs 38b and 50a. These are shown in Table 33.

Table 33. Comparisons Between Runs 38b and 50a.

Criteria	Early Feed 38b	Early Feed 50a
Evaporation rate (g/hr)	~ 25	~ 70 for burkeite region and ~ 25 for nitrate and carbonate region
Condensate-to-Feed Ratio	0.481	0.475
Washes necessary for major mother liquor removal	3	3-4[4]
Filtration & Washing Time	Typical	Typical
Slurry cake composition	Powder-like with large-medium crystals	Powder-like with large-medium crystals
Mass of final crystals	Typical (210 g)[5]	Increased (262 g)
Color of final crystals	White with slight yellow color	White with slight yellow color
Ease of operation	No filter plugging, easy to stir	Very slight filter plugging, still easy to stir

A key point illustrated in Table 33 is the difference between the masses of final crystals from the two runs; Run 50a generated far more product crystals. The main explanation for this is

[1] Three washes were necessary for major removal and no change in color was observed after the fourth wash.
[2] The value of 210 g in Run 38b corresponds to the final mass of crystals collected after the washing steps. This does not account for the samples collected from the unwashed crystals or those collected after each wash step, which totaled 19 g. The discrepancy between the two values may be explained by the difference in accumulation collected at the end of Run 38b (135 g) and Run 50a (85 g).

the accumulation difference between the two runs. Run 50a had 50 grams less accumulation than Run 38b, and this mass was collected as product crystals. Both runs were however very similar concerning the solid-liquid separation step

5.1.2.5 Crystal identification

Samples were taken from the sieved crystals of Run 50a for PLM analysis. Images from this analysis displayed the presence of sodium nitrate, sodium carbonate monohydrate, burkeite, sodium sulfate, and sodium oxalate. Selected images are shown in Figure 97.

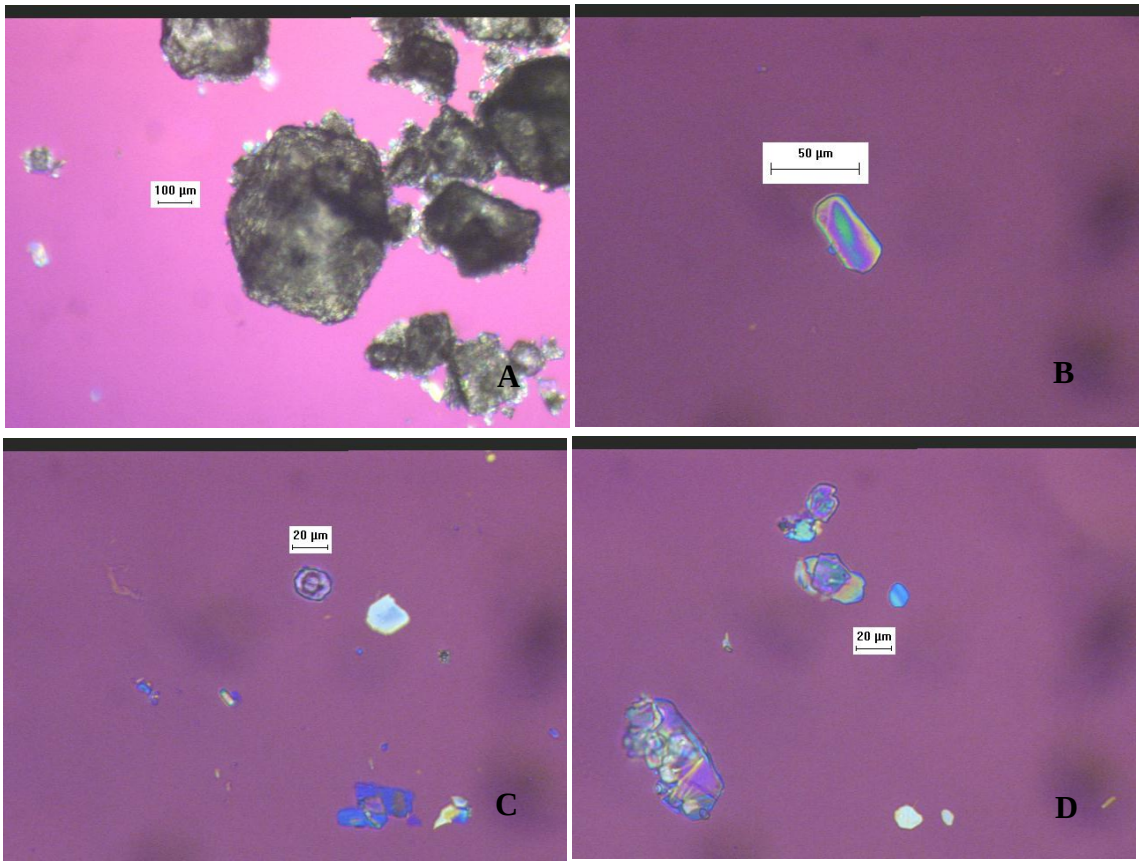

Panel A, sodium nitrate at mode size, panel B, sodium carbonate monohydrate with sizes ranging from 50 to 100µm, panel C, homogenous burkeite crystals with a size equal to 20µm, panel D, trace of sodium sulfate and sodium oxalate crystals

Figure 97. PLM Images from Sieved Crystals of Run 50a

5.1.2.6 Conclusions

Run 50a achieved its main objective. By applying a convex evaporation profile, burkeite crystals were produced at higher number but lowered size. The size range of burkeite crystals displayed in run 50a represents the lowest obtained by crystallization with Early Feed. By creating a lot of burkeite nuclei, burkeite grown on the existing burkeite more in this run than on nitrate nuclei. Consequently, the proportion of heterogeneous burkeite crystals was reduced which should have an effect on decontamination. On the other hand, no real improvement or deterioration of the conditions of solid liquid separation was noticed compared to run 38B.

5.2 INFLUENCE OF EVAPORATION RATE VALUE

5.2.1 Objectives

A crystallization run (run 48) was performed on the FY06 simulated Early Feed solution. The purpose of Run 48 was to study the effect of an elevated evaporation rate on crystal size distribution and on the solid-liquid separation. The results of run 48 would be compared to those from Certification Run 38b to assess any improvement concerning the filtration operation.

5.2.2 Operating conditions

Run 48 was performed in a single-stage and had an average evaporation rate of 58 g/h. Results from this run were compared to those of Stage 1 from Certification Run 38b, which had an average evaporation rate of 25 g/h.

Temperature and pressure profiles from Run 48 are shown in Figure 98. The run temperature was controlled to within +/- 1 ^{o}C of the target value of 66 ^{o}C, except for one excursion 10.5 hours into the experiment. The pressure profile reflects the step-wise changes in vacuum that are associated with manual adjustments of the regulating valve.

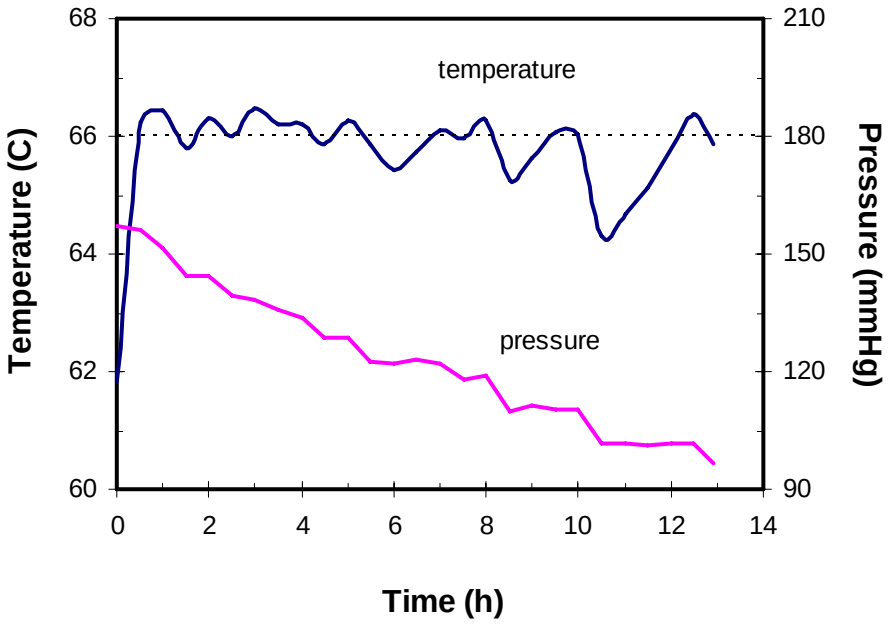

Figure 98. Temperature and Pressure profiles for Run 48. The dotted line represents the target operating temperature of 66 ^{o}C.

The mass of vapor generated as a function of time is shown in Figure 99. The target and actual condensate-to-feed ratios for this run were 0.474 and 0.491, respectively. The operating time for the run was 12.9 hours, and the average evaporation rate was about 58 g water/h. Overall and detailed mass balances are provided in Appendix L.

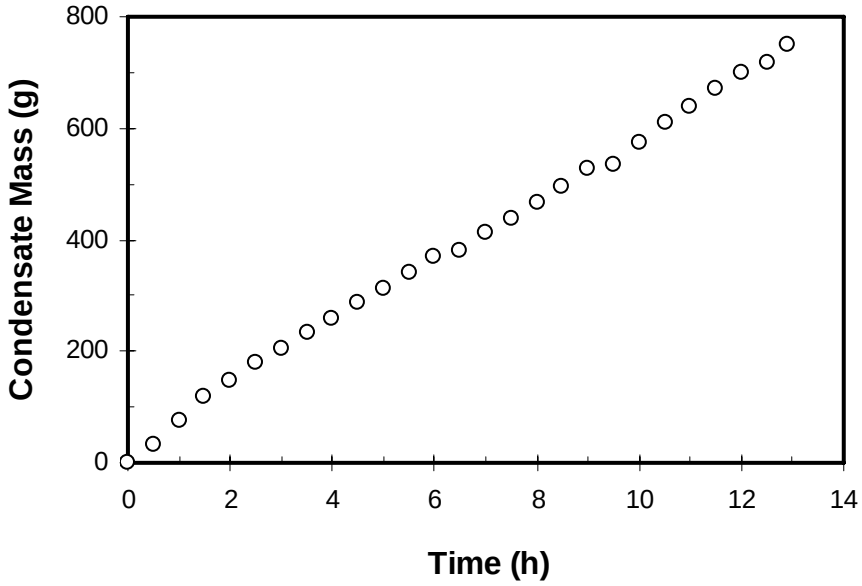

Figure 99. Evaporation profile for Run 48.

5.2.3 Slurry composition and CSD

Samples were taken from the slurry of Run 48 for PLM analysis. Images from this analysis displayed the presence of sodium nitrate, sodium carbonate monohydrate, burkeite, sodium sulfate, and sodium oxalate. Selected images are shown in Figure 100.

The sodium nitrate crystals were observed in very large amounts. Their size ranged from several microns up to sizes of 300-400 μm. There were very few large (>500 μm) single sodium nitrate crystals observed. The amount of small crystals is significant and the average size of the sodium nitrate crystals appears to be smaller than in Run 38b. The small crystals had well-defined shapes, which allowed their identification as sodium nitrate. These crystals, with a size of only a few microns, are expected to go through the medium-frit filter and be collected in the filtrate.

Sodium carbonate monohydrate crystals were present in important amounts. Their average size was around 50 µm, which is smaller than those produced in Run 38b. More sodium carbonate monohydrate crystals are likely to be recovered in the sieves smaller than 50 µm.

Sodium oxalate crystals were observed in trace amounts, similar to Run 38b. The burkeite crystals were observed in reasonable amounts, although their proportion was less than in Run 38b. This observation could be associated with the presence of an increased amount of sodium sulfate crystals in Run 48. Burkeite crystals were present at a lower size range (20 microns or less) than in Run 38b (30-50 µm) and generally appeared as single crystals. Only a few heterogeneous crystals were observed.

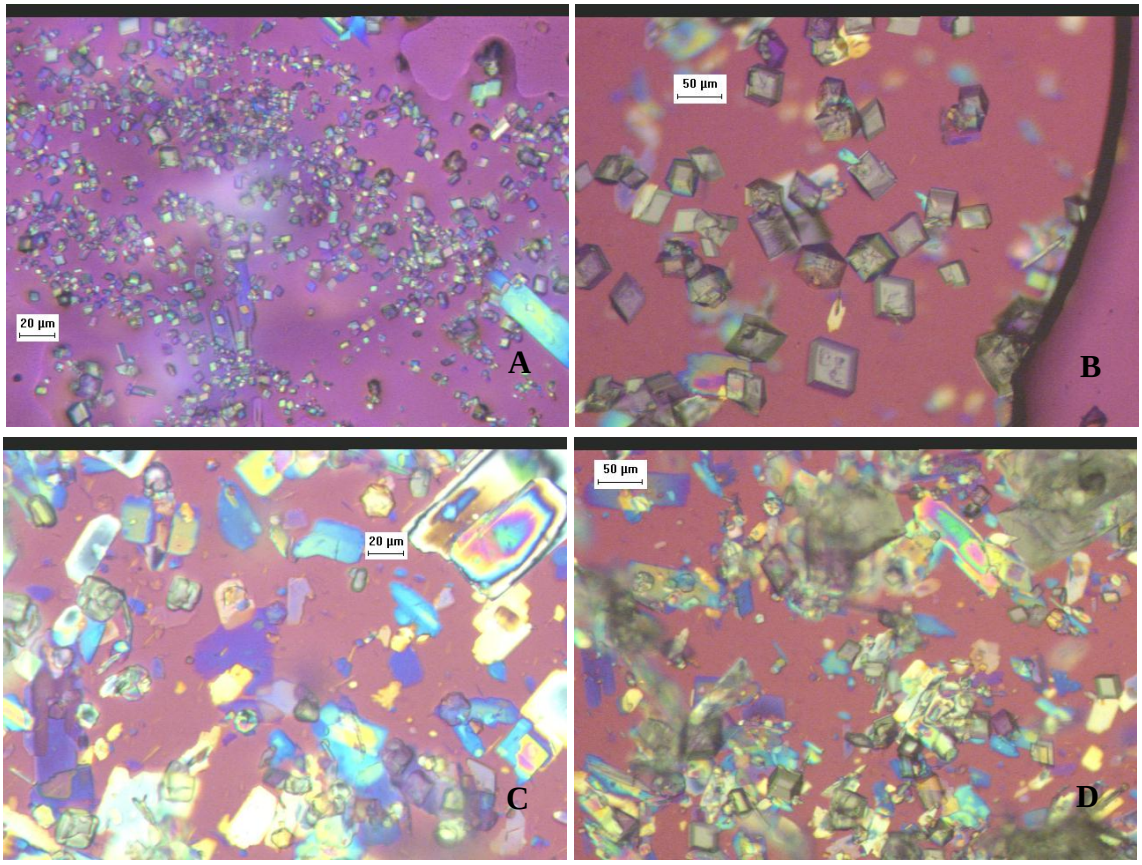

Panel A and B, sodium nitrate crystals as nuclei and lower size, panel C, burkeite crystals with sizes less than or equal to 20µm, panel D, sodium carbonate with sizes ranging from 50 to 100µm.

Figure 100. PLM Images of Sieved Crystals from Run 48

The increased evaporation rate in Run 48 increased the nucleation rate of the crystal species, with sodium nitrate and sodium carbonate monohydrate being the most evident. This increased nucleation led to more crystals with a smaller average size, making the effective growth rate appear lower.

The CSD of Run 48 is shown in Figure 101. The figure displays (1) the same mode size as Run 38b, but with a smaller percentage of crystals at this size, (2) a slightly larger general spread, and (3) a greater amount of fines (crystals under 50 μm). For analysis purposes, the curve will be divided into two sections (from 0-200 μm and 200-600 μm).

In the first section of the CSD, Run 48 produced more crystals between 0 and 50 μm, whereas they were less numerous between 50 and 200 μm. The crystals between 0 and 50 μm have not been grown to the size of 50-200 μm, as they were in Run 38b. The crystals corresponding to this size range (0-50 μm) are mainly burkeite and sodium carbonate. Hence, the sodium carbonate crystals have an average size smaller than those from Run 38b. Slurry images display that sodium nitrate crystals are present in this size range, attesting to an increased nucleation rate of sodium nitrate crystals.

In the second section of the curve, between 200 and 600 μm, there are two distinct parts. Between 200 and 300 μm, Run 48 produced more crystals, whereas Run 38b produced more crystals in the range of 300 and 600 μm. This proves that the sodium nitrate crystals obtained between 200 and 300 μm were not grown to the higher size range, as they were in Run 38b. As a result, the effective growth rate of sodium nitrate crystals was reduced in Run 48. The discrepancy in the CSDs obtained from these runs is highlighted further in Figure 102 and Table 34 below.

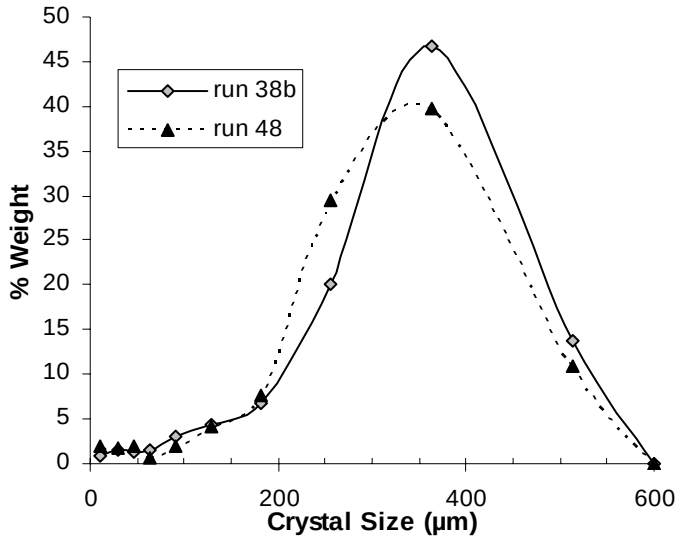

Figure 101. CSDs for Runs 38b and 48

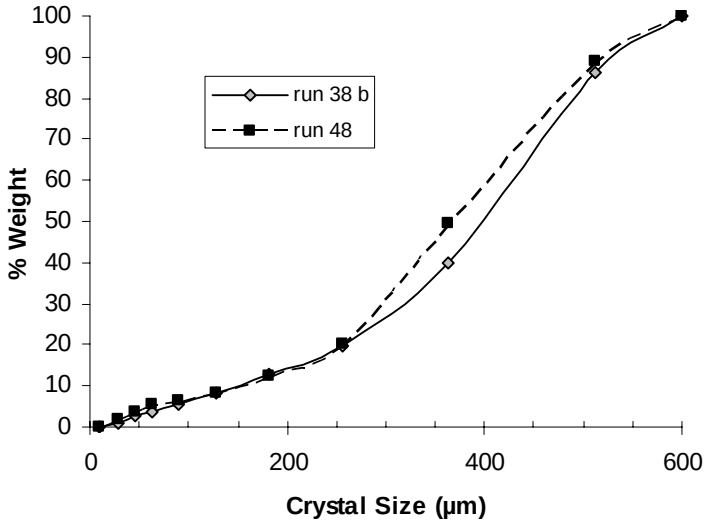

Figure 102. Cumulative Mass Distributions for Runs 38b and 48.

Table 34. CSD Comparison for Runs 38b and 48.

Criteria	Early Feed 38b	Early Feed 41
Coefficient of variation	34.7	35.5
Percent crystal mass at mode size	46.62	39.64
Percent crystal mass below 50µm	3.82	5.64

5.2.4 Solid-liquid separation

Several criteria were used to evaluate the effect of evaporation rate on the solid-liquid separation steps in Runs 38b and 48. These are shown in Table 35.

Table 35. Comparisons between Runs 38b and 48.

Criteria	Early Feed 38b	Early Feed 48
Evaporation rate (g/hr)	~ 25	~ 58
Condensate-to-Feed Ratio	0.481	0.491
Washes necessary for major mother liquor removal	3	5
Filtration & Washing Time	Typical (~ 30min)	Increased (~ 60min)
Slurry cake composition	Powder-like with large-medium crystals	Fine powder with small-medium crystals
Mass of final crystals	Typical (210 g)[6]	Increased (284 g)
Color of final crystals	White with slight yellow color	White with yellow color
Ease of operation	No filter plugging, easy to stir	Some filter plugging, more difficult to stir, increased time.

A key point illustrated in Table 35 is differences in the mass of final crystals from each run; Run 48 generated far more product crystals. One partial explanation for this is the fact that the condensate-to-feed ratio was higher for Run 48: 0.491 in run 48 compared to 0.481 in Run 38b. Another contributing factor is the amount of wash solution used, which caused slightly more crystals to be dissolved in Run 38b. The slurry mass recovered at the end of each crystallization stage was the same for both runs and the accumulation was also nearly identical, which make the discrepancy in final product mass more comparable.

The increased product mass was apparent during the filtration and washing processes and contributed to the processing difficulty. The difficulty was made worse by the apparent crystal

[6] The value of 210 g in Run 38b corresponds to the final mass of crystals collected after the washing steps. This does not account for the samples collected from the unwashed crystals or those collected after each wash step, which totaled 19 g.

size distribution (CSD) of the filter cake. The cake from Run 48 was composed of smaller crystals, which gave the product more of powdery appearance. The fine crystals tended to plug the filter occasionally. Given this CSD, it is clear that the increased evaporation rate favored crystal nucleation over growth, and that the median size of each crystalline species was smaller in Run 48 than in Run 38b.

The CSD in the filter cake from Run 48 had an effect on the ease of solid-liquid separation and crystal washing. The slurry cake obtained at the higher evaporation rate retained more interstitial mother liquor than in Run 38b. This observation is in agreement with a smaller crystal size distribution. The number of washes necessary to remove the interstitial mother liquor from the filter cake (judged by the change in yellow color of the cake over successive washes) increased with the higher evaporation rate, as shown in Table 35. As in the filtration step, filter plugging was an issue due to the accumulation of very small crystals at the surface of the medium frit filter. Along with the filter plugging, the increased mass of crystals from this run made manual stirring more difficult and made this step more time consuming. The crystals recovered from the washing step were of good quality, but with a yellow color more pronounced than those from Run 38b.

5.2.5 Crystal identification

Samples were taken from the sieved crystals of Run 48 for PLM analysis. Images from this analysis displayed the presence of sodium nitrate, sodium carbonate monohydrate, burkeite, sodium sulfate, and sodium oxalate. Selected images are shown in Figure 103.

PLM images showed that the main crystals were grown at a lower size than the certification run 38b. Burkeite crystals were observed at an average size of 15-20μm. Sodium nitrate crystals and sodium carbonate crystals were also affected and their average size was

reduced and distribution was broader. PLM images displayed also that the proportion of heterogeneous burkeite was reduced compared t run 38b and the presence of greater amount of sulfate crystals in run 48.

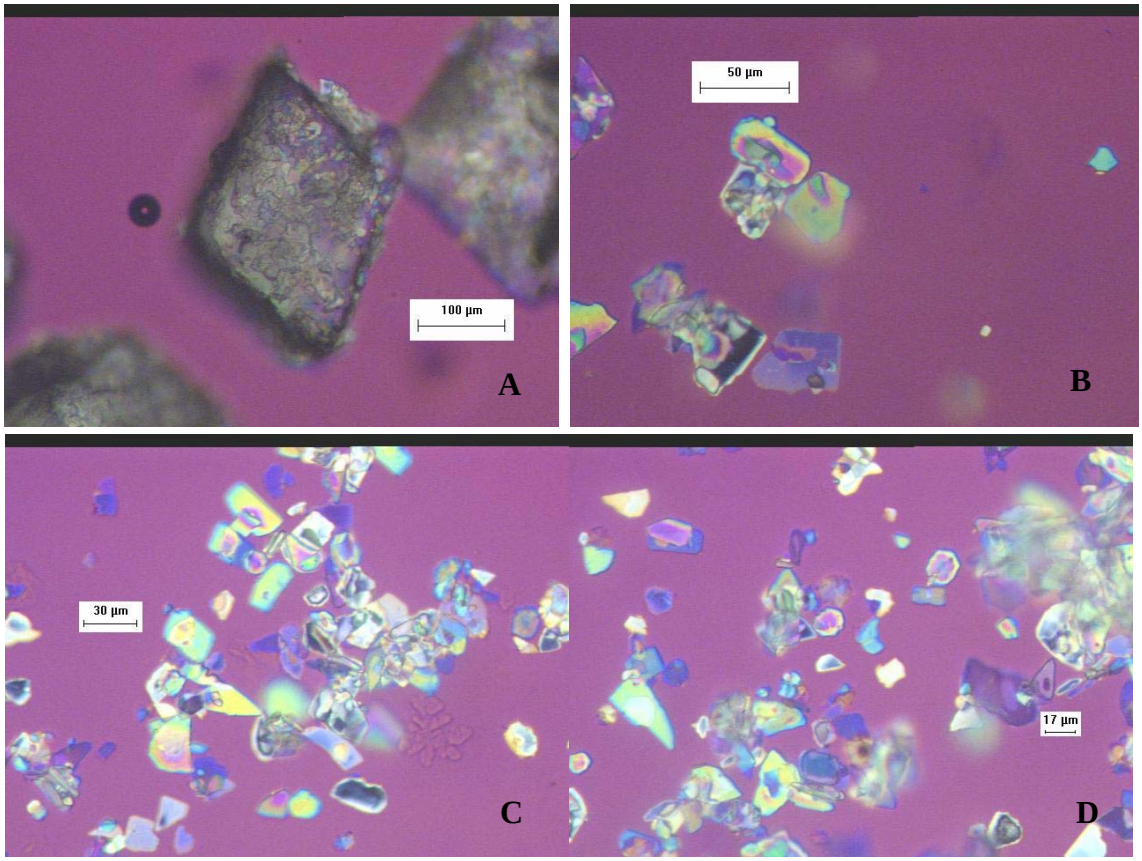

Panel A, sodium nitrate crystals with an average size of 200-250µm, panel B, sodium carbonate with an average size of 50 µm, panel C and D, sodium sulfate and homogenous burkeite.

Figure 103. PLM Images on Sieved Crystals from Run 48

5.2.6 Limitation of evaporation rate value

The run 48 displayed the presence of non negligible amount of sulfate crystals and slightly reduce amount of burkeite crystals. This is one of the impacts of evaporation rate on the crystallization. An additional run performed previous to run 50a proved that by increasing the

evaporation rate further burkeite will not be produced and only sodium sulfate and carbonate will. This outcome would be in opposition to our objectives.

5.2.7 Conclusions

Run 48 displayed the influence of the evaporation rate on the crystallization. As expected, the increase in evaporation rate seemed to have increased nucleation in opposition to crystal growth. As a consequence, the recovered crystals displayed a lower average size. Following the same idea developed in section 5.1.2, the amount of heterogeneous burkeite was reduced. However two main impacts are to take into consideration. First the presence of smaller crystals increased the process difficulties associated with the solid-liquid separation. Secondly the increase in evaporation rate leads to formation of non negligible amount of sodium sulfate, sign that the amount of burkeite crystal might have been reduced.

5.3 INFLUENCE OF OPERATING TEMPERATURE

5.3.1 Objectives

A crystallization run (run 49) was performed on the FY06 simulated Early Feed solution. The first stage of the Early Feed Run 49 was performed under the operating temperature of 55 °C and the same evaporation rate as Certification Run 38b. Results of this run were compared to the certification run in terms of ease of solid-liquid separation and impact on crystallization

5.3.2 Operating Conditions

The first stage has been completed and the temperature and pressure profiles are presented in Figure 104. Throughout the run the temperature was controlled to within +/- 1 ^{o}C of

the target value of 55 °C. The pressure profile reflects the step-wise changes in vacuum that are associated with manual adjustments of the regulating valve.

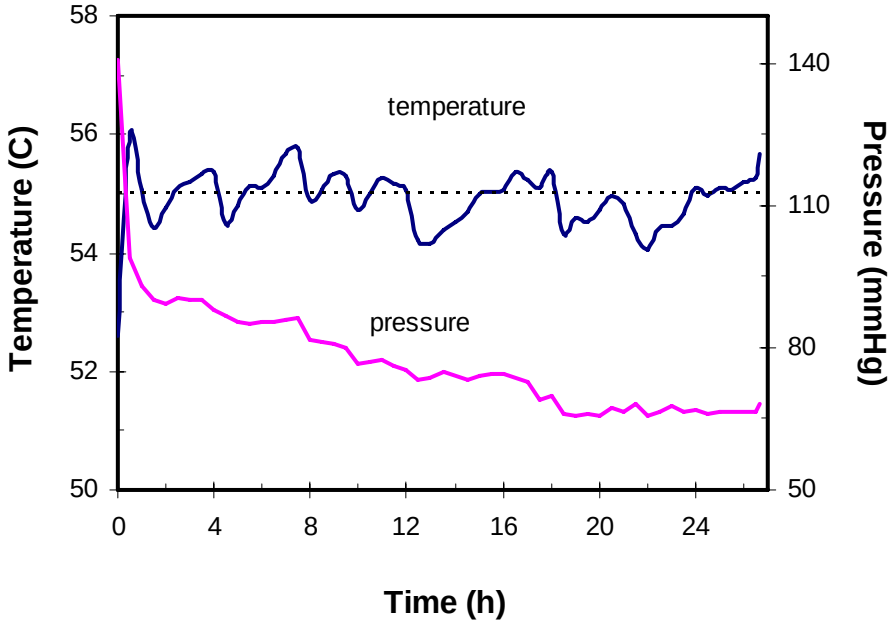

Figure 104. Temperature and Pressure Profiles for Stage 1 of Run 49. The dotted line represents the target operating temperature of 55 °C.

The evaporation profile for Stage 1 of Run 49 is shown in Figure 105. The target and actual condensate-to-feed ratios were 0.461 and 0.471, respectively. The operating time for the first stage was 26.7 hours, and the average evaporation rate was about 27.4 g/h. The Overall mass balance information for the runs 49 and 38b are provided in the Tables 36 and 37.

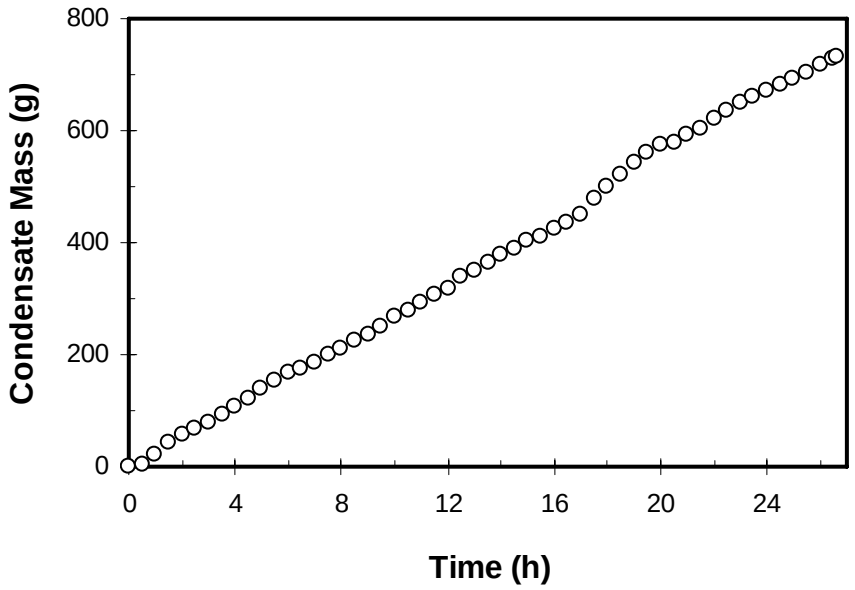

Figure 105. Evaporation Profile for Stage 1 of Run 49.

The mass balance closure for Run 49 was 1.69 % (reduced to 0.51 % after loss accounting). The amounts of feed used for both runs were comparable. The overall mass balance displays that Run 49 produced more final crystal mass than did Run 38b. This increase in crystal mass is displayed without accounting for the samples taken from Run 38b and besides a slightly lower condensate-to-feed ratio for Run 49 (Table 36). The decrease in temperature has hence increased the crystal mass recovered from Early Feed Run 49.

Table 36. Mass balance Run 38b Stage 1

	Input (g)		Output (g)				Accum (g)	Loss (g)
Species	**Feed**	**Wash**	**Cond**	**Washed Solids**	**Filtrate**	**Spent Wash**	**Solids**	
Feed	1565.45							
H_2O			753.03					
Solution		334.28		209.71	385.86	377.31	136.9	
Total	1565.45	334.28	753.03	209.71	385.86	377.31	136.9	36.92
Combined	1899.73		1862.81					36.92
								1.9%
							Corrected Loss	0.4%

30.03 grams were accounted for from this stage, leading to a corrected loss of 0.4%.

Table 37. Mass Balance Run 49 Stage 1

	Input (g)		Output (g)				Accum (g)	Loss (g)
Species	**Feed**	**Wash**	**Cond**	**Washed Solids**	**Filtrate**	**Spent Wash**	**Solids**	
Feed	1587.57							
H_2O			748.47					
Solution		303.68		228.14	372.87	369.99	139.72	
Total	1587.57	303.68	748.47	228.14	372.87	369.99	139.72	32.06
Combined	1891.25		1859.19					32.06
								1.69%
						Corrected Loss		0.51%

22.34 grams were accounted for from this stage, leading to a corrected loss of 0.51 %.

Table 38. Condensate-to-feed ratio Run 38b and Run 49

Criteria	Early Feed 38b	Early Feed 49
Condensate-to-feed ratio	0.481	0.471

5.3.3 Slurry composition and csd

Figure 106 displays the PLM images taken of samples from the slurry of Run 49. The species identified were (1) burkeite crystals, (2) sodium carbonate monohydrate, (3) sodium nitrate, (4) sodium sulfate and (5) sodium oxalate. Another crystalline species was detected in the slurry and were not identified as a round shape carbonate or burkeite crystal.

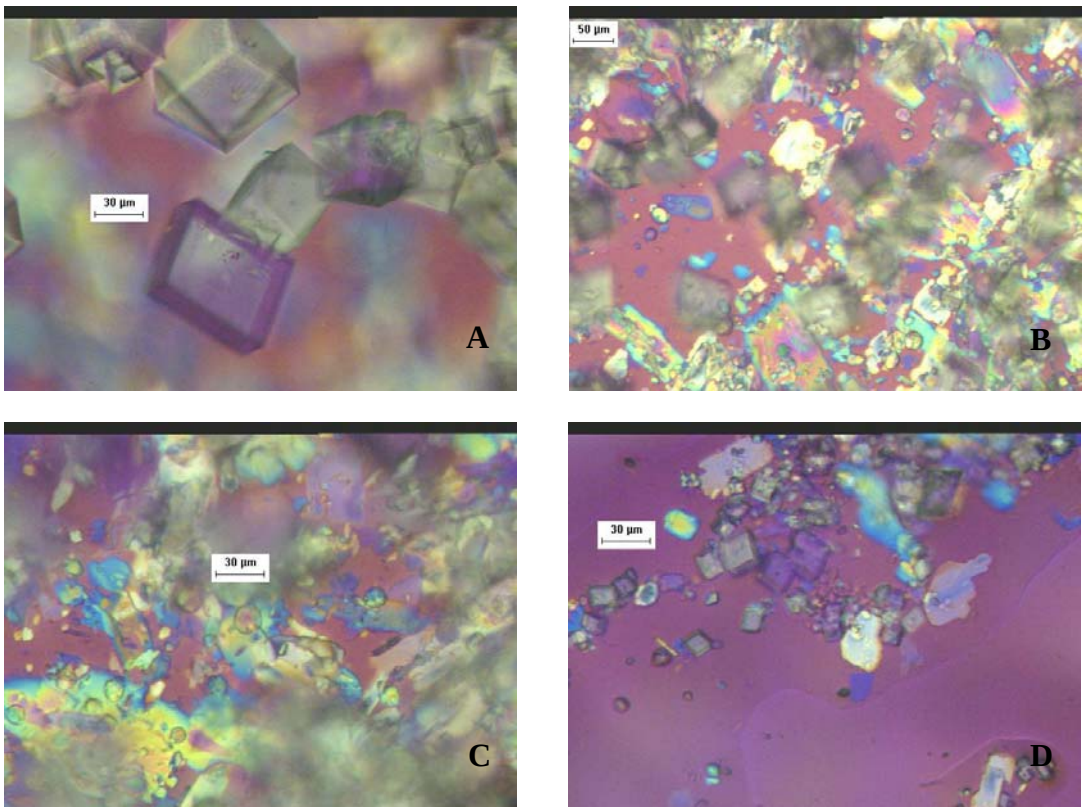

(a) sodium nitrate crystals, (b) sodium carbonate monohydrate and sodium sulfate crystals, (c) burkeite crystals, (d) small sodium nitrate crystals and trace of sodium oxalate crystals.

Figure 106. PLM Images from Run 49 Slurry

The burkeite crystals were observed as single non-heterogeneous crystals at an average size of 15 µm. This represents a relatively small size compared to the burkeite crystals that were observed at a higher size range in Run 38b (30 to 50 µm). The growth rate of burkeite crystals was hence reduced.

The observed sodium nitrate crystals were smaller than those in Run 38b, indicating a reduced growth rate. This observation is in agreement with the expectation that the temperature decreases the solubility of the sodium nitrate and affects the growth rate. A large number of small crystals were observed, which indicates an increase in the nucleation rate of the sodium nitrate crystals. Figure 107 displays images of sodium nitrate crystals.

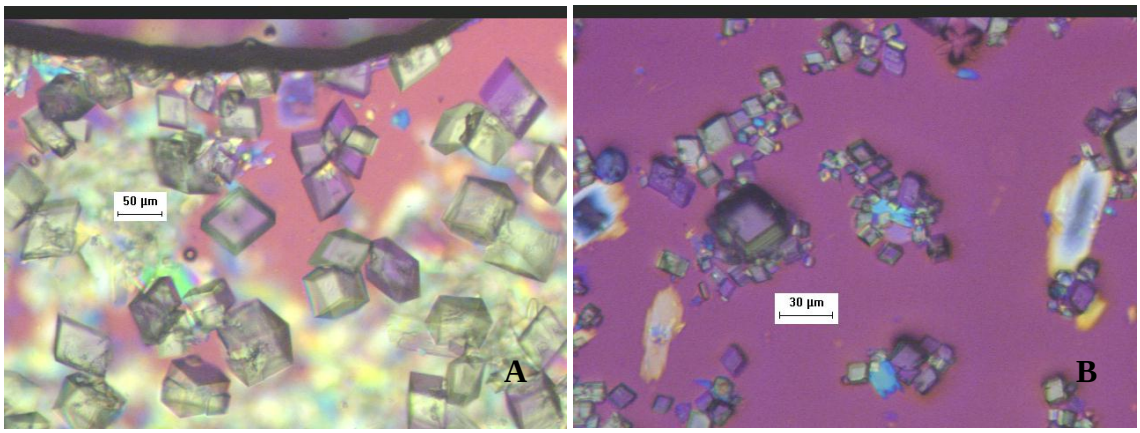

(a) medium-sized sodium nitrate crystals and (b) non-negligible amount of small sodium nitrate crystals.

Figure 107. Sodium Nitrate crystals from Run 49 Slurry

The sodium carbonate monohydrate crystals were observed in a size ranging between 20 to 100 µm. Based on the slurry images it is difficult to estimate the impact of temperature on the sodium carbonate; however the apparent smaller size of sodium carbonate crystals and the absence of large sodium carbonate in the slurry samples tends to confirm a decrease in the growth rate of sodium carbonate monohydrate crystals.

As in the preceding run, a round shaped crystalline form was observed. This species might be either burkeite (based on round shape and size) or carbonate (color and rainbow).

Sieving was performed on the final product of Run 49, and the results for two samples are given in Figure 108. The CSD displays a primary mode size around 250 µm. This curve is bimodal and the secondary mode is observed around 45 µm. In addition, the curves show that less than 5% of the crystal mass is below 100 µm. Comparison with Run 38b CSD confirms that the crystals obtained in Run 49 are smaller than those from Run 38b. The mode size has been reduced from Run 38b to run 49 showing that the sodium nitrate growth rate has been particularly affected by the change in temperature (the sodium nitrate is the only species grown

at a size exceeding 200 μm). The distribution is relatively narrow and gives a coefficient of variation of 32.6 %, where

$$CV = \frac{100(d_{84\%} - d_{16\%})}{2d_{50\%}}$$

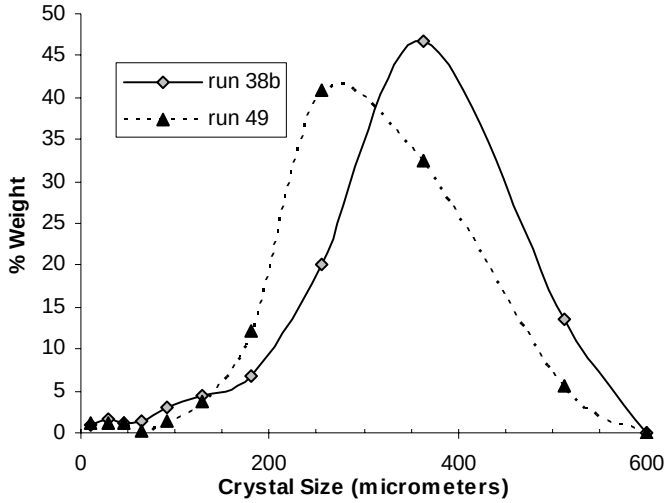

Figure 108. CSDs of Run 38b and 49.

The comparison of the coefficients of variation for Runs 38b and 49 are presented in Table 39, which shows that the overall distribution is narrower for Run 49 than for the Certification Run 38b. This observation implies modifications in the nucleation and growth rate from Run 38b to Run 49.

Table 39. Coefficient of Variation Run 38b and Run 49

Criteria	Early Feed 38b	Early Feed 49
Coefficient of variation	34.7 %	32.6 %

Figure 109 shows the cumulative mass distributions from Runs 38b and Run 49, which highlight the fact that Run 49 produced smaller sodium nitrate crystals than run 38b. The amount of fines (crystal size lower than 100 μm) collected for both runs are equivalent. An effect on the separation process is hence expected due to higher crystal mass and smaller crystal size but no filter plugging is expected as it is linked to the amount of fines.

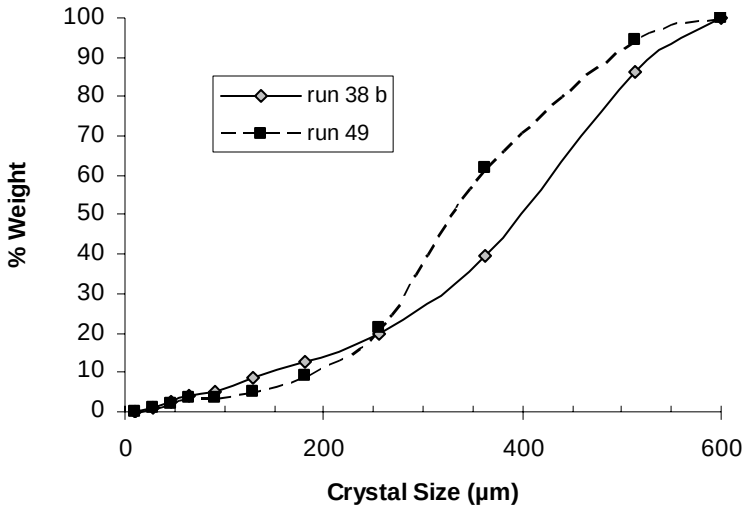

Figure 109. Cumulative Mass Distribution of Run 38b and 49.

5.3.4 Solid-liquid separation

Table 40 quantifies a comparison of the solid-liquid separation of slurries from Runs 38b and 49. The increases in mass of crystals and the smaller crystals (especially sodium nitrate crystals) have increased the time of separation and the stirring. On the other hand no filter

plugging was observed and the color of the recovered final crystals were identical for Runs 38 b and 49.

Table 40. Effect of Crystal Distribution on Solid-Liquid Separation

Criteria	Early Feed 38b	Early Feed 41
Evaporation rate value (g/h)	~ 25	~ 27.4
Washes necessary for major mother liquor removal	3	3-4
Time	Typical (~ 30min)	Slightly Increased (~ 45min)
Slurry cake	Powder like with large-medium crystals	Finer powder with smaller crystals
Mass of crystals	Typical (210 g)	Increased (230 g)
Color of final crystals	White with slight yellow color	White with slight yellow color
Ease of operation	No filter plugging, easy to stir.	No filter plugging, more difficult to stir.

5.3.5 Conclusions

Run 49 provided valuable information on the impacts of temperature on the SST Early Feed crystallization. The crystals obtained from run 49 were smaller than the certification run 38b, indicating a reduced growth rate. This observation is in agreement with the expectation that the temperature decreases the solubility especially of the sodium nitrate and affects the growth rate. The reduced size of the crystal leads to more difficulty during the separation step as important proportions of small crystals have the tendency to plug the apparatus.

5.4 INFLUENCE OF CONDENSATE TO FEED RATIO

5.4.1 Objectives

Run 50b was performed in a single-stage and the condensate-to-feed ratio was increased to assess the effects of varying evaporation profile and extended evaporation. The profile used was similar to the one applied in Run 50a.

5.4.2 Operating conditions

Temperature and pressure profiles from Run 50b are shown in Figure 110. The run temperature was controlled to within +/- 1 ^{o}C of the target value of 66 ^{o}C. The pressure profile reflects the step-wise changes in vacuum that are associated with manual adjustments of the regulating valve.

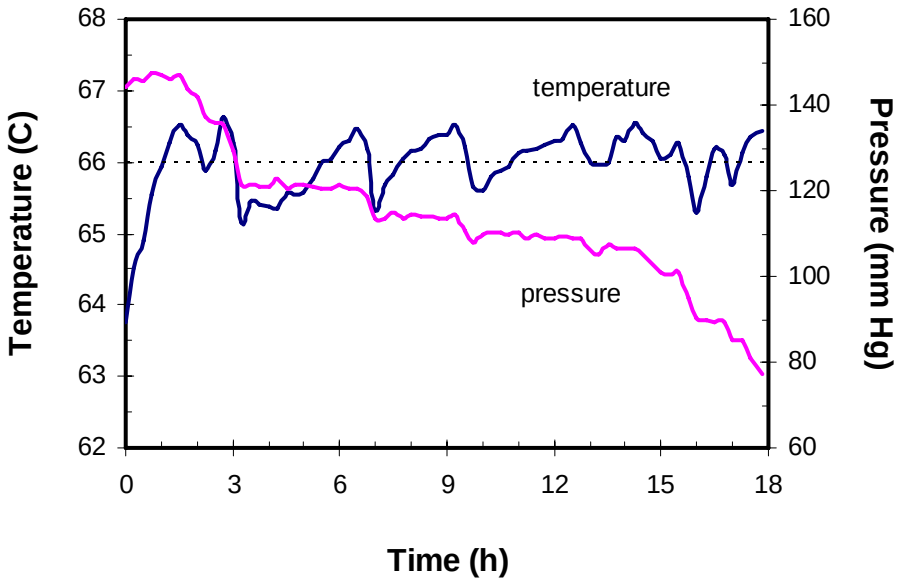

Figure 110. Temperature and Pressure Profiles for Run 50b. The dotted line represents the target operating temperature of 66 ^{o}C.

The mass of vapor generated as a function of time is shown in Figure 111. The target and actual condensate-to-feed ratios for this run were 0.474 and 0.538, respectively. The operating time for the run was 18 hours. Overall and detailed mass balances are provided in Appendix K.

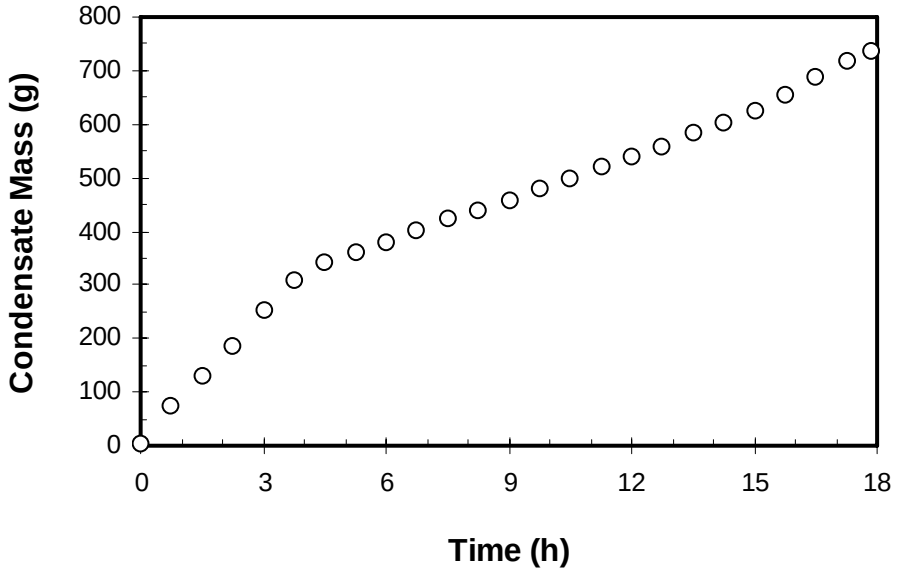

Figure 111. Evaporation profile for Run 50b**.**

5.4.3 Slurry composition and csd

Samples were taken from the slurry of Run 50b for PLM analysis. Images from this analysis displayed the presence of sodium nitrate, sodium carbonate monohydrate, burkeite, sodium sulfate, and sodium oxalate. Selected images are shown in Figure 112.

The sodium nitrate crystals were observed in very large amounts. Their size ranged from several microns up to sizes of 300-400 μm. There were non-negligible amounts of large (>500

μm) single sodium nitrate crystals observed. The average size was increased, whereas the amount of small sodium nitrate crystals appears to be less than in Run 38b. The small sodium nitrate crystals, with a size of only a few microns, are expected to go through the medium-frit filter and be collected in the filtrate.

Sodium carbonate monohydrate crystals were present in important amounts. Their average size was around 100 μm. An increased amount of sodium carbonate monohydrate crystals are likely to be recovered in the sieves greater than 50 μm.

Sodium oxalate crystals were observed in trace amounts, similar to Run 38b. The burkeite crystals were observed in reasonable amounts, although their average size was smaller than in Run 38b. Burkeite crystals were present at a lower size range (20 microns or less) than in Run 38b (30-50 μm) and generally appeared as single crystals. The burkeite crystals observed in the slurry displayed a greater proportion of homogenous crystals than in Run 38b. Both observations are directly linked to the increased evaporation rate applied to the burkeite crystals and might lead to lesser proportion of burkeite crystals recovered in the final product (loss through filter).

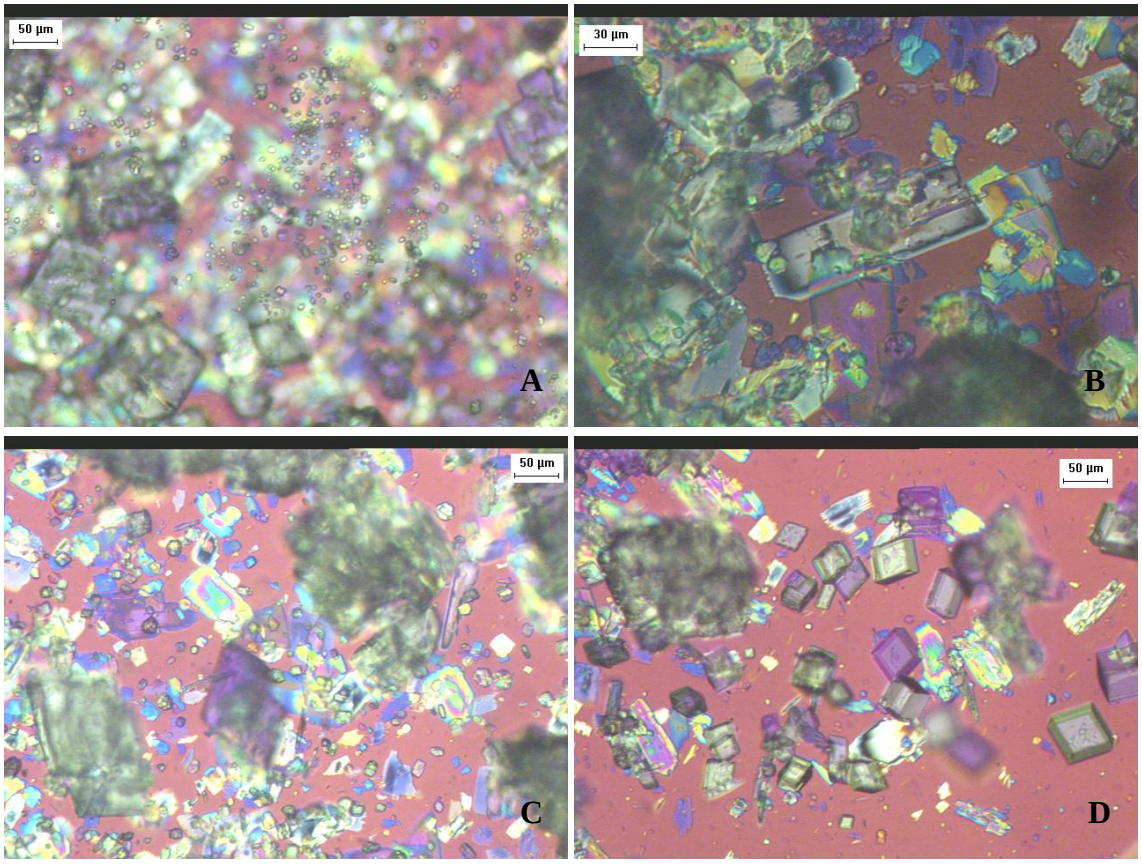

Panel A, sodium nitrate nuclei, panel B, sodium carbonate with a size around 100µm,panel C, burkeite crystals with a size less than or equal to 20 µm, panel D, sodium nitrate and trace of sodium oxalate in the background.

Figure 112. PLM Images of Slurry from run 50b

The evaporation profile used in Run 50b seems to have had the same effect on the burkeite crystals as seen in Run 50a. Both runs increased burkeite nucleation, leading to a smaller average size and less heterogeneous crystals. The increase in condensate-to-feed ratio has apparently only affected the growth of sodium nitrate and sodium carbonate monohydrate crystals.

The CSD of Run 50b is shown in Figure 113. The figure displays (1) a higher mode size than Run 50a, (2) a slightly smaller general spread, (3) a slightly different first mode and (4) a greater amount of larger crystals (crystals over 500 μm).

In the first section of the CSD, Run 50b is close to the results obtained for Run 50a. The amount of crystals collected in the first mode (between 0 and 50 μm) is slightly smaller because the burkeite crystals have similar size to Run 50a but the sodium carbonate monohydrate crystals have a higher size. A smaller amount of crystals was collected between 50 and 200 μm since the sodium nitrate crystals were grown to a larger size in Run 50b. The collection of a greater amount of sodium nitrate crystals decrease the percentage of final mass attributed to the sodium carbonate monohydrate and burkeite crystals.

In the second section of the curve, between 200 and 600 μm, the crystals obtained (mainly sodium nitrate crystals) are larger for Run 50b than for Run 50a. This discrepancy is completely dependent on the increase of operating time and condensate-to-feed ratio.

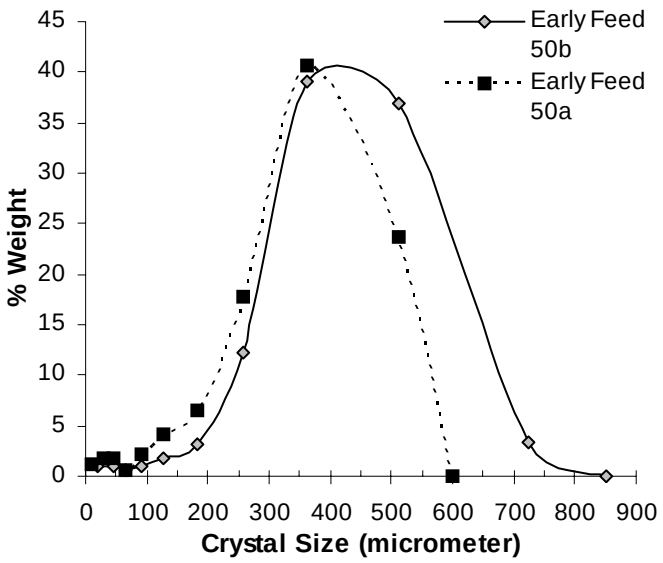

Figure 113. CSDs for Runs 50a and 50b.

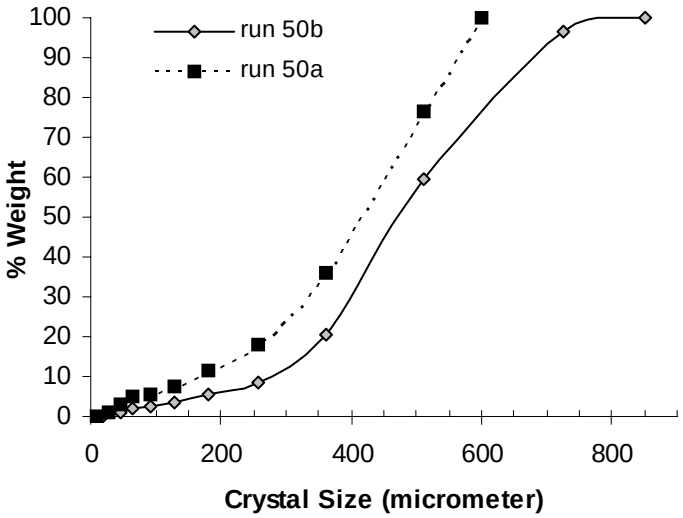

Figure 114. Cumulative Mass Distributions for Runs 50a and 50b.

These observations are further illustrated in Figure 114 and Table 41

Table 41. CSD comparison for Runs 38b and 50b

Criteria	Early Feed 38b	Early Feed 50a	Early Feed 50b
Coefficient of variation	34.7	39.4	30.9
Percent crystal mass at mode size	46.62	39.7	39.1
Percent crystal mass below 50μm	3.82	5.2	0.89

5.4.4 Solid-liquid separation

Several criteria were used to evaluate the effect of evaporation rate on the solid-liquid separation steps in Runs 38b and 50b. These are shown in Table 42.

Table 42. Solid Liquid Separation Comparison between Run 38b and 50b

Criteria	Early Feed 38b	Early Feed 50b
Evaporation rate (g/hr)	~ 25	~ 70 for burkeite region and ~ 25 for nitrate and carbonate region
Condensate-to-Feed Ratio	0.481	0.538
Washes necessary for major mother liquor removal	3	4-5[7]
Filtration & Washing Time	Typical	Typical[8]
Slurry cake composition	Powder-like with large-medium crystals	Powder-like with large crystals
Mass of final crystals	Typical (210 g)[9]	Increased (296 g)
Color of final crystals	White with slight yellow color	White with slightly more pronounced yellow color
Ease of operation	No filter plugging, easy to stir	Slight filter plugging, easy to stir

[7] The main change in color occurred during the first 4 washes, however the color change was still significant the fourth and fifth wash.
[8] The larger crystal size made the washing easier and compensated for the important mass increase.
[9] The important discrepancy in crystal mass is due to the higher condensate-to-feed ratio for Run 50b.

A key point illustrated in Table 42 is the difference in mass of final crystals from each run; Run 50b generated far more product crystals. The main explanation for this is the fact that the condensate-to-feed ratio was greatly increased for Run 50b.The crystal washing was apparently less effective albeit the sodium carbonate and sodium nitrate crystals were larger. This might be due to the large amount of crystal product and the fact that the smaller burkeite crystals have the tendency to accumulate at the bottom of the filter cake. Although Run 50b did not represent an improvement in terms of solid-liquid separation, these steps were still easy to perform with the larger amount of final crystals recovered.

5.4.5 Crystal identification

Samples were taken from the sieved crystals of Run 50b for PLM analysis. Images from this analysis displayed the presence of sodium nitrate, sodium carbonate monohydrate, burkeite, sodium sulfate, and sodium oxalate. Selected images are shown in Figure 115.

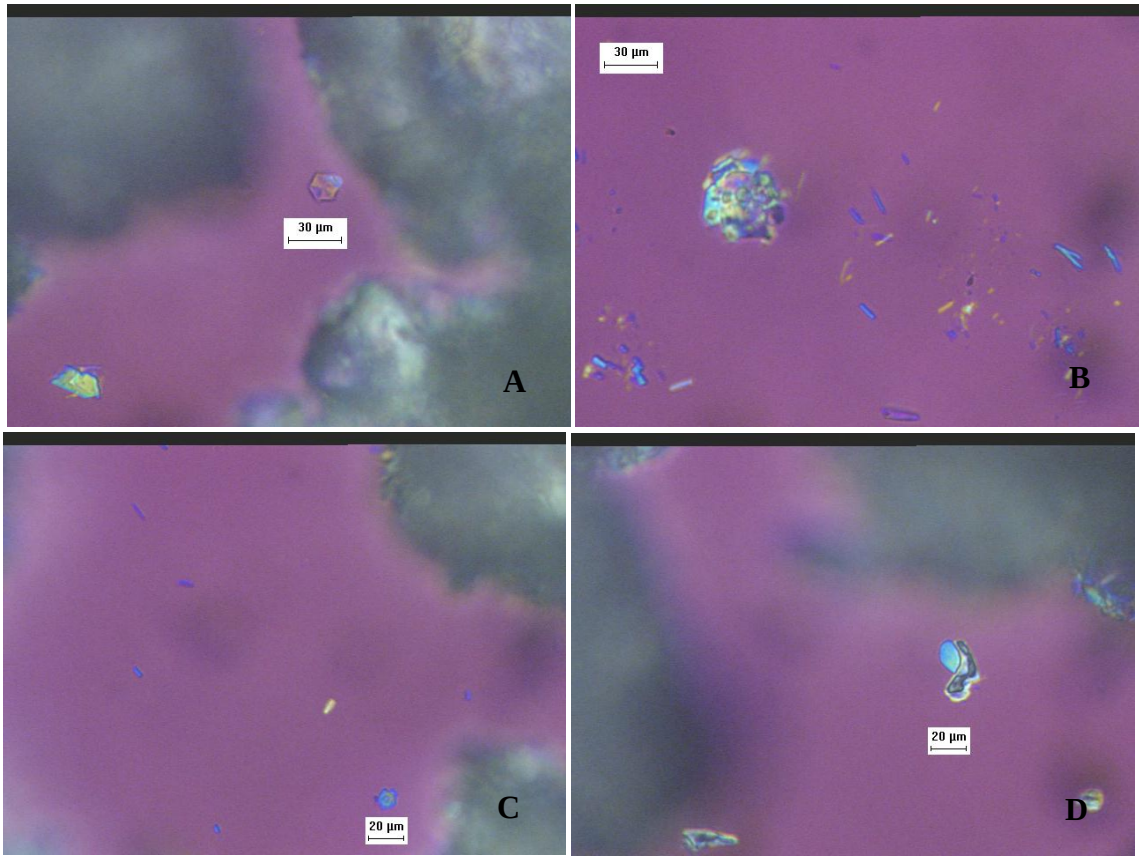

Panel A, hexagonal shape crystal, panel B, trace of sodium oxalate, panel C, homogenous burkeite crystals with a size equal to 20µm, panel D, trace of sodium sulfate crystals.

Figure 115. PLM Images on Sieved Crystals from Run 50b

5.4.6 Conclusions

The increase in condensate to feed ratio did not affect the burkeite crystals. However the sodium nitrate and sodium carbonate crystals were grown until larger sizes. This prove that the burkeite stop its growth during the run, whereas sodium nitrate and sodium carbonate continue growing with a high growth rate.

CONCLUSIONS

The purpose of this Section is to review the key findings from the study and to put them in context relative to the work still to be performed on SST Feed crystallization and modeling.

In the research conducted, the evaporation rates were controlled so as to balance three objectives: (1) to reduce nucleation rates so that crystals produced were as large as possible, (2) to minimize run times and (3) to simplify operations under hot-cell environment.

As shown in Section 3.0 for each of the first two certification runs, the evaporation was run relatively rapidly until crystals were observed in the system. A that point, the evaporation was stopped and additional feed solution was added to return the operating level in the crystallizer to its initial location and, very importantly, to re-dissolve all crystals that had been formed. Without re-dissolution, the characteristics of the crystal population would be influenced by the initial rapid evaporation, which is expected to enhance nucleation kinetics. Instead, once the level in the crystallizer had been returned to its initial value and initially formed crystals re-dissolved, the evaporation was restarted, but this time at a much lower rate than initially. The purpose of the slow evaporation was to generate supersaturation slowly, and thereby produce larger crystals than would be the case with more rapid generation. For the third certification run (performed on SST Early Feed solution FY06), the evaporation rate was kept at a constant value of 26grams of water collected per hour. This was performed in order to simplify the operation of the Early Feed crystallization and palliate to any variation in operating conditions.

The design of each of the certification runs was based on an operating temperature for each stage in the run and a final solids fraction in the slurry from each stage. The solubility of key salts was a key factor in selecting the operating temperature; on the other hand, selection of a target for solids fraction was based on maintaining good mixing and flow characteristics of the slurry.

The mass of crystals produced in each stage of a given run, as well as the composition of that mass, was estimated from modeling based on the ESP (Environmental Simulation Program) software with the MSE (Mixed Solvent Electrolyte) supplement, obtained from OLI Systems, Inc (OLI Systems, Morristown, NJ, http://www.olisystems.com/), and implemented by COGEMA. With this model, the amount of water that had to be evaporated in order to obtain that crystal mass was determined and used as a guide in operating a run.

In case it is not apparent, it should be pointed out that the mass produced from the batch crystallizer should correspond to what could be expected from a continuous unit. In other words, if the total mass fed to the batch crystallizer were fed to a continuous unit at a specific rate, then the production rate of condensate divided by the feed rate should be the same as the condensate-to-feed ratio from the batch operation. The solids fraction of the product (or, in case selective removal has been implemented, the value resulting if all product streams are combined) would correspond to that in the batch unit.

Irrespective of the rate of evaporation, the compositions and amounts of the resulting phases are fixed if the solid-liquid slurry is allowed to reach equilibrium. However, as already pointed out, the nucleation and growth kinetics of each species formed determine the respective crystal size distributions and therefore the handling characteristics of the product. Hence the last

three steps (separation, washing, and drying) are greatly influenced by the kinetics and can vary substantially from one run to the next of a batch operation.

How each certification run was conducted and the details of the outcomes of each were provided in Section 3.0. Table 43 summarizes comparisons of the process criteria with experimentally determined (actual) values for the three SST Feed certification runs performed.

Table 43: Comparison of Required and Desired Outcomes to Experimental Results

SST Early Feed FY05	Stage	Required	Actual	Desired
Cs Decon Factor	1	1.15	5.9	48
	2	1.15	6.7	48
	Total	1.15	6.0	48
Sodium Recovery	Total	50%	58.1%	90%
Sulfate to Sodium	1	0.01	0.0027	0.0022
	2	0.01	0.0017	0.0022
	Total	0.01	0.0023	0.0022
SST Late Feed				
Cs Decon Factor	1	-	24.5	14
	2	-	11.2	14
	Total	-	14.8	14
Sodium Recovery	Total	50%	74.7%	90%
Sulfate to Sodium	1	0.01	0.008	0.0022
	2	0.01	0.0191	0.0022
	Total	0.01	0.01	0.0022
SST Early Feed FY06				
Cs Decon Factor	1	1.15	210	48
	2	1.15	66	48
	Total	1.15	162	48
Sodium Recovery	Total	50%	63.4%	90%
Sulfate-to-Sodium	1	0.01	0.0032	0.0022
	2	0.01	0.0052	0.0022
	Total	0.01	0.0037	0.0022

There are two types of criteria to be met by the process: one type has to do with the exclusion of species (i.e., Cs) from the crystals produced while the other is related to the fractions of sodium and sulfate in the feed solutions that are removed in the crystalline product. In essence, the Cs is supposed to go with the filtrates from each stage, while the sodium and sulfate go with the crystals. Hence, the cesium requirement is based on crystal purity while the sodium and sulfate requirements are based on yield.

As shown, for the first two certification runs essentially all of the actual values exceed those required, but fall short of those desired. On the other hand, results obtained for the third certification run displays that values of decontamination factor meets the desired value and that the sodium recovery increased keeping the requirement on sodium to sulfate molar ratio in the order of magnitude of the desired target. In other words, improvements on the requirement values have been made from certification run 26 to 38b, by obtaining values that meets or are in the same order of magnitude of the desired targets.

The mechanisms by which Cs could become part of the crystalline product include the formation of inclusions through overgrowth of mother liquor by the crystal surface, entrapment of mother liquor in either the irregularities of individual crystals or in the crystal cake, in lattice substitution or in interface between two different matrices in the case of heterogeneous crystal formation. Because cesium has such a high solubility in the feed solutions, it is unlikely that it would be captured by lattice substitution, which leaves the possibility of inclusions, heterogeneous crystallization effect and entrapment.

Inclusions typically are formed when crystal growth occurs at high supersaturations. In the certification runs, attempts were made to control the supersaturation at which nucleation and growth occurred, but it is highly likely that some inclusions were formed for the homogeneous

crystals obtained. This is obvious in some of the PLM images taken of product crystals and displayed in Sections 3.0, 4.0 and 5.0. Moreover, it is important to add that the operation of a continuous crystallizer would undoubtedly maintain a significantly lower system supersaturation, and there should be less possibility of forming inclusions in homogenous crystals.

Inclusions in heterogeneous crystals are however more important. In heterogeneous crystallization, a crystal is formed following a specific matrix until the system conditions are changed and growth of a different species, following a different matrix, occurs on the first crystal. The interface between the two matrices is a location where inclusions (in particular cesium inclusions) occur. PLM images displayed in Sections 4.1.9 and 4.2.2 attest of the presence of this type of inclusions and crystal identification performed on certification run 38b shows that this phenomenon is not negligible.

Entrapment of mother liquor in the irregularities of individual crystals or in the void spaces of multi-crystal agglomerates or cakes formed during filtration present problems quite different from inclusions. In principle, mother liquor can be flushed from crystal surfaces provided wash liquid flows through all void spaces. An excellent example of the effect of washing was provided in the experiments described in Appendix H.2. In that work, crystals produced from SST Early Feed Solution were subjected to a series of washing steps and the color of the crystals was used as a measure of how well the washing had been performed. The yellowish color of the freshly produced crystals, which was attributed to the presence of chromium, was gradually eliminated each successive wash until after four washing stages the crystals were white. The washing done in this experiment involved mixing the crystals in a saturated wash liquid, so that there was no issue of flow through a filter cake, and filtering the

resulting slurry. Table 44 displays the evolution of the decontamination factor for both stages of run 38b with respect to the successive wash performed.

Table 44: Decontamination Factor Evolution for Run 38b

Sample	DF Value Stage 1	DF Value Stage 2
Feed	N/A	N/A
Unwashed	2.8	1.2
1 Wash	6.3	3.1
2 Washes	21.7	10.8
3 Washes	69.3	24.2
4 Washes	76.7	46.2
Final Crystals	210	66.2

It is unlikely that an operation like that described in the preceding paragraph would be possible in a full-scale unit, and that is why so much effort went into studying the influence of process variables on the crystal size distribution. As pointed out earlier, the crystal size distribution plays a very significant role in determining how easily solid-liquid separation occurs. It also greatly impacts washing and all other downstream operations. In the present work, attempts to produce crystals that were as large as possible, reduce the amount of heterogeneous crystals (and hence inclusions effect) and obtain a crystal size distribution as homogeneous as possible, were performed by studying the effect of the evaporation rate, evaporation profile, operating temperature and condensate to feed ratio. Results obtained for each of this parameter variation are presented in Section 5.0.

In essence results of this study may be summarized as

- the increase in evaporation rate has favored the nucleation rate of all main species and led to a crystal size distribution shifted to the smaller crystal size. Associated

to this modification of the CSD, complications on the solid-liquid separation steps had arised.

- the decrease in operating temperature reduced the crystal sizes indicating a reduced growth rate. Temperature has decreased the solubility especially of the sodium nitrate and affected the growth rate. Complications during the separation step were observed as important proportions of small crystals have the tendency to plug the apparatus.
- the application of a concave evaporation profile produced burkeite crystals at lower number but increased size and increased the spread of the sodium nitrate crystals producing a more homogenous crystal population and facilitating the solid-liquid separation.
- the application of a convex evaporation profile produced burkeite crystals at higher number but lowered size. By creating a lot of burkeite nuclei, burkeite grown on the existing burkeite more than on nitrate nuclei. Consequently, the proportion of heterogeneous burkeite crystals was reduced, reducing crystal inclusions. No real improvement or deterioration of the conditions of solid liquid separation was created.
- the increase in condensate to feed ratio did not affect the burkeite crystals. However the sodium nitrate and sodium carbonate crystals were grown until larger sizes proving that the burkeite stop its growth during the run, whereas sodium nitrate and sodium carbonate continue growing with a high growth rate.

The effects exposed in Section 5 of cry

The results obtained in performing the Certification Runs described in Section 3.0 and in the supporting activities leading up to those runs provide guidance on important activities that should be performed in support of future research on FC from the Hanford wastes covered by this study. The purpose is to support the development of process flowsheets and the design of an operation that can be used to accelerate the treatment of Hanford waste.

Study of variables such as evaporation rate, evaporation profile, operating temperature and condensate to feed ratio described in Section 5 proved to affect crystal size distribution and is a first step leading to modeling of crystallization of SST Feed solution and more generally kinetics parameters of multi-salts crystallization.

However, predicting the actual impact of operating variables on size distribution is again complicated by the fact that several crystal species are produced in fractional crystallization. Each species is characterized by a crystal size distribution determined by species-specific nucleation and growth kinetics, one or several occurrences (terms including shapes, habits and crystalline system) and growth mechanism (heterogeneous, by agglomeration, etc...) inside the crystallizer and under the specific system conditions. Study of these different elements for the SST Early and Late Feed solutions were presented in Section 4 along with a first estimate of growth kinetics for the three main species produced. This study represents also a step forward leading to multi-salts crystallization modeling.

APPENDICES

APPENDIX A

WASHING-FILTRATION APPARATUS DESIGN

Figure A1. Illustration of the Custom Designed Washing-Filtration Apparatus as per Chemglass Drawing.

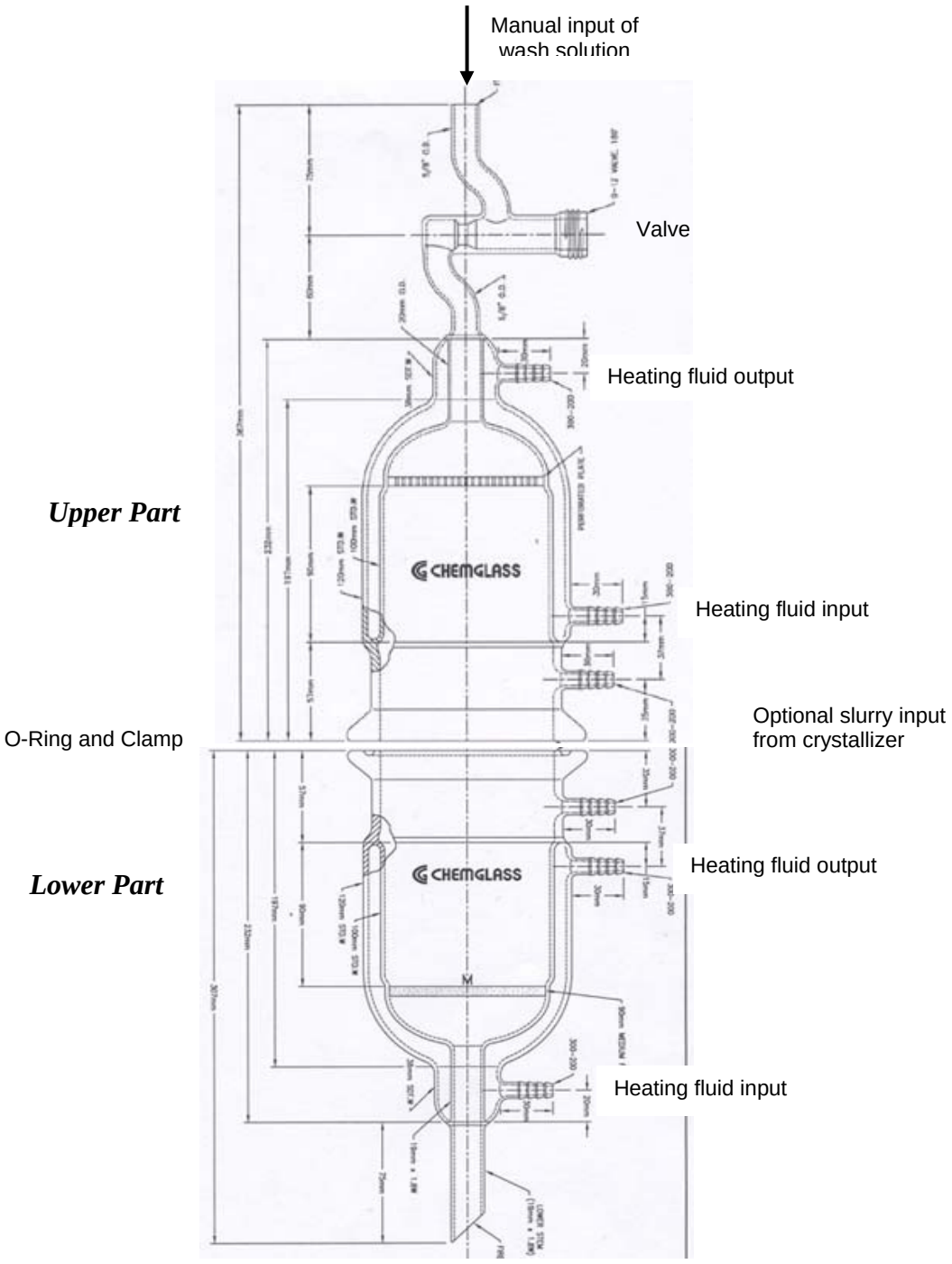

Figure A2. Detailed Components of the Filtration and Washing Apparatus.

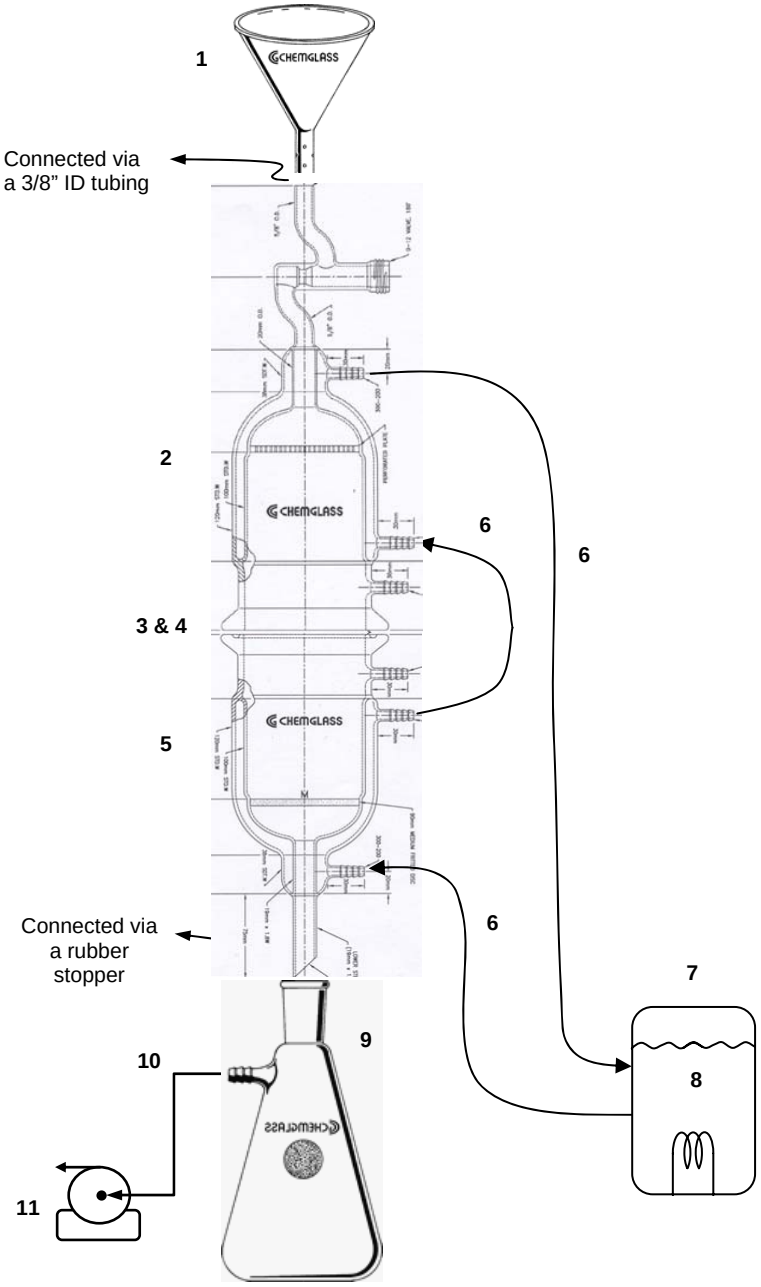

Table A1. Itemized List of Filtration/Washington Apparatus Components According to Figure 2.

Item	Description	Provider	Catalog No.	Notes
1	Funnel	GA Tech		
2	Jacketed Buchner Funnel, 90mm Diameter Perforated Plate, 0-12mm Chem-Vac Valve on top, 100mm ID Schott Flat Flange on the bottom, 10mm OD Hose Connection@90° located between the Jacket and Flange per Chemglass Drawing	Chemglass	Special/GT-0507-011JS	Special design
3	Clamp for Duran® reaction PER Quote# JS-16810	Chemglass	CG-141-02	
4	O-ring, Viton®, 100mm Flange	Chemglass	CG-147-21	
5	Jacketed Buchner Funnel, 90mm Diameter Medium Frit, 100mm ID Schott Flat O-ring Flange on the top, 10mm OD Hose Connection@90° located between the Jacket and Flange, 3/4" OD Lower Drain, per Chemglass Drawing	Chemglass	Special/GT-0507-012JS	Special design
6	Tygon Tubing, 1/2” OD x 3/8 ID, 10ft	GA Tech		
7	VWR Heating bath 13l programmable 1157P	VWR	13271-106	
8	Heating fluid DC 200 5 cs	Ashland, GA	3311089 600	
9	Vacuum Filtration flask, 1000 mL	GA Tech		
10	Vacuum tubing, 5/16" ID	Fisher	14-175D	
11	Dry pressure/vacuum pump, Welch	Fisher	01-051-1C	

Figure A3. Detailed Crystallizer Components.

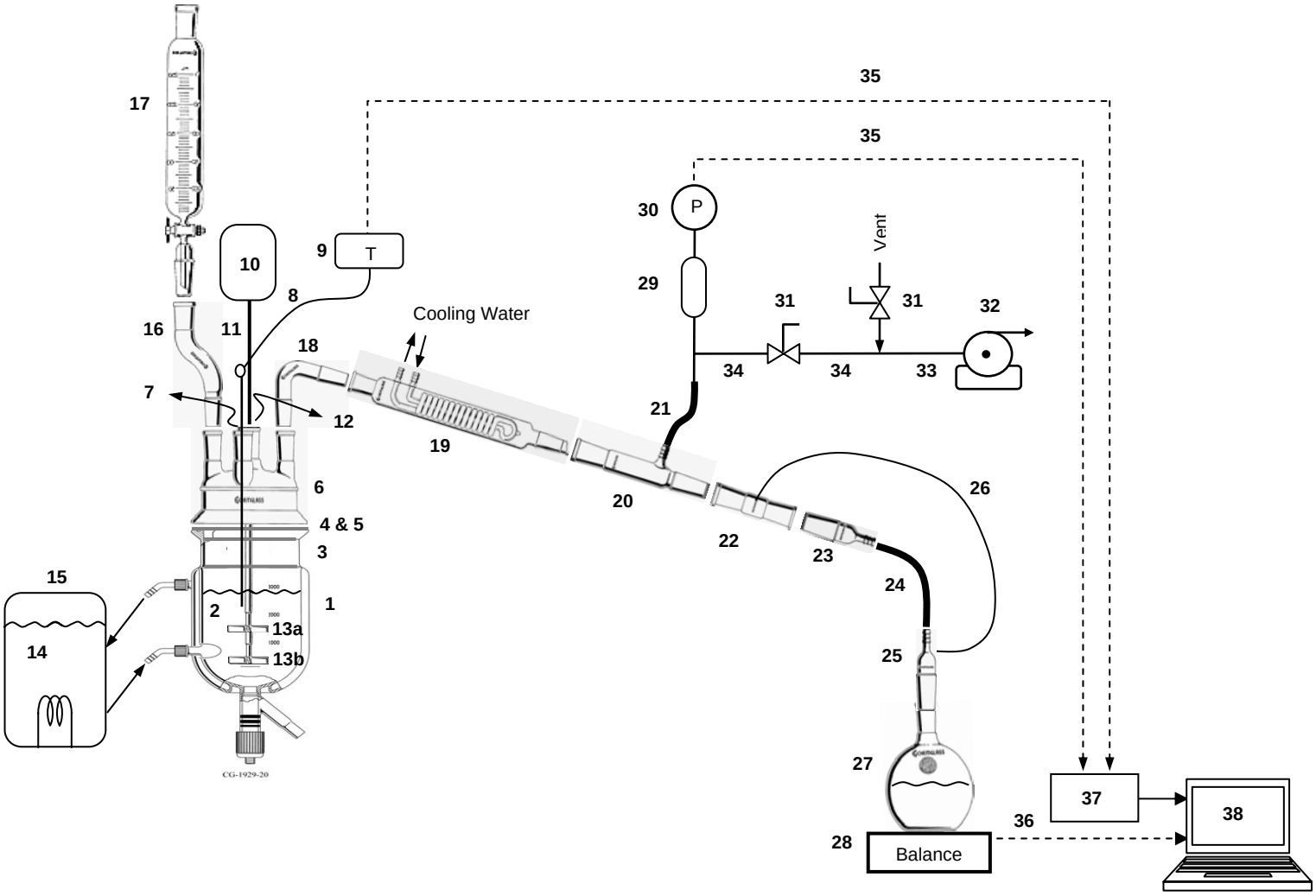

Table A2. Itemized List of Crystallizer Components According to Figure A3.

Item	Description	Provider	Catalog No.	Notes
1	Jacketed Reaction Vessel, 1-Liter	Chemglass	CG-1929-14	
	Jacketed Reaction Vessel, 300 mL	Chemglass	CG-1929-10	
2	Baffles	GA Tech		Home made
3	Clamp, 100mm	Chemglass	CG-141-02	
4	Viton O-Ring, 100mm	Chemglass	CG-147-21	
5	Support clamp, 100 mm	Chemglass	CG-1947-01	
6	Reaction Vessel Lid, 4-necks, all 24/40 joints	Chemglass	CG-1941-01	
7	Thermocouple, Hastalloy C-276, Type “T”, 1/8”, 12” long	Chemglass	CG-3498-302	
8	Thermocouple Adapter, 24/40, 1/8"	Chemglass	CG-1042-E-01	
9	Analog Temperature Controller/Display	Omega	CNi3253	
10	Stirrer motor, IKA Model RW 16	Fisher	14-260-31	
11	Stirrer Shaft, 555 mm	Chemglass	CG-2075-B-03	
12	Stirrer Bearing, Chemvac™, Teflon®, 24/40, 10mm	Chemglass	CG-2077-G-01	
13a	Agitator, TFE, 10 mm Stir Shaft, 4 Blades, 45°, 75 mm Diameter	Chemglass	CG-2091-02	
13b	Agitator, TFE, 10 mm Stir Shaft, 4 Blades, 45°, 50 mm Diameter	Chemglass	CG-2091-01	
14	Heating fluid DC 200 5 cs	Ashland, GA	3311089 600	
15	VWR Heating bath 13l programmable 1157P	VWR	13271-106	
16	Offset Adapter, 24/40 joint size	Chemglass	CG-1033-01	
17	250 mL Graduated separatory funnel, 2mm Teflon stopcock, 24/40 joint size	Chemglass	CG-1734-03	
18	Adapter, Distillation, 75°, 24/40	Chemglass	CG-1010-01	
19	Reflux Condenser, 175mm Coil Length, 24/40	Chemglass	CG-1213-L-21	
20	Inlet adapter, straight, 24/20 joint, hose connection	Chemglass	CG-1062-01	
21	TYGON Vacuum Tubing, 3/8"ID x 7/8"OD	Cole-Parmer	EW-06413-30	
22	Adapter, 24/40 Outer Jt. to 24/40 Outer Jt. with a ¼”-28 Thread sealed in between the Jts., supplied complete with ¼”-28 Tefzel Union	Chemglass	GT-0505-061JS	Custom designed
23	Inner adapter, 24/40 Inner Joint, 86mm Height	Chemglass	CG-1012-01	
24	Nalgen 980 Braided Clear PVC Tubing, 1/4" ID	Fisher	14-169-10A	
25	Inlet Adapter, Top Hose Connection, Lower 24/40 Inner Jt. with a ¼”-28 Thread sealed in between the Jts., supplied complete with ¼”-28 Tefzel Union	Chemglass	GT-0505-062JS	Custom designed
26	Teflon Tubing, .062” ID x .125” OD, 10 ft.	Chemglass	CG-1164-02	
27	Flat Bottom Flask, 24/40, 1000 mL	Chemglass	CG-1500-07	

Item	Description	Provider	Catalog No.	Notes
28	Balance PB1502-S, Mettler Toledo	VWR	11274-918	
29a	Pressure Transducer, 0-50 psia, Current Output)	Omega	PX305-050AI	
29b	Snubber	Swagelok	SS-4-SA-EA	
30	Process Meter and Controller	Omega	DP25B-E	
31	Stainless 1-Piece Ball Valve, 1/4 in. Tube Fitting	Swagelok	SS-42S4	
32a	Two-stage Welch Vacuum Pump	Fisher	01-129-4	
32b	Regulating Valve for Welch Pump	Fisher	NC9186594	
33	PTFE Tubing,1/8" ID x 1/4" OD	Cole-Parmer	EW-06605-13	
34	316/316L Seamless Stainless Steel Tubing	Swagelok	SS-T4-S-035	
35	Teflon Coated Cable, 10 ft	Omega	TECT10-11	
36	RS-232 Serial Port	Measurement Computing	PCI-COM232/4-9	
37	USB Based Data Acquisition Module	Measurement Computing	PMD-1208FS	
38	LabView software on a PC			

APPENDIX B

OPTICAL SETUP AND ILLUMINATION ADJUSTMENT FOR THE PLM

B1.0 OPTICAL SETUP AND ILLUMINATION ADJUSTMENT FOR THE PLM

This procedure is supplementary to the description of the use of the PLM given in Section 2.0.

1. Turn on the illuminator and place the slide on the microscope stage (11) and fix it with the clamp. Slide out the analyzer (16) and compensator (21 placed in 14) plates from the light path then rotate the 10X objectives into position for focus.
2. Move the substage condenser up to its top position using the substage focusing control (7). Check to make sure that both the field iris (3a) and the aperture iris (3b) are fully open.
3. Focus down on the specimen slide (9) without bombing the objective into the slide until details can be seen in the eyepiece (18). Adjust the light brightness using the intensity control knob (6).
4. Adjust the distance between the two binocular eyepieces (18a and 18b) to fit the observer's eyes.
5. Fine focus (9b) to get a sharp image in the right eyepiece (18b) using your right eye.
6. Using your left eye, adjust the diopter adjustment collar on the left eyepiece (18a) (not the fine focus) to get the sharpest image.
7. Now turn the field iris adjustment ring (3a) until the field iris is seen.
8. Raise or lower the substage condenser (7) to focus the field iris sharp in the plane of the specimen. Then open out the field iris until it is just outside the field of view.
9. Remove one of the eyepieces (18) and reduce the intensity of the disc of light coming from the back of objective to about 75% using the aperture iris (3b).
10. Similar adjustments should be repeated for each objective.

* All numbers in parenthesis correspond to element numbers appearing in Figure 14.

B2.0 PLM OBJECTIVE CENTERING PROCEDURE

This procedure is supplementary to the description of the use of the PLM given in Section 2.0.

The objectives should be precisely seated in the optical axis. If it is even lightly off the axis the specimen image will stray from the center of view upon rotation of the stage. If this happens then the objective needs centering using two hexagon keys supplied with microscope as follows:

1. Remove the analyzer and compensator plates from the light path and swing in the 10X objective which is mounted in the non-centerable opening. All other objectives are mounted in floating centerable nosepiece holes.
2. Focus down on the specimen and memorize the pinpoint appearing on the eyepiece cross-line center (18b).
3. Turn the nosepiece (13) and bring the higher power objective to position and focus then see if the memorized specimen pinpoint is located at the cross mark. If not, insert the two centering screws into the key holes on the nosepiece ring above the objective and turn to move the pinpoint to the cross point.
4. Repeat the same procedure for the remaining objectives.

All numbers in parenthesis correspond to element numbers appearing in Figure 14.

B3.0 OBJECTIVE SCALE CALIBRATION

This procedure is supplementary to the description of the use of the PLM given in Section 2.0.

1. Turn on the illuminator and place the standard micrometer slide on the stage (11). Slide out the analyzer (16) and rotate desired objective, e.g., 10X, into position for focus. Turn on the Digital camera and start the Image-Pro Plus software and the live preview.
2. Focus down on the micrometer slide (9) and adjust the light intensity (6) until the graduated micro-ruler appears clearly on the live preview. Record the image of the micro-ruler by pressing "Snap."
3. On the Image-Pro Plus main menu, select *Measure* → *Calibration* → *Spatial* sequence where the Spatial Calibration window is displays. This window is linked to the active image of interest. Press "New" to create a new set of calibration value or to edit current ones. Edit the name to desired Objective power value, e.g., 10X, and then select the desired unit from the *Unit* list, preferably microns. This will be the unit of measurement that will appear on the graphs. On the "Pixels/Unit" group box press the "Image" button, where a scaling dialog box opens, and draw a straight horizontal line on the recorded micro-slide reference image between two grids of known length, e.g., 25 μm. Then write this value in the scaling dialog box and press OK to close the box and return the Spatial Calibration menu. Keep other values un-changed and press OK.
4. Repeat steps 1-3 for all other objectives to calibrate them.

All numbers in parenthesis correspond to element numbers appearing in Figure 14.

APPENDIX C

SIEVE TEST PROCEDURE

C1.0 Sieve Test Simplified Procedure

Sample Preparation

1- Dispose the final dried crystals into a cookie dish and spread them evenly

2- Separate the weak aggregates with a Teflon spatula.

3- Choose the eleven sieves[1] to be used for the sieving analysis (refer to the last paragraph for more precision on this topic).

4- With a large spatula collect the crystals and sieve them manually through the sieve presenting the highest size among the selected sieves.

5- Collect these crystals on a weighing paper until reaching 35 g of crystals.

6- Separate the 35 g of crystals into three samples of 15 g each. Place them on a weighing paper. Label them by writing the sample number on the paper[2].

Sieving Preparation

7- Wash the sieves to be used with hot water and allow them to dry for 30 minutes to one hour in an oven.

8- Place the sieves to be used in "sieve number" increasing order when going from top to the bottom of the sieve column[3].

9- Measure the weigh of the empty sieves and record this number. At the end of the sieving, the difference in mass will determine how many crystals were collected.

10- Insert the crystals evenly on the top sieve and place the cover on the sieve column.

Sieving Performing

11- Place the column in the Rotap apparatus. Place the Rotap cover and position the agitated arm above the cover[4].

12- Set the sieving time to 30 minutes[5]. Press the "power "button.

13- Close the sieving doors (keep the noise from spreading in the sieving machine surroundings) and let the sieving being performed during the 30 minutes.

Results Collection and Analysis

14- At the end of the sieving, collect the weight of each of the sieves with the crystals recuperated inside. Determine the mass of crystals in each sieve by making difference with the weigh recorded in step 9.

15- Plot on Excel or any appropriate software the "cumulative mass"[6] and CSD graphs.

16- Perform three times the procedure (steps 7 to 14) for the three samples prepared in 6.

Compare each of the three graphs obtained and conclude on crystal size distribution of the studied sample.

Validation with PLM Imaging and XRD

17- Weight and label eleven plastic cups. Labels have to present the type of feed (i.e. Early, Late, DST), the Stage (i.e. 1 or 2) and the crystal size range for each sieve

18- Collect the crystals contained in each sieve inside the properly labeled plastic container. Record the final weigh.

19- Determine the sample mass of crystals by subtracting the weight recorded in 19 to the one recorded in 18.

20- Prepare at least 3 slides for each crystal size. Preparation consists in disposing a sample of crystal in one slide, adding some silicone oil, and placing a round shape slide to cover the sample.

21- Take pictures of each sample for each size range and conclude on the content of each sieve in terms of crystals species collected and potential agglomeration or breakage.

22- Collect at least 0.7 g of crystals for each sieve to prepare the sample to be used for XRD analysis.

23- Perform XRD on each sample and conclude on crystals species identification and CSD.

C.2.0 Sieve Size Selection

The sieves may be selected by (1) performing the sieving of one of the three samples selected in 6, (2) performing the sieving of an additional sample, or (3) by following the tables presented in appendix A and B.

[1] Eleven represents the maximum number of sieves that can be used with the Rotap Apparatus.

[2] Refer to figure 1.

[3] refer to figures 2 and 3.

[4] refer to figure 3.

[5] The sieving time is important when operating sieving analysis. A fairly large sieving time would eventually lead to crystals breakage inside the sieving due to chocks with the sieves walls or between crystals. On the other hand a small sieving time would lead to poor segregation between the crystal sizes and hence would bias the sieving experiment. 30 minutes sieving time associated with a sample size of 15 g have been determined as appropriate sieving conditions.

[6] An example calculation of cumulative mass is presented in appendix C.

Figure C1: Random samples

Figure C2: Sieves available for sieving

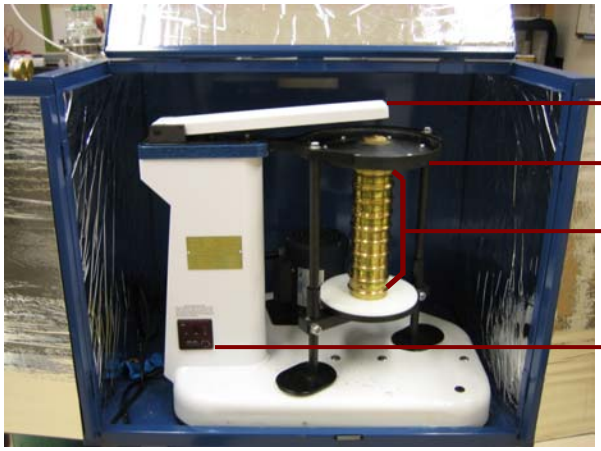

Figure C3: Sieving apparatus

Table C1. Sieves used for the First Stage of Early Feed Run

No.	ASTM Sieve No.	Nominal Sieve Opening (μm)
1	16	1180
2	20	850
3	30	600
4	40	425
5	50	300
6	70	212
7	100	150
8	140	106
9	200	75
10	270	53
11	Pan	0

Table C2. Sieves used for the Second Stage of Early Feed Run

No.	ASTM Sieve No.	Nominal Sieve Opening (μm)
1	20	850
2	30	600
3	40	425
4	50	300
5	70	212
6	100	150
7	140	106
8	200	75
9	270	53
10	400	38
11	Pan	0

Table C3. Sieves used for the First Stage of Late Feed Run.

No.	ASTM Sieve No.	Nominal Sieve Opening (μm)
1	20	850
2	30	600
3	40	425
4	50	300
5	70	212
6	100	150
7	140	106
8	200	75
9	270	53
10	400	38
11	635	20
12	850	10
13	Pan	0

For the first stage a first sieving was performed with the sieves numbered from 1 to 11. A second sieving was then performed on the crystals collected in the sieve 11 by replacing sieves 1 and 2 by sieves 11 and 12.

Table C4. Sieves used for the Second Stage of Late Feed Run

No.	ASTM Sieve No.	Nominal Sieve Opening (μm)
1	20	850
2	30	600
3	40	425
4	50	300
5	70	212
6	100	150
7	140	106
8	200	75
9	270	53
10	400	38
11	Pan	0

C3.0 Sample calculation for CSD and Cumulative mass distribution

Sample Name	Late feed stage 1
Sample weight (g)	14.06
Sieving time (min)	30

Sieve no.	Mesh opening	Range	Ave. Size (micron)	Before sieving (g)	After sieving (g)	Crystal weight (g)	Collected %	Cumulative %
20	850	>850	850	126.74	126.74	0.00	0.00	100.00
30	600	600-850	725	125.02	125.16	0.14	1.00	100.00
40	425	425-600	512.5	115.98	116.44	0.46	3.27	99.00
50	300	300-425	362.5	110.7	111.99	1.29	9.17	95.73
70	212	212-300	256	112.5	116.85	4.35	30.94	86.56
100	150	150-212	181	106.69	110.07	3.38	24.04	55.62
140	106	106-150	128	105.23	106.53	1.30	9.25	31.58
200	75	75-106	90.5	105.1	105.93	0.83	5.90	22.33
270	53	53-75	64	103.93	104.52	0.59	4.20	16.43
400	38	38-53	45.5	102.78	103.3	0.52	3.70	12.23
635	20	20-38	29	104.56	105.1456	0.59	4.17	8.53
850	10	10-20	15	107.7	108.3144	0.61	4.37	4.37
Pan	0	0-10	5	82.9	82.9	0.00	0.00	0.00
					TOTAL	14.06	100.00	100

The “crystal weight” column corresponds to the mass of crystals collected on each pan. This mass is obtained by subtracting the “before sieving” and “after sieving” recorded mass.
This mass is converted in percent (collected percent column) by using the total crystal weigh (total mass of the sample). The crystal size distribution presented in figure C1 corresponds to the plot of the “crystal weight” column with respect to the “average crystals size”.
The “cumulative percent” is obtained by adding the collected percent of each preceding crystal size. The cumulative mass distribution presented in figure C2 corresponds to the plot of the “cumulative percent” column with respect to the “average crystal size” column.

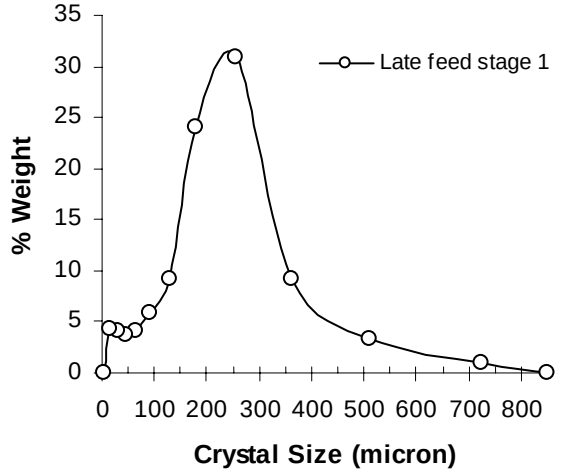

Figure C4. Crystal size distribution

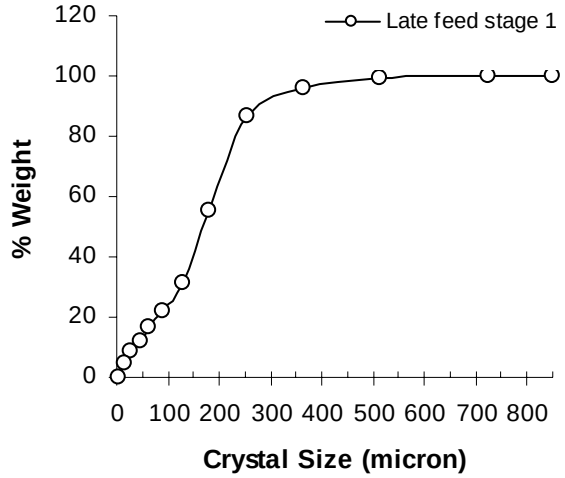

Figure C5. Cumulative mass distribution

APPENDIX D

CONDENSATE-TO-FEED RATIO

D1.0 CONDENSATE-TO-FEED RATIO

Each certification run followed the corresponding simulation file provided by COGEMA (shown in parenthesis in the table) and the endpoint for the operation of each stage was determined by the amount of condensate collected. The Table C1 gives the target condensate-to-feed ratios along with the actual experimental results. Since the laboratory experiments involved adding dilution water to the filtrate from the first stage, the target ratios had to be adjusted for the second stage of each run. The feed to the second stage of each run was a portion of the diluted filtrate from the first stage. An example of the adjusted target ratio calculations is given for the SST Early Feed Solution Run 26.

Example calculation of the revised condensate-to-feed ratio for the SST Early Feed Solution certification run:

$$AdjustedRatio = \frac{(Filtrate \times OldRatio + DilutionWater)}{(Filtrate + DilutionWater)} \tag{D-1}$$

$$AdjustedRatio = \frac{(1080.25 \times 0.189 + 500.33)}{(1080.25 + 500.33)} = 0.446 \tag{D-2}$$

Table D1.

Experimental Stage	Experimental Value	Early Feed (SST1SIM.xls)		Late Feed (SST2SIM1.xls)	
		Simulation	**Experimental**	**Simulation**	**Experimental**
Stage 1	Feed (g)	1000.1	3214.81	1000	5698.37
	Condensate (g)	332.4	1056.84	681	3877.78
	Condensate-to-Feed Ratio	**0.329**	**0.332**	**0.681**	**0.681**
	Filtrate from Stage 1 (g)	333.4	1080.25	282.3	1510.02
	Dilution water to filtrate (g)		500.33		1074.07
Stage 2	Feed (g)	333.4	1102.88	282.3	967.7
	Condensate (g)	63.1	496.91	58.7	471.57
	Adjusted Target Ratio		**0.446**		**0.537**
	Condensate-to-Feed Ratio	0.189	**0.451**	0.208	**0.487**

D2.0 SAMPLE IDENTIFICATION FOR THE CERTIFICATION RUNS

The following tables give the sampling information necessary to accurately calculate the species balances. Each table identifies the samples taken and gives the amounts of pure sample and water added to each sample container. As shown in the tables, the only samples sent in solid form were the final crystals from each stage.

Early Feed Stage 1

Code	Name	Pure sample	Water added	Total mass	State
EF2-ST1-1	filtrate	50.89	23.57	74.46	L
EF2-ST1-2	spent wash	177.01	0	177.01	L
EF2-ST1-3	final crystals	9.38	0	9.38	S
EF2-ST1-4	accumulation	33.82	112.08	145.9	L
EF2-ST1-5	unwashed solids	9.6	93.7	103.3	L
EF2-ST1-7	feed (CH2M HILL)	93.66	0	93.66	L

Early Feed Stage 2

Code	Name	Pure sample	Water added	Total mass	State
EF2-ST2-1	filtrate	77.94	86.03	163.97	L
EF2-ST2-2	spent wash	77	73.49	150.49	L
EF2-ST2-3	final crystals	6.21	0	6.21	S
EF2-ST2-4	accumulation	32.17	114.04	146.21	L
EF2-ST2-5	unwashed solids	7.72	122.78	130.5	L

Late Feed Stage 1

Code	Name	Pure sample	Water added	Total mass	State
LF3-ST1-1	filtrate	60.07	42.73	102.8	L
LF3-ST1-2	spent wash	92.70	61.32	154.01	L
LF3-ST1-3	final crystals	7.83	0	7.83	S
LF3-ST1-4	accumulation	6.33	128.03	134.36	L
LF3-ST1-5	unwashed solids	13.03	125.04	138.07	L
LF3-ST1-6	feed (CH2M HILL)	30.78	0	30.78	L
LF3-ST1-7	feed (lab)	39.53	0	39.53	Ll

Late Feed Stage 2a

Code	Name	Pure sample	Water added	Total mass	State
LF3-ST2-1a	filtrate	9.38	126.76	136.14	L
LF3-ST2-2a	spent wash	84.90	55.08	139.98	L
LF3-ST2-3a	final crystals	12.14	0	12.14	S
LF3-ST2-4a	accumulation	9.83	109.88	119.71	L
LF3-ST2-5a	unwashed solids	6.06	124.8	130.86	L

Early Feed 38b Stage 1

Code	Name	Pure sample	Water added	Total mass	State
EF38b-ST1-1	feed hanford	129.92	0	128.92	L
EF38b-ST1-2	feed mixed	114.39	0	114.39	L
EF38b-ST1-3	accumulation	136.9	880.74	1017.64	L
EF38b-ST1-4	filtrate	385.86	498.06	883.92	L
EF38b-ST1-5	wash solution	36.80	74.32	111.12	L
EF38b-ST1-6	spent wash	51.09	69.01	120.1	L
EF38b-ST1-7	unwashed solids	3.20	85.36	88.56	L
EF38b-ST1-8	first wash	1.99	102.09	104.08	L
EF38b-ST1-9	second wash	2.03	95.73	97.77	L
EF38b-ST1-10	third wash	2.13	100.31	102.45	L
EF38b-ST1-11	fourth wash	2.58	107.08	109.66	L
EF38b-ST1-12	fifth wash	6.99	111.22	118.22	L

Early Feed 38b Stage 2

Code	Name	Pure sample	Water added	Total mass	State
EF38b -ST2-1	accumulation	100.73	619.54	120.27	L
EF38b -ST2-2	filtrate	126.33	374.4	500.73	L
EF38b -ST2-3	wash solution	19.97	86.03	106.01	L
EF38b -ST2-4	spent wash	56.98	80.16	137.15	L
EF38b -ST2-5	unwashed solids	1.91	111.37	113.29	L
EF38b-ST2-6	first wash	2.04	121.81	123.85	L
EF38b-ST2-7	second wash	1.53	112.12	113.66	L
EF38b-ST2-8	third wash	1.00	122.97	123.97	L
EF38b-ST2-9	fourth wash	1.76	114.46	116.22	L
EF38b-ST2-10	fifth wash	2.54	113.71	116.25	L

D3.0 TEMPERATURE AND PRESSURE PROFILES FOR THE CERTIFICATION RUNS

Figure D2. Temperature and Pressure Profiles for the SST Early Feed Solution Certification Run. Dotted Lines Represent Target Temperatures.

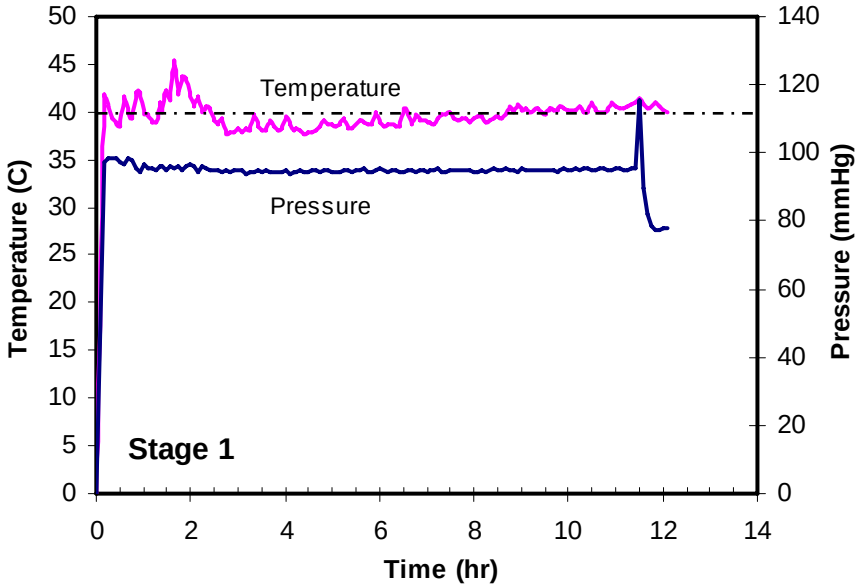

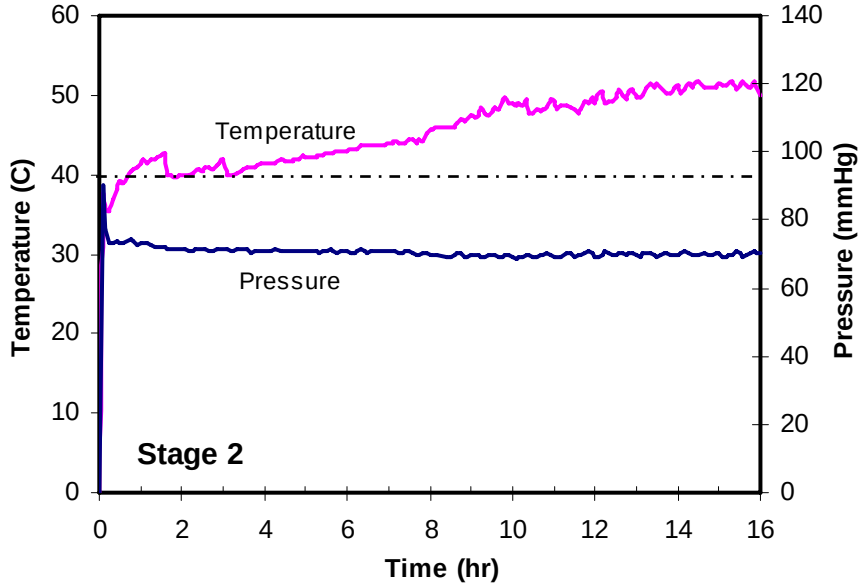

Figure D3. Temperature and Pressure profiles for the SST Late Feed Solution Certification Run. Dotted Lines Represent Target Temperatures.

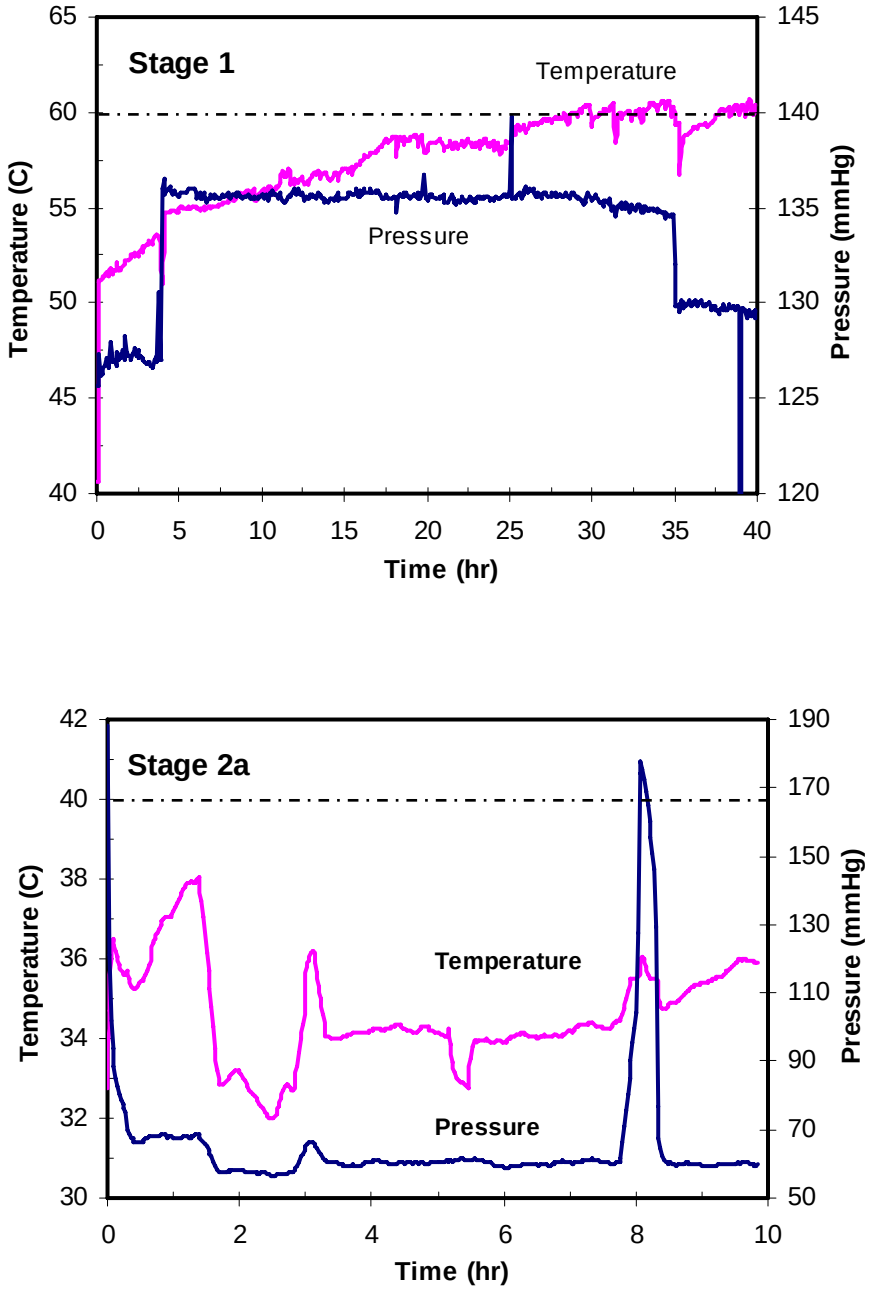

APPENDIX E

SST EARLY FEED SPILL

E1.0 DETAILS ON THE SPILL IN THE SST EARLY FEED SOLUTION CERTIFICATION RUN 26

Closure of the mass balances on the SST Early Feed Solution Certification Run 26 was considered an important component of the analysis of that run. Since there was a slurry spill during the run, considerable effort went into estimating the quantity and characteristics of the lost material. Here is a summary of how that estimation was performed.

The slurry loss can be estimated in two ways: 1) by a rough estimate of the volume lost, and 2) from the detailed mass balance.

1. Volume Lost

   The volume processed during the filtration step corresponded roughly to 1200 mL (750 mL for the new filtration-washing apparatus and 450 mL for the other medium frit filter). In order to estimate the mass of slurry lost from the spill, the simulation file SST1SIM.xls was used to approximate the slurry density. The simulation file predicts a slurry density of 1.67 for the first stage. The actual slurry density is expected to be lower than that predicted by the simulation file due to the fact that the achieved condensate-to-feed ratio was slightly below the target value.

   The volume that was lost during filtration corresponded to almost 1/3 of the volume sent to the medium frit filter, which would be 150 mL. This corresponds to a mass of 250 g. Since the actual density should be less than 1.67, the mass of slurry lost by first approximation is expected to be between 200 and 250 g.

2. Detailed Mass Balance

   The total input to the evaporative crystallizer is 3214.81 g.

   The total output from the evaporative crystallizer, including condensate, accumulation, vessel loss, and recovered slurry is 3000.4 g.

   Therefore, there is a loss of 214.41 g in transporting material from the evaporation step to the filtration step. Because the vessel loss was estimated to be 25.23 and this value has been as high as 35 g, the mass lost in the spill was estimated to be 200 g.

The stirrer in the crystallizer was left on during drainage of the slurry to assist in maintaining its flow characteristics. Moreover, the heating jacket maintained the temperature constant during this process so as avoid cooling and further crystallization. For these reasons, the slurry in the vessel and in the 600-mL beaker into which the slurry flowed was homogenous. As the filtration step was completed rapidly, the suspended solids had no opportunity to settle and, therefore, the material spilled was assumed to have the same composition as the slurry that was filtered.

APPENDIX F

SEEDING

F1.0 SEEDING OF BATCH RUNS

The addition of seed crystals is a well-accepted procedure for controlling nucleation and the resulting crystal size distribution produced in batch crystallization; on the other hand, seeding is unnecessary, except in special circumstances, when the operation is of a continuous nature. It is thought that burkeite is the most suitable candidate for seeding for the following reasons: (1) it is one of the major species and it grows relatively slowly, and (2) crystals larger than 20 μm may facilitate solids separation.

Seeding was examined in experiments involving a 3-salt solution of sodium nitrate, sodium carbonate and sodium sulfate. The main purposes of these experiments were to study the effect of seeding on product properties and to investigate potential modifications in procedures that would reduce the amount of crystal accumulation on the walls of the crystallizer. Seeded 3-salt experiments (Runs 17 and 18) used sodium sulfate and sodium carbonate crystals as seed crystals.

The objective of using burkeite seed crystals in the 3-salt crystallization experiments was to obtain larger burkeite product crystals. The seed crystals were obtained from an earlier burkeite run performed according to the simulation Lab1B.xls. The product from that run was sieved, and the crystals retained on the smallest sieve (35 to 58 μm) were used as seeds in Run 18. Unfortunately, after performing Run 18, some question as to the actual composition of the seed crystals arose and they may have instead been a physical mixture of sodium sulfate and sodium carbonate.

The amount of seed crystals added in Run 18 was 10% of the expected mass of burkeite crystal yield as predicted by the simulation. The majority of the seed crystals appeared to be agglomerates comprised of constituent fine crystals whose shapes were similar to that of sodium sulfate. These agglomerates were close to 35 μm in size. The addition of seed crystals was expected to lead to larger product crystals. Since it was thought originally that the seed crystals were burkeite, larger crystals of this species were expected. PLM observations of the product from this run showed larger sodium carbonate and sodium sulfate crystals than in previous non-seeded 3-salt crystallization runs. There appeared to be little effect of the seed crystals on the size of the burkeite crystals in the product, and it was this observation that threw the composition of the seed crystals into question.

The product from Run 18 was washed with acetone, dried, and sieved to give the results shown in the following figure. The distribution is quite uniform and exhibits no significant post-washing agglomeration.

Figure F1. Size Distribution of the Seeded 3-Salt Experiment (Run 18).

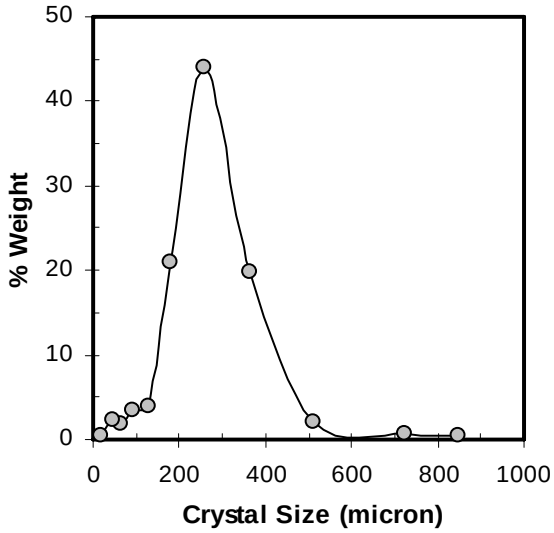

APPENDIX G

CRYSTALLIZATION RUNS

Table G1. List of Crystallization Runs Performed

Run #	Stage	Crys Nom. Vol. (mL)	Date	Feed Solution	Comments
1	1	1000	3/24/2005	NaNO3	
2	1	1000	3/30/2005	burkeite	
3	1	1000	4/5/2005	NaNO3	
4	1	1000	4/7/2005	NaNO3	
5	1	1000	4/12/2005	burkeite	
6	1	1000	4/15/2005	NaNO3	
7	1	1000	4/22/2005	NaNO3	
8	1	1000	4/28/2005	3-salt	
9	1	1000	5/2/2005	3-salt	
10	1	1000	5/6/2005	NaNO3	
11	1	1000	5/11/2005	NaNO3, CsNO3, NaOH	Cesium used as a tracer
12	1	1000	5/12/2005	3-salt	tested two-stage experiment
	2	600	5/13/2005	3-salt	
13	1	1000	5/17/2005	Early Feed	initial examination of simulant
	2	600	5/19/2005	Early Feed	sent samples for analysis
14	1	1000	5/24/2005	3-salt	
	2	600	5/26/2005		
15	1	1000	6/2/2005	3-salt	
16	1	1000	6/6/2005	DST Feed	DST practice run
	2	600	6/7/2005	DST Feed	initial examination of simulant
17	1	1000	6/14/2005	3-salt	used seed crystals from earlier burkeite run
18	1	1000	6/15/2005	3-salt	used seed crystals from earlier burkeite run
19	1	1000	6/16/2005	burkeite	grow new burkeite seed crystals
20	1	600	6/21/2005	3-salt	test spray nozzle for washing crystallizer walls during run
21	1	600	6/22/2005	3-salt	initial test of semi-batch operation
22	1	1000	6/27/2005	Late Feed	test operations with late feed simulant
	2	600	6/28/2005	Late Feed	
23	1	600	7/1/2005	3-salt	operate at a constant level with a semi-

					continuous feed
24	1	600	7/8/2005	burkeite	attempt to grow burkeite seed crystals
25	1	1000	7/21/2005	Late Feed #2	test operation at constant level in preparation for a certification run
	2	300	7/23/05	Late Feed	
26	1	1000	7/26/05	Early Feed	Certification Run
	2	300	7/28/05	Early Feed	
27	1	1000	8/1/2005	Late Feed #3	Certification Run
	2	300	8/4/2005	Late Feed	reduced evaporation rate for both stages
	2a	300	8/11/2005	Late Feed	
28	1	1000	8/7/2005	DST	carbonation on first stage, batch experiment
	2	600	8/15/05		
29	1	1000	8/17/2005	DST	carbonation on both stages, batch experiment
	2	600	8/17/05		
30	1	1000	8/23/05	DST	test operation for certification run
	2	300	8/25/05		identified gelling problems
31	1	1000	8/28/05	DST	Certification Run
	2	300	8/31/05		
32	1	300	11/20/05	Early Feed	tested small-scale apparatus with constant-level procedure
	2	100	11/29/05		
33	1	300	1/16/06	Early Feed	small scale/variable level => high accumulation
	2	100	1/18/06		Stage 2 aborted
34	1	300	2/8/06	Early Feed	compare results from small-scale apparatus to Run 32
	2	100	2/12/06		
35	1	100	2/22/06	Late Feed	demonstration run for CH2M Hill representatives; inadequate filtrate for operation of second stage, test FY 2006 simulant
36	1	300	4/10/06	Early Feed	Test water as heating

					medium, temperature control, new saturated solution composition and acetone alternative, test FY 2006 simulant
37	1	300	4/23/06	Early Feed	New Procedure Testing On Laboratory feed
	2	100	4/26/06		
38	1	300	4/30/06	Early Feed	Certification Run On Hanford Feed
	2	100	5/3/06		
38a	1	300	5/22/06	Early Feed	Certification Run, evaporation rate issues
38b	1	300	5/25/06	Early Feed	Final Certification Run
	2	100	5/29/06		
39	1	100	6/1/06	Late Feed	Procedure testing Run on Laboratory Feed
40	1	100	6/7/06	Late Feed	Certification Run on Hanford Feed
41					
42					
43					
44					
45					
46					
47					
48	1	300	7/18/06	Early Feed	Fast evaporation rate, ~58 g/h (originally Run 41)
49	1	300	7/25/06	Early Feed	Temperature target of 55^{o}C
50a	1	300	8/30/06	Early Feed	Concave-down evaporation rate
50b	1	300	8/23/06	Early Feed	Concave-down evaporation rate, increased C:F ratio
51	1	300		Early Feed	Concave-up evaporation rate

APPENDIX H

GALBRAITH LABORATORIES SAMPLE ANALYTICAL RESULTS

H1.0 CHEMICAL ANALYSES FROM GALBRAITH LABORATORIES

Identification of Samples from Crystallization from SST Early Feed Solution Certification Run 26, SST Late Feed Solution Certification Run 27, and DST Feed Solution Certification Run 31 Sent to Galbraith Laboratories for Analysis

Sample ID	Description	Condition
EF2-ST1-1	Filtrate from Stage 1	Liquid
EF2-ST1-2	Spent wash from Stage 1	Liquid
EF2-ST1-3	Washed crystals from Stage 1	Solid
EF2-ST1-4	Accumulation from Stage 1 crystallizer	Liquid
EF2-ST1-5	Unwashed crystals from Stage 1	Liquid
EF2-ST2-7	SST Early Feed Solution	Liquid
EF2-ST2-1	Filtrate from Stage 2	Liquid
EF2-ST2-2	Spent wash from Stage 2	Liquid
EF2-ST2-3	Washed crystals from Stage 2	Solid
EF2-ST2-4	Accumulation from Stage 2 crystallizer	Liquid
EF2-ST2-5	Unwashed crystals from Stage 2	Liquid
LF2-ST1-1	Filtrate from Stage 1	Liquid
LF2-ST1-2	Spent wash from Stage 1	Liquid
LF2-ST1-3	Washed crystals from Stage 1	Solid
LF2-ST1-4	Accumulation from Stage 1 crystallizer	Liquid
LF2-ST1-5	Unwashed crystals from Stage 1	Liquid
LF2-ST2-6	SST Early Feed Solution (CH2M HILL)	Liquid
LF2-ST2-7	SST Early Feed Solution (Lab)	Liquid
LF2-ST2-1a	Filtrate from Stage 2	Liquid
LF2-ST2-2a	Spent wash from Stage 2	Liquid
LF2-ST2-3a	Washed crystals from Stage 2	Solid
LF2-ST2-4a	Accumulation from Stage 2 crystallizer	Liquid
LF2-ST2-5a	Unwashed crystals from Stage 2	Liquid
DST5-ST1-1	Filtrate from Stage 1	Liquid
DST5-ST1-2	Spent wash from Stage 1	Liquid
DST5-ST1-3	Washed crystals from Stage 1	Solid
DST5-ST1-4	Accumulation from Stage 1 crystallizer	Liquid
DST5-ST1-5	Unwashed crystals from Stage 1	Liquid
DST5-ST2-6	SST Early Feed Solution	Liquid
DST4-ST2-0	Carbonated Feed Solution	Liquid
DST4-ST2-1	Filtrate from Stage 2	Liquid
DST4-ST2-2	Spent wash from Stage 2	Liquid
DST4-ST2-3	Washed crystals from Stage 2	Solid
DST4-ST2-4	Accumulation from Stage 2 crystallizer	Liquid
DST4-ST2-5	Unwashed crystals from Stage 2	Liquid

LABORATORY REPORT

Dr Ronald W Rousseau
Georgia Institute of Technology
School of Chemical & Biomolecular Engineering
311 Ferst Drive
Atlanta GA 30332-0100

Reanalysis Request: 09/23/05
Previous Lab ID #: X-3191-3225, X-0051-62, X-3191-
Report Date: 09/23/05

E-mail Addresses: EANelson@cogema-eng.com
FRRenz@cogema-eng.com

SAMPLE ID	LAB ID	ANALYSIS	RESULTS		DUPLICATE RESULTS	MATRIX SPIKE RECOVERY
DST5-ST1-1	X-1834	Oxalate	<200 [(a)]	ppm		
		Sodium	11.7	%		
		Aluminum	2.61	%		
		Chromium	190	ppm		
		Cesium	15	ppm		
		Fluoride	<7	ppm		
		Nitrate as Nitrogen	1.80	%		
		Nitrite as Nitrogen	2.33	%		
		Sulfate as Sulfur	<100	ppm		
		Carbonate	0.14	%		
		Hydroxide	4.05	%		
		Karl Fischer Water	61.19	%		
		Phosphate as Phosphorus	200	ppm		
		Density	1.333	g/mL		
	X-3191	Loss on Drying	55.34	%		
DST5-ST2-3	X-1835	Oxalate	<100	ppm		
		Sodium	29.3	%		
		Aluminum	0.957	%		
		Chromium	65	ppm		
		Cesium	5.1	ppm		
		Fluoride	76	ppm		
		Nitrate as Nitrogen	1.22	%		
		Nitrite as Nitrogen	0.859	%		
		Sulfate as Sulfur	<100	ppm		
		Carbonate	29.0	%		
		Hydroxide	3.21	%		
		Karl Fischer Water	7.60	%		
		Phosphate as Phosphorus	105	ppm		
	X-3192	Loss on Drying	22.25	%		

LABORATORY REPORT

Dr Ronald W Rousseau
Georgia Institute of Technology

Report Date: 09/23/05
Lab ID#: X-3191-3225

SAMPLE ID	LAB ID	ANALYSIS	RESULTS		DUPLICATE RESULTS		MATRIX SPIKE RECOVERY
DST5-ST1-3	X-1836	Oxalate	819	ppm			
		Sodium	30.5	%			
		Aluminum	0.429	%			
		Chromium	36	ppm			
		Cesium	2.7	ppm			
		Fluoride	304	ppm			
		Nitrate as Nitrogen	1.35	%			
		Nitrite as Nitrogen	0.443	%			
		Sulfate as Sulfur	885	ppm			
		Carbonate	31.4	%			
		Hydroxide	2.61	%			
		Karl Fischer Water	41.59	%			
		Phosphate as Phosphorus	<100	ppm			
	X-3193	Loss on Drying	22.38	%			
DST5-ST1-2	X-1837	Oxalate	234	ppm			
		Sodium	14.0	%			
		Aluminum	1.38	%			
		Chromium	96	ppm			
		Cesium	7.4	ppm			
		Fluoride	13	ppm			
		Nitrate as Nitrogen	3.04	%			
		Nitrite as Nitrogen	1.20	%			
		Sulfate as Sulfur	273	ppm			
		Carbonate	0.84	%			
		Hydroxide	4.93	%			
		Karl Fischer Water	61.83	%			
		Phosphate as Phosphorus	123	ppm			
		Density	1.379	g/mL			
	X-3194	Loss on Drying	46.01	%	46.29	(a) %	

LABORATORY REPORT

Dr Ronald W Rousseau
Georgia Institute of Technology

Report Date: 09/23/05
Lab ID#: X-3191-3225

SAMPLE ID	LAB ID	ANALYSIS	RESULTS		DUPLICATE RESULTS		MATRIX SPIKE RECOVERY
DST5-ST1-4	X-1838	Oxalate	<200 [a]	ppm			
		Sodium	1.83	%			
		Aluminum	0.177	%			
		Chromium	13	ppm			
		Cesium	0.94	ppm			
		Fluoride	11	ppm			
		Nitrate as Nitrogen	0.143	%			
		Nitrite as Nitrogen	0.155	%			
		Sulfate as Sulfur	<100	ppm			
		Carbonate	1.50	%			
		Hydroxide	0.240	%			
		Karl Fischer Water	96.29	%			
		Phosphate as Phosphorus	<100	ppm			
	X-3195	Loss on Drying	94.59	%			
DST5-ST1-5	X-1839	Oxalate	<200 [a]	ppm			
		Sodium	3.04	%			
		Aluminum	0.202	%			
		Chromium	2.9	ppm			
		Cesium	1.1	ppm			
		Fluoride	35	ppm			
		Nitrate as Nitrogen	0.268	%			
		Nitrite as Nitrogen	0.175	%			
		Sulfate as Sulfur	105	ppm			
		Carbonate	2.67	%			
		Hydroxide	0.348	%	0.269 [b]	%	
		Karl Fischer Water	92.87	%			
		Phosphate as Phosphorus	<100	ppm			
	X-3196	Loss on Drying	91.70	%			

LABORATORY REPORT

Dr Ronald W Rousseau
Georgia Institute of Technology

Report Date: 09/23/05
Lab ID#: X-3191-3225

SAMPLE ID	LAB ID	ANALYSIS	RESULTS		DUPLICATE RESULTS		MATRIX SPIKE RECOVERY
DST5-ST1-6	X-1840	Oxalate	241	ppm			
		Sodium	11.8	%			
		Aluminum	1.99	%			
		Chromium	136	ppm			
		Cesium	11	ppm			
		Fluoride	21	ppm			
		Nitrate as Nitrogen	1.63	%			
		Nitrite as Nitrogen	1.83	%			
		Sulfate as Sulfur	231	ppm			
		Carbonate	3.72	%			
		Hydroxide	3.13	%	3.09 [b]	%	
		Karl Fischer Water	64.43	%			
		Phosphate as Phosphorus	162	ppm			
		Density	1.331	g/mL			
	X-3197	Loss on Drying	46.89	%			
DST5-ST2-0	X-1841	Oxalate	<200 [a]	ppm			
		Sodium	11.6	%			
		Aluminum	2.68	%			
		Chromium	186	ppm			
		Cesium	14	ppm			
		Fluoride	<7	ppm			
		Nitrate as Nitrogen	1.81	%			
		Nitrite as Nitrogen	2.27	%			
		Sulfate as Sulfur	<100	ppm			
		Carbonate	2.75	%			
		Hydroxide	2.56	%			
		Karl Fischer Water	61.15	%			
		Phosphate as Phosphorus	186	ppm			
		Density	1.335	g/mL			
	X-3198	Loss on Drying	53.37	%			

LABORATORY REPORT

Dr Ronald W Rousseau
Georgia Institute of Technology

Report Date: 09/23/05
Lab ID#: X-3191-3225

SAMPLE ID	LAB ID	ANALYSIS	RESULTS		DUPLICATE RESULTS		MATRIX SPIKE RECOVERY
DST5-ST2-1	X-1842	Oxalate	151	ppm			
		Sodium	11.4	%			
		Aluminum	3.27	%			
		Chromium	223	ppm			
		Cesium	17	ppm			
		Fluoride	<4	ppm			
		Nitrate as Nitrogen	2.20	%			
		Nitrite as Nitrogen	2.75	%			
		Sulfate as Sulfur	79	ppm			
		Carbonate	0.27	%			
		Hydroxide	3.07	%			
		Karl Fischer Water	57.13	%			
		Phosphate as Phosphorus	191	ppm			
		Density	1.357	g/mL			
	X-3199	Loss on Drying	57.15	%			
DST5-ST2-2	X-1843	Oxalate	<200 [a]	ppm			
		Sodium	12.4	%			
		Aluminum	0.575	%			
		Chromium	41	ppm			
		Cesium	3.1	ppm			
		Fluoride	4	ppm			
		Nitrate as Nitrogen	2.23	%			
		Nitrite as Nitrogen	0.544	%			
		Sulfate as Sulfur	<100	ppm			
		Carbonate	1.84	%			
		Hydroxide	4.71	%			
		Karl Fischer Water	74.05	%			
		Phosphate as Phosphorus	<100	ppm			
		Density	1.299	g/mL	1.317 [b]	g/mL	
	X-3200	Loss on Drying	63.96	%			

LABORATORY REPORT

Dr Ronald W Rousseau
Georgia Institute of Technology

Report Date: 09/23/05
Lab ID#: X-3191-3225

SAMPLE ID	LAB ID	ANALYSIS	RESULTS		DUPLICATE RESULTS		MATRIX SPIKE RECOVERY	
DST5-ST2-4	X-1844	Oxalate	<200 [a]	ppm			117 [b]	%
		Sodium	2.57	%				
		Aluminum	0.181	%				
		Chromium	121	ppm				
		Cesium	0.90	ppm				
		Fluoride	<4	ppm				
		Nitrate as Nitrogen	0.137	%			105 [b]	%
		Nitrite as Nitrogen	0.177	%			101 [b]	%
		Sulfate as Sulfur	<100	ppm			102 [b]	%
		Carbonate	2.58	%				
		Hydroxide	0.171	%				
		Karl Fischer Water	97.47	%				
		Phosphate as Phosphorus	<100	ppm			108 [b]	%
	X-3201	Loss on Drying	92.49	%				
DST5-ST2-5	X-1845	Oxalate	<200 [a]	ppm				
		Sodium	2.22	%	2.17 [b]	%	100 [b]	%
		Aluminum	0.327	%	0.324 [b]	%	101 [b]	%
		Chromium	23	ppm	22 [b]	ppm	99 [b]	%
		Cesium	1.7	ppm	1.7 [b]	ppm	95 [b]	%
		Fluoride	<4	ppm				
		Nitrate as Nitrogen	0.225	%				
		Nitrite as Nitrogen	0.286	%				
		Sulfate as Sulfur	<100	ppm				
		Carbonate	1.45	%				
		Hydroxide	0.344	%				
		Karl Fischer Water	95.49	%				
		Phosphate as Phosphorus	<100	ppm				
	X-3202	Loss on Drying	92.86	%				

LABORATORY REPORT

Dr Ronald W Rousseau
Georgia Institute of Technology

Report Date: 09/23/05
Lab ID#: X-3191-3225

SAMPLE ID	LAB ID	ANALYSIS	RESULTS		DUPLICATE RESULTS			MATRIX SPIKE RECOVERY		
LF3-ST1-1	X-0051	Cesium	0.45	ppm	0.43	(b)	ppm	122	(b)	%
		Sodium	8.93	%	8.97	(b)	%	114	(b)	%
		Aluminum	0.237	%	0.237	(b)	%	99	(b)	%
		Chromium	0.169	%	0.170	(b)	%	104	(b)	%
		Fluoride	15	ppm						
		Nitrite as Nitrogen	0.179	%				98	(b)	%
		Nitrate as Nitrogen	3.98	%				104	(b)	%
		Phosphate as Phosphorus	0.276	%				88	(b)	%
		Sulfate as Sulfur	997	ppm				97	(b)	%
		Oxalate	244	ppm				102	(b)	%
		Carbonate as Carbon	0.374	%						
		Karl Fischer Water	68.80	%						
		Hydroxide	0.384	%						
		Density	1.256	g/mL						
	X-3203	Loss on Drying	67.81	%	67.79	(b)	%			
LF3-ST1-2	X-0052	Cesium	0.032	ppm						
		Sodium	8.57	%						
		Aluminum	185	ppm						
		Chromium	122	ppm						
		Fluoride	189	ppm						
		Nitrite as Nitrogen	122	ppm						
		Nitrate as Nitrogen	3.87	%						
		Phosphate as Phosphorus	329	ppm						
		Sulfate as Sulfur	971	ppm						
		Oxalate	145	ppm						
		Carbonate as Carbon	0.604	%						
		Karl Fischer Water	71.00	%						
		Hydroxide	0.035	%	0.027	(b)	%			
		Density	1.232	g/mL						
	X-3204	Loss on Drying	71.04	%						

LABORATORY REPORT

Dr Ronald W Rousseau
Georgia Institute of Technology

Report Date: 09/23/05
Lab ID#: X-3191-3225

SAMPLE ID	LAB ID	ANALYSIS	RESULTS		DUPLICATE RESULTS	MATRIX SPIKE RECOVERY
LF3-ST1-3	X-0053	Cesium	0.042	ppm		
		Sodium	30.9	%		
		Aluminum	682	ppm		
		Chromium	215	ppm		
		Fluoride	5.30	ppm		
		Nitrite as Nitrogen	<170	(a) ppm		
		Nitrate as Nitrogen	3.33	%		
		Phosphate as Phosphorus	0.260	%		
		Sulfate as Sulfur	10.7	%		
		Oxalate	1.45	%		
		Carbonate as Carbon	2.14	%		
		Karl Fischer Water	13.91	%		
		Hydroxide	0.107	%		
	X-3205	Loss on Drying	10.93	%		
LF3-ST1-4	X-0054	Cesium	<0.025	ppm		
		Sodium	1.53	%		
		Aluminum	62	ppm		
		Chromium	<49	ppm		
		Fluoride	0.426	%		
		Nitrite as Nitrogen	<100	ppm		
		Nitrate as Nitrogen	547	ppm		
		Phosphate as Phosphorus	<100	ppm		
		Sulfate as Sulfur	0.637	%		
		Oxalate	432	ppm		
		Carbonate as Carbon	0.016	%		
		Karl Fischer Water	98.65	%		
		Hydroxide	<0.01	%		
	X-3206	Loss on Drying	95.66	%		

LABORATORY REPORT

Dr Ronald W Rousseau
Georgia Institute of Technology

Report Date: 09/23/05
Lab ID#: X-3191-3225

SAMPLE ID	LAB ID	ANALYSIS	RESULTS		DUPLICATE RESULTS	MATRIX SPIKE RECOVERY
LF3-ST1-5	X-0055	Cesium	<0.024	ppm		
		Sodium	2.86	%		
		Aluminum	117	ppm		
		Chromium	67	ppm		
		Fluoride	0.408	%		
		Nitrite as Nitrogen	<100	ppm		
		Nitrate as Nitrogen	0.284	%		
		Phosphate as Phosphorus	329	ppm		
		Sulfate as Sulfur	0.888	%		
		Oxalate	0.127	%		
		Carbonate as Carbon	0.169	%		
		Karl Fischer Water	93.00	%		
		Hydroxide	0.026	%		
	X-3207	Loss on Drying	91.65	%		
LF3-ST1-6	X-0056	Cesium	0.21	ppm		
		Sodium	5.57	%		
		Aluminum	0.119	%		
		Chromium	821	ppm		
		Fluoride	0.189	%		
		Nitrite as Nitrogen	905	ppm		
		Nitrate as Nitrogen	1.97	%		
		Phosphate as Phosphorus	0.137	%		
		Sulfate as Sulfur	0.481	%		
		Oxalate	771	ppm		
		Carbonate as Carbon	0.246	%		
		Karl Fischer Water	82.49	%		
		Hydroxide	0.216	%		
		Density	1.148	g/mL		
	X-3208	Loss on Drying	83.64	%		

LABORATORY REPORT

Dr Ronald W Rousseau
Georgia Institute of Technology

Report Date: 09/23/05
Lab ID#: X-3191-3225

SAMPLE ID	LAB ID	ANALYSIS	RESULTS		DUPLICATE RESULTS	MATRIX SPIKE RECOVERY
LF3-ST1-7	X-0057	Cesium	0.13	ppm		
		Sodium	5.27	%		
		Aluminum	0.114	%		
		Chromium	777	ppm		
		Fluoride	0.186	%		
		Nitrite as Nitrogen	871	ppm		
		Nitrate as Nitrogen	1.90	%		
		Phosphate as Phosphorus	0.138	%		
		Sulfate as Sulfur	0.459	%		
		Oxalate	759	ppm		
		Carbonate as Carbon	0.242	%		
		Karl Fischer Water	83.25	%		
		Hydroxide	0.205	%		
		Density	1.144	g/mL		
	X-3209	Loss on Drying	81.88	%		
LF3-ST2-1A	X-0058	Cesium	0.095	ppm		
		Sodium	1.02	%		
		Aluminum	628	ppm		
		Chromium	449	ppm		
		Fluoride	<4	ppm		
		Nitrite as Nitrogen	486	ppm		
		Nitrate as Nitrogen	0.310	%		
		Phosphate as Phosphorus	369	ppm		
		Sulfate as Sulfur	271	ppm		
		Oxalate	<100	ppm		
		Carbonate as Carbon	0.056	%		
		Karl Fischer Water	98.17	%		
		Hydroxide	0.071	%		
		Density	1.024	g/mL		
	X-3210	Loss on Drying	96.45	%		

LABORATORY REPORT

Dr Ronald W Rousseau
Georgia Institute of Technology

Report Date: 09/23/05
Lab ID#: X-3191-3225

SAMPLE ID	LAB ID	ANALYSIS	RESULTS		DUPLICATE RESULTS		MATRIX SPIKE RECOVERY
LF3-ST2-2a	X-0059	Cesium	0.11	ppm			
		Sodium	8.60	%			
		Aluminum	610	ppm			
		Chromium	454	ppm			
		Fluoride	44	ppm			
		Nitrite as Nitrogen	497	ppm			
		Nitrate as Nitrogen	3.44	%			
		Phosphate as Phosphorus	994	ppm			
		Sulfate as Sulfur	276	ppm			
		Oxalate	<100	ppm			
		Carbonate as Carbon	0.798	%			
		Karl Fischer Water	72.04	%			
		Hydroxide	<0.01	%			
		Density	1.240	g/mL	1.258 [b]	g/mL	
	X-3211	Loss on Drying	70.72	%	70.74 [b]	%	
LF3-ST2-3a	X-0060	Cesium	0.077	ppm			
		Sodium	25.8	%			
		Aluminum	872	ppm			
		Chromium	311	ppm			
		Fluoride	237	ppm			
		Nitrite as Nitrogen	<100	ppm			
		Nitrate as Nitrogen	12.4	%			
		Phosphate as Phosphorus	0.220	%			
		Sulfate as Sulfur	209	ppm			
		Oxalate	98	ppm			
		Carbonate as Carbon	1.16	%			
		Karl Fischer Water	6.08	%			
		Hydroxide	0.322	%			
	X-3212	Loss on Drying	8.94	%			

LABORATORY REPORT

Dr Ronald W Rousseau
Georgia Institute of Technology

Report Date: 09/23/05
Lab ID#: X-3191-3225

SAMPLE ID	LAB ID	ANALYSIS	RESULTS		DUPLICATE RESULTS		MATRIX SPIKE RECOVERY
LF3-ST2-4a	X-0061	Cesium	0.052	ppm			
		Sodium	1.77	%			
		Aluminum	321	ppm			
		Chromium	222	ppm			
		Fluoride	31	ppm			
		Nitrite as Nitrogen	251	ppm			
		Nitrate as Nitrogen	0.869	%			
		Phosphate as Phosphorus	427	ppm			
		Sulfate as Sulfur	144	ppm			
		Oxalate	<100	ppm			
		Carbonate as Carbon	0.054	%			
		Karl Fischer Water	98.65	%			
		Hydroxide	0.055	%			
	X-3213	Loss on Drying	93.69	%			
LF3-ST2-5a	X-0062	Cesium	<0.025	ppm			
		Sodium	1.10	%			
		Aluminum	134	ppm			
		Chromium	87	ppm			
		Fluoride	11	ppm			
		Nitrite as Nitrogen	121	ppm			
		Nitrate as Nitrogen	0.475	%			
		Phosphate as Phosphorus	327	ppm			
		Sulfate as Sulfur	<100	ppm			
		Oxalate	<100	ppm			
		Carbonate as Carbon	0.061	%			
		Karl Fischer Water	98.50	%			
		Hydroxide	0.035	%	0.035 [(b)]	%	
	X-3214	Loss on Drying	96.20	%			

LABORATORY REPORT

Dr Ronald W Rousseau
Georgia Institute of Technology

Report Date: 09/23/05
Lab ID#: X-3191-3225

SAMPLE ID	LAB ID	ANALYSIS	RESULTS		DUPLICATE RESULTS		MATRIX SPIKE RECOVERY	
EF2-ST1-1	W-9700	Cesium	2.7	ppm				
		Sodium	12.2	%				
		Aluminum	1.76	%				
		Chromium	0.430	%				
		Fluorine	4	ppm				
		Nitrite as Nitrogen	1.31	%			110	%
		Nitrate as Nitrogen	2.30	%			87	%
		Phosphate as Phosphorus	508	ppm			104	%
		Sulfate as Sulfur	453	ppm			105	%
		Oxalate	<100	ppm			99	%
		Carbonate	0.45	%				
		Karl Fischer Water	74.68	%				
		Hydroxide	4.35	%	4.32 [b]	%		
		Density	1.316	g/mL				
	X-3215	Loss on Drying	54.17	%				
EF2-ST1-2	W-9701	Cesium	0.19	ppm				
		Sodium	13.3	%				
		Aluminum	0.127	%				
		Chromium	288	ppm				
		Fluorine	5	ppm				
		Nitrite as Nitrogen	957	ppm				
		Nitrate as Nitrogen	5.19	%				
		Phosphate as Phosphorus	<100	ppm				
		Sulfate as Sulfur	965	ppm				
		Oxalate	97	ppm				
		Carbonate	5.24	%				
		Karl Fischer Water	99.49	%				
		Hydroxide	0.374	%				
		Density	1.389	g/mL				
	X-3216	Loss on Drying	56.58	%				

LABORATORY REPORT

Dr Ronald W Rousseau
Georgia Institute of Technology

Report Date: 09/23/05
Lab ID#: X-3191-3225

SAMPLE ID	LAB ID	ANALYSIS	RESULTS		DUPLICATE RESULTS	MATRIX SPIKE RECOVERY
EF2-ST1-3	W-9702	Cesium	0.64	ppm		
		Sodium	28.4	%		
		Aluminum	0.462	%		
		Chromium	0.113	%		
		Fluorine	91	ppm		
		Nitrite as Nitrogen	0.331	%		
		Nitrate as Nitrogen	11.3	%		
		Phosphate as Phosphorus	<200	(a) ppm		
		Sulfate as Sulfur	0.966	%		
		Oxalate	959	ppm		
		Carbonate	10.85	%		
		Karl Fischer Water	5.30	%		
		Hydroxide	<0.01	%		
	X-3217	Loss on Drying	3.80	%		
EF2-ST1-4	W-9703	Cesium	0.28	ppm		
		Sodium	5.57	%		
		Aluminum	0.195	%		
		Chromium	470	ppm		
		Fluorine	4	ppm		
		Nitrite as Nitrogen	0.150	%		
		Nitrate as Nitrogen	2.08	%		
		Phosphate as Phosphorus	<100	ppm		
		Sulfate as Sulfur	0.168	%		
		Oxalate	182	ppm		
		Carbonate	1.28	%		
		Karl Fischer Water	20.71	%		
		Hydroxide	0.426	%		
	X-3218	Loss on Drying	81.03	%		

LABORATORY REPORT

Dr Ronald W Rousseau
Georgia Institute of Technology

Report Date: 09/23/05
Lab ID#: X-3191-3225

SAMPLE ID	LAB ID	ANALYSIS	RESULTS		DUPLICATE RESULTS	MATRIX SPIKE RECOVERY
EF2-ST1-5	W-9704	Cesium	0.08	ppm		
		Sodium	2.44	%		
		Aluminum	571	ppm		
		Chromium	136	ppm		
		Fluorine	4	ppm		
		Nitrite as Nitrogen	427	ppm		
		Nitrate as Nitrogen	1.07	%		
		Phosphate as Phosphorus	<100	ppm		
		Sulfate as Sulfur	385	ppm		
		Oxalate	<100	ppm		
		Carbonate	0.32	%		
		Karl Fischer Water	7.83	%		
		Hydroxide	0.114	%		
	X-3219	Loss on Drying	91.56	%		
EF2-ST1-7	W-9705	Cesium	0.16	ppm		
		Sodium	6.08	%		
		Aluminum	0.135	%		
		Chromium	844	ppm		
		Fluorine	0.187	%		
		Nitrite as Nitrogen	982	ppm		
		Nitrate as Nitrogen	1.96	%		
		Phosphate as Phosphorus	0.135	%		
		Sulfate as Sulfur	0.463	%		
		Oxalate	755	ppm		
		Carbonate	1.27	%		
		Karl Fischer Water	83.15	%		
		Hydroxide	0.316	%		
		Density	1.155	g/mL		
	X-3220	Loss on Drying	80.11	%		

LABORATORY REPORT

Dr Ronald W Rousseau
Georgia Institute of Technology

Report Date: 09/23/05
Lab ID#: X-3191-3225

SAMPLE ID	LAB ID	ANALYSIS	RESULTS		DUPLICATE RESULTS		MATRIX SPIKE RECOVERY
EF2-ST2-1	W-9706	Cesium	2.7	ppm			
		Sodium	10.5	%			
		Aluminum	1.92	%			
		Chromium	0.467	%			
		Fluorine	26	ppm			
		Nitrite as Nitrogen	1.32	%			
		Nitrate as Nitrogen	0.887	%			
		Phosphate as Phosphorus	565	ppm			
		Sulfate as Sulfur	249	ppm			
		Oxalate	<100	ppm			
		Carbonate	0.10	%			
		Karl Fischer Water	59.24	%			
		Hydroxide	4.61	%			
		Density	1.257	g/mL			
	X-3221	Loss on Drying	64.43	%	64.63 [b]	%	
EF2-ST2-2	W-9707	Cesium	0.053	ppm			
		Sodium	7.27	%			
		Aluminum	393	ppm			
		Chromium	90	ppm			
		Fluorine	5	ppm			
		Nitrite as Nitrogen	505	ppm			
		Nitrate as Nitrogen	2.89	%			
		Phosphate as Phosphorus	<100	ppm			
		Sulfate as Sulfur	<100	ppm			
		Oxalate	<100	ppm			
		Carbonate	2.96	%			
		Karl Fischer Water	77.37	%			
		Hydroxide	0.729	%			
		Density	1.188	g/mL	1.197 [b]	g/mL	
	X-3222	Loss on Drying	76.10	%			

LABORATORY REPORT

Dr Ronald W Rousseau
Georgia Institute of Technology

Report Date: 09/23/05
Lab ID#: X-3191-3225

SAMPLE ID	LAB ID	ANALYSIS	RESULTS		DUPLICATE RESULTS	MATRIX SPIKE RECOVERY
EF2-ST2-3	W-9708	Cesium	0.54	ppm		
		Sodium	27.2	%		
		Aluminum	0.760	%		
		Chromium	0.202	%		
		Fluorine	59	ppm		
		Nitrite as Nitrogen	0.630	%		
		Nitrate as Nitrogen	13.3	%		
		Phosphate as Phosphorus	<200	ppm		
		Sulfate as Sulfur	0.133	%		
		Oxalate	121	ppm		
		Carbonate	4.51	%		
		Karl Fischer Water	3.67	%		
		Hydroxide	0.622	%		
	X-3223		(c)			
EF2-ST2-4	W-9709	Cesium	0.44	ppm		
		Sodium	5.38	%		
		Aluminum	0.325	%		
		Chromium	809	ppm		
		Fluorine	4	ppm		
		Nitrite as Nitrogen	0.265	%		
		Nitrate as Nitrogen	2.26	%		
		Phosphate as Phosphorus	133	ppm		
		Sulfate as Sulfur	194	ppm		
		Oxalate	<100	ppm		
		Carbonate	0.31	%		
		Karl Fischer Water	86.82	%		
		Hydroxide	0.734	%		
	X-3224	Loss on Drying	80.83	%		

LABORATORY REPORT

Dr Ronald W Rousseau
Georgia Institute of Technology

Report Date: 09/23/05
Lab ID#: X-3191-3225

SAMPLE ID	LAB ID	ANALYSIS	RESULTS		DUPLICATE RESULTS	MATRIX SPIKE RECOVERY
EF2-ST2-5	W-9710	Cesium	0.087	ppm		
		Sodium	1.67	%		
		Aluminum	643	ppm		
		Chromium	157	ppm		
		Fluorine	9	ppm		
		Nitrite as Nitrogen	893	ppm		
		Nitrate as Nitrogen	0.645	%		
		Phosphate as Phosphorus	<100	ppm		
		Sulfate as Sulfur	114	ppm		
		Oxalate	<100	ppm		
		Carbonate	0.19	%		
		Karl Fischer Water	96.18	%		
		Hydroxide	0.133	%		
		Loss on Drying	94.19	%		

LABORATORY REPORT

Dr Ronald W Rousseau		Report Date:	09/23/05
Georgia Institute of Technology		Lab ID#:	X-3191-3225

TECHNICAL INFORMATION:

(a) We regret that we are unable to achieve lower quantitation limits due to matrix interference. If you have any questions, please contact our technical staff.

QUALITY ASSURANCE INFORMATION:

(b) Duplicate analyses were performed as part of our internal Quality Control Program. There is no additional charge for duplicate values.

(c) There was not sufficient sample remaining to perform the Loss on Drying analysis.

Authorized Release of Data

_____
Jeffry L. Dillener, Technical Manager

H2.0 WASHING EFFICIENCY

To determine qualitatively the effect of multiple wash steps on product purity, crystals recovered from run using an SST Early Feed simulant were washed and filtered four times in series. The following figure displays the change in color of crystals at the bottom of the sample bottles (from left to right) as the product crystals were washed. The sample labeled –1 corresponds to the filtered slurry obtained from the crystallization and bottle 0 is a sample of the washed crystals produced in the experiment. Bottles 1 through 4 are samples taken after each of four additional wash steps. Each wash was performed by slurrying the crystals in a saturated solution of sodium nitrate. The experiment was stopped when the color between two successive samples remained unchanged. At this point the amount of adhering mother liquor and its associated impurities can be assumed negligible and the remaining color is a result of the crystal inclusions. The progression of the color to a virtually white sample after three additional washings leads to the conclusion that the majority of the remaining liquid (mother liquor remaining after the filtration operation) is present in a form other than inclusions.

Effects of Washing on Crystal Color

The graph presented in the figure to the right shows the chromium analyses of the washed crystals. Clearly, the expected coloration of the crystals due to the presence of chromium corresponds to the visual observations described above and the quantitative analysis shown on the graph.

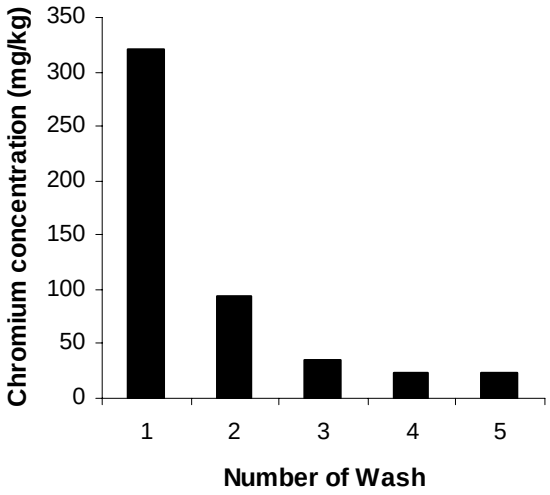

Chromium Evolution with Washing

APPENDIX I

COEFFICIENT OF VARIATION SAMPLE CALCULATIONS

I1.0 COEFFICIENT OF VARIATION

Table I 1: Sieve Test Results for certification run 38b Stage 1

Sample Name	Early Feed 38b_Stage 1
Sample weight (g)	15.96
Sieving time (min)	30

Sieve no.	Mesh opening	Range	Ave. Size (micron)	Before sieving (g)	After sieving (g)	Crystal weight (g)	Fractional Mass %	Cumulative oversize %	Cumulative undersize %
30	600	600-850	600	125.06	125.06	0	0.00	0.00	100.00
40	425	425-600	512.5	115.9	118.08	2.18	13.66	13.66	86.34
50	300	300-425	362.5	110.71	118.15	7.44	46.62	60.28	39.72
70	212	212-300	256	112.52	115.72	3.2	20.05	80.33	19.67
100	150	150-212	181	106.69	107.78	1.09	6.83	87.16	12.84
140	106	106-150	128	105.25	105.96	0.71	4.45	91.60	8.40
200	75	75-106	90.5	105.13	105.62	0.49	3.07	94.67	5.33
270	53	53-75	64	103.95	104.19	0.24	1.50	96.18	3.82
400	38	38-53	45.5	102.81	103.01	0.2	1.25	97.43	2.57
635	20	20-38	29	104.58	104.84	0.26	1.63	99.06	0.94
Pan	0	0-20	10	82.89	83.04	0.15	0.94	100.00	0.00

The coefficient of variation is calculated based on the cumulative undersize percent data. Cumulative undersize values are plotted in graph displaying in the Y axis the cumulative undersize and in the X axis the mesh opening (Figure I 1). The coefficient of variation is calculated based on the relation: $CV = \frac{100(d_{84\%} - d_{16\%})}{2d_{50\%}}$, where the values $d_{84\%}$, $d_{16\%}$ and $d_{50\%}$ corresponds to the sizes (X axis) for 84%, 16% and 50% cumulative undersize weight percent respectively. Figure I1 led to the values 415 µm, 187.5 µm and 327.5µm for $d_{84\%}$, $d_{16\%}$ and $d_{50\%}$ respectively leading to a coefficient variation of 34.7%

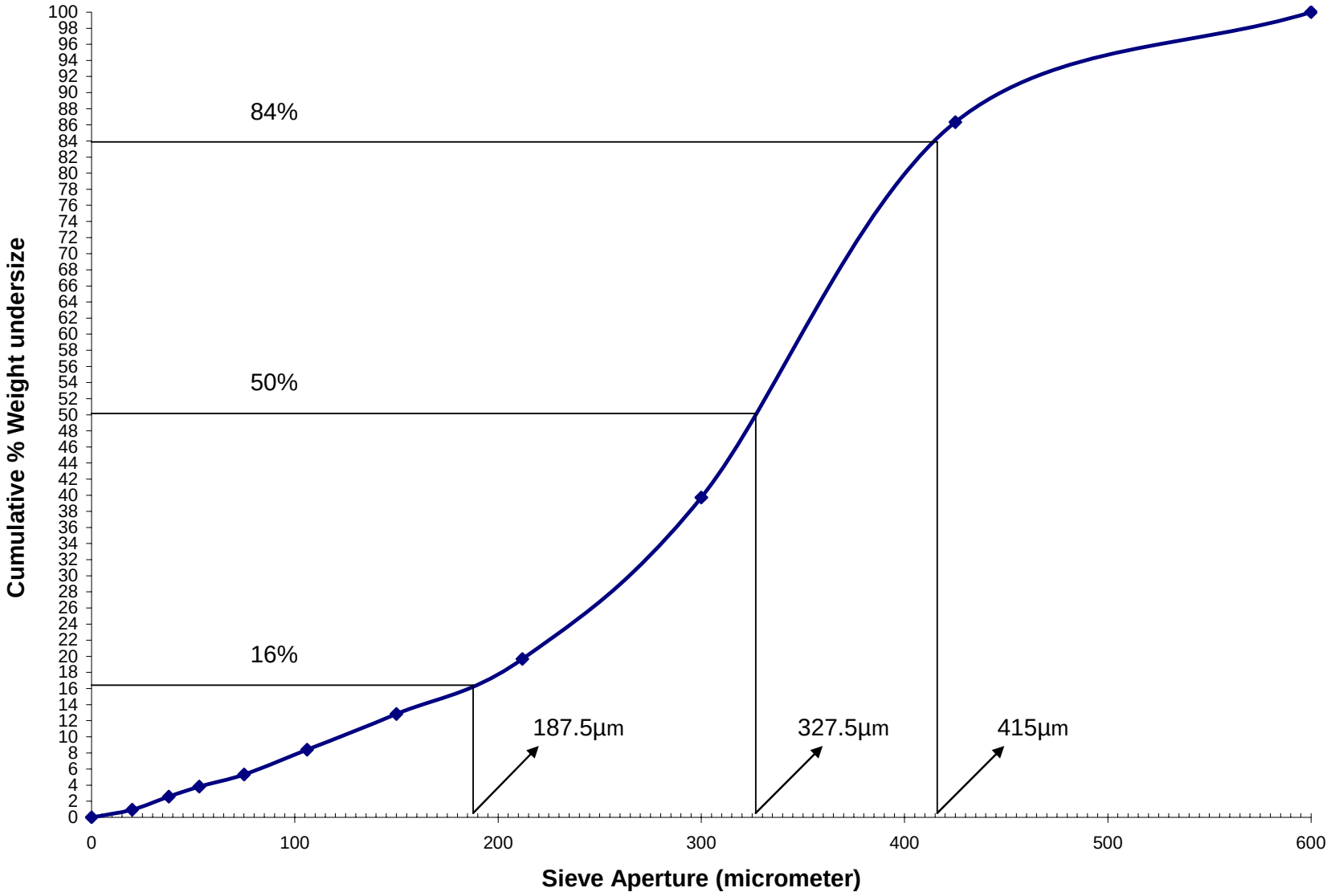
Cumulative % Weight undersize
Sieve Aperture (micrometer)
84%
50%
16%
187.5µm
327.5µm
415µm
0
100
200
300
400
500
600

APPENDIX J

GTRI LABORATORIES SAMPLE ANALYTICAL RESULTS

J1.0 CHEMICAL ANALYSES FROM GTRI LABORATORIES

Identification of Samples from Crystallization from SST Early Feed Solution Certification run 38b sent to GTRI Laboratories for Analysis

			Concentration (% or ppm)					
GTRI ID #	Sample ID	Sample Name	Al	Cr	Cs	SO4	P	Na
52418	EF38B-ST1-01	Hanford Feed	0.75%	810	3.300	<10.0	0.150%	15.0%
52419	EF38B-ST1-02	Mixed Feed	0.76%	0.15%	3.150	1.19%	0.160%	15.0%
52420	EF38B-ST1-03	Accumulation	0.11%	260	0.391	0.443%	230	4.10%
52421	EF38B-ST1-04	Filtrate	1.10%	0.22%	3.340	0.125%	0.180%	9.50%
52422	EF38B-ST1-05	Wash Solution	20.0	<0.10	<0.002	<100	2.20	6.50%
52423	EF38B-ST1-06	Spent Wash	0.21%	440	0.568	0.120%	430	8.80%
52424	EF38B-ST1-07	Unwashed Crystals	230	50.0	0.082	0.111%	45.0	1.10%
52425	EF38B-ST1-08	1 Wash	63.0	13.0	0.019	560	13.0	0.57%
52426	EF38B-ST1-09	2 Washes	16.0	3.80	0.006	661	3.60	0.62%
52427	EF38B-ST1-10	3 Washes	6.30	1.60	<0.002	635	<2.00	0.66%
52428	EF38B-ST1-11	4 Washes	3.70	1.30	<0.002	702	<2.00	0.73%
52429	EF38B-ST1-12	Final Crystals	5.10	2.40	<0.002	0.166%	2.20	2.00%
52430	EF38B-ST2-01	Accumulation	0.16%	350	0.511	195	480	2.50%
52431	EF38B-ST2-02	Filtrate	0.93%	0.19%	3.020	0.119%	0.110%	5.50%
52432	EF38B-ST2-03	Wash Solution	2.40	<0.10	<0.002	<100	<2.00	3.50%
52433	EF38B-ST2-04	Spent Wash	0.22%	460	0.813	350	370	8.40%
52434	EF38B-ST2-05	Unwashed Crystals	260	53.0	0.073	29.0	41.0	0.43%
52435	EF38B-ST2-06	1 Wash	82.0	17.0	0.029	<10.0	21.0	0.43%
52436	EF38B-ST2-07	2 Washes	20.0	4.00	0.007	<10.0	11.0	0.36%
52437	EF38B-ST2-08	3 Washes	2.80	0.550	<0.002	<10.0	3.90	0.23%
52438	EF38B-ST2-09	4 Washes	3.20	0.620	<0.002	<10.0	5.00	0.44%
52439	EF38B-ST2-10	Final Crystals	3.60	0.710	<0.002	<10.0	4.90	0.63%
52440	LF40-ST1-01	Hanford Feed	0.12%	170	0.546	0.165%	750	3.10%
52441	LF40-ST1-02	Accumulation	860	110	0.328	0.172%	640	2.50%
52442	LF40-ST1-03	Filtrate	0.32%	430	1.310	<10.0	120	3.40%
52443	LF40-ST1-04	Wash Solution	2.10	<0.10	<0.002	<100	<2.00	4.20%
52444	LF40-ST1-05	Spent Wash	0.38%	490	1.420	562	580	13.0%
52445	LF40-ST1-06	Unwashed Crystals	160	21.0	0.067	465	240	0.69%
52446	LF40-ST1-07	1 Wash	32.0	4.70	0.015	354	180	0.49%
52447	LF40-ST1-08	2 Washes	18.0	3.10	0.008	438	200	0.64%

52448	LF40-ST1-09	3 Washes	8.40	1.80	0.003	522	220	0.74%
52449	LF40-ST1-10	4 Washes	5.60	1.80	0.002	781	300	1.10%
52450	LF40-ST1-11	Final Crystals	<1.00	<0.10	<0.002	993	430	1.40%
52451	LF40-ST1-12	GT Feed	0.13%	340	0.713	0.159%	870	3.30%

APPENDIX K

GROWTH RATE ESTIMATE CALCULATIONS

K1.0 NUCLEATION TIME VALUES

The nucleation time of the three main species (sodium nitrate, sodium carbonate monohydrate and burkeite crystals) was determined by performing a run under similar operating conditions than certification run 38b.Sampling was performed during this run and the nucleation time was determined based on the sample time. Both experimental nucleation and nucleation time according to the simulation files are displayed in Table K1.

Table K1. Experimental and Simulation Time and Condensate to Feed Ratio at Nucleation

Parameters	Sodium nitrate	Sodium carbonate	Burkeite
Condensate to feed ratio at nucleation (simulation)	0.38	0.33	0.09
Condensate to feed ratio at nucleation (experimental)	0.24	0.28	0.09
Time at nucleation (simulation) (in min)	720	1067	232.6
Time at nucleation (experimental) (in min)	669.6	841	232.6

K2.0 MAXIMUM CRYSTAL SIZES

PLM analysis performed on run 38b leads to sieve sizes where each of the species where observed at their maximum sizes. At least three samples on each of these pan were taken and analyzed through PLM to determine the maximum size for each species. The maximum size is determined on single homogenous crystals and corresponds to the length of the larger side when the shape is not regular. In other words, the heterogeneous or agglomerated burkeite crystals are excluded from this study and a crystal with the dimensions 15 x 30 x 15 μm has a maximum size of 30μm. Table K2 displays the maximum sizes for the three main species observed in run 38b.

Table K2. Sodium Nitrate, Sodium Carbonate and Burkeite Maximum sizes during Run 38b

Parameters	Sodium nitrate	Sodium carbonate	Burkeite
Maximum crystal size (in μm)	550	250	45

K3.0 AVERAGE GROWTH RATE ESTIMATE CALCULATION

The average growth rate is calculated based on the equation $G = \frac{(L_{MAX})}{(t_{end} - t_{nucleation})}$ (E-4) where LMAX represents the maximum crystal size (displayed in Table K2), tend represent the time at the end of the certification run 38b (1830minutes) and tnucleation the time at nucleation.

In other words, performing calculations on sodium nitrate crystals leads to a Growth rate G of:

$G = \frac{550}{(1830 - 669.6)} = 0.474 \mu m \bullet \min^{-1}$ for the experimental growth rate and a value of $G = \frac{550}{(1830 - 720)} = 0.495 \mu m \bullet \min^{-1}$ for the simulation growth rate estimate.

APPENDIX L

OVERALL AND DETAILLED MASS BALANCE OF RUNS IN SECTION 5

L1.0 OVERALL MASS BALANCE ON RUNS DESCRIBED IN SECTION 5

Table L1. Mass balance Run 48 Stage 1

	Input (g)		Output (g)				Accum (g)	Loss (g)
Species	**Feed**	**Wash**	**Cond**	**Washed Solids**	**Filtrate**	**Spent Wash**	**Solids**	
Feed	1576.76							
H_2O			774.09					
Solution		278.41		284.13	309.07	306.58	142.94	
Total	1576.76	278.41	774.09	284.13	309.07	306.58	142.94	38.36
Combined	1855.17		1816.81					38.36
								2.1%
						Corrected Loss		1.2%

16.72 grams were accounted for from this stage, leading to a corrected loss of 1.2%.

Table L2. Mass balance Run 49 Stage 1

	Input (g)		Output (g)				Accum (g)	Loss (g)
Species	**Feed**	**Wash**	**Cond**	**Washed Solids**	**Filtrate**	**Spent Wash**	**Solids**	
Feed	1587.57							
H_2O			748.47					
Solution		303.68		228.14	372.87	369.99	139.72	
Total	1587.57	303.68	748.47	228.14	372.87	369.99	139.72	32.06
Combined	1891.25		1859.19					32.06
								1.69%
						Corrected Loss		0.51%

22.34 grams were accounted for from this stage, leading to a corrected loss of 0.51 %.

Table L3. Mass balance Run 50a Stage 1

	Input (g)		Output (g)				Accum (g)	Loss (g)
Species	**Feed**	**Wash**	**Cond**	**Washed Solids**	**Filtrate**	**Spent Wash**	**Solids**	
Total	1547.16	289.57	736.17	262.29	414.98	299.82	85.45	
Combined	1836.73		1798.71					38.02
								2.1%
						Corrected Loss		1.2%

15.93 grams were accounted for from this stage, leading to a corrected loss of 1.2%.

Table L4. Mass balance Run 50b Stage 1

	Input (g)		Output (g)				Accum (g)	Loss (g)
Species	**Feed**	**Wash**	**Cond**	**Washed Solids**	**Filtrate**	**Spent Wash**	**Solids**	
Total	1563.29	298.22	842.38	296.56	141.36	307.60	234.60	
Combined	1861.51		1822.50					39.01
								2.1%
						Corrected Loss		1.3%

14.02 grams were accounted for from this stage, leading to a corrected loss of 1.3%.

Table L5. Mass balance Run 51 Stage 1

	Input (g)		Output (g)				Accum (g)	Loss (g)
Species	**Feed**	**Wash**	**Cond**	**Washed Solids**	**Filtrate**	**Spent Wash**	**Solids**	
Total	1545.72	347.60	746.64	274.52	390.94	372.46	70.88	37.88
Combined	1893.32		1855.44					37.88
								2.0%
						Corrected Loss		1.1%

16.14 grams were accounted for from this stage, leading to a corrected loss of 1.1%.

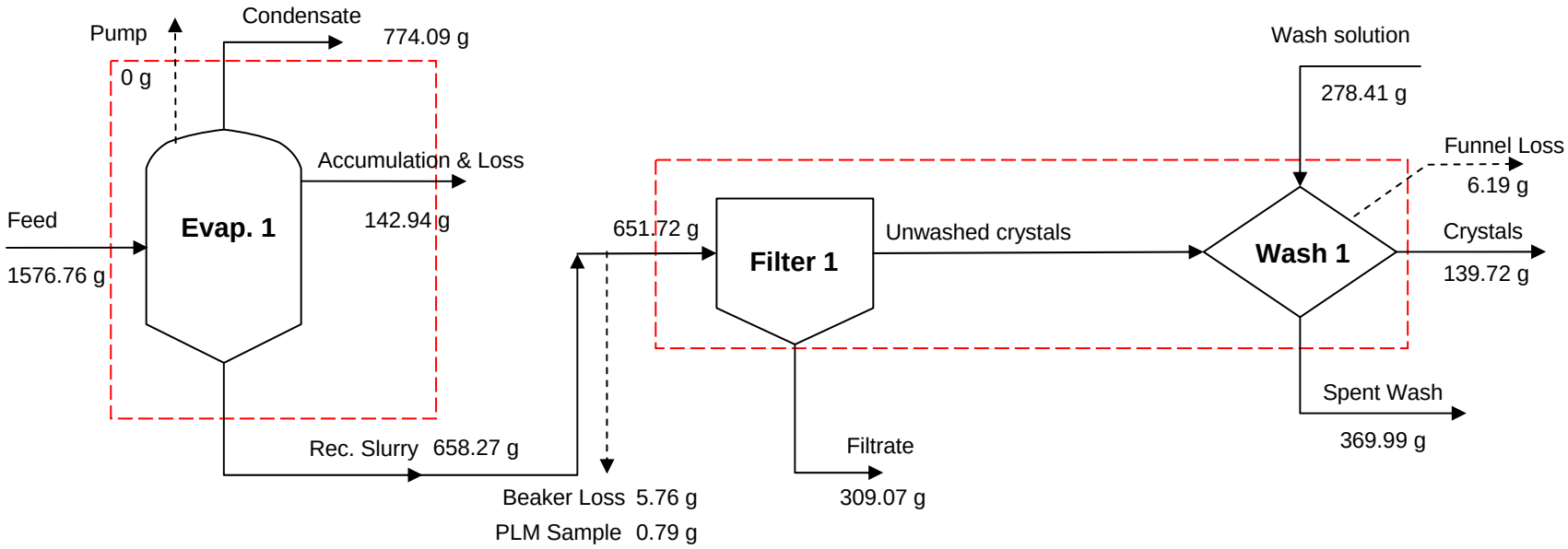

Pump	Mass of the condensate collected in the cold trap protecting the vacuum pump.
Rec. Slurry	Mass of slurry recovered from the crystallizer.
Accumulation & Loss	Mass recovered by washing the vessel with a known amount of water.
Funnel Loss	Mass recovered by washing the funnel with a known amount of water and then drying with paper of a known weight. Performed after the filtration and washing operations.
Beaker Loss	Mass of slurry lost in the beaker necessary for the transfer from the vessel to the filter.
PLM Sample	Mass taken from the slurry for PLM imaging.

Figure L1. Overall mass balance of Early Feed Run 48. Solid arrows are the process streams and the dotted arrows represent the quantified losses. Closure on a total mass balance was performed for each dashed box around a process unit.

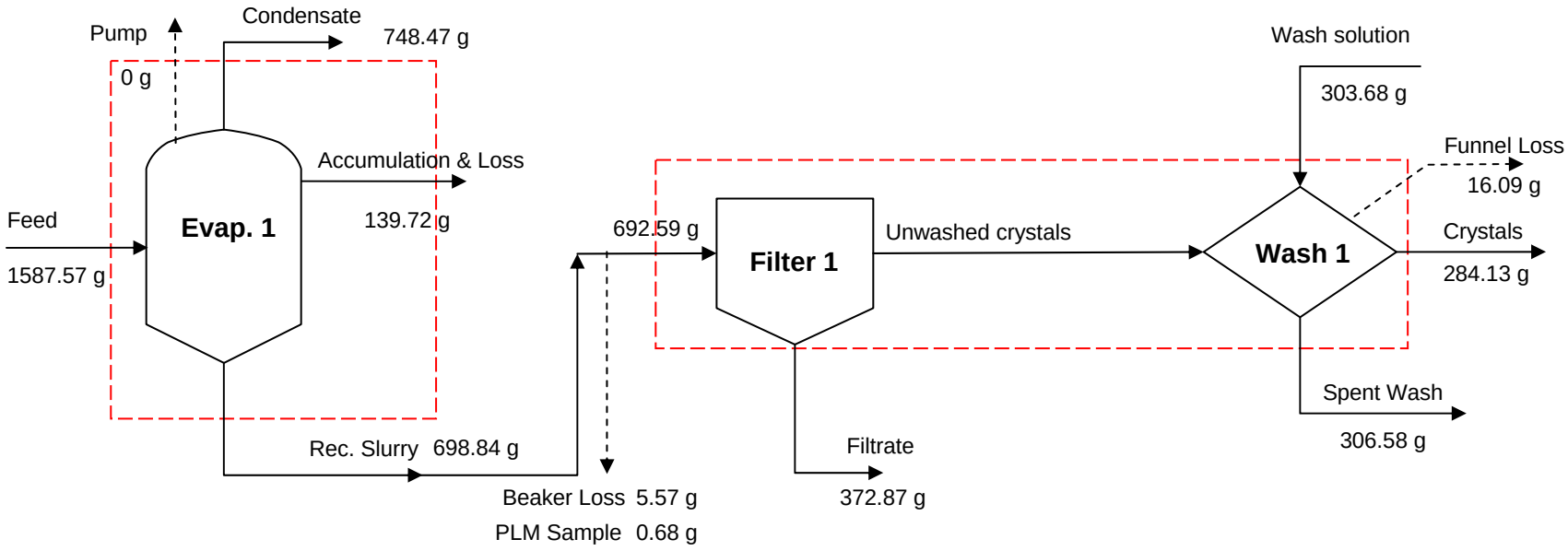

Pump	Mass of the condensate collected in the cold trap protecting the vacuum pump.
Rec. Slurry	Mass of slurry recovered from the crystallizer.
Accumulation & Loss	Mass recovered by washing the vessel with a known amount of water.
Funnel Loss	Mass recovered by washing the funnel with a known amount of water and then drying with paper of a known weight. Performed after the filtration and washing operations.
Beaker Loss	Mass of slurry lost in the beaker necessary for the transfer from the vessel to the filter.
PLM Sample	Mass taken from the slurry for PLM imaging.

Figure L2. Overall mass balance of Early Feed Run 49. Solid arrows are the process streams and the dotted arrows represent the quantified losses. Closure on a total mass balance was performed for each dashed box around a process unit.

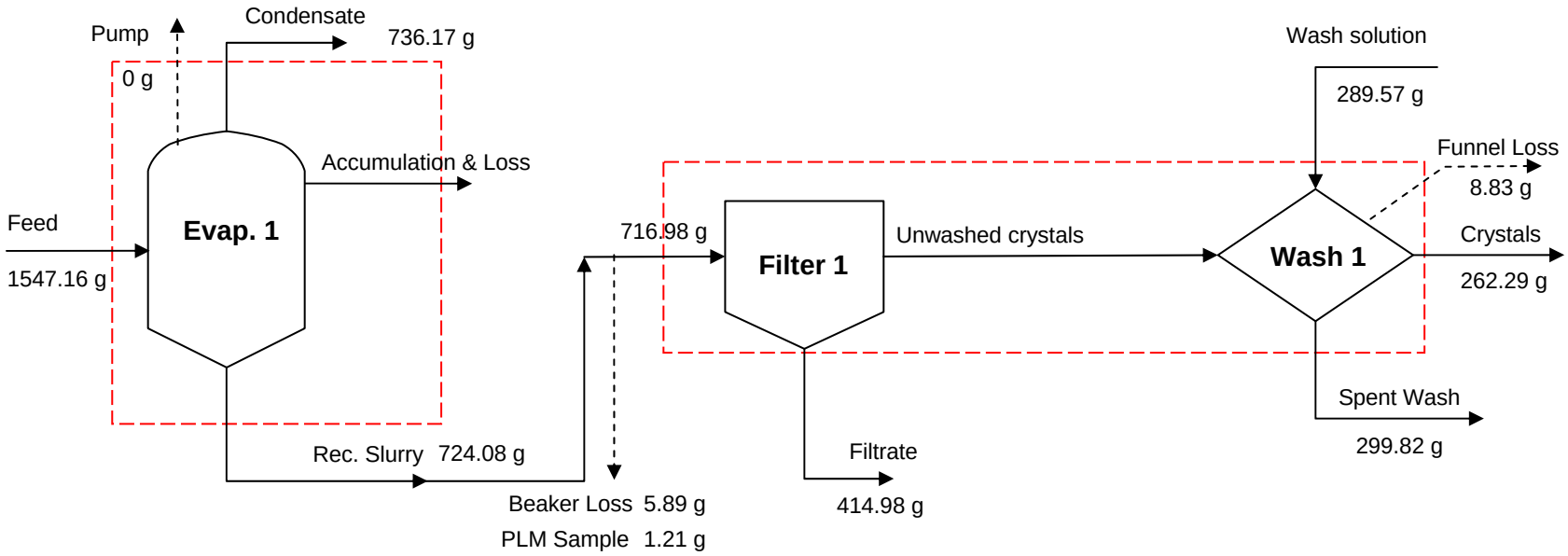

Pump	Mass of the condensate collected in the cold trap protecting the vacuum pump.
Rec. Slurry	Mass of slurry recovered from the crystallizer.
Accumulation & Loss	Mass recovered by washing the vessel with a known amount of water.
Funnel Loss	Mass recovered by washing the funnel with a known amount of water and then drying with paper of a known weight. Performed after the filtration and washing operations.
Beaker Loss	Mass of slurry lost in the beaker necessary for the transfer from the vessel to the filter.
PLM Sample	Mass taken from the slurry for PLM imaging.

Figure L3. Overall mass balance in Early Feed Run 50a. Solid arrows are the process streams and the dotted arrows represent the quantified losses. Closure on a total mass balance was performed for each dashed box around a process unit.

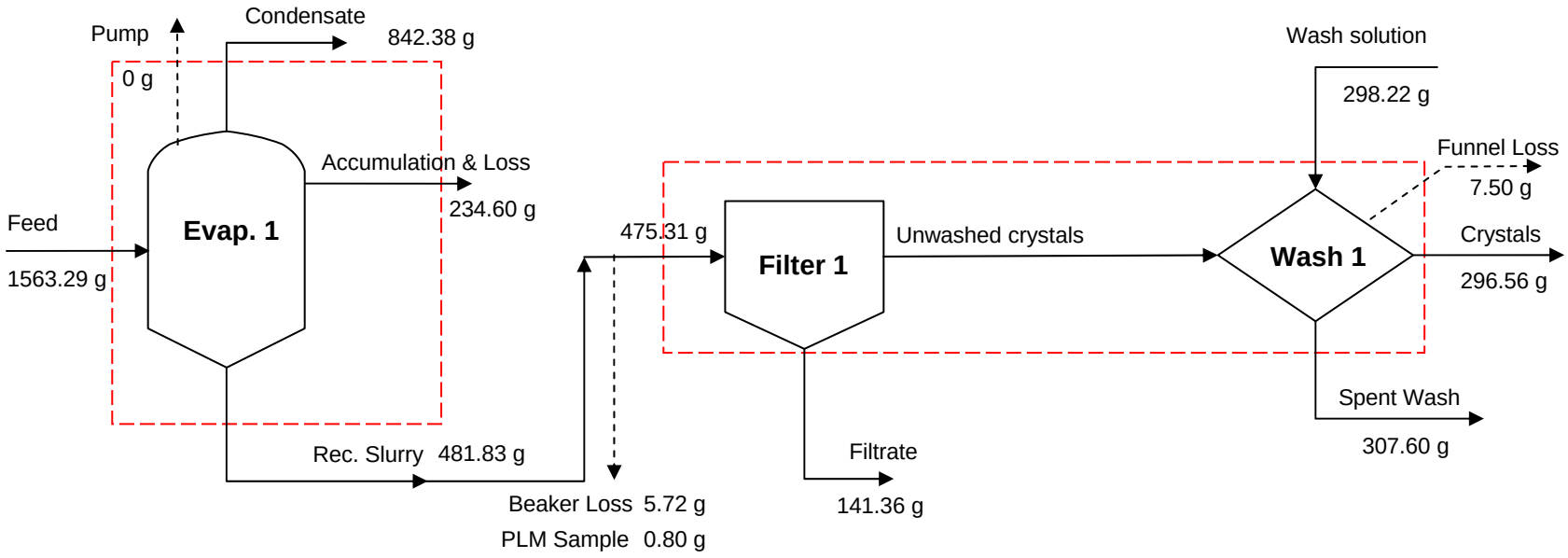

Pump	Mass of the condensate collected in the cold trap protecting the vacuum pump.
Rec. Slurry	Mass of slurry recovered from the crystallizer.
Accumulation & Loss	Mass recovered by washing the vessel with a known amount of water.
Funnel Loss	Mass recovered by washing the funnel with a known amount of water and then drying with paper of a known weight. Performed after the filtration and washing operations.
Beaker Loss	Mass of slurry lost in the beaker necessary for the transfer from the vessel to the filter.
PLM Sample	Mass taken from the slurry for PLM imaging.

Figure L4. Overall mass balance in Early Feed Run 50b. Solid arrows are the process streams and the dotted arrows represent the quantified losses. Closure on a total mass balance was performed for each dashed box around a process unit.

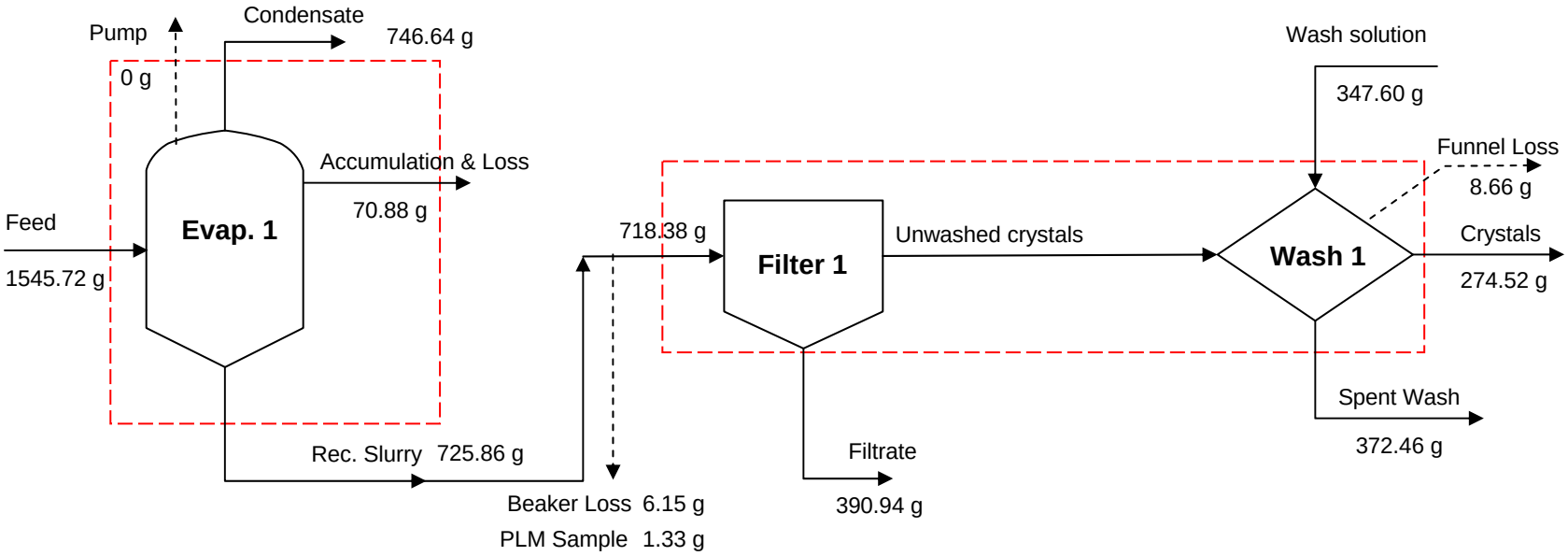

Pump	Mass of the condensate collected in the cold trap protecting the vacuum pump.
Rec. Slurry	Mass of slurry recovered from the crystallizer.
Accumulation & Loss	Mass recovered by washing the vessel with a known amount of water.
Funnel Loss	Mass recovered by washing the funnel with a known amount of water and then drying with paper of a known weight. Performed after the filtration and washing operations.
Beaker Loss	Mass of slurry lost in the beaker necessary for the transfer from the vessel to the filter.
PLM Sample	Mass taken from the slurry for PLM imaging.

Figure L5. Overall mass balance in Early Feed Run 51. Solid arrows are the process streams and the dotted arrows represent the quantified losses. Closure on a total mass balance was performed for each dashed box around a process unit.

REFERENCES

The research team drew on several references during the course of this project, and these are catalogued in the following list.

Aloise, Gene. United States Government Accountability Office April 6 (2006). "Hanford Waste Treatment Plant". GAO-06-602T.

Bryan, Sam. June 12-14 (2003). "Flammable gas issue in stored Hanford Waste". American Chemical Society, Bozeman, MT. Pacific Northwest National Laboratory, Richland, WA.

Carreon, Rudy; Mauss, Billie M.; Johnson, Mike E.; Holton, Langdon K.; Wright, Todd G.; Peterson, Reid A.; Rueter, Ken J. (2002)."Selection of Pretreatment Processes for Removal of Radionuclides from Hanford Tank Waste". WM'02 Conference, February 24-28, 2002, Tucson, A.

Chapman, C.C.; Buelt, J.L.; Slate, S.C.; Katayama, Y.B.; Bunnell, L.R.. (1979). " Vitrification of Hanford wastes in a joule-heated ceramic melter and evaluation of resultant canisterized product". Abstract, Energy Res. Battelle Pac. Northwest Lab., Richland, WA, USA.

Chitry, Frederic; Pellet-Rostaing, Stephanie; Nicod, Laurence; Gass, Jean-Louis; Foos, Jacques; Guy, Alain; Lemaire, Marc. Cesium/Sodium Separation by Nanofiltration-Complexation in Aqueous Medium. Separation Science and Technology, 2001.

P. Colombo ; G. Brustatin; E. Bernardo; G. Scarinci. (2003). "Inertization and reuse of waste materials by Vitrification and fabrication of glass-based products." Solid State and Materials Science, August 2003.

Cowley, W.L.; Vail, T.S.; Reynolds, D.A.; Herting, D.L. April 19-23 (1998). "Technical basis for selecting radionuclide concentrations for use in Hanford tank basis for interim operation source term". Technologies for the New Century topical conference, Nashville. American Nuclear Society, La grange Park, III.

DOE/EM-0319. January (1997). "Connecting the Cold War Nuclear Weapons Production Processes To Their Environmental Consequences". Linking Legacies, US Department of Energy DOE/EM-0319, United States Department of Energy, Washington, DC 20585 .

DOE/EM-0266. (1996). "Closing the Circle on the Splitting of the Atom: The Environmental Legacy of Nuclear Weapons Production and What the Department is Doing About It".

DOE/EM-0232 and DOE/EM-0290. (1995-1996). "Estimating the Cold War Mortgage: The 1995 Baseline Environmental Management report".

DOE. (1996). "Risks and the Risk Debate: Searching for Common Ground".

Felder R. M. and Rousseau R. W., *Elementary Principles of Chemical Processes*, 3rd ed., John Wiley & Sons, Inc., New York, 2000.

Fullam, H.T.(1976). "Solubility and dissolution behavior of strontium-90 difluoride in aqueous media". ERDA Energy Res. Abstract. Battelle Pac. Northwest Lab., Richland, WA, USA.

Geniesse, Donald James; (2004). "Volume reduction of Aqueous Waste by Evaporative Crystallization of Burkeite and Sodium Salts". US Patent. Cogema Engineering Corporation, Richland, WA, USA.

Hammitt, A.P.; Schulz, W.W.. (1979). "Hot Cell Facility and Equipment for Tests of the Hanford Radionuclide Removal Process". Proceedings of the Conference on Remote Systems Technology, Volume No. 26 413-29. Rockwell Hanford Oper., Richland, WA, USA.

Hassan, N.M.; McCabe, D.J.; King, W.D.; Hamm, L.L.; Johnson, M.E.. Ion exchange removal of cesium from Hanford tank waste supernates with SuperLig® 644 resin. Journal of Radioanalytical and Nuclear Chemistry. Vol. 254, No. 1 (2002), pp. 33-40.

Herting, D.L. (1992). "Identification of crystals in Hanford nuclear waste using polarized light microscopy". Energy Res. Abstract, 17(08), Abstract No. 22486. Westinghouse Hanford Co., Richland, WA, USA.

Herting, Daniel L. September 7-11 (1997). "Clean salt process for Hanford nuclear waste treatment". Book of Abstracts, 214th ACS National Meeting, Las Vegas, NV. American Chemical Society, Washington, D.C.

Herting D. L., G. A. Cooke, R. W. Warrant, *Identification of Solid Phases in Saltcake from Hanford Site Waste Tanks,* CD of typical product characterization, Fluor Hanford, Richland, 2002.

Herting, Dan. June 12-14 (2003). "Inorganic tank waste speciation". Abstracts, 58th Northwest Regional Meeting of the American Chemical Society.

Herting D. L., *Fractional Crystallization of Waste from Tank 241-S-112*, Technical Report, 2005.

Hrma P., Crum J.V., Bates D.J., Bredt P.R., Greenwood L.R., Smith H.D. (2005). "Vitrification and testing of a Hanford high-level waste sample. Part 1: Glass fabrication, and chemical and radiochemical analysis."Journal of Nuclear Materials 345 (2005) 19-30

Hrma P., Crum J.V., Bredt P.R., Greenwood L.R., Arey B.W., Smith H.D. (2005). "Vitrification and testing of a Hanford high-level waste sample. Part 2: Phase identification and waste form leachability."Journal of Nuclear Materials 345 (2005) 31-40

Huang, Frank H.; Mitchell, Dolores E.; Conner, John M.. (1994). "Low-Level Radioactive Hanford Wastes Immobilized by Cement-Based Grouts". Nuclear Technology. Westinghouse Hanford Company, Richland, WA,USA.

Kaldor, R.A.; McDaniel, E.W.; Treat, R.L.. September 7-11 (1985). "Immobilization of Selected Low-Level Hanford Wastes in Grout". Waste Management (Tucson, Arizona). Pacific Northwest Lab., Richland, WA, USA.

Kaminski, Michael D.; Nunez, Luis. Cesium Extraction from a Novel Chemical Decontamination Process Solvent Using Magnetic Microparticles. Separation Science and Technology Vol. 37, No. 16 2002.

Lewis, R E.; Butler, T.A.; Lamb, E. (1965). "Recovery of 137Cs from fission-product wastes and transport by an aluminosilicate ion exchanger". U.S. At. Comm. Oak Ridge Natl. Lab., Oak Ridge, TN, USA.

Mika. M; Patek. M; Maixner.J; Randakova.S; Hrma.P;. (2001)."The effect of temperature and composition on spinel concentration and crystal size in high-level radioactive waste vitrification." Proceedings of the International Conference on radioactive Waste Management and Environmental Remediation, 2001.

Moyers C. G. and Rousseau R. W., "Crystallization Operations," in *Handbook of Separation Process Technology*, Chapter 11, pp. 578–643, John Wiley and Sons, Inc., 1987.

Mullin John W., *Crystallization*, 4th ed., Butterworth-Heinemann, Oxford, 2001.

Myerson A. S., ed., *Handbook of Industrial Crystallization*, Butterworth-Heinemann, Boston, 1993.

Ponder, Sherman M.; Helkowski, Robert; Mallouk, Thomas E. Continuous-Flow Process for the Separation of Cesium from Complex Waste Mixtures. Ind. Eng. Chem. Res. Vol. 40, No. 15 2001.

Rabiger K. ; Keldenich K. ; Scheffer J.. Glastech Ber. (1995). "Experience in operation of a pilot plant melting residual substances."
Glass Sci technol, Vol. 68, 84-90, 1995.

Randolph A. D. and Larson M. A., Theory of Particulate Processes: Analysis and Techniques of Continuous Crystallization, 2nd ed., Academic Press, San Diego, 1988.

Reynolds, D.A.; Herting, D.L. (1985). "Solubilities of Sodium Nitrate, Sodium Nitrate, Sodium Nitrite, and Sodium Aluminate in simulated nuclear waste ". Energy Res. Abstr.. Rockwell Hanford Oper., Rockwell Int. Corp., Richland, WA, USA.

Robert A. Smith ; David H. Nyman; B. Nick Anderson. (1990) "Getting ready to build the Hanford Waste Vitrification Plant." Nuclear Engineering International, Vol. 35, No 428, 40-43, March 1990.

Rousseau R. W., "Crystallization," in *Kirk-Othmer Encyclopedia of Chemical Technology*, Volume 7, 4th ed., John Wiley & Sons, Inc., pp. 683–730, 1993.

Rousseau R. W., "Crystallization," in *Encyclopedia of Separation Technology*, Douglas M. Ruthven, Ed., Volume 1, Wiley Interscience, pp. 393–439, 1997.

Rousseau R. W., "Crystallization Processes," in *Encyclopedia of Physical Science and Technology*, 3rd ed., Academic Press, Volume 4, pp. 91–119, 2002.

Sohnel O. and Garside J., *Precipitation*, Butterworth-Heinemann, Oxford, 1992.

Teja A. S. and Rousseau R. W., "Thermodynamics of Crystallization," Chapter 20 in *Chemical Thermodynamics for Industry*, T. Letcher, editor, Royal Society of Chemistry, Cambridge, UK, pp. 230–242. 2004.

Thompson, LE.; Lowery, P.S. (2003). "Development of the bulk vitrification treatment process for the low activity fraction of Hanford single shell tank waste" Conference, February 23-27,2003 Tucson, AZ

Toghiani, Rebecca K.; Lindner, Jeff S.; Herting, D.L. March 11-14 (2002). "Modeling of Hanford saltcake dissolution". American Institute of Chemical Engineers, Spring National Meeting, New Orleans, LA, USA.

Tyree Geoff.."First glass made at Hanford via bulk vitrification."
CH2M Hill Hanford group Publication

Vance, E.R.; Hart, K.P.; Carter, M.L.; Hambley, M.J.; Day, R.A.; Begg, B.D.(1998). "Further studies of Synroc immobilization of HLW sludges and Tc for Hanford tank waste remediation". Materials Research Society. Materials Division, ANSTO, Menai, Australia.

Wilson.B.K; Hrma.P; Alton.J; Plaisted.T.J; Vienna.J.D . (2002). “The effect of composition on spinel equilibrium and crystal size in high-level waste glass.” Journal of Materials Science, Vol 37 (24), 5327-5331, 2002.